

Preparation and Characterization of Polymer/Dendrimer Blends

Final Report, March 2000

Eric J. Amis, Barry J. Bauer, Andreas Topp, Franziska Gröhn, Ty J. Prosa, Brent D. Viers, Dawei Liu, Kathleen A. Barnes, Catheryn L. Jackson, Giovanni Nisato, Ginam Kim, and Alamgir Karim

Polymers Division

National Institute of Standards and Technology

Gaithersburg, MD 20899

Introduction to the Report

This report is a summary of the results of measurement and characterization of dendritically branched polymers that was done for the Army Research Office under contract 35109-CH. Three previous NISTIR's¹⁻³ reported investigations covering consecutive 12 month periods. This report gathers information from previous reports and new information gathered within the last year.

The report describes three areas of research on dendrimers. In section 1 we report on our study of individual dendrimer properties in solution. In section 2, we describe materials made from a combination of dendrimers and conventional polymers, and in section 3 materials made from a combination of dendrimers and metals.

The dendrimer solution properties are divided into six categories, size measurement, internal segment density distribution, comparison of different types of dendritic polymers, location of dendrimer terminal units, interactions of dendrimers at high concentrations, and effect of solvent on dendrimer size. This research area was the first to be explored, and detailed information has been given in several published papers that can be used to obtain detailed information. In this report, summaries are given of these results in a concise review.

The research areas of dendrimer/polymer combinations are blends, interpenetrating polymer networks, and dendrimers tethered to linear chains. The blend work is divided into four subcategories, hydrogen bonding blends of dendrimers, fatty acid modified dendrimer/polyolefin blends, ternary blends, and dendrigraft blends. The ability to disperse a dendrimer in a polymeric matrix is examined by different synthetic approaches. Methods of structure characterization are developed and thermodynamic explanations of the results are offered.

The dendrimer/metal combinations have three subcategories, metal containing polyamidoamine dendrimers in aqueous solution, metal containing hydrophobically modified polypropyleneimine dendrimers in hydrophobic solvents, and metal containing dendrimer interpenetrating polymer networks. Measurement methods and techniques of data interpretation are developed that can be used to identify structural features. These methods are then used to identify thermodynamic principles that govern the structure formation process. These principles can then be used on generic materials

Most of the work that is described in this report gives completed areas of research on generic dendritic materials the results of which may be applied to individual materials of interest.

General Information And Acknowledgments

Throughout this report certain conventions will be used when describing uncertainties in measurements. Plots of small angle scattering data have been calculated from circular averaging of two-dimensional files. The uncertainties are calculated as the estimated standard deviation of the mean and the total combined expanded uncertainty is not given as comparisons are made with data obtained under the same conditions. In cases where the limits are smaller than the plotted symbols, the limits are left out for clarity. In data plots with uncertainties larger than the symbols, representative 95% confidence intervals are plotted at appropriate places. Fits of the scattering data are made by a least squares fit of the data giving an average and a standard deviation to the fit. This would be correct for fit values such as radius of gyration and exponents. Temperatures are given as expected ranges of values based on previous work.

All concentrations are calculated from weighed samples and are reported as mass fractions and are nominal values for naming purposes. The ranges of the concentrations calculated from mass are within one percent of the reported values. The conventional notation “molecular weight” has been replaced by “relative molecular mass” according to ISO 31-8 in most cases. occasionally, the conventional notation is used to conform to previous publications.

Certain commercial materials and equipment are identified in this paper in order to specify adequately the experimental procedure. In no case does such identification imply recommendation by the National Institute of Standards and Technology nor does it imply that the material or equipment identified is necessarily the best available for this purpose.

This work has been preceded by three progress reports that list in detail the participants in individual projects from outside of NIST.¹⁻³ We gratefully thank them for the samples provided and their characterization results. This work is supported in part by the U.S. Army Research Office under contract number 35109-CH.

1	Characterization of Dendritically Branched Polymers by SANS, SAXS, and TEM.....	14
1.1	Synopsis	12
1.2	Introduction.....	12
1.2.1	Unique Structures	12
1.2.2	History of Dendrimer Characterization.....	13
1.2.3	Important Technological Questions.....	14
1.2.4	Measurement Methods Used.....	15
1.3	Dendrimer Size vs. Generation.	16
1.4	Dendrimer Internal Segment Density Distribution.....	17
1.5	Comparison of Dendrimers, Hyperbranched, and Dendrigrraft.....	18
1.6	Location of the Terminal Groups	20
1.7	Dendrimer-Dendrimer Interactions	22
1.8	Dendrimer Size Change in Different Solvents.....	24
1.9	Summary	25
2	Dendrimer/Polymer Blends	27
2.1	Blends of Dendrimers and Hydrogen-Bonding Polymers	27
2.1.1	Synopsis	27
2.1.2	Introduction	27
2.1.3	Experimental.....	27
2.1.4	Results and Discussion.....	28
2.1.5	Summary	29
2.2	Blends of Fatty Acid Modified Dendrimers with Polyolefins	29
2.2.1	Synopsis	29
2.2.2	Introduction	30
2.2.3	Experimental.....	30
2.2.4	Results and Discussion.....	31
2.2.5	Summary	32
2.3	Ternary Dendrimer Blends.....	32
2.3.1	Synopsis	32
2.3.2	Introduction	32
2.3.3	Experimental.....	33
2.3.4	Results and Discussion.....	33
2.3.5	Summary	35
2.4	Blends of Dendrigrraft Polymers with Linear Polymers	35
2.4.1	Synopsis	35
2.4.2	Introduction	35
2.4.3	Experimental.....	37
2.4.4	Results and Discussion.....	38
2.4.5	Conclusions	42
2.5	Dispersing Dendrimers in a Solid Polymer Matrix	42
2.5.1	Synopsis	42
2.5.2	Introduction	43
2.5.3	Experimental.....	44
2.5.4	Results and Discussion.....	45
2.5.5	Conclusions:	48
2.6	End Linked Dendrimer Networks	48

2.6.1	Synopsis	48
2.6.2	Introduction	48
2.6.3	Experimental.....	49
2.6.4	Results and Discussion.....	50
2.6.5	Summary	55
3	Metal Containing Dendrimers.....	56
3.1	Dendrimers as Templates for the Formation of Inorganic Nanoclusters.....	56
3.1.1	Synopsis	56
3.1.2	Introduction	56
3.1.3	Experimental.....	57
3.1.4	Results and Discussion.....	58
3.1.5	Conclusions	64
3.2	Hydrophobically Modified Dendrimers.....	65
3.2.1	Synopsis	65
3.2.2	Experimental.....	66
3.2.3	Results and Discussion.....	67
3.2.4	Conclusion.....	70
	References:	151

Table 1 Major technological issues. Key to symbols, ++, best technique for measurement; +, acceptable technique for measurement; -, unsuitable for measurement.....	71
Table 2 Comparison of different dendritically branched polymer types, see Figure 7.....	72
Table 4 Characteristics of Arborescent Polymers with 5000 g/mol Branches	73
Table 5. Characteristics of deuterated polystyrene and deuterated poly(vinyl methyl ether).....	74
Table 6. Diameter of G6 – G11 PAMAM dendrimers in methanol solution and in IPN's as measured by SAXS and TEM at mass fraction 1 % and 10 %.....	75

Figure 1 Classical Dendrimer Cartoon showing core, branch points and terminal groups.	76
Figure 2 SAXS R_g of PPI and PAMAM dendrimers. Straight line is the limit of PAMAM dendrimers collapsed to bulk density. The 1/3 power law suggests uniform spherical shape.....	77
Figure 3 TEM of G5, G6, G8, and G10 PAMAM dendrimers. Individual molecules are seen.....	78
Figure 4 PAMAM dendrimer diameter from SAXS and TEM.....	79
Figure 5 SAXS curves for PAMAM mass fraction 1% dendrimer/methanol solutions of generation G3 (top) through G10 (bottom). Power law behavior continuously varies from $-5/3$ to -4	80
Figure 6 Fits of the G10 PAMAM dendrimer data to a distribution of spheres and a single ellipsoid of revolution.....	81
Figure 7 Cartoons representing dendritically branched polymers listed in Table 2	82
Figure 8 Zimm and Guinier plots of G4 PAMAM dendrimer and G5 hyperbranched polyol. The dendrimer fits Guinier (Spherical) and the hyperbranched fits Zimm (Gaussian).....	83
Figure 9 Kratky plots of G1 PS dendrigraft, G3 PS dendrigraft, G4 PAMAM dendrimer, and G10 PAMAM dendrimer. . Flat high q shows star-like structure, higher order features shows sphere-like structure.....	84
Figure 10 Volume fraction interior polymer segments in dendrimer solution. PPI dendrimer in methanol, PAMAM dendrimer in methanol, hyperbranched polyol in methanol, and PS dendrigraft in cyclohexane.....	85
Figure 11 Cartoon of possible end group locations. A) whole dendrimer end groups outside, b) whole dendrimer end groups backfolded, a) matched dendrimer end groups backfolded, a) matched dendrimer end groups backfolded. Outside end groups have a larger R_g	86
Figure 12 SANS of G7(H) in CD_3OH , G7(D) in contrast match methanol, and G7(H) in contrast match solvent. Labeled dendrimer in core match solvent shows scattering from labeled terminal generation.	87
Figure 13 Cartoon showing dendrimers at different concentrations.....	88
Figure 14 SANS of G5 PPI dendrimer at various mass fractions. Peaks move to higher q (smaller separation distance) with increased concentration.	89
Figure 15 Kratky plot of SAXS of G5 PPI dendrimer at various mass fractions. Higher order feature moves to higher q suggesting shrinkage with increased concentration.	90
Figure 16 TEM of aqueous PAMAM G10. Note dendrimers are touching but not interpenetrating.....	91
Figure 17 R_g of G8 PAMAM dendrimer in alcohol of various types from SANS. R_g of G8 PAMAM dendrimer calculated from HRS results in reference. ⁵²	92
Figure 18 SANS from G8 PAMAM dendrimer with and without acid and salt additions. Note constant position of higher order features showing constant size.	93
Figure 19 SANS from blends of G4 PAMAM and PMMA-r-PMAA.....	94
Figure 20 SANS from Blends of G4.5 PPI and PMMA-r-PMAA. Parameter of the plot is the temperature as indicated in the figure.....	95

Figure 21 SANS from blends of mass fraction 2% dendrimer-h in 98% mass fraction HDPE-d ₄ . (), G1; ('), G3; (, G5.	96
Figure 22 Guinier plot of the scattering from blends of 2% mass fraction dendrimer-h in HDPE-d ₄ . Symbols are the same as in.....	97
Figure 23 Mass fraction 2% G5 Dendrimer-d in PP,) ; LPDE, ' ; and E-co-B, (.....	98
Figure 24 SANS from a 1:9 PSD/PVME blend that contains a mass fraction of 1% PPI-C ₈ dendrimer for temperatures in the range 90 °C ≤ T ≤ 140 °C.....	99
Figure 25 SANS from 3:7 PSD/PVME blends that contain a mass fraction 0% and 1% PPI-C ₈ dendrimer.	100
Figure 26 . Effect of the dendrimer PPI-C ₈ on the spinodal temperature of PSD/PVME blends.....	101
Figure 27 SANS of PSD/PVME = 1/9 with and without mass fraction 1 % dendrimer at 140 °C and 150 °C.....	102
Figure 28 SANS of PSD/PVME = (1/9 and 3/7) with and without mass fraction 1 % dendrimer at 70 °C.	103
Figure 29 TEM of PSD/PVME blend ED-1. The scale bar is one micron.....	104
Figure 30 Schematic representation of the growth of arborescent polymers by successive grafting reactions.....	105
Figure 31 SANS curves for all arborescent polymer generations in d-polystyrene at 120 °C.....	106
Figure 32 R _g of arborescent polymers in solutions and in blends as a function of generation number.....	107
Figure 33 Temperature dependence of R _g for arborescent polymers in d-PVME.....	108
Figure 34 (a) R _g versus molecular mass for arborescent polymers in d-PVME. (b) R _g versus molecular mass for arborescent polymers in d-polystyrene.....	109
Figure 35 (a) Scattering functions for power law model compared with G3 polymer in d-PVME. (b) Scattering functions for power law model compared with G3 polymer in d-polystyrene.....	110
Figure 36 Density profiles for G3 arborescent polymer in solutions and blends.	111
Figure 37 I(q) versus q for G3 polymer in d-PVME from 80 °C to the phase separation temperature.	112
Figure 38 Temperature dependence of R _g for G3 polymer in d-PVME.	113
Figure 39 R _g of G3 arborescent polymer as a function of molecular mass of the matrix d-polystyrene.....	114
Figure 40 SAXS for G10 dendrimer solution and IPN's. High concentration low q peaks are indicative of dendrimer ordering. The first minimum in the scattering indicates dendrimer size. The shift to higher q of the minimum for the mass fraction 10% dendrimer in the IPN shows shrinking.	115
Figure 41 SAXS and TEM-FFT dendrimer R _g in solution and IPN's. The size in mass fraction 10 % dendrimer in the IPN is considerable smaller than in dilute solution or IPN.....	116
Figure 42 TEM of mass fraction 10 % G11 dendrimer in the IPN with osO ₄ staining. Picture contains images of dendrimers at different levels.	117
Figure 43 TEM of mass fraction 1 % G10 dendrimer in PHEMA with Phosphotungstic acid staining.....	118

Figure 44 SAXS of mass fraction 2 % G8 PAMAM dendrimer and mass fraction 2 % G8-MAA dendrimer stained with phosphotungstic acid. Leveling off at low q is an incipient peak showing uniform spacing. Peak at higher q shows spherical nature and first minimum gives information on size.	119
Figure 45 TEM of mass fraction 2 % G8 dendrimer in PHEMA with Phosphotungstic acid staining.....	120
Figure 46 TEM of mass fraction 2 % G8 PAMAM dendrimer in PHEMA-co-PMAA with Phosphotungstic acid staining.....	121
Figure 47 Fast Fourier transform of TEM micrographs. Features at high q are representative of spherical shape, the first minimum indicates an average R. Peak in mass fraction 2 % G8 PAMAM dendrimer samples at low q represents incipient ordering and is not seen for the mass fraction 1 % G9 or G10.....	122
Figure 48 Kratky plots of 32 arm stars with DSM G5 cores. The choice of endlinking chemistry will affect the ultimate number of arms added.	123
Figure 49 GPC on the 32 arm stars (Figure 48) demonstrating the differences in reactive endlinking chemistries.	124
Figure 50. Kinetically Resolved GPC on DSM G4 stars of expected functionality 32. The star (at low elution volumes) is clearly delineated from the free, reacting arms. A ratio of the two peaks provides a measure of the conversion.	125
Figure 51 Kinetic Analysis of Figure 50. The dotted line demonstrates the fit expected from Equation (2.12). A better fit is obtained when the reaction order is allowed to float (Equation (2.13)). This demonstrates that arms add very rapidly in early stages, but further addition is very sterically hindered at late stages.	126
Figure 52. DSM G5 networks with differing PEG/DSM stoichiometry. The most lightly crosslinked gels swell most, and there is little variance in swelling for high crosslink functionality in accord with Equation (2.14) and (2.15)	127
Figure 53. PAMAM G4 networks with differing PEG/PAMAM stoichiometries (see. Figure 52).....	128
Figure 54. PAMAM networks swollen in solutions of decreasing pH. Gels with the lowest functionality swell the most, and all gels demonstrate a maximum in swelling due to repulsion of the (acid charged) dendrimers. The swelling decreases at lower pH (higher HCl:NR ₃) due to screening of the repulsive interactions.	129
Figure 55. Dendrimer nanotemplating in aqueous solution. In a first step, the dendrimer is loaded with a precursor salt (H ⁺ AuCl ₄ ⁻) resulting in a charged dendrimer with the precursor as counterions. In a second step, the chemical reduction is performed which yields a colloid inside the dendrimer.	130
Figure 56 UV-VIS spectra for gold-dendrimer hybrid colloids in aqueous solution. The spectra correspond to G9-PAMAM dendrimer samples loaded with different amounts of gold (the molar ratio of gold ions to dendrimer end groups is indicated in the figure.).....	131
Figure 57. TEM of gold containing G9 PAMAM-dendrimer obtained for 1:1 loading. The dendrimer has been stained with phosphotungstic acid, it appears gray, the gold appears black. A: fast reduction (NaBH ₄ in 0.1 mol/L NaOH) b: slow reduction (NaBH ₄ in 0.3 mol/L NaOH)	132
Figure 58 a: Small angle x-ray scattering curve I(q) for the plain G9 PAMAM-dendrimer along with fit to the data. Error bars are the measured standard deviation in I(q).	134

Figure 59 a) Small angle x-ray scattering curve $I(q)$ for the gold containing G9 PAMAM dendrimer of figure 3 along with fit to the data. B) Pair distribution function $P(r)$ obtained by indirect Fourier transformation of the scattering data $I(q)$ (program ITP). A layered-sphere structure with a total diameter of 13 nm becomes evident.	135
Figure 60 a) Theoretical pair distribution function $P(r)$ calculated for layered spheres with different relative contrast of the inner sphere (solvent contrast = 0, outer sphere contrast = 1, inner sphere contrast as given in the figure). The basic shape of the experimental function in Figure 4b cannot be modeled.	136
Figure 61 a) Small angle x-ray scattering curves $I(q)$ for gold containing G9 PAMAM-dendrimers obtained for different loading ratios 1:1, 1:2 and 1:4. Pair distribution functions $P(r)$ obtained by indirect Fourier transformation of the scattering data $I(q)$ in b) The decreasing gold diameter but constant dendrimer diameter upon decreasing loading is visible.	137
Figure 62 a) TEM of gold containing G8 PAMAM dendrimer obtained for 1:1 loading and slow reduction. (The dendrimer has been stained with phosphotungstic acid.)	138
Figure 63 a) Small angle x-ray scattering curves $I(q)$ for gold-dendrimers hybrid structures obtained with PAMAM dendrimers of generation 7 to 10.	139
Figure 64 Small angle neutron scattering curve for the initial G5 poly(propyleneimine) dendrimer in toluene at 55°C and small angle neutron scattering curve and small-angle x-ray scattering curve after solubilization of gold salt.	140
Figure 65 Small angle neutron scattering curve $I(q)$ for the gold-salt loaded G5 poly(propyleneimine) dendrimer along with fit to the data.	141
Figure 66 Pair distance distribution function $P(r)$ obtained by indirect Fourier transformation of the scattering data $I(q)$ (program ITP). A cylindrical structure with a diameter of 6 nm and a length of 21 nm becomes evident.	142
Figure 67 Cross-sectional pair distance distribution function $P_c(r)$ obtained by indirect Fourier transformation of the scattering data $I(q)$ under assumption of a cylindrical particle geometry.	143
Figure 68. Radial scattering length density profile $\rho(r)$ obtained by square-root deconvolution of the cross sectional pair distance distribution function $P_c(r)$ in figure 68. The dotted line represents the result from the first multi-step approximation. The solid line represents the final solution, i.e. the easiest profile corresponding to the best fit of the data: A two step cross-sectional profile becomes evident.	144
Figure 69 Small angle x-ray scattering curve $I(q)$ for the gold-salt loaded G5 poly(propyleneimine) dendrimer along with fit to the data.	145
Figure 70 Pair distance distribution function $P(r)$ obtained by indirect Fourier transformation of the scattering data $I(q)$ (program ITP). A cylindrical structure with a diameter of 4 nm becomes evident.	146
Figure 71 Cross-sectional pair distance distribution function $P_c(r)$ obtained by indirect Fourier transformation of the SAXS data $I(q)$ under assumption of a cylindrical particle geometry (program ITP).	147
Figure 72 Schematic of the multi-dendrimer cylindrical structure as deduced from the SAXS and SANS results.	148
Figure 73 Small angle neutron scattering curve $I(q)$ for gold-dendrimer hybrid structures.	149

Figure 74 TEM of gold colloids obtained from hydrophobically modified G5 poly(propyleneimine) dendrimers loaded with gold-salt after reduction with sodium borohydrate. 150

1. Characterization of Dendritically Branched Polymers by SANS, SAXS, and TEM

1.1 Synopsis

Small angle neutron scattering (SANS), small angle x-ray scattering (SAXS), and transmission electron microscopy (TEM) have been used to characterize the size, shape and interactions of dendrimers, hyperbranched, and dendrigraft polymers. Size in terms of radius of gyration (R_g) from scattering and diameter from microscopy can be routinely measured. Five technologically important factors of dendritically branched polymers have been identified and measured. Dendrimers have a uniform spherical structure without a greatly depressed segment density distribution (SDD) at the center or a broad outer interfacial transition. Dendrimers are spheres with a uniform SDD and an abrupt outer transition, hyperbranched polymers are polydisperse in size and have Gaussian SDD, dendrigrafts have a uniform interior with a star-like outer transition. The terminal units of dendrimers are predominately on the exterior of the molecule. Dendrimers at high concentrations tend to align and will shrink rather than interpenetrate at high concentration. There is negligible size change of dendrimers in solvents of different quality or when charged.

1.2 Introduction

1.2.1 Unique Structures

Ever since the introduction of the synthetic techniques that produce dendrimers, it has been quite obvious that they produce structures unlike all previous synthetic polymers.^{4,5} The stepwise layering of generations with uniform branching present in every step produces molecules of elegant symmetry that have become immediately recognizable. Figure 1 is a classical dendrimer cartoon that is instructive on the synthetic steps necessary to form the dendrimer, and of the topology of the resultant structure.

At the center of the dendrimer is the core that represents the first synthetic step in divergent synthesis, or the last step in convergent synthesis. Each concentric circle of branched units is a generation X, designated GX, of identical repeat units. Hundreds of chemical repeat units have been reported,^{6,7} but our characterization has primarily been for polyamidoamine (PAMAM), $-(\text{CH}_2\text{CH}_2\text{CONHCH}_2\text{CH}_2\text{N})_n$,⁴ or polypropyleneimine (PPI), $-(\text{CH}_2\text{CH}_2\text{CH}_2\text{N})_n$ ^{8,9} dendrimers. The discontinuous lines at the perimeter of the circle in Figure 1 are the terminal units of the dendrimer which are $-\text{NH}_2$ for the full generations of both PAMAM and PPI dendrimers. We are interested in the structure of a generic dendrimer, however, whose properties result from the connections within a dendrimer and not primarily from the chemistry involved in the synthesis.

Although the synthetic techniques of dendrimer production have been extensively studied,^{6,7} characterization of the size, shape, and interactions of dendrimers have lagged behind. While the cartoon of Figure 1 is very instructive for learning about the

connections resulting from the synthesis, it can be very misleading if it is used to describe how a dendrimer actually distributes itself in space. If dendrimers were shaped as depicted by Figure 1 they would be round (circular in 2 dimensions, spherical in 3 dimensions), have a lower segment density on the inside than at the outside, and have all of the terminal units at the outside. Since these factors have very important technological implications, it is imperative that measurements be made to characterize the reality of dendrimers.

The doubling that is inherent in dendrimer chemistry is the dominant process that controls the dendrimer shape ⁴. With each generation, the number of terminal units usually doubles. Since the mass of each generation doubles, the total molecular mass also approximately doubles with each generation, as does the number of branch points. While the dendrimer mass doubles with generation, the space to fit the units increases at a much slower rate. The contour length of any chain from the core to the terminal units is proportional to the number of chemical bonds and hence the number of generations. Equations (1.1) to (1.3) show the relationship between the molecular mass, M , and the molecular volume, V , for a dendrimer of generation G . The ratio of M to V gives a relative local density ρ and the inverse of this quantity gives an intrinsic viscosity $[\eta]$.

$$M \propto 2^G \quad (1.1)$$

$$V \propto G^3 \quad (1.2)$$

$$\rho \propto [\eta]^{-1} \propto M/V \propto 2^G / G^3 \rightarrow \infty \quad (1.3)$$

The increase of the molecular mass proceeds much more rapidly than the space available and means that after a few generations, there will not be enough room to fit in all of the required units of the next generation. The result is that the chemistry at a certain generation cannot be complete and a fraction less than 100 % chemical conversion will result. It is of interest to study dendrimers up to this limit to find the effect of such extreme crowding.

1.2.2 History of Dendrimer Characterization

The earliest work on dendrimer characterization was concerned with aspects of the organic chemistry – did the proposed chemical reaction take place without side reactions and what was the conversion? Since near 100 % conversion and near perfect removal of excess reactants is required for making pure dendrimer, common methods of spectroscopy and chromatography can be used to verify the structure. In a wide variety of dendrimer chemistries, nearly perfect structures have been produced, at least for earlier generations where the techniques are more quantitative.

The development of mass spectroscopic techniques such as MALDI and electrospray mass spectrometry has allowed the absolute determination of dendrimer perfection.^{10,11} For divergent dendrimers such as PAMAM and PPI, single flaws in the chemical structure can be measured such as an unreacted site of the previous generation, or a side reaction producing a loop. Mass spectrometric results on dendrimers certainly

demonstrate the extreme sensitivity of the technique, but they also demonstrate the uniformity of the molecular mass. The polydispersity index of M_w/M_n for a G6 PAMAM dendrimer can be < 1.0006 which is narrower than that of “living” polymers of the same molecular mass.¹⁰

Hydrodynamic sizes from intrinsic viscosity (IV), gel permeation chromatography (GPC), and holographic relaxation spectroscopy (HRS) map the changes in size with generation. For example, IV of PAMAM¹² and PPI⁹ dendrimers goes through a maximum with generation suggesting that the dendrimers become more densely packed. While these techniques give valuable information, they are most sensitive to the external size of the dendrimers rather than to their internal structure.

Scattering techniques measure the radius of gyration (R_g) of dendrimers which is an average of the spatial distribution of all of the units. Aharoni and Murthy¹³ have used scattering to measure the R_g of dendrimers with alanine repeat units and conclude that they are spherical. These molecules differ from conventional dendrimers, however, in that the branch unit is asymmetric and therefore the internal segment distributions are modified. Other laboratories have begun to publish results of small angle neutron scattering (SANS)¹⁴ and small angle x-ray scattering (SAXS)^{15,16} of dendrimers, but only a few studies have had sufficient resolution to resolve the higher order features characteristic of uniform dendrimers.¹⁷⁻²⁰

Transmission electron microscopy (TEM)^{4,21-23} has been used to image individual dendritic molecules, usually the larger generations. Recently atomic force microscopy (AFM)²⁴ has also been used to image dendritic molecules.

1.2.3 Important Technological Questions

The unique shape and organization of dendrimers suggests that some important applications may be possible. We have identified five important factors that pose questions concerning technological applications. Table 1 lists these factors along with the applicability of SANS, SAXS, and TEM to address the questions.

The first question concerns the segment density distribution (SDD) of the atoms in the interior of a dendrimer. Predictions vary from the extremes of a very hollow structure with a densely packed exterior²⁵ to a high central segment density with a gradually tapering concentration of units²⁶ and a variety of intermediate structures.²⁷⁻³¹ If dendrimers have a micelle-like structure, they may be able to solubilize molecules in the interior for applications such as drug delivery,³² phase transfer,³³ etc. If dendrimers have tapered distributions, they may not be significantly different from linear or slightly branched polymers for these applications.

Another important factor is the difference between different branched types such as hyperbranched³⁴ and dendrimers. The different synthetic requirements between the

two types make dendrimers orders of magnitude more expensive than hyperbranched. Are the structures as significantly different as the prices are?

The terminal groups of a dendrimer are large in number and can have functionalities capable of chemical reactions. If the reactive terminal groups were near the periphery, they would be readily accessible for attachment to surfaces or to reagents. Block copolymers or networks with dendrimers as crosslink points would benefit from having them on the outside.

When dendrimers come in contact by increasing their concentration in solution, or by placing them on a surface, do they freely pass through one another or do they avoid interpenetration and align themselves? Dendrimers have sizes in the range (1 to 20) nm and would be excellent candidates for nanoscopic structures if ordering does occur.

Finally, do dendrimers change greatly in size when placed in different solvents? For applications as size standards or molecular probes dendrimers having a relatively fixed size would be preferable. For applications using the release of stored molecules, however, it would be preferable to “open” and “close” dendrimers by adding appropriate solvents.

1.2.4 Measurement Methods Used

Dendritically branched polymers have been characterized at NIST primarily by SANS, SAXS, and TEM. All three techniques are capable of measuring the size of dendritic materials. SAXS and SANS probe a size scale that reveals information about the average size of the molecules, the radius of gyration (R_g).^{17,18,20,35,36} But more complex fits of the scattering give information on the internal structure of the whole dendrimer or individual parts of dendrimers.^{20,35,37} Scattering can also give information on the spacing between dendrimers.^{35,38,39} TEM can be used to image individual polymer molecules, giving direct information on size, shape, polydispersity, and alignment²³.

Both SANS and SAXS probe the same size scale characterized by the scattering vector q (with $q = (4\pi/\lambda) \sin(\theta/2)$, θ being the scattering angle and λ being the wavelength of the probing radiation). The intensity of the scattering as a function of angle (q) gives information on the arrangement and spacing of the polymer segments. The scattering from a collection of particles can be broken into contributions from a single particle, $P(q)$, and between particles, $S(q)$.

$$I(q) \propto P(q)S(q) \quad (1.4)$$

The form factor term, $P(q)$, contains information on the distribution of segments within a single dendrimer. Models can be used to fit the scattering from various types of particles, common ones being a Zimm function which describes scattering from a collection of units with a Gaussian distribution (equation (1.5)), a Guinier function which describes the

scattering from sphere-like objects (equation (1.6)), and the Sphere function which gives the exact scattering from a perfect sphere where $R = (5/3)^{1/2}R_g$ (equation (1.7)).

$$P(q) = (1 + q^2 R_g^2 / 3)^{-1} \quad (1.5)$$

$$P(q) = \exp(-q^2 R_g^2 / 3) \quad (1.6)$$

$$P(q) = 9(\sin(qR) - qR \cos(qR))^2 / (qR)^6 \quad (1.7)$$

Therefore, a fit of the scattering data not only gives information on an average size, R_g , but also information on the segment density distribution within the dendrimers.

Table 1 compares the usefulness of the three techniques in addressing the questions posed. SANS has the ability to label parts of the molecule by replacing hydrogen with deuterium. This allows for the location of parts of the molecules, such as the end groups, to be measured. SAXS has the advantage of very low background radiation, which gives the best resolution of the higher q features which are weak in intensity. TEM is the only way of seeing individual molecules and offers direct visualization.

Descriptions of the experimental scattering and microscopy conditions have been published elsewhere and are referenced in each section. Throughout this report certain conventions will be used when describing uncertainties in measurements. Plots of small angle scattering data have been calculated from circular averaging of two-dimensional files. The uncertainties in the text, tables, and figures are calculated as the estimated standard deviation of the mean and the total combined uncertainty is not given as comparisons are made with data obtained under the same conditions. In cases where the limits are smaller than the plotted symbols, the limits are left out for clarity. In data plots with uncertainties larger than the symbols, representative confidence limits are plotted at appropriate places. Fits of the scattering data are made by a least squares fit of the data giving an average and a standard deviation to the fit, this is the case for fit values such as radius of gyration and exponents.

1.3 Dendrimer Size vs. Generation.

SANS and SAXS have been used to measure the average R_g of dendrimers in dilute solution.^{17,18,20,36} Figure 2 is a plot of R_g vs. Theoretical M_w for both PPI and PAMAM dendrimers. A line giving the theoretical R_g of spheres with a density of 1.23 g/cc, the value reported for PAMAM dendrimers, is also plotted. Therefore, the line would be the limit of PAMAM dendrimers that have excluded all solvent and shrunk to single dendrimers of bulk density. The distance of the PAMAM points to the line gives the relative segment density within the dendrimers. The data points roughly parallel the line, with the points getting slightly closer to the line for the largest generations.

A slope of 1/3 would suggest that the dendrimers are spherical with similar internal density profiles. There seems to be a slight increase in internal segment density as the dendrimers get larger. For the highest PAMAM generations, it is known that the

theoretical molecular mass is not reached due to crowding.⁴ This would shift the high generation data points to the right and may indicate that the internal densities are uniform after a certain generation.

TEM has been used to measure the average diameter of PAMAM dendrimers from G5 to G10.²³ Figure 3 shows micrographs of G5, G6, G8, and G10. The G5 micrograph also has a small amount of G10 dendrimers added to help focus the microscope and to identify the relative sizes. Single dendrimers can easily be distinguished over the whole size range shown. Individual polymer molecules can easily be seen, while conventional linear polymers in this molecular mass range are difficult to image. This attests to the fact that the dendrimers are much more spherical in shape and have a very high internal segment density compared to conventional polymers.

Size ranges are tabulated from the TEM images and are reported elsewhere.²³ Each generation has a well defined average with a relatively narrow range of sizes. Figure 4 is a plot of the average diameter from TEM²³ and from SAXS²⁰ assuming that the dendrimers are spheres and that therefore the diameter $D = (20/3)^{1/2} R_g$. There is good agreement between the two types of measurement.

1.4 Dendrimer Internal Segment Density Distribution

While microscopy can give important information on the average size of dendrimers, scattering gives much more detailed information on their internal structure. As has been previously mentioned, there are a variety of predictions on the type of segment density distributions on the inside of a dendrimer, from a hollow structure with a dense shell²⁵ to a dense center with a gradually tapering outward distribution.²⁶

The angular dependence of the scattered intensity contains information on the SDD. In principle, if the SDD is known exactly, then the scattering can be calculated exactly and vice versa. The uncertainties in the scattering become translated into uncertainties in the SDD, however, and direct transformation is not practical for samples that do not scatter strongly. There are some characteristics of the scattering at intermediate or high q that can provide insight into relative structures, easily distinguishing the structural class.

Figure 5 is a plot of the SAXS from G3 through G10 PAMAM dendrimers over a very wide q range³⁷. The scattering at low q is a measure of dendrimer R_g , and a gradual transition is easily seen from G3 to G10 indicating increasing R_g with generation number. The high q scattering also has a gradual transition in the limiting power law slope that is sensitive to the transition of segment densities at the outside of the dendrimer. The G3 dendrimer has a high q power law of $-5/3$ which is characteristic of a polymer in a good solvent such as linear polymers or star polymers.³⁵ This indicates a relatively diffuse outer boundary. The G10 dendrimer, however, has a power law slope of -4 which is characteristic of an object with a very sharp outer boundary.³⁵ There is a

gradual transition from G3 to G10 showing that dendrimers transform from star-like to sphere-like.

Another important factor is the appearance of inflections in the high q data that become multiple peaks as the generation number increases. Equation (1.7), which describes scattering from a monodisperse, uniform sphere has multiple peaks at high q . These features also appear in the SAXS data, indicating that the large generation PAMAM dendrimers are becoming quite sphere-like. Even the relatively small G5 dendrimer is beginning to show this feature and the G10 dendrimer shows at least five additional peaks in the data.

The strong scattering from the G10 dendrimers and the multitude of subtle features make it the best candidate for thorough fitting of the structure. Figure 6 is a plot of the G10 SAXS data in a Porod plot, Iq^4 vs. Q . A Porod plot is a convenient way of looking at the scattering from objects with sharp outer boundaries since scattering with a -4 power law will be horizontal line in this type of plot. The data points oscillate around a horizontal line showing a sphere-like structure with a sharp outer boundary. The diminished size of the oscillations with increased q is due to the polydispersity of the sizes of the objects.

The polydispersity can be fit by two limiting cases, as a population of perfect spheres with a range of diameters, or as a single randomly oriented ellipsoid. The solid line in Figure 6 is the theoretical scattering from a population of spheres with a Gaussian distribution of radii with a mean of 69.9 Å and a distribution half width of 4.9 Å. The dashed line is for a randomly oriented ellipsoid with a major axis of 74.1 Å and a minor axis of 59.8 Å. It is not possible to distinguish between these two types of polydispersities, but it is likely that both types are present, resulting from a population of slightly elliptical molecules with a small size variation.

Therefore, the shapes of dendrimers span the range from stars to spheres. Small G3 dendrimers have a diffuse, open structure while large G10 dendrimers are spheres with a uniform interior, sharp outside transition, and low polydispersity.

1.5 Comparison of Dendrimers, Hyperbranched, and Dendrigraft

Dendrimer synthesis involves a repetitive building of generations through alternating steps which double the size with every generation as has been discussed earlier^{4,21}. Hyperbranched synthesis involves self-condensation of multifunctional monomers, usually in a single step³⁴. Hyperbranched polymers and dendrimers of comparable molecular mass have the same number of branch points and terminal units, and any application requiring only these two characteristics could be satisfied by either one. Since dendrimer synthesis requires many synthetic steps and purification processes while hyperbranched synthesis can have only one synthetic step with no purification step, the dendrimers will necessarily be a much more expensive material to produce.

A third type of branched molecule has been described recently, known alternatively as dendrigraft⁴⁰ or arborescent⁴¹ molecules. They are made in a stepwise synthesis as are dendrimers, but the steps involve conventional grafting reactions of end functionalized linear polymers onto a polymer substrate. Ungrafted linear polymer is removed by fractionation and the grafting reaction is repeated, forming the next generation of dendrigrafts. Since many grafts can be added to the previous generation each time, the molecular mass increases by much more than the doubling that is usual for dendrimers, with increases of 10 to 100 per generation being typical. Figure 7 is a cartoon showing the three different types of dendritically branched molecules. The dendrimer has a uniform doubling of the structure with generation producing a monodisperse structure. The hyperbranched molecule has polydispersity in both molecular mass between different molecules, but also internally with the path between the core and different terminal units varying greatly. A dendrigraft is made by repeated grafting of “living” linear polymers, each having a very narrow molecular mass distribution, making the overall distribution narrow.

Table 2 lists some of the typical characteristics of the three types. All have some characteristics in common, such as a high amount of branching as is defined by having a low number (typically < 10) of covalent bonds between branch points and a large number of terminal groups. The most important differences are in the polydispersity, the size of the end groups, and the number of synthetic and purification steps. The last factor is mirrored in the resultant cost that can be different by orders of magnitude. It is important to measure the differences between these three types and linear polymers to see if the differences are sufficient to justify their enormously different costs.

SANS⁴²⁻⁴⁴ and SAXS^{20,37} have been used to measure the form factors of various types of dendritic molecules at NIST. As was described earlier, different structures have different form factors and if the scattering fits a given model over a wide q range, then the molecular structure is well described by the model distribution. Figure 8 is a plot of the SANS from a G4 PAMAM dendrimer and a G5 hyperbranched polyol both of which have the same nominal M_w , 14,000 g/mol. Both SANS curves are plotted as a Zimm plot (I^{-1}) and a Guinier plot ($\ln(I)$). It is quite clear that the dendrimer is linear in the Guinier plot and curved in the Zimm plot, with the opposite being true for the hyperbranched. A Zimm plot describes the scattering from particles such as a linear chain having a Gaussian distribution of segments, while a Guinier plot in this q range fits the scattering from a uniform spherical object. Therefore, to a first approximation, the segment density distribution of a dendrimer is relatively uniform while that of a hyperbranched is quite tapered, with a high density in the center and a gradual decrease in segment density as one moves outward.

The low q range shown in Figure 8 gives important information, but the most sensitive q range is at somewhat higher values of q . Figure 9 is a Kratky plot, of scattering from low generation (G4) and high generation (G10) PAMAM dendrimers²⁰ along with low generation (G1) and high generation (G3) polystyrene dendrigrafts.⁴⁵ A Kratky plot, Iq^2 vs. Q , emphasizes the differences in scattering at higher q values. The uppermost curve is the theoretical scattering from a linear polymer. All of the others

show a peak in the scattering which is characteristic of dense internal structure. The G1 dendrigraft has the shape characteristic of a star polymer with a broad peak and leveling off at higher q . The G4 dendrimer also has this shape, but the peak is much narrower. This suggests a star-like structure on the outside, but more of a tendency for uniform a spherical interior than the G1 dendrigraft. As has been seen previously, the G10 dendrimer has several higher order peaks typical of a very sphere-like distribution. The G3 dendrigraft has a weak higher order peak, but the uniformity is less pronounced than the G10 dendrimer.

Figure 10 is a plot of the average local segment density (volume fraction polymer) for typical dendrimers, dendrigrafts, and hyperbranched. The average size is calculated from the R_g as measured from SAXS or SANS, assuming a spherical shape. The size of a collapsed molecule calculated from M_w and bulk density, ρ , is then used to calculate the average internal volume fraction of polymer segments, ϕ_p , as is shown in equation (1.8).

$$\phi_p = \frac{4\pi \left(\frac{5}{3} \langle R_g \rangle \right)^3}{M_w / N_{Av} \rho} \quad (1.8)$$

Where N_{av} is Avagadro's number. The hyperbranched molecules have the most open structure, with values of ϕ_p , in the range of (2 to 3) %. PPI and PAMAM dendrimers form a composite curve with ϕ_p , ranging from (20 to 75) % from the smallest to the largest dendrimers. The dendrigrafts ϕ_p , ranges from (10 to 50) % from G0 to G3.

The results are summarized in Table 2. A low generation dendrimer has the shape of a dense star with an interior having a more uniform density than a low generation dendrigraft. As the generation number increases, the shape becomes more sphere-like. At the limit of a G10 PAMAM dendrimer, the molecules have a uniform interior with an abrupt transition in segment density at the outside, and low polydispersity. A G0 dendrigraft is like a conventional multi-arm star, but a G3 dendrigraft has a uniform interior with a narrow, star-like zone of transition at the outside. Hyperbranched molecules have polydispersity both in molecular mass and in the internal structure of each molecule. They have a much more open structure with a broad, tapered segment density distribution than do dendrimers of similar size.

1.6 Location of the Terminal Groups

The cartoon representation of a dendrimer is shown in Figure 11 in two forms, Figure 11a being the classical picture with all of the terminal groups (shown as circles connected with a single bond) at the outside of the dendrimer. Figure 11b shows how the terminal groups could enter the interior of the dendrimer by backfolding. SANS of unlabelled dendrimers can give detailed information on the SDD as was demonstrated in the SAXS studies²⁰. However, the calculated density distribution cannot distinguish between the terminal units and all of the other units. Therefore, the types of distributions described in Figure 11a and Figure 11b would give identical scattering.

To distinguish the terminal groups from the groups of the earlier generations, deuterium labeling is used. PAMAM dendrimers having a tetrafunctional core of ethylene diamine (EDA) were synthesized according to reported methods⁴⁶. Fully hydrogenated G7 PAMAM dendrimers and partially deuterated versions were prepared. The partially deuterated dendrimer was prepared by reacting the fully hydrogenous G6 dendrimer with partially deuterated methyl acrylate, $\text{CD}_2=\text{CDCO}_2\text{CH}_3$ to form G6.5 dendrimer with a hydrogenated interior and deuterated terminal units. The G6.5 was converted to the partially deuterated G7(D) dendrimer by reaction with hydrogenated EDA.

Solutions for SANS experiments were prepared with methyl alcohol, CH_3OH , and its partially deuterated counterpart, CD_3OH . For the determination of the contrast match point of the unlabeled parts of the dendrimer, two stock solutions of equal G9 dendrimer concentrations were made in CH_3OH and CD_3OH . Various amounts of the two stock solutions were mixed to make a series of solution with different isotopic contents. The $\text{CH}_3\text{OH} / \text{CD}_3\text{OH}$ match point was determined as the point at which the coherent SANS scattering goes to zero. The procedure is described elsewhere.⁴⁶

After the match point was determined, solutions were made of labeled G7(D) and unlabeled G7(H) dendrimer in the match solvent along with the unlabeled G7(H) in CD_3OH . Figure 12 shows the SANS of the three samples. The unlabeled in match solvent is completely flat, showing only incoherent scattering. This proves that the match solvent completely masks the hydrogenous parts of the dendrimer. The unlabeled G7(H) in CD_3OH shows strong scattering characteristic of dendrimer scattering. The labeled dendrimer in the match solvent still shows some coherent scattering. This scattering is from the deuterated half of the last generation.

To ensure that instrumental artifacts do not perturb the results, we collected two independent data sets for G7(D) in the matching solvent by measuring the solutions on both 30 m SANS instruments at NIST.^{47,48} The absolute values of the coherent scattering intensity of the G7(D) labeled segments were reproduced to high accuracy, independent of the SANS instrument and its configuration. The values of the R_g are determined by weighted linear least squares fits to equation 1.6 and give an R_g of non-labeled dendrimer of $(34.4 \pm 0.2) \text{ \AA}$. For the deuterated segments of the partially deuterated dendrimer, the results are $R_g(\text{G7(D)}) = (38.8 \pm 1.2) \text{ \AA}$ and $R_g(\text{G7(D)}) = (39.8 \pm 1.2) \text{ \AA}$ for the data taken on NG3 and NG7, respectively (uncertainties are based on the standard deviation of the fits). We can take the average value of $R_g(\text{G7(D)})$ as $(39.3 \pm 1.0) \text{ \AA}$ for the deuterated segments of G6.5 in a G7 dendrimer. If a uniform distribution of end groups were present throughout the dendrimer, we would see the same R_g for both the labeled and the whole dendrimer. This is demonstrated by the cartoon in Figure 11 where the end groups have different locations. Instead, we see a clear difference between the R_g values for the labeled units and the unlabeled dendrimers. The distribution of dendrimer terminal groups is not uniform throughout the interior of the dendrimer but rather the terminal groups are localized near the periphery of the dendrimer.

There have been solid state NMR studies⁴⁹ on the distribution of end groups by site-specific stable-isotope-labeling, rotational-echo double-resonance (REDOR) NMR. REDOR experiments which measure dipolar couplings between C-13 atoms located near the chain ends and an F-19 label placed at the core of benzyl ether dendrimers (generations 1-5). They find that average distances are quite small, suggesting that terminal units do approach the core unit. The important difference between the NMR and the SANS studies is the moment of the average distribution. The weighting of the R_g from SANS goes as the square of the distance, R^2 , so that segments with large distances from the center of mass are weighted heavily and ones near the core have little weighting. The NMR technique, however, weighs the cube of the inverse distance, R^{-3} so that small distances are weighted heavily and large distances are not seen. Therefore SANS and NMR are complimentary measurements with the SANS showing that most, but not all of the terminal units are predominately on the outside of the dendrimer, but some can approach the core through backfolding.

Most, but not all of the terminal units are near the outside of the dendrimer at any given time. The SAXS studies²⁰ of the segment density distribution have shown that there is an abrupt transition region at the outside of large PAMAM dendrimers. The combination of these two factors suggests that the terminal functionalities of dendrimers are accessible from the outside and available for chemical reactions such as attachment to surfaces, mounting of a catalyst, or for use as a crosslink junction.

1.7 Dendrimer-Dendrimer Interactions

As was demonstrated earlier, the internal SDD of dendrimers is quite high compared to conventional polymers and there is a narrow zone of transition at the outside. When linear polymers are forced together by increasing their concentration in a solvent, they freely interpenetrate each other due to their open structure. Dendrimers may represent a different case, however, due to their compact size. At low concentrations, dendrimers may avoid interpenetrating each other by occupying space available away from other dendrimers. As the dendrimer concentration is increased, the solvent swollen dendrimers will encroach upon each other, first touching, and then interacting more strongly. Two results could occur, first, the dendrimers could retain the dilute solution size and start to interpenetrate, mixing the outer segments. The other extreme result would be for the dendrimers to collapse upon themselves, avoiding interpenetration. Figure 13 is a cartoon of the three possible states with Figure 13a showing a dilute solution, Figure 13b showing the overlap concentration at which point the dendrimers contact one another, Figure 13c showing dendrimer collapse and non-interpenetration, and Figure 13d showing a concentration above the overlap concentration where the dendrimers retain their size and interpenetrate.

SANS was used to measure the scattering of G4 and G5 PPI dendrimers at concentrations up to a mass fraction of 80 %.⁵⁰ The partially deuterated solvent CD₃OH was used throughout the study. It is used instead of CD₃OD to prevent exchange of deuterium with the hydrogen of the terminal primary amines. The scattering experiments

were performed at the 30 m SANS facility at NIST.^{47,48} The spectrometer was operated at a configuration giving a wide range of the scattering vector, q , $0.05 \text{ \AA}^{-1} \leq q \leq 0.55 \text{ \AA}^{-1}$. The maximum q was required to resolve the scattering at high concentrations. Figure 14 is a plot of the coherent scattering from a G5 PPI dendrimer as a function of concentration. At concentrations below a mass fraction of 5 % the scattering monotonically decreases with q . This is typical of dilute solution scattering with no interactions. A peak in the SANS appears at a mass fraction of 10 % indicating that long range fluctuations have been suppressed because the dendrimers avoid each other. The overlap concentration can be calculated from the R_g assuming a spherical shape and is equal to a mass fraction of about 25 %. At the overlap concentration and higher, the peak is strong and moves to higher q as the dendrimers are forced together.

A previous SANS study of concentrated PPI dendrimers also noted that the peak appears and moves in a way consistent with increased concentration⁵¹. This peak suggests ordering, but cannot easily distinguish between dendrimers shrinking or interpenetrating. It is interesting to note, however, that in Figure 14 at q values higher than the peak position, there is an excess scattering over the incoherent background. As was shown earlier, higher order features in scattering from spheres can be used to fit the size of the sphere. As the sphere size decreases, this feature moves to higher q . If this feature could be resolved, the size of a dendrimer could be measured at high concentrations.

SANS often has a large amount of incoherent scattering that is a flat background containing no structural information. The higher order peaks are in a q range that has low coherent scattering so that a large fraction of the scattering is a noisy baseline, and resolving features becomes difficult. SAXS, however, has only weak background scattering in this angular region. The experiments were repeated at the Advanced Polymers PRT beamline (X27C; SUNY Stony Brook/ NIST/GE/Allied Signal/Montell) at the National Synchrotron Light Source, Brookhaven National Laboratory. Figure 15 is a Kratky plot of the scattering of a G5 PPI dendrimer at various concentrations. The mass fraction 1% scattering can be fit with the scattering from a sphere giving $R = 18.6 \text{ \AA}$ and $R_g = 14.4 \text{ \AA}$ which is consistent with previous results of fitting the low q scattering alone. It is easy to distinguish the higher order features in these plots. As the concentration increases, the minimum remains stationary until the overlap concentration of 25 % is reached. Beyond this point, the minimum moves to higher q showing that the dendrimers are becoming smaller. At the highest concentration, the resolution is lost, but at moderate concentrations above the overlap concentration, the dendrimers tend to shrink in size rather than overlap. Figure 16 is a cryo-TEM image of G10 PAMAM dendrimers in water. The cryo technique involves flash freezing of the solvent that is in a thin film on a grid and is described in detail elsewhere.²³ Individual dendrimers can be seen that are lined up in what is probably an array of a single dendrimer thickness. While there are complicating factors due to the sample preparation, the picture is consistent with dendrimers touching, but not interpenetrating. AFM studies of G3 dendrigraft polystyrene can resolve individual molecules in a surface monolayer²⁴. This is consistent with our PAMAM results and is further evidence of dendrimer non-interpenetration.

Dendrimers remain discrete objects in dilute solution, avoiding interpenetration. As the concentration increases above overlap, the dendrimers preferentially shrink in size rather than interpenetrating. When dried to a solvent free condition, the dendrimers must either deform from their spherical shape into polyhedrons, or must interpenetrate. The solvent free condition would require deuterium labeled dendrimers, and experiments are underway to probe this last concentration regime.

1.8 Dendrimer Size Change in Different Solvents

The effect of solvent quality on the dimensions of linear chains has been studied for many years, and chain dimensions can change a large amount, especially at high molecular mass. There are reports in the literature that the size of dendrimers is largely influenced by the solvent quality. A molecular dynamics study by Murat and Grest²⁹ resulted in an increasing internal segment density of dendrimers when the dendrimer-solvent interactions are less favorable, which leads to a considerable decrease of the average dimensions of the simulated structures. A holographic, relaxation spectroscopy, HRS, study by Stechemesser and Eimer⁵² concluded that the radius of higher generation PAMAM dendrimers would be extremely sensitive to solvent conditions. The effect of charging of the dendrimer in aqueous solution was investigated by Welch and Muthukumar⁵³ through Monte Carlo simulations. They found that charging a simulated PPI dendrimer could change its linear dimension by as much as a factor of 1.8.

Small angle scattering is a direct method of determining dendrimer size. SANS was used to measure dendrimer size by two methods. Dilute solutions of noninteracting dendrimers can be fit by equation (1.6) to determine R_g as a function of dendrimer generation, solvent type, and temperature. The effect of charging is more complex because long range ionic interactions can impose a uniform spacing between dendrimers that affects the low angle scattering. In this case, higher q scattering can be used to measure a size if a higher order feature can be resolved as was the case for the high concentration dendrimer solutions discussed earlier.

The SANS experiments were performed at the NIST 8 m facility. SANS experiments were performed with solutions of G8 PAMAM dendrimer in D_2O , methyl- d_4 , ethyl- d_6 , and n-butyl- d_{10} alcohol at a temperature of $T = 20.0$ °C. PAMAM dendrimers do not dissolve in acetone, but they readily dissolve in methyl alcohol/acetone mixtures over a wide range of composition. Solvents of different composition, were prepared and added to a weighed amount of dried G5 or G8 dendrimer. In a separate set of experiments, the NIST NG7 30 m instrument was used to measure the effects of charging on the dendrimer size. PAMAM G8 dendrimers in D_2O were charged by addition of HCl. Various amounts of NaCl were also added to the charged dendrimers to screen the electrostatic interactions.

Guinier plots were made of the scattering from G8 PAMAM dendrimers to measure the R_g in alcohols of different chain length. Figure 17 is a plot of the R_g values vs. Alcohol chain length. There is a small but consistent drop in R_g as the length of the

hydrocarbon chain goes from 0 to 4, with the total relative change being 10 %. The range of solvents goes from very good (water) to very poor (n-butanol). This is considerably lower than the range predicted from dynamic calculations. Also plotted in Figure 17 are results of holographic relaxation spectroscopy from the literature.⁵² The large changes in the reported hydrodynamic size are not found in the SANS results.

Similar results were found with mixtures of acetone-d₆ and methanol-d₄. The R_g of the dendrimers is not significantly affected by the fraction of acetone in the solvent. The same result is found over the whole range of temperature studied, i.e. In the range $-10\text{ }^\circ\text{C} \leq T \leq 50\text{ }^\circ\text{C}$. Only the data taken in the solvent of the composition $x_s = 0.50$ show some consistent decrease of R_g , relative to the other solvent compositions. This may indicate the onset of a shrinkage of the dendrimers in the vicinity of the solubility gap, which is around $x_s \approx 0.52$. However, the difference from the value of R_g for $x_s = 0.50$ is less than 5 % of the mean value of R_g for the other solvent compositions.

Ionic effects were used in an attempt to modify the size of a G8 PAMAM dendrimer. Monte Carlo calculations⁵³ have predicted that there should be a strong effect, with R_g varying by as much as 1.8 by charging with acid and by screening the charges by addition of salts. Figure 18 shows SANS of the dendrimer under three conditions⁵⁴. A dendrimer solution without acid or salt addition has a pH of 10.1 and has scattering typical of a dilute non-interacting sphere. The R_g of the dendrimer can be calculated from the position of the higher order feature of the sphere scattering and is consistent with previous measurements. The dendrimer is then charged by addition of acid until the pH becomes 4.7. At this point the low q scattering changes dramatically, developing a peak that is characteristic of ordering of the dendrimers by long range ionic effects. As with the high concentration dendrimer studies, the minimum in the scattering can be used to calculate a dendrimer R_g , even when the interactions occur. The R_g has changed only very slightly, increasing by no more than 5 %. Upon addition of salt to screen the long range interactions, the peak disappears, indicating that the long range ordering has been lost. The position of the minimum has not changed, however, indicating that charging and screening the dendrimers does not significantly modify the dendrimer size.

Both large (G8) and small (G5) PAMAM dendrimers do not significantly change size when the solvent environments are changed. When the solvent is made increasingly hydrophobic by increasing the hydrocarbon chain length, only a 10 % change occurs. Also the addition of a nonsolvent to a good solvent does not significantly change the dendrimer size up to the point of phase separation. Charging a dendrimer in aqueous solution also does not change the size of the dendrimer by more than 5 %.

1.9 Summary

Dendritically branched molecules have shapes and interactions that are radically different from conventional linear polymers. SANS, SAXS, and TEM have been used to measure the properties of dendrimers and a generic understanding of their properties has

emerged. Five technologically important questions on the nature of dendrimers have been posed and generalized observations can be made.

Dendrimers are very spherical in shape when compared to conventional linear polymers.^{20,37} The lowest generation dendrimers have internal segment density distributions similar to star molecules, but even the smallest are more compact than stars. As the generation number increases, the sphere-like characteristics increase and the largest dendrimers form a population of spheres with uniform internal density (roughly half dendrimer units - half solvent)⁵⁰, sharp interfaces on the outside, and a small polydispersity in shape.

Dendrigraft molecules are star-like in the 0th generation, but have a uniform interior with an exterior transition zone for G3.^{20,37} Hyperbranched molecules have broad distributions in molecular mass and in shape.²⁰ The scattering from hyperbranched is more similar to that of linear polymers than to spheres, indicating that there is a gradually tapering distribution on units from the center to the exterior.

The terminal units of a dendrimer are predominately towards the exterior of the dendrimer.⁴⁶ While some terminal units may fold inwards, most of the terminal units are on the outside. Combined with the fact that there is a narrow interface on the outside of large dendrimers,²⁰ most terminal groups should be accessible for chemical manipulation such as attachment to surfaces, mounting of catalysts, or attachment of linear chains.

As dendrimers are forced together by increasing the concentration, they avoid interpenetrating each other and preferably shrink in size rather than overlap.^{38,50} This should provide a strong thermodynamic force for ordering dendrimers on surfaces or in the bulk. Dendrimers seem to be well suited for forming well ordered nanostructures.

The size of dendrimers in dilute solution is relatively constant. Changing the quality of the solvent or charging the dendrimers results in only a very small change in dimensions. Therefore, dendrimers seem well suited for applications as standards or as probes of other materials.

2 Dendrimer/Polymer Blends

2.1 Blends of Dendrimers and Hydrogen-Bonding Polymers

2.1.1 Synopsis

Blends of PAMAM and PPI dendrimers were made with linear polymers. SANS of these blends indicated good mixing between the linear components, but heating the mixtures to temperatures above 100 °C causes irreversible changes in the scattering. The samples became insoluble due to crosslinking after the heating cycles of the SANS experiments. This is due to covalent bonds formed between the components. While hydrogen-bonding seems capable of making dendrimers miscible with linear polymers, the side reactions make further processing impossible. This is probably due to the dendrimer samples available to this study and is not representative of dendrimers in general.

2.1.2 Introduction

Miscible blends of high molecular weight polymers have been studied for many years. They are polymer combinations that form thermodynamically favorable interactions causing the polymers to dissolve in each other giving intimate mixing and molecular level dispersions. Combinations of polymers that form miscible blends, however, are exceedingly rare. Arbitrary combinations of two linear polymers overwhelmingly form immiscible blends. This is primarily due to unfavorable heats of mixing that dominate the thermodynamics and result in morphologies with relatively large domains of individual polymers.

An important way to induce miscibility in polymer blends is to make the heat of mixing more favorable through the use of hydrogen bonding.^{55,56} By placing hydrogen-bonding groups on one polymer and hydrogen-bond acceptors on the others, the favorable heat of mixing can be used to induce miscibility. This approach has been successful with linear polymers and may be an important approach in forming miscible dendrimer blends.

The most commonly available dendrimers, PAMAM and PPI, both have internal tertiary amino groups and terminal primary amino groups which are candidates for ionic or hydrogen-bonding interactions. The PAMAM dendrimers also have carbonyl groups in amide linkages that may be susceptible to hydrogen-bonding. It was therefore of interest to use linear polymers with a few hydrogen bonding or ionic groups to determine if miscibility could be induced.

2.1.3 Experimental

Full generation G4 and G11 PAMAM, and generation G5 PPI, each terminated with primary amines (-NH₂) were used as hydrogen bond donors. Half generation G4.5 PPI dendrimers dendrimers of generation 4 (G4) were purchased from Aldrich Chem.

Comp., And G11 PAMAM (Starburst™) dendrimers were obtained from Dendritech (Michigan Molecular Institute, Michigan). The PPI (Astramol™) dendrimers were provided by DSM (Geleen, The Netherlands). The full generation dendrimers are terminated by primary amines (-NH₂), while half generation PPI dendrimers have cyano groups (-CN) as terminal units. These dendrimers were used as received. Random copolymers were synthesized from mixtures of methylmethacrylate-d₈ or styrene-d₈ (PSD) with methacrylic acid or 1,1,1,3,3,3-hexafluoro-2-hydroxy-isopropyl- α -methyl styrene (HFIS) with azobisisobutyronitrile as initiator in bulk at 60 °C for 2 hours. They were purified by dissolution in THF and precipitation into methanol.

Blends were prepared by dissolving the components in a mixture of methanol and THF and evaporating the solvents slowly in a fluorinated copolymer dish. They were then pressed into disks of 0.5 mm thickness for the neutron scattering experiments. The NIST 8 m instrument was used in the standard manner. A sample to detector distance of 3.6 m was used with a wavelength $\lambda = 6 \text{ \AA}$ and a wavelength spread of $\Delta\lambda/\lambda = 0.25$.

2.1.4 Results and Discussion

The blends of hydrogen bonding polymers with dendrimers were first screened for cloudiness by simple visual inspection. Out of all the combinations tried, a large majority could be identified as phase separated, and were rejected from further study. Among these are mixtures of PAMAM and full generation PPI dendrimers with poly(styrene)-d₈ that contained a small fraction of comonomers of either methacrylic acid or FHIS.

Figure 19 shows the scattering from a blend of G4 PAMAM dendrimer with PMMA-r-PMAA containing mass fraction 2 % PMAA. The scattering is typical of a single phase mixture. The scattering decreased with increasing the temperature from 140 °C to 180 °C, indicating decreased concentration fluctuations due to enhanced mixing. DSC results from this combination, with the blend having a T_g intermediate between the pure materials. At higher temperatures, the blend showed an anomalous change in the heat flow. This is often found in systems that are undergoing chemical reactions.

Blends of a copolymer of methyl methacrylate-d₈ with mass fraction 1 % methacrylic acid produced films that were optically transparent when blended with PAMAM dendrimers or the cyano terminated half generation PPI dendrimers. Both of these were examined with SANS for miscibility, and the temperature dependence of the scattering was studied.

Figure 19 shows an example of the SANS results of PAMAM dendrimers in poly(methacrylate) as described above, heating the sample from 130 °C up to 180 °C and cooling back to 130 °C. The scattering intensity decreases with increasing temperatures, suggesting that an upper critical solution temperature might be present. However, when the sample is cooled back to previous temperatures, the scattering is not reproducible, i.e. Does not regain the intensity recorded previously at 155 °C or 130 °C. This can be

caused by a chemical reaction between the dendrimer and the methacrylate polymer during the time of study. After the SANS experiments, the samples were no longer soluble, indicating that crosslinking took place.

Figure 20 shows the SANS results from a blend of mass fraction 5 % G4.5 PPI dendrimer with a PMMA-d₈ copolymer containing mass fraction 2 % PMAA. As the temperature is increased, the scattering increases as the phase boundary is approached. For short periods of heating of only a few hours, lowering the temperature reproduces the previous scattering, but longer times at high temperatures produced samples that did not reproduce the scattering as in the previous example. After the scattering experiment was concluded, the samples did not redissolve, indicating crosslinking.

The terminal units of both the PAMAM and the PPI dendrimers are possible sites for chemical reactions. Although, the SANS experiments show that the dendrimers can be dispersed in this polymeric matrix, the material does not exhibit the characteristics of a truly miscible polymer blend, but rather should be considered as a covalent dendrimer/polymer network after reaction.

2.1.5 Summary

Hydrogen bonding can increase the miscibility of PAMAM and PPI dendrimer/polymer blends, forming systems where dendrimers are uniformly dispersed in a polymeric matrix. Elevated temperatures cause chemical reaction to result in a crosslinked network, however. This limitation is due to the fact that only PAMAM and PPI dendrimers were available for this study. We can make no conclusions on the dendrimeric nature of the molecules on the thermodynamic drive for miscibility.

This technique is available for producing molecularly dispersed dendrimers in a matrix of linear polymers. Other methods such as IPN and end-linked polymers also form intractable structures, but have several synthetic advantages of structure control over the ones shown in this section.

2.2 Blends of Fatty Acid Modified Dendrimers with Polyolefins

2.2.1 Synopsis

Blends were made by solution and melt mixing fatty acid modified dendrimers with various polyolefins. Small angle neutron scattering (SANS) was used to determine the miscibility of the blends. Poly propylene imine (PPI) dendrimers G1, G3, and G5 (DAB-*dendr*-(NH₂)_y) with y = 4, 16, and 64, were reacted with stearic acid or stearic acid-d₃₅ forming amide bonds. The modified dendrimers were then blended with high density polyethylene (HDPE), high density polyethylene-d₄ (HDPE-d₄), low density polyethylene (LDPE), amorphous polypropylene (PP), or an ethylene-butylene copolymer (E-co-B). Limiting power law behavior shows that all of the blends are immiscible. It is likely that the dendrimers form a second phase, being finely dispersed, but thermodynamically immiscible.

2.2.2 Introduction

Recently, dendrimers have been modified by attaching hydrophobic groups to the terminal units of dendrimers.^{57,58} This further accentuates the micellar nature of the dendrimers. Hydrophylic dendrimers such as polyethyleneimine dendrimers (ASTRAMOL™)⁵⁹ can be reacted with stearic acid resulting in amide bonds between the dendrimer and the hydrophobic stearic acid groups. The solubility characteristics are changed dramatically, with the dendrimers becoming soluble in hydrocarbon solvents.

From recent work it appears that the combination of fatty acid modified dendrimers (FAD's) with polyolefins leads to interesting new applications. It turns out that FAD's can stabilize the dispersion of polar dye molecules in apolar polyolefins such as polyethylene,⁵⁹ by complexing the dye molecules as guests into the modified dendrimer, followed by blending the dendrimer-dye complex into the polymer matrix. Another application, which makes use of FAD's, is a dendrimer-modified polypropylene (PP) fiber. This is obtained by blending a small quantity of FAD with PP, followed by spinning. The resulting dendrimer-containing fibers can be dyed by aqueous solutions or dispersions of conventional dyes.

The nature of the dispersion of the FAD's in the polyolefins in these applications is not known. One possibility is that the dendrimers are molecularly dispersed in the polymeric matrix. Another possibility is that the dendrimers form a second phase, being finely dispersed, but thermodynamically immiscible.

2.2.3 Experimental

In order to gather this information from a SANS experiment, it is necessary that sufficient neutron contrast exists. This is most commonly achieved by deuterium labeling of one of the components. In this study, three generations G1, G3, and G5 of poly(propylene imine) dendrimers,⁸ with $y = 4, 16,$ and 64 primary amine groups (DAB-*dendr*-(NH₂)_y), were modified with fatty acid (octadecanoic, C₁₈). The modification consisted of the conversion of the primary amine groups into amides.⁶⁰ In this case, about 2.5 mmoles of fatty acid, hydrogenous or deuterated, was added to an equivalent amount of poly(propylene imine) dendrimer and 20 ml of xylene. The mixture was heated to 160 °C while stirring under a slow stream of nitrogen in a two-necked flask with a gas inlet and a Dean-Stark trap. After 1 h. Of reaction at 160 °C all xylene was distilled off carefully, and the product was allowed to cool to room temperature. The dendrimer modified with octadecanoic acid-d₃₅ is designated dendrimer-d and with octadecanoic acid-h₃₅ is designated dendrimer-h.

HDPE-d4 was purchased from Cambridge Isotope Laboratories (DLM-220). HDPE 42,799-3, PP 42,818-3, LLDPE 42,809-4, LDPE 42,804-3, and E-co-B 43,473-6 were purchased from Aldrich. All were used as received except for the PP which was

extracted with toluene at 60 °C and precipitated into methanol to produce an atactic, amorphous polymer.

Samples were prepared by two methods, solution mixed and melt mixed. The solution mixed samples are dissolved in xylene at 140 °C and precipitated into methanol. They were dried in vacuum and pressed at 150 °C into disks for SANS. The melt mixed samples were pressed at 150 °C and folded twice and repressed. The folding and pressing is repeated 10 times.

SANS experiments were carried out on the 8m (NG1) and 30m (NG7) instruments in the standard manner. The wavelength λ of the incident beam was 6Å.

2.2.4 Results and Discussion

Differential scanning calorimetry was used to determine the melting points of the crystalline regions of the polyolefins so that blending and SANS could be carried out on amorphous samples. Miscible blends can be made to phase separate upon crystallization of one component. The highest melting point was for HDPE-d4 which showed complete melting by 130 °C. Therefore all of the melt mixing was carried out at 150 °C and the scattering was done at 140 °C.

The first set of experiments checked for miscibility of HDPE-d₄ with dendrimers of different size. Figure 21 is a plot of the SANS from binary blends of mass fraction 2 % dendrimer-h in HDPE-d₄. A log-log plot shows that there is an extensive region with a slope of q^{-4} .³⁵ This is characteristic of Porod scattering from a morphology that is strongly phase separated with negligible mixing within the phases and a negligible interfacial region between the phases. In this q range, there is no leveling off of the scattering intensity at low q . This extended range of power-law behavior indicates that the characteristic size of the two phase morphology is larger than can be measured under these instrumental conditions.

Figure 22 is a Guinier plot of the scattering from blends of mass fraction, 2 % dendrimer-h HDPE-d₄. The measurement was taken with the 8 m SANS instrument which had a low q value of 0.008 Å⁻¹. An estimate can be made of the characteristic phase size if data is available in the range $q R_g \ll 1$. As can be seen, there is still curvature in the lowest accessible q region, so fits in this region only give a lower bound of the phase size. The fits over a q range of $0.008 < q/\text{Å}^{-1} < 0.012$ give $R_g = 220$ Å, 200 Å, and 190 Å for G1, G3, and G5 respectively. Since $q R_g > 1$ under these conditions, the measured size is limited by the instrument resolution. These sizes therefore represent a lower bound of the true phase size.

Other polyolefins were blended with dendrimers to see if miscibility was possible for other combinations. Figure 23 is a log-log plot of mass fraction 2 % G5 dendrimer-d in PP, LDPE, and E-co-B. As with the blends of PE described earlier, there is an extended region with a slope of q^{-4} , indicating strong phase separation. Since there is no plateau region at low q , as was the case of the other blends, these also have relatively

large phase sizes, larger than the resolution of the SANS instrument. Also, the results shown are for both melt (LDPE, E-co-B) and solution processed (PP) samples with both giving identical power law scattering. No differences could be seen resulting from different preparation methods.

2.2.5 Summary

While melt mixed samples of fatty acid modified PPI dendrimers appear transparent when kept above the melting temperature, SANS shows that they are actually phase separated on a size scale much greater than the individual dendrimer size. This was true for all of the fatty acid modified dendrimers studied, G1, G3, and G5, in both hydrogen and deuterium forms. All polyolefins tested were immiscible with the dendrimers, HDPE, LDPE, PP, and E-co-B, in both hydrogen and deuterium forms. Melt mixing by mechanical kneading of virgin material or with samples previously solution mixed all produced immiscible blends. Premixing in solution also did not change the miscibility of the binary blends. Extended annealing did not produce any morphological changes in a size scale accessible to SANS.

The ultimate goal of blending fatty acid modified dendrimers is to promote long time stability of additives to the polyolefins. Even if the size scale of the dendrimer phase is relatively large, small molecules such as dyes that are permanently affixed to the dendrimers may be lodged in the polyolefin matrix. If this is the case, then the use of fatty acid modified dendrimers to promote long time stability of additives may be applicable to a wide range of polymers other than polyolefins, independent of specific miscibility conditions.

2.3 Ternary Dendrimer Blends

2.3.1 Synopsis

Miscible blends were made of polystyrene- d_8 (PSD) and poly(vinylmethyl ether) (PVME) with and without addition of a fatty acid modified PPI dendrimer. SANS shows that the phase separation of the PSD/PVME blends can be inhibited by several °C with the addition of a small amount of dendrimer. The scattering from the ternary blends shows an upturn at lowest q , however, suggesting a large size component in the morphology. TEM reveals very large aggregations of the dendrimer in a matrix of a miscible PSD/PVME phase, so that while the dendrimer affects the phase boundary of the miscible binary blend, it itself is not miscible at a mass fraction 1 % level.

2.3.2 Introduction

Dendrimers may act as modifiers of binary blends if they could change the point of phase separation. The branched structure of dendrimers may act as an interfacial agent and modify the thermodynamics or rate of phase separation. Hydrophobically modified PPI dendrimers are soluble in toluene which is the preferred solvent for casting films of PSD/PVME. The binary blend of PSD/PVME has been extensively studied by SANS. It

has a lower critical solution temperature and phase separates at temperatures around 150 °C. A ternary blend of PSD/PVME/dendrimer is a good candidate for the study of the effect of dendritically branched additives on blend miscibility.

2.3.3 Experimental

Hydrophobically modified dendrimers were synthesized from a G5 PPI dendrimer with -NH₂ terminal groups by addition of an excess mass fraction 80 % 1,2-epoxy octane in vacuum at 140 °C for 8 h. Fatty acid modified G5 PPI was synthesized as described in the experimental section of the Blends of Fatty Acid Modified Dendrimers with Polyolefins section.

Blends were made with PSD and PVME by solution in toluene, evaporation of the solvent, drying in vacuum, and pressing into disks. SANS from blends with and without added dendrimer demonstrate that the presence of the dendrimer gives the sample stability, causing it to remain miscible when blends without the dendrimer phase separate.

All SANS experiments were performed in the normal manner. A sample to detector distance of 3.6 m was used with a wavelength $\lambda = 6 \text{ \AA}$ and a wavelength spread of $\Delta\lambda/\lambda = 0.25$.

The PSD:PVME (1:9) samples, ED-1 and ED-4 (containing mass fraction (1 to 10) % G5 DSM dendrimer reacted with 1-2 epoxy octane), were ultramicrotomed to a thickness of (60 to 80) nm at -70 °C and transferred to 200-mesh, carbon coated Cu grids. The sections were stained with OsO₄ vapors by exposing the grids to a aqueous solution containing 0.04 g OsO₄/g H₂O at room temperature for 2 h. The blend samples were imaged by transmission electron microscopy (TEM) at 120 kV in a Philips 400T using low-dose conditions.

2.3.4 Results and Discussion

A series of SANS experiments was run on the ternary system consisting of the hydrophobically modified dendrimer PPI-C₈ and the polymer blend PSD/PVME. Samples were prepared with between mass fraction 0 % and mass fraction 10 % of the dendrimer added to a blend of PSD/PVME having mass ratios of 1:9, 3:7, 5:5, and 7:3. The samples with 1:9 and 3:7 were optically clear, but were hazy for higher PSD content. Figure 24 shows the scattering for a 1:9 blend containing mass fraction 1 % PPI-C₈. The scattering is plotted in the Ornstein-Zernike (OZ) method, i.e. As $I(q)^{-1}$ versus q^2 . The scattering fits the OZ relation well, suggesting a miscible blend. The scattering was shown to be reproducible in temperature cycles, and the samples could be redissolved after the SANS experiments. Size exclusion chromatography before and after the SANS experiments showed that the PSD and PVME had not degraded or crosslinked during the experiment.

Figure 25 shows the SANS of a 3:7 blend containing mass fraction 0 % or mass fraction 1 % dendrimer. Both samples show OZ type of scattering at 120 °C, indicating

miscibility, but the mass fraction 1 % sample shows a much higher scattering intensity suggesting that it is closer to phase separation. The 130 °C results confirm this observation. The intensity of the 1 % sample has shifted slightly, being closer to the phase separation temperature, but remaining a single phase. The mass fraction 0 % sample had phase separated at this temperature, however, as is indicated by the negative intercept of the OZ plot, and was confirmed by its optical cloudiness.

The results shown in Figure 25 suggest that the ternary blends have an increased range of miscibility over blends that do not contain the dendrimer. Fits were made to an OZ form as

$$S(q) = S(q = 0)/(1 + \xi^2 q^2) \quad (2.1)$$

Where $S(q)$ is the scattered intensity and ξ is the correlation length. In a mean field polymer system, $S(q = 0)$ and ξ vary with temperature as:

$$S(q = 0)^{-1} = T_s^{-1} + k_1 T^{-1} \quad (2.2)$$

$$\xi^{-1/2} = T_s^{-1} + k_2 T^{-1} \quad (2.3)$$

Plots of $S(q = 0)^{-1}$ versus T^{-1} or $\xi^{-1/2}$ versus T^{-1} give the value T_s^{-1} as an intercept, T_s being the spinodal temperature (e.g. Critical onset of phase separation).

Figure 26 is a plot of the relative shift in T_s as a function of dendrimer content for 1:9 and 3:7 blends. There is a dramatic increase in the spinodal temperature when dendrimer is added, with as large as a 30 °C shift for the 1:9 blend. These results suggest that for PSD/PVME blends with high PVME content, the addition of dendrimer improves the miscibility significantly.

Experiments were continued with G5 PPI dendrimers that were modified by reaction with stearic acid forming amide bonds on all 64 terminal amino groups. Figure 27 shows the SANS from PSD/PVME = 1/9 blends with and without mass fraction 1 % of the dendrimer added. Two types of dendrimer were used, one that had stearic acid -d₃₅ and one that was -h36. At 140 °C, all three samples has scattering typical of a miscible blend. At 150 °C, however, the blend without dendrimer showed increased scattering at low q indicating phase separation is taking place. The blends with the dendrimer still showed scattering typical of micibility at 150 °C. These results are qualitatively similar to previous results of blends with the 1,2-epoxy octane modified dendrimers.

Experiments were repeated under experimental conditions that gave results extending to lower values of q . Figure 28 shows SANS of blends of PSD/PVME = 1/9 and PSD/PVME = 3/7 containing mass fraction 1 % dendrimer. The data were taken at 70 °C which is well within the range of miscibility for the blend without dendrimer. At lower q there is an upturn in the scattering which is typical of a large dispersed phase. The q range shown in Figure 28 gives a linear relationship, but when lower q is probed, the 2 phase structure is evident.

Figure 29 is the TEM result of ED-1. It shows dark domains of sizes <100 nm, presumed to be aggregates of the dendrimers in the single phase, PS/PVME blend. A PS/PVME (1:9) blend without dendrimer was examined as a control and did not contain any similar domains; this control sample showed a single phase morphology. ED-4 (mass fraction 10 % dendrimer) contained dark domains of larger and more varied sizes, from 100 nm-1.0 μm , also presumed to be the dendrimer aggregates.

2.3.5 Summary

The addition of dendrimer promotes miscibility of binary PSD/PVME, blends as is demonstrated by SANS, causing the phase separation temperature of the PSD and PVME components to increase by several $^{\circ}\text{C}$. However, the dendrimer itself is not itself miscible with the PSD/PVME binary blend. This is apparent from the upturn in the very low q of the scattering curves and by TEM. The cause of the effect is not known. It may be that a small amount of dendrimer does enter the PSD/PVME phase.

2.4 Blends of Dendrigrraft Polymers with Linear Polymers

2.4.1 Synopsis

Small angle neutron scattering (SANS) was used to measure the size and shape of styrene-based arborescent polymers blended with linear deuterated polystyrene (d-PS) and linear deuterated poly(vinyl methyl ether) (d-PVME). For generation 0, 1, and 2 arborescent polymers, the R_g values were the same in going from d-PVME to d-PS as the matrix material while for generation 3 (G3) the R_g in d-PS was found to be smaller than in d-PVME. For comparison, the R_g of a sphere was calculated assuming the size of the sphere was equivalent to a G3 molecule collapsed to bulk density. The R_g obtained was 162 \AA , which is quite close to the R_g of the G3 polymer in d-PS ($R_g = 164$ \AA). This indicates that the G3 molecules should behave as essentially non-interpenetrating spheres with the linear d-PS matrix chains being largely excluded from the interior of the arborescent molecules. In the single phase region of the phase diagram it was difficult to establish a clear temperature dependence of the R_g for the generation 0, 1 and 2 molecules in d-PVME. For the G3 molecules in d-PVME a small decrease in R_g with increasing temperature was observed in the single phase region with an abrupt decrease in R_g of 21 % on phase separation between 110 $^{\circ}\text{C}$ and 115 $^{\circ}\text{C}$. The single particle form factor of arborescent polymers in blends was studied using a power law model for the density profile. In comparison with a hard sphere or a shell model, the scattering function calculated from the power law function for the density profile provided the best fit to the experimental scattering data.

2.4.2 Introduction

Various types of dendritic polymers with a controlled architecture such as dendrimers, hyperbranched polymers, and arborescent polymers have been developed recently.^{4,24,34,41,61-66} This special class of branched polymers has gained increasing

interest from both theoretical and practical points of view. For example, they can be used as crosslinking agents, sensors, catalysts, size standards, and drug release systems.^{4,30} For many applications it is necessary to have detailed information on the intramolecular density profile, molecular size and shape in solution and in mixtures with other polymers.

Arborescent polymers are branched macromolecules synthesized by successive cycles of functionalization and grafting reactions.^{4,24,30,41,62-66} The structure of arborescent polymers is represented schematically in Figure 30. The structure of arborescent polymers has features distinct from the classical dendrimer molecules. The building blocks used in the synthesis of arborescent polymers are polymer chains rather than small molecules. The grafting sites in arborescent polymer molecules are randomly distributed, rather than strictly controlled like in dendrimer molecules. In our previous paper the size of arborescent polystyrenes in solution was measured as a function of temperature and molecular mass using small angle neutron scattering (SANS).⁴⁵ In this paper small angle neutron scattering is used to study arborescent polystyrenes in blends with linear polymers for comparison to the results obtained in solutions. Deuterated polystyrene (d-PS) and deuterated PVME (d-PVME) are used as matrix polymers to study arborescent polymer blends as a function of molecular mass and temperature.

According to classical Flory theory for a linear polymer chain in a good and a theta solvent, the scaling exponent for $R_g \sim M^{\nu}$ is 0.6 and 0.5, respectively, where R_g is the radius of gyration and M is the molecular mass (or chain length). Linear polymer chains are fractal objects which means that as the molecular mass of a linear polymer chain increases, the average density of the linear chain decreases. The density is taken as an average coil density estimated as $\rho \sim M/R_g^3$.⁶⁷ In the work by Zimm and Stockmayer who studied this scaling relation for branched polymers, the scaling exponent was found to be 0.25 for a Cayley tree in the limit of large molecular mass.⁶⁸ This value of the scaling exponent is smaller than the value of 1/3 for a constant density object, which means that as the size of a (highly) branched polymer increases the (average coil) density of branched polymer increases.⁶⁸ de Gennes and Hervet studied the scaling relation for dendrimers using an analytical calculation and the scaling exponent was found to be 0.2.²⁵ According to numerous computer simulations and limited experimental work on dendrimers, the values of this scaling exponent have been reported in the range of 0.2-0.4.^{26-29,52} In our previous work on arborescent polymers in solution, the scaling exponent was found to be $\nu = 0.25 \pm 0.01$ in deuterated cyclohexane and $\nu = 0.32 \pm 0.01$ in deuterated toluene.⁴⁵ These values of ν are less than 1/3, indicating again that the average segment density in the polymer coil is increasing. This creates a self-limiting condition where the coil density approaches bulk density, and arborescent polymers of higher generations can no longer be synthesized with a constant branching density.

The intramolecular radial density profile of dendrimer molecules proposed by de Gennes and Hervet has a minimum density at the center of the molecule.²⁵ However, a number of computer simulations^{25,27-29,52} and theoretical work by Boris and Rubinstein³⁰ predict a maximum in the radial density profile at the center of the

molecule, and a decreasing density gradient to the outer edge of the molecule. According to recent small angle x-ray scattering (SAXS) work, generation 10 polyamidoamine (PAMAM) dendrimers in solution do not exhibit any sizable minimum in density near the core.²⁰ More recent results by Prosa et al. Show that the dendrimers exhibit sphere-like characteristics.³⁷ In our previous work on arborescent polymer in solution, a power law model for the radial density profile which has a maximum density at the center of molecule was used to successfully model the single particle form factor.⁴⁵ This function has a relatively constant interior density and an outer zone of transition that is dependent on the solvent used.

2.4.3 Experimental

The arborescent polymers used in this study were synthesized by successive grafting reactions of polystyryl anions onto a linear polystyrene substrate.⁶⁵ The molecular mass of the *branches* used for grafting for each generation was determined by gel permeation chromatography (GPC). The molecular mass of the arborescent polymers was not determined by GPC, but was measured in this work as part of the SANS analysis. The characteristics of the arborescent polymers used in the study and the branches are given in Table 3. The relative precision in molecular mass from GPC is $\pm 10\%$ as is typical of this technique. The core and the side chains used in the synthesis of each generation had a molecular mass of around 5000 g/mol. The total number of branches in a given generation G polymer was calculated using eq (2.4);

$$f_w(tot) = f_w(G-1) + \frac{M_w(G) - M_w(G-1)}{M_w(branch)} \quad (2.4)$$

Where $M_w(G)$, $M_w(G-1)$ and $M_w(branch)$ are the molecular masses of a generation G polymer, of the previous generation and of the grafted side chains, respectively. If the molecular mass of the branches for all generations is the same, eq (2.4) can be reduced to simpler form:

$$f_w(tot) = \frac{M_w(G) - M_w(linear\ core)}{M_w(branch)} \quad (2.5)$$

The branching density of the core portion of a generation G polymer is given by eq (2.6):

$$\text{Branching Density} = \frac{\text{number of branches added per molecule in a grafting reaction}}{\text{total number of repeat units of previous generation}} \quad (2.6)$$

Blends of the arborescent and linear polymers were prepared using deuterated linear polystyrene or deuterated linear poly(vinyl methyl ether). The deuterated linear polystyrene samples were either purchased or synthesized, depending on the molecular mass. Deuterated styrene purchased from Cambridge Isotope Laboratories, Inc and a tetramethylpiperidinyloxy (TEMPO) based unimolecular initiator obtained from Dr. C.

Hawker of IBM Almaden Research Center were used to synthesize deuterated linear polystyrene by living free radical polymerization.⁶⁹ Deuterated linear PVME was synthesized by cationic polymerization of d_3 -vinyl methyl ether, $CH_2=CHOCD_3$, in toluene using boron trifluoride-ethyl ether complex as the initiator.⁴³ The molecular mass of deuterated polystyrene and deuterated PVME were determined using GPC and the mass average molecular masses were found to be 102,900 g/mol and 8,280 g/mol, respectively. Universal calibration was used with the Mark-Houwink-Sakurada parameters $a = 0.739$ and $k = 1.35 \times 10^{-4}$ for d-PVME in tetrahydrofuran (THF) at 30 °C.⁴³ In addition to the deuterated polystyrene synthesized by living free radical polymerization, several anionically polymerized deuterated polystyrenes of different molecular masses were purchased from Polymer Laboratories, Ltd. The characteristics of the linear polymers are summarized in Table 4. Samples for neutron scattering were prepared by dissolving the appropriate deuterated linear polymer and the arborescent polymer in toluene and then allowing the solution to evaporate in a Teflon petri dish to form a thin film. The film was then dried in vacuum to remove any remaining toluene. The film was pressed into disk of 1.4 cm diameter and 0.05 cm thickness for the SANS experiments using a hot press at approximately 150 °C. The concentration range of the blends studied was mass fraction (0.5 to 2) % arborescent polymer.

Small angle neutron scattering experiments were carried out at the Center for Neutron Research of the National Institute of Standards and Technology on the 30 m NIST-NG3 instrument in the normal manner.⁴⁷ The q range was from 0.0046 \AA^{-1} to 0.0520 \AA^{-1} with a neutron wavelength, $\lambda = 6 \text{ \AA}$ and a wavelength spread, $\Delta\lambda/\lambda = 0.15$. All temperatures reported are within $\pm 1 \text{ }^\circ\text{C}$ as determined by previous experience.

2.4.4 Results and Discussion

A typical set of SANS data for all generations ($T = 120 \text{ }^\circ\text{C}$, mass fraction 1 % in deuterated polystyrene) is shown in Figure 31. The radii of gyration were measured using Guinier plots at small q as given by eq (2.7):

$$I(q) = I(0) \exp\left(-\frac{R_g^2 q^2}{3}\right) \quad (2.7)$$

Where R_g is radius of gyration of the object.^{70,71} A typical Guinier plot of $\ln I(q)$ versus q^2 for a generation 3 (G3) polymer is displayed as an inset in Figure 31. The R_g of the arborescent polymer molecules in blends was plotted as a function of generation number (molecular mass) and compared with data from solutions measured previously in Figure 32.⁴⁵ The error bars in Figure 32 represent **one** standard deviation calculated from the linear least-squares fit of the Guinier plot data. The R_g decreases in going from solutions to blends, and the observed R_g is smaller in linear deuterated polystyrene than in deuterated PVME (Note that the molecular masses of the two polymers are quite different at 103 k and 8.2 k, respectively). As will be discussed in detail later in the paper, the R_g of the G3 polymer was studied as a function of the molecular mass of the d-PS matrix

polymer. The R_g of the G3 polymer in d-PS with $N = 38$ ($M_w = 4.3$ k) and $N = 238$ ($M_w = 27$ k) was found to be 206 Å and 182 Å, respectively, while R_g in d-PVME with $N = 131$ ($M_w = 8.2$ k) was 205 Å (N is the average number of monomer units in the chains). Although the d-PVME chain length falls between the two d-PS molecular masses studied, it appears that for equivalent chain lengths the R_g would be smaller with d-PS as the matrix.

The radii of gyration for the arborescent polymers in deuterated PVME are plotted as a function of temperature in Figure 33. Polystyrene/poly(vinylmethylether) blends are well known to exhibit a low critical solution temperature (LCST) type phase diagram with a critical point between 110 °C and 160 °C depending on molecular mass and deuteration effects.³⁵ The polystyrene/poly(vinylmethyl ether) blends studied in this work contain deuterated PVME. All previous neutron scattering work on PS/PVME blends used polystyrene as the deuterated component. All the data in Figure 33 are from blends in the single phase region of the phase diagram. It is difficult to interpret the data in Figure 33 in terms of any systematic temperature dependence of R_g in the single phase region of the phase diagram. The temperature dependence of R_g for arborescent polymers in deuterated polystyrene was not studied.

A scaling relation given by $R_g = kM_w^{\nu}$ exists between the R_g and the molecular mass, M_w , where ν is the scaling factor and k is a constant. A log-log plots of R_g versus M for the arborescent polymers in deuterated PVME and deuterated polystyrene are shown in Figure 34(a,b). Two dashed lines are shown in Figure 34(a,b), one calculated for a Gaussian linear polystyrene chain and one for a sphere with the bulk density of polystyrene, assuming the chain is completely collapsed. As observed in previous work on arborescent polymers in solution, the arborescent polymers exhibit a crossover between a Gaussian linear chain ($\nu=1/2$) and an object with constant density ($\nu = 1/3$).⁴⁵ The exponent of ν for the arborescent polymers in deuterated PVME and deuterated polystyrene was found to be $\nu = 0.28 \pm 0.02$ and $\nu = 0.26 \pm 0.06$, respectively, which indicates that the average polymer segment density inside the sphere defined by the R_g increases with increasing generation.

A power law function for the radial density was used to calculate the expected scattering and fit to the SANS data for the G3 polymer. The fitting procedures and uncertainties are reported elsewhere. The fit was optimized by varying the value of α . The power law function is given by

$$\rho(r) = 1 - \left(\frac{r}{R_{\max}} \right)^{\alpha} \quad (2.8)$$

Where R_{\max} corresponds to the hydrodynamic radius. The scattering was calculated using eq (2.9).³⁵

$$I(q) \propto \left[\int dr \rho(r) \frac{\sin(qr)}{qr} r^2 \right]^2 \quad (2.9)$$

The best fit to the SANS data for the G3 molecule was found when $\alpha = 12$ and $\alpha = 18$ for deuterated PVME and deuterated polystyrene, respectively, and the fits to the scattering data are shown in Figure 35(a,b). The fits to the data in Figure 35(a,b) include a 9 % polydispersity of the polymer and the effect of instrumental smearing with $I(0)$, R_{\max} and a base line as floating parameters.^{72,73} The values of $R_{\max}=(260 \pm 4) \text{ \AA}$ and $R_{\max}=(221 \pm 4) \text{ \AA}$ were obtained from the fit of the scattering data in Figure 35(a,b) for the G3 polymer in deuterated PVME and deuterated polystyrene, respectively. The error bars for the values of R_{\max} were calculated from the errors in q based on the SANS instrument configuration. A comparison of the radial density profiles in blends with those previously obtained for solutions is shown in Figure 36.⁴⁵ The density profile for arborescent polymers in blends with linear chains decreases more rapidly at the outside edge of molecules in comparison with that in solutions ($\alpha = 4$). The density profile for arborescent polymers in deuterated polystyrene is close to that of a hard sphere. Using the power law density function given by Equation (2.8), the radius of gyration can be calculated from Equation (2.10).

$$R_g^2 = \frac{\int dr \rho(r) r^4}{\int dr \rho(r) r^2} \quad (2.10)$$

The relation between R_g and R_{\max} for arborescent polymer in deuterated polystyrene was found to be $R_g = (63/115)^{1/2} R_{\max}$ (for $\alpha = 18$) and the calculated R_g was 164 \AA . For comparison the R_g of a sphere was calculated assuming that the G3 molecules were collapsed to bulk density. The R_g obtained was approximately 162 \AA , which is close to the R_g of the G3 polymer in deuterated polystyrene. This indicates that the G3 molecules in deuterated polystyrene should be non-interpenetrating and the deuterated linear polystyrene is largely excluded from the interior of the arborescent molecules.

The measured scattering for the G3 in deuterated poly(vinylmethyl ether) (PVME) was essentially constant as the temperature was changed from 80 $^{\circ}\text{C}$ to 105 $^{\circ}\text{C}$. No increase in the concentration fluctuation scattering was observed as the phase separation was approached, as is typically observed for polymer blends.^{74,75} Phase separation occurs above 105 $^{\circ}\text{C}$ and two peaks develop as shown in Figure 37. Upon phase separation, the single particle form factor peak (the second peak located at $q = 0.023 \text{ \AA}^{-1}$) shifts to higher q , indicating that the size of the molecules decreased. The size of the molecules after phase separation was estimated from the position of the second form factor peak using the power law model and plotted as a function of temperature in Figure 38. As noted previously, there is no appreciable temperature dependence of R_g in the single phase region, but a collapse of the G3 molecules by about 21 % is observed with phase separation. The collapse transition has long been of interest and has generated

much theoretical and experimental work, because of its relevance to local polymer structure, fractionation, and biological applications such as protein folding.^{76,77} To the authors' best knowledge this is the first direct observation of a collapse transition observed in polymer blends, although it has been predicted in simulations⁷⁸ and theoretically.⁷⁹ It should also be noted that the deuterated PVME is of quite low molecular mass. The variation in the size of a linear polystyrene chain in cyclohexane as a function of temperature near the theta temperature has been studied by many authors and the collapse transition for a linear chain in deuterated cyclohexane has been observed below the theta temperature.^{76,77,80-84} In our previous experiments on arborescent polymers in deuterated cyclohexane there was a 15% decrease in R_g when phase separation occurred.⁴⁵ At 115 °C two peaks are found in the $I(q)$ versus q data for the G3 in deuterated poly(vinyl methyl ether). The first peak is due to the interference between molecules, while the second peak arises from the single particle form factor. The scattering intensity for a particulate system can be expressed as²⁰

$$I(q) = k_n N P(q) S(q) \quad (2.11)$$

Where k_n is the contrast factor for neutrons, N is the concentration of the scatterers (arborescent polymer molecules), $P(q)$ is the single particle form factor (intraparticle interference), and $S(q)$ is the structure factor (interparticle interference). In the single phase blends, the molecules are in the dilute concentration range and non-interacting, and only $P(q)$ is observed. For the phase separated G3 arborescent polymers in d-PVME at high temperature, it is expected that $S(q)$ should play a role. The first peak observed in the scattering curve from the phase separated solution is due to the first neighbor interference (i.e. $S(q)$), as observed in many systems such as latex spheres and spherical block copolymers.⁸⁵⁻⁸⁹ The second peak in the scattering curve has the same general shape and is in the same general q range as the peak observed in $P(q)$ for the non-phase separated samples. The interpretation of this peak as being associated with $P(q)$ is also consistent with previous work on latex spheres and block copolymer systems.^{85,90,91} From the position of the first peak the center to center distance between nearest neighbor molecules was estimated using the relation, $d = (1.23 \times 2\pi)/q$, which is valid for a structure controlled by two body (noncrystalline) correlations.^{70,71} This distance was found to be $(505 \pm 14) \text{ \AA}$. From the position of the second peak, the diameter of a single molecule was estimated using the single particle scattering function derived from the power law function density profile (Equation (2.8)). The data in the range $q = (0.018 \text{ to } 0.05) \text{ \AA}^{-1}$ was fitted to the scattering function calculated using the power law model with $\alpha=12$. R_{max} was found to be $(232 \pm 4) \text{ \AA}$ and the calculated density profile for phase-separated G3 polymer in deuterated PVME is shown in Figure 7. The error on the value of R_{max} was calculated from the errors in q based on the SANS instrument configuration. The diameter of a single dendrimer molecule is $d_{\text{max}} = 2R_{\text{max}} = (464 \pm 8) \text{ \AA}$, which is smaller than the distance between nearest neighbors, indicating that the molecules are not quite in contact with each other. Using the power law density function given by Equation (2.8) the radius of gyration was calculated from eq 7 and found to be $R_g = (9/17)^{1/2} R_{\text{max}}$ (for $\alpha = 12$). The R_g for a G3 arborescent polymer in

deuterated PVME at 115 °C (which is slightly inside the two-phase region of the phase diagram) calculated using this relation is (169 ± 3) Å. This is close to the R_g calculated for a sphere assuming the G3 molecule is collapsed to bulk density. This indicates that deuterated PVME is largely excluded from the interior of the arborescent molecules after phase separation occurs.

The R_g of G3 arborescent polymer molecules was studied as a function of the molecular mass of the linear d-polystyrene matrix. The matrix molecular mass was varied from 4,300 g/mol to 430,000 g/mol. The R_g obtained using Guinier analysis, is plotted as a function of the molecular mass of the matrix polymer in Figure 39 shows that as the molecular mass of the matrix polymer increases, the R_g of the G3 polymer decreases. The largest decrease in R_g is observed when the matrix molecular mass increases from 4300 g/mol to 26600 g/mol. There appears to be additional small decreases in R_g with further increases with molecular mass of the matrix polymer, but their magnitude is close to the errors on the measurements. The larger R_g observed for the lowest molecular mass matrix polymer indicates that the regions within the volume of the G3 arborescent polymer are limited in size and shape and only accessible to the shortest chains. The configurational entropy penalty for higher molecular mass polymers to penetrate the coil of the arborescent polymer is too great compared to the (relatively small) gain in mixing energy.

2.4.5 Conclusions

The radius of gyration of arborescent polymers decreases in going from solutions to polymer blends. The size of arborescent polymers in deuterated polystyrene is smaller than in deuterated poly(vinyl methyl ether). The scaling exponent for $R_g \sim M^v$ is found to be $v = 0.28 \pm 0.02$ in d-PVME and $v = 0.26 \pm 0.06$ in d-PS, which indicates that arborescent segment density is increasing as a function of generation. The scattering curve calculated using a power law model is in reasonable agreement with the measured scattering. The value of α in the power law model is largest for arborescent polymers in deuterated polystyrene, and the sequential density calculated from the molecular mass divided by the volume of coil of the arborescent polymer in deuterated polystyrene is found to be close to bulk density. This indicates that the molecules are essentially non-interpenetrating and exclude the linear matrix chains. For G3 polymer in deuterated poly(vinylmethyl ether), two peaks in the $I(q)$ versus SANS data are observed above the phase separation temperature (105 °C) and the R_g of the phase separated sample decreases by about 21 % upon phase separation. In the two phase blends, G3 polymer molecules are found to be not in contact with each other.

2.5 Dispersing Dendrimers in a Solid Polymer Matrix

2.5.1 Synopsis

Dendrimers can be uniformly dispersed in a solid, polymeric matrix by the use of interpenetrating polymer network (IPN) synthetic methods. Small angle x-ray scattering (SAXS) and transmission electron microscopy (TEM) demonstrate that polyamidoamine

(PAMAM) dendrimers are well dispersed in a poly(2-hydroxyethyl methacrylate) PHEMA matrix that has been crosslinked with mass fraction 0.5 % ethylene glycol dimethacrylate. The dendrimer size can be measured by SAXS through fitting of the minimum before the first higher order feature of the sphere-like scattering. The size can also be measured by TEM through either measurement of individual dendrimers in the micrograph, or by taking a fast Fourier transform (FFT) of the micrograph and comparing the features of the transform to those of circles. All three methods give equal sizes within the error estimates. When the concentration of dendrimers in the IPN reaches mass fraction 10 %, a shrinkage of the dendrimers occurs with the dendrimers shrinking to near bulk density. This concentration is lower than the concentration at which the dendrimers shrink when in solution. The G8 dendrimers at mass fraction 2 % have a weak peak in the FFT indicating that a correlation in the spacing is beginning, but the addition of acid to the IPN polymerization does not increase order.

2.5.2 Introduction

Various applications of dendrimers take advantage of the spherical shape, such as the use as covalently bonded micelles or as an agent for encapsulation (“dendritic box”).⁹² The design of materials with specialized optical properties, or for use as high-capacity magnetic storage devices is currently being discussed.^{93,94} These applications require the isolation of entrapped functionalities from their counterparts in neighboring dendrimers. Recently, PAMAM dendrimers have been used as templates to produce metallic nanoclusters that are incorporated into the dendrimer structure.⁹⁵

To fabricate a useful device based on these ideas, incorporation of the dendrimers into solid polymeric matrices is desirable. It would be very advantageous to be able to “freeze” the dispersion of dendrimers in solution by replacing the solvent with polymer. This could possibly be accomplished by the use of interpenetrating polymer network (IPN) techniques.

IPN technology has been studied for many years⁹⁶. It involves forming an intimate mixture of two polymer types, with at least one of the polymers being polymerized in the presence of the other. The word “interpenetrating” described the attempts to make two polymers form continuous, independent structures, either as intertwined networks in a single phase, or more commonly, as a two phase morphology with co-continuous phases. While the word “interpenetrating” implies a certain morphology, the designation, IPN, has taken on a broader meaning than the morphology alone. In this paper “IPN” will be used to describe the method of polymerization as is commonly used, and does not imply that the dendrimer phase is continuous.

A Semi-II IPN is formed when a linear polymer is dissolved in a monomer of another type which acts as a solvent. The monomer is then polymerized, most often with a certain amount of multifunctional comonomer present to form a crosslinked network. In most cases, the dissolved polymer phase separates during the polymerization of the second polymer, forming a multi-phase morphology. The presence of the crosslinked second phase, however, can induce a very fine size scale on the phase separation.

Previous work on semi-II IPN's of linear polymers has shown that there is a strong thermodynamic push to phase separation.^{42,97,98} Only when the first polymer is of low molecular mass, generally having a lower molecular weight than the molecular mass between crosslinks, does the linear chain stay molecularly dispersed. If this is also the case with dendrimers, large dendrimers, which can be greater than 1,000,000 g/mole, may be difficult to disperse in an IPN matrix at a molecular level.

2.5.3 Experimental

2.5.3.1 Synthesis

PAMAM dendrimers diluted with methanol to produce the desired concentration. The ipns were prepared by dissolving the dendrimers in 2-hydroxyethylmethacrylate (HEMA) containing either mass fraction (1/2 or 1) % ethylene glycol dimethacrylate with AIBN as an initiator^{99,100}. They were polymerized at 35 °C for 72 h and at 70 °C for an additional hour.

2.5.3.2 SAXS

SAXS experiments were measured in the standard manner. The IPN samples were soaked in aqueous HBr to increase the x-ray contrast. They were then dried in vacuum for the SAXS experiments. A second set of samples were soaked in the same Phosphotungstic acid solution as was used in the TEM experiments.¹⁰¹ The stained samples were mounted in a solution cell.

2.5.3.3 TEM

Samples of thickness approximately (60-80) nm were ultramicrotomed at -80 °C, transferred to carbon-coated Cu grids of 200 mesh, and stained with OsO₄ vapors by exposing the grid to a solution of 0.04 g OsO₄/g H₂O at room temperature for 1 h. The images were obtained at magnification of 17,000X or less on a Philips 400T model TEM operated at 120 kV using low-dose conditions^{99,100}.

Dendrimer blends were stained with a mass fraction 2% aqueous phosphotungstic acid (PTA) solution that has been neutralized with sodium hydroxide (ph = 7), for 1 d and dried for 3 d in air. The blends looked optically transparent, even after Na-PTA staining. Electron transparent films of (60 to 80) nm thickness were cryo-microtomed at -30 °C, transferred to carbon coated Cu TEM grids, and the morphology of these materials was studied using TEM (Philips EM 400T) operated at 120 kV under low-dose conditions¹⁰¹.

2.5.3.4 Data Analysis

The R_g values of solutions were from Guinier fits of the scattering data.³⁵ The values for the IPNs were calculated from the positions of the higher order features^{38,50} and are reported as a relative range of $\pm 10\%$ that is typical of such measurements.

Micrographs were scanned at (40 to 120) pixels/cm. Sections 512 by 512 pixels were cut and fast Fourier transforms were taken with Scion Image¹⁰² to produce 2-dimensional images that were anisotropic in all cases. The 2-dimensional images were averaged to produce $I(q)$ files and calibrated by taking transforms of model objects.

2.5.4 Results and Discussion

Figure 40 shows the SAXS from a G10 dendrimer at high and low concentration, in methanol solution and in a PHEMA matrix. The IPN contrast was enhanced by treatment with hbr as described in the experimental section. The maxima at $q > 0.05 \text{ \AA}^{-1}$ in Figure 40 result from $P(q)$ with the higher order scattering features from spherical particles (Equation (1.7)³⁵). This function has minima at $qr = 4.49, 7.73, 10.90 \dots$ which can be used to estimate the R and R_g of a sphere. This is useful at high concentrations where $S(q)$ interferes with the size measurements at low q . Such a procedure has been used to measure dendrimer size at high concentrations^{38,50}. It is easy to see in Figure 40 that the first minimum of $P(q)$ is quite similar for the G10 dendrimer at mass fraction 1% in both solution and IPN. At mass fraction 26% solution concentration, the minimum is the same as the low concentrations, indicating that the dendrimer is unchanged in size. At mass fraction 10% dendrimer in the IPN, however, the minimum is shifted to higher q , showing that the dendrimer has shrunk in size. This is similar to the findings that dendrimers shrink in size at concentrations higher than overlap concentration, even though the mass fraction 10% dendrimer in IPN is presumably below the overlap concentration.

Figure 41 is a plot of dendrimer size in dilute solution and in ipns at mass fraction (1 and 10)% versus generation. There is a consistent trend in the range G6 through G11 where the dilute solution sizes are similar in both methanol solution and in HEMA IPN. At mass fraction 10% concentration, however, the size has shrunk by about 20%. Such sizes are close to dendrimers that have excluded all of the linear PHEMA chains.

The peaks at low q of the mass fraction 10% dendrimer in the IPN and the mass fraction 26% dendrimer in solution are from the $S(q)$ contributions and can be used to calculate the characteristic spacing between dendrimers, D , from the peak position, q_{\max} by $D = 1.23 \times 2\pi / q_{\max}$.³⁵ The spacing of the mass fraction 26% dendrimers in solution is $(187 \pm 19) \text{ \AA}$ and of the mass fraction 10% dendrimer in the IPN is $(224 \pm 22) \text{ \AA}$. Also, there is no sign of an upturn at the lowest resolvable q that would be an indication of dendrimer aggregation. Therefore, SAXS shows that dendrimers from G6 through G11 can be uniformly distributed in IPNs.

Figure 42 is a TEM of a G11 PAMAM dendrimer at mass fraction 10% concentration. Individual dendrimers can be seen, but due to the thickness of the sample,

dendrimers at different levels can be seen, making them appear to overlap. The dendrimers appear round, with uniform sizes and distributions. Lower magnification images of this sample showed that the dendrimer concentration was uniform without any sign of clustering. These results are consistent with the SAXS results.

Figure 43 is a TEM of an IPN with mass fraction 1 % PAMAM G10. The staining in this sample was with a mass fraction 2 % aqueous PTA as was described in the experimental section. Individual dendrimers can be seen. A comparison to results using OsO_4 stain for the mass fraction 10 % G11 dendrimer in the IPN shown in Figure 42. The dendrimers are visible in this image, but the differentiation between dendrimer and matrix is much less apparent than seen in Figure 40 for the same sample stained with NaPTA.

Previous work^{54,103} has shown that the addition of acid to an aqueous dendrimer solution causes ordering of the dendrimers. If such ordering can be induced in the solid IPN, it may produce morphologies with potential applications as electrical, optical, or information storage devices^{93,94}. SAXS was performed on samples that were stained with phosphotungstic acid. The samples were made with mass fraction 2 % G8 dendrimer (G8) and with added methacrylic acid comonomer (G8-MAA) as was described in the experimental section. Figure 44 shows the scattering from the two samples. The two curves are nearly identical, suggesting that the morphology is unchanged with and without the acid addition. In previous solution studies^{54,103} a strong peak appears when the acid is added. This peak is from the $S(q)$ function which can be used to calculate a characteristic spacing. While no peak is apparent, there is a leveling of the intensity at low q , which may be a shoulder or an incipient peak. The absence of a strong peak shows that no pronounced ordering exists in these samples. The electrostatic forces that cause the ordering in dilute aqueous solution are not sufficient to increase the ordering under the IPN conditions since the scattering from.

Figure 45 is a TEM of sample G8. Individual dendrimers can be seen, and they appear to be well dispersed in the matrix. Micrographs of all of the different areas examined in this sample were indistinguishable from this one, suggesting that the dispersion is macroscopically uniform. Figure 46 is of a sample similar to the one in Figure 45, except that the matrix is made from PHEMA containing a small amount of methacrylic acid sample G8-MAA, an amount calculated to be the molar equivalent to the PAMAM dendrimer terminal amine groups. These are the same samples that were used in the SAXS experiments shown in Figure 44.

Figure 45, however, is indistinguishable from Figure 44 showing that there is no detectable change in the morphology. This is in agreement with the SAXS results. To better estimate the size and dispersion of the dendrimers, a 2-dimensional Fourier transform was performed on the micrographs and the resulting anisotropic pattern was circularly averaged to produce the curves shown in Figure 47. The SAXS and TEM-FFT curves differ in that the SAXS scattering is from a 3-dimensional array, while the TEM-FFT is from a 2-dimensional projection. Both, however, have similar features. First, the curves of the two samples are identical in both samples in each figure, indicating that the

morphology is not significantly affected by the addition of the MAA to the IPN. Second, the incipient peak at low q in the SAXS has become a weak peak in the TEM-FFT indicating that there is a weak correlation between the dendrimer spacing. A TEM-FFT of the mass fraction 1 % G9 and G10 dendrimers in IPN's is included in Figure 47 to show the complete absence of a peak in the transform. Third, both figures show higher order features in the scattering which can be used to measure the R and R_g of the dendrimers. The sizes from SAXS are $R_g = (37.4 \pm 3.7$ and $36.2 \pm 3.6) \text{ \AA}$ for the G8 and G8-MAA sample respectively. The TEM-FFT size is $R_g = 36.8 \pm 3.7 \text{ \AA}$ for both samples.

Table 5 is a compilation of the sizes of the dendrimers in IPNs and in solution of samples of various generations. Also listed in Table 5 are the sizes from TEM calculated by measuring the sizes of a population of dendrimers from each micrograph^{23,101}. As can be seen in Table 5 and in Figure 41, all of the dendrimer sizes form a composite line except for the mass fraction 10 % dendrimer in IPN samples which are approximately 20 % smaller. Therefore there appears to be a shrinkage in size with increased concentration as was seen in previous solution studies,^{38,50} however, the shrinkage comes at a somewhat lower concentration for the solid ipns.

All of the SAXS and TEM results suggest that the dendrimers are well dispersed in the matrix with no dendrimer aggregation evident. This is contrary to previous results on ipns made from linear polymers. Bauer and Briber⁴² have found that ipns made with poly(vinylmethyl ether) in a crosslinked polystyrene (PS) matrix will phase separate when the crosslink density is large enough. In this study, the Flory-Huggins interaction parameter was negative, which is a strong driving force for miscibility. Even under these favorable conditions, phase separation was induced by the crosslinking. Similarly, linear PS phase separated from a deuterated PS network during the IPN polymerization.⁹⁷ Another study^{98,104} with dilute linear PS in a deuterated PS network found that the linear chains collapsed as the network density was increased and phase separated, even at low concentrations, when the molecular mass between crosslinks was equal to the molecular mass of the linear chains.

For the dendrimer ipns, however, phase separation did not occur, even though the dendrimer molecular weight of the largest dendrimers was around 1,000,000 g/mol. The dendrimer/PHEMA interaction parameter is unfavorable as is evident since a solution cast film of PAMAM G8 and linear PHEMA phase separations upon solvent evaporation. The fact that the dendrimer ipns do not phase separate upon polymerization may be due to their compact size. In linear ipns, phase separation occurs when the size of linear chain is approximately that of the size of the linear chain between crosslink points. For a mass fraction 0.5 % ethylene glycol dimethacrylate, the molecular mass between crosslink points is approximately 80,000 g/mol. For a mer step length of 7 \AA , this makes the average spacing between crosslink points of 170 \AA which is smaller than the dendrimer diameters. The compact size of the dendrimers may contribute to the stability of the ipns.

2.5.5 Conclusions

Dendrimers can be uniformly dispersed in a solid, polymeric matrix by the use of IPN synthetic methods. PAMAM dendrimers from G6 – G11 were placed in IPN's of PHEMA crosslinked with mass fraction 0.5 % ethylene glycol dimethacrylate. SAXS and TEM show that there is a uniform dispersion of dendrimers at mass fraction 1 % dendrimer. SAXS of mass fraction 10 % dendrimer IPN's also shows good dispersion, with a peak forming that indicated ordering. G8 dendrimers at mass fraction 2 % dendrimer show an incipient peak in SAXS and a weak peak in TEM-FFT. This may be the concentration at which ordering first appears. The addition of MAA to the IPN does not measurably change the ordering of the dendrimers.

The dendrimer size can be measured by SAXS through fitting of the minimum before the first higher order feature of the sphere-like scattering. The size can also be measured by TEM through either measurement of individual dendrimers in the micrograph, or by taking a Fourier transform of the micrograph and comparing the features of the transform to those of circles. All three methods give equal sizes within the error estimates.

When the concentration of dendrimers in the IPN reaches mass fraction 10 %, a shrinkage of the dendrimers occurs with the dendrimers shrinking to near bulk density. This concentration is lower than the concentration at which the dendrimers shrink when in solution.

2.6 End Linked Dendrimer Networks

2.6.1 Synopsis

Networks and star polymers are formed by reacting end functionalized polyethylene glycol (PEG) with PAMAM or PPI dendrimers. Four end functionalities, Vinyl Sulfone (VS), Isocyanate (IS), Acrylate (AC), and Epoxide (EP) are used and SANS and GPC are used to measure the extent of reaction. The EP is unreactive under the conditions used, AC reacted efficiently but quickly hydrolyzed in aqueous conditions, and IS reacted well, but formed large size byproducts in aqueous conditions. The VS proved best, giving high conversion and hydrolytically stable linkages. Swelling experiments show similar swelling for samples with high crosslink functionality, but the amount of swelling is methanol < water < acid. Aqueous solutions swell with acid addition, reaching a maximum, and then deswelling with more acid addition.

2.6.2 Introduction

A variety of model networks made from end functionalized low polydispersity linear polymers have been studied. The functionality of the crosslinks is either small molecules with 3 or 4 functionality or a polydisperse, multifunctional gel such as divinyl benzene. The use of dendrimers as a multifunctional branch point should give

high functionality since dendrimers have up to several thousand attachment sites and low polydispersity

Dendrimers are polymeric molecules that are made in a stepwise synthesis that doubles the terminal functionality with each set of two synthetic steps, or generation.^{4,21} Dendrimers have been found to be spherical with a narrow interfacial transition on the outside.²⁰ The terminal units are predominately on the outside.⁴⁶ These factors make dendrimers ideal multifunctional crosslinking agents, with many functional units easily accessible at the periphery of the dendrimer. Dendrimers also have a very narrow polydispersity with between 4 and 4096 theoretical crosslink sites.^{4,21}

The efficiency of the reaction is difficult to measure in networks, analytical methods that measure end group conversion are difficult and subject to uncertainties at high conversions. Extraction experiments are also inexact at high conversions. Studies of the reactions of polymers with a single end functionality are simpler since they form stars rather than networks which are soluble and can be more easily characterized.

Reactions of end functionalized PEG with dendrimers have been reported for amino terminated dendrimers and NHS terminated PEG.¹⁰⁵ High conversions have been reported forming stars with large numbers of arms. Only the high conversion results were studied, however. No measures of the kinetics were made. This work reports the use of chromatography to follow the conversion of arms to stars.

By changing the generation of the dendrimer, the crosslink functionality can be continuously changed. Similarly, by changing the ratio of linear chains to dendrimer terminal units, the crosslink functionality can be changed. Thus, samples can be made with a constant degree of polymerization, N , between crosslinks, but with a wide range of functionalities. Swelling of the networks with solvents of varying power, i.e. Varied Flory-Huggins interaction parameter, χ , can be used to measure the effect of crosslink functionality.

2.6.3 Experimental

All endfunctionalized poly(ethylene glycol) was used as received from Shearwater Polymers. Monofunctional Vinyl Sulfone (VS), Isocyanate (IS), Acrylate (AC), and Epoxide (EP) terminated PEG had nominal $M_n = 5,000 \text{ g mol}^{-1}$ and $M_w/M_n < 1.1$. Difunctional Vinyl Sulfone (VS) terminated PEG had nominal $M_n = 20,000 \text{ g mol}^{-1}$ and $M_w/M_n < 1.1$. Polyamidoamine (PAMAM) dendrimers G5 through G10 were obtained from Dendritech and generations G2 through G4 were purchased from Aldrich Chemical Company. Polypropyleneimine (PPI) G5 dendrimer was purchased from Aldrich Chemical Company.

Stars were formed by reacting the monofunctional PEGs with PPI or PAMAM dendrimers in methanol, water, or DMSO solution. Networks were made in a similar way and fluorinated polymeric containers were used for easy removal of the gels for swelling measurements. Swelling measurements were made by immersing the gels in a

large excess of the new solvent. Swelling ratios were measured by weight and soluble fractions were measured by evaporation of the extracting solvent. Ipns were synthesized by swelling the gels with methyl methacrylate containing mass fraction 0.5 % axobisisobutyronitrile as a free radical initiator and polymerizing at 35 °C for 72 hours and an additional hour at 70 °C.

Gel permeation chromatography (GPC) was done with volume fraction 0.1 % triethylamine in H₂O as a mobile phase with a Phenomenex Polysep-GFC P column. Kinetic GPC runs were done by adding appropriate amounts of VS-PEG and dendrimer at total mass fraction 10 % in the mobile phase solvent were mixed and 10 µl quantities were repeatedly injected. Detection was by an evaporative light scattering detector (Varex, model Mark iia).

The SANS experiments were performed at the 8 m facility at the National Institute of Standards and Technology Center for Cold Neutron Research (Gaithersburg, Maryland) in the normal manner. Scattering was done at ambient temperatures which were nominally (20 ± 2) °C. A sample to detector distance of 360 cm was maintained throughout the study, operating at a wavelength $\lambda = 6 \text{ \AA}$, with a wavelength spread of $\Delta\lambda/\lambda = 0.25$. Based on the hydrogen content of the materials, an estimate for the incoherent scattering was subtracted from the values of the absolute solution scattering intensity, to give the final form of the experimental data, which is the absolute intensity of the coherent scattering, I , as a function of q .

SAXS data were collected at the Advanced Polymer Beamline at Brookhaven National Laboratory, X27C. X-ray contrast was enhanced by soaking the samples in dilute sodium phosphotungstinate solution as is described in the experimental section of the dendrimer IPN section. The usable span of scattering vector q , was in the range $0.07 \text{ \AA}^{-1} < q < 0.3 \text{ \AA}^{-1}$.

2.6.4 Results and Discussion

PEG has many advantages over other end functionalized polymers. It has solubility characteristics similar to that of PAMAM and PPI dendrimers, being soluble in water, alcohols, and DMSO. Solubility in common solvents is a requirement for the chemical reaction to form a large, uniform sample. PEG is also soluble in non-solvents for dendrimers such as benzene. Also PEG forms miscible blends with polymers such as poly(methyl methacrylate) (PMMA) and poly(methyl acrylate) (PMA) which can be exploited in forming solvent-free samples.

PEG is available with a variety of end functionalizations that are capable of forming covalent bonds with the terminal primary amines of PAMAM or PPI dendrimers. It is important that the reaction takes place at a rate fast enough for high conversions to be reached in a reasonable time, but slow enough so that mixing and film casting can take place before gelation takes place. Side reactions that would cause unwanted bonding or polymerizations or cleave the functionalities from the chain have to be avoided.

Four functionalities were chosen for screening, acrylate, epoxy, isocyanate, and vinyl sulfone. An acrylate reacts with a primary amine through a Michael addition. This is the same reaction that is used to form half generations in both PAMAM and PPI dendrimers. The vinyl sulfone also reacts through a Michael addition. The isocyanate forms a urethane linkage and is perhaps the most common reaction used in linking polymers. The epoxy forms an amine linkage and generated a hydroxy group. The epoxy-amine reaction is commonly used in forming networks, but usually requires high temperatures.

PEGs of $M_w = 5000$ g/mol with these four functional groups on one end were reacted with PPI G5 dendrimer. The ratio of PEG end groups to PPI end groups examined was 1:2, which would produce 32 arm stars at 100 % conversion. Mixtures were made in DMSO- d_6 at a total mass fraction of 10 % and allowed to react for one week. The mixtures were placed in 1 mm thick quartz cells for SANS experiments. Figure 48 shows Kratky plots of the results of mass fraction 0.5 % dilutions of the four samples. The plot is $Iq^{5/3}$ vs q which gives a plateau region at high q for flexible chains in a good solvent. The plots are normalized so that the curves go to 1 at this point. The IS, VS and AC samples all have a strong peak in the Kratky plots which is characteristic of many arm stars.³⁵ The ratio of the peak to the plateau is function of the average number of arms. Assuming that the scattering is from a mixture of stars and unreacted arms with an arm conversion, p , the scattering can be calculated for stars with Gaussian arms, and an estimate of conversion and arms per star can be made.

The conversion of the IS, VS, and AC, is 0.76, 0.73, and 0.66, respectively. The average arms per star are 24.4, 23.3, and 21.6. It is clear that the reaction is efficient and produces large star molecules. The EP sample, however does not produce a peak in the Kratky plot. A peak appears in the Kratky plot at a conversion of 0.21 under these conditions, so it is obvious that the reaction is quite incomplete. Also plotted is the SANS of a mass fraction 5 % PEG arm for comparison. It appears that the epoxy does not react significantly under these conditions.

The SANS samples were examined with GPC to separate the stars from the unreacted arms. Figure 49 shows chromatograms of the four groups and an unreacted VS terminated PEG. The chromatographic conditions used gives good separation of the two peaks. The VS star shows good conversion into a narrow star peak, with only a small peak from the unreacted PEG, giving a conversion of 0.82. The IS chromatogram shows good conversion of the arms, but an additional peak appears at even lower elution volume, indicating a larger hydrodynamic volume. This peak is at the exclusion limit of the column and indicated that very large structures exist. This additional peak is probably due to a side product from the isocyanate reaction producing larger molecules. It seems likely that the reactions happened when the sample was placed in the aqueous solution since the SANS results do not show such large structures. The EP sample shows little conversion, consistent with the SANS results. The AC sample also shows no star molecules present, in contrary to the SANS results which indicated high conversion. The EP terminated PEG was the only sample that has an ester linkage. It probably has hydrolyzed under the aqueous GPC conditions.

Out of the four reactions, the EP is not useful due to the low conversion under the reaction conditions. The IS reacts well, forming stars, but side reactions make the product heterogeneous. The AC reaction is quite efficient and the bond formed stable in aprotic solvents such as DMSO, but is sensitive to impurities such as water. The VS is by far the most useful of the four reactions. It gives good yield in a reasonable time and is not subject to side reactions. The bond formed is hydrolytically stable, and good conversions can be obtained even with water or methanol as a reaction solvent.

The VS reaction allows for detailed study of the kinetics of the linking due to its reaction in aqueous media. GPC was done on a reaction mixture in which the dendrimer and PEG-VS was mixed in water with volume fraction 0.1 % triethylamine which was the GPC mobile phase. Roughly equimolar amounts of a G4 PPI dendrimer (32 terminal $-NH_2$ groups) and PEG-VS at a total mass fraction of 10 %. A slight excess of G4 PPI dendrimer would give 30 arms at complete conversion. Injections were repeatedly made from this reaction mixture over the period of one day. Figure 50 shows the GPC of six injections over this time period. The PEG-VS peak drops continuously during this time span and the star peak increases in size. The position of the star peak also shifts to lower elution volume and becomes narrower with conversion. This suggests that the stars are becoming larger and more uniform. Figure 51 shows the conversion of arms with time with GPC data were taken between (4 and 1383) min. The kinetics of the reaction can be modeled by kinetics that are first order in VS-PEG and first order in dendrimer end groups as in equation (2.12).

$$\partial[PEG]/\partial t = -k[PEG][NH_2] \quad (2.12)$$

The solid line in Figure 51 is a fit of equation (2.12) to the first order kinetics. The fit is quite poor, underestimating the rates at low conversion and overestimating the rates at high conversion. The reaction seems to be slowing down considerably with conversion due to the crowding that occurs when a large number of arms are placed on the star. If the crowding that occurs when a large number of arms are on the dendrimer, the reaction may not obey first order kinetics in the concentration of available dendrimer terminal groups. The kinetics was refit to equation (2.13), which allows the order of the reaction with respect to dendrimer end groups to float.

$$\partial[PEG]/\partial t = -k[PEG][NH_2]^a \quad (2.13)$$

It is quite possible that the reaction is also not first order in PEG-VS concentration, but the reaction orders will be too closely correlated to separate them from a single kinetic run. The dashed line is a fit of Equation (2.13) and it is quite good, giving an exponent $a = 3.6$ with a standard deviation of ± 0.2 . The kinetic experiment has been repeated with different concentrations, stoichiometries, and dendrimer type and the slowing down of the conversion is typical of this reaction, but high conversions can still be reached. In Figure 51 a conversion of 80 % is reached within a day. A more detailed investigation of the kinetics will be published separately.

A network with degree of polymerization, N_C , when swollen with a solvent with a solvent having a Flory-Huggins interaction parameter, χ , will swell from the volume fraction polymer during synthesis, v_{2c} , to a swollen volume fraction, v_2 , according to equation (2.14).

$$N_C = \frac{(1 - 2/f)(v_2/v_{2c})^{1/3}(1 + K(\lambda))}{\ln(1 - v_2) + v_2 + \chi v_2^2} \quad (2.14)$$

Where f is the functionality of the crosslinks and $K(\lambda)$ is an elastic contribution that is a function of chain extension ratio, λ , which depends on the elasticity theory used. Therefore the swelling ratio of a network is a constant for any given value of $N_C/(1 - 2/f)$. Therefore changing the crosslink functionality has the effect of changing the molecular mass between crosslinks. The change in going from $f = 4$ to $f \rightarrow \infty$ involves an effective change of N_C by a factor of 2.

Equation (2.14) has different forms depending of the theory of elasticity used. For the Phantom Network assumption, where the chains do not experience the effects of neighboring chains, the term $K(\lambda) = 0$ so equation (2.14) described the swelling without the final term. For an Affine Network assumption, where the microscopic crosslink sites move proportionate to macroscopic deformation, the term $K(\lambda) = 1 - \lambda^{-2}$. The functional form for the swelling is given in equation (2.15), and is known as the Flory-Rehner equation.

$$N_C = \frac{(v_2/v_{2c})^{1/3}(1 + 2/f(v_2^{2/3}/v_{2c}))}{\ln(1 - v_2) + v_2 + \chi v_2^2} \quad (2.15)$$

Two series of networks were synthesized with PEG-VS₂ chains attached to PPI or PAMAM dendrimers. In the PPI series, G5 dendrimers were used in all samples, but the stoichiometry was changed giving between 4 and 64 theoretical crosslink functionality for 100 % conversions. Therefore, the mass fraction dendrimer and the fraction of reacted terminal groups changed in the samples of the series, but the dendrimers were all the same size. In the PAMAM series, the dendrimer generation changed from G2 to G7, but the ratio of VS groups to dendrimer terminal groups was kept at 1:2 in all cases giving between 16 and 256 theoretical crosslink functionality. Therefore, the mass fraction dendrimer and the fraction of reacted terminal groups were constant in the samples of the series, but the dendrimers changed in size.

Both series had a mass fraction of 10 % solids in methanol during the synthesis and the reaction was allowed to proceed for seven days. In the PPI series, three additional samples were made but were reacted for only one day. Figure 52 is a plot of the mass swelling ratio of the PPI series samples. The samples were first placed in excess methanol and allowed to swell to equilibrium. The samples were then placed in excess water and the water was exchanged twice. HCl was then added in a stoichiometric amount to that of the dendrimer terminal groups. The increased mass in methanol was quite small with the exception of the lowest crosslink functionality. In water, the

swelling ratio increases for all samples and was relatively constant with the exception of the lowest functionality again. This is qualitatively in agreement with equations 3 and 4 which predict only a weak effect of the crosslink functionality on the swelling for large f and an increase of swelling as f gets close to the critical value of 2.

The data points for the one day reaction time all lie above the seven day points. This is due to the lower extent of reaction. The theoretical value of f is not achieved and the curves would be shifted to the left if the actual values of f were printed. In fact, the study of the reaction rate of the stars shows that the reaction is not complete and this is undoubtedly true for the networks also. In an effort to judge the effectiveness of equations (2.14) and (2.15), fits can be made to the swelling data. There are considerable uncertainties in the variables needed for the fits, particularly the crosslink functionality, but the fits can give qualitative trends that can provide some insight in the swelling.

Equations (2.14) and (2.15) were fitted to the swelling data, using χ as the fitting parameter. When 100 % conversion is assumed and the theoretical f is used, the fits are poor, with the low f swelling values underestimated and the high f values overestimated. The fits were repeated but the average conversion was also fitted. An assumption that the probability of a chain attaching, p , is the same for all samples. While there is undoubtedly different conversions for the samples, the results should qualitatively be the same.

The fits of the PPI series are shown in Figure 52 for both the Phantom and Affine networks. Fits of both theories have common features, a relative level swelling at high f with an upturn at low f . The fit parameters merely show that the value of c is small and the conversion is around one half. Extraction studied of these samples gives an average extractable fraction of (2.9 ± 2.7) % which represents a value of $p = (83 \pm 16)$ %. The fits of equations (2.14) and (2.15) are therefore qualitatively consistent with other measurements.

The addition of acid causes the samples to swell considerably more than with neutral water. Figure 53 shows the swelling that results when HCl is added to the aqueous solution in a stoichiometric amount to the terminal amines. The amount of swelling is also no longer flat for the larger crosslink functionality, but varies continuously. For these samples, the mole fraction dendrimer increases proportionately to the crosslink functionality so that the acid amount increases also.

Another set of samples was made with PAMAM dendrimers of generations 2 through 7. The molar ratio was kept at one PEG end group to two PAMAM terminal units. These samples therefore have a constant mass fraction dendrimer in each case, but the crosslink functionality changed continuously with the generation number. The swelling curves shown in Figure 54 look qualitatively like those of PPI dendrimers in Figure 53. The fits also give values similar to those in Figure 53, but as before, they can be considered qualitative only. As with the PPI networks, the swelling ratios increase as methanol > water > acid.

The PAMAM samples were titrated with HCl and swelling measurements were taken from well below to well above the stoichiometric amounts. The swelling results are shown in Figure 54 and clearly show a maximum swelling ratio at intermediate acid additions. There is a large initial increase with the first relatively small acid addition with a maximum at approximately the stoichiometric amount to the total amine concentration, both the internal tertiary amines, and the terminal amines, both unreacted and attached to the PEG vinyl sulfone. Additional acid additions causes a decrease in swelling ratio, but no abrupt volume decrease is seen.

2.6.5 Summary

Networks can be synthesized by reacting α - ω end functionalized PEG with the terminal amines of PAMAM or PPI dendrimers. The relative reactivity and susceptibility to side reactions of four functional groups, EP, AC, IS, and VS were examined by SANS and GPC. The EP group did not react at ambient temperatures. The AC reacted efficiently, but upon solution in basic water, the bonds broke to the dendrimer, probably due to hydrolysis of the ester linkage from the PEG to the dendrimer. The IS reacted efficiently, but upon solution in basic water, very large structures formed, possibly due to additional side reactions. The VS proved to be best with 80 % conversion possible and was hydrolytically stable.

The reaction kinetics of the VS-dendrimer reaction can be conveniently followed by repeatedly injecting a reaction mixture into a GPC column. The reaction was found to slow down considerably with conversion, probably due to the crowding that results when a large fraction of the dendrimer terminal units have reacted with a PEG chain. Even with the crowding, a conversion of more than half of the terminal amines was possible.

Swelling of dendrimer networks shows that there is a strong effect of going from relatively poor (methanol) to relatively good (water) solvents. The swelling of the networks is only weakly affected by the crosslink functionality, however. Addition of aqueous acid to the dendrimer increases the swelling a large amount, with a maximum in swelling being seen when there is a stoichiometric amount of acid to amine added.

3 Metal Containing Dendrimers

3.1 Dendrimers as Templates for the Formation of Inorganic Nanoclusters

3.1.1 Synopsis

Charged poly(amidoamine) (PAMAM) dendrimers are used to create organic-inorganic hybrid colloids in aqueous solution. The formation of gold colloids upon reduction of a gold salt precursor serves as a model reaction to study the influence of reaction conditions and dendrimer generation on the resulting nanostructures. Characterization by transmission electron microscopy (TEM), small angle neutron scattering (SANS), and small angle x-ray scattering (SAXS) show that the gold particles are formed inside the dendrimer and located offset from the center. Although lower generation dendrimers aggregate when stabilizing the metal particles formed, dendrimers of generation 6 to 9 can template one gold colloid per dendrimer molecule, the size of which is well-controlled by the number of gold atoms added per dendrimer. For generation 10, multiple smaller gold particles per dendrimer are observed. The effectiveness of PAMAM dendrimers as templates in the host-guest nanoscale synthesis is confirmed for different chemical reactions.

3.1.2 Introduction

Organic-inorganic hybrid nanostructures have generated great interest due to a variety of potential applications as electrical, optical, medical and information storage materials. In order to design hybrid structures of organic and inorganic material, templating a growing inorganic crystal within a polymeric matrix, a method that was initially inspired by nature, has been evaluated as an effective synthetic route for a variety of polymer-inorganic systems.¹⁰⁶

Since dendrimers are well defined organic molecules in the size range of (1 to 15) nm and are known to act as hosts for guest molecules,^{107,108} they are promising candidates as templates for the formation of inorganic nanoclusters. Organic-inorganic hybrid materials based on dendrimers have been recently reported by several authors.¹⁰⁹⁻¹¹⁴ The results from these studies show that dendrimers are able to stabilize metal clusters in solution. Furthermore, the nanoclusters have been demonstrated to be effective high surface area catalysts in solution that allow substrates to penetrate the dendrimer interior and access the cluster surface.¹¹² Predictions have been made about the selectivity of such catalysts.¹¹⁵ Although several studies propose that dendrimers can act as “nanotemplates”,¹⁰⁹⁻¹¹⁴ none of those studies show whether the colloid is formed inside the dendrimer nor investigate how the colloids formed can be influenced by varying the so-called “template”.

Our motivation for using dendrimers comes from a desire to understand the mechanisms of polymer nanotemplating with a model system. Dendrimers are monodisperse and well characterized molecules.²⁰ The size of different generation

dendrimers spans the characteristic sizes of low molecular mass molecules, polymers and colloids, thereby offering a unique mesoscopic system.

In this study, we use charged poly(amidoamine) (PAMAM) dendrimers in aqueous solution as potential nanotemplates. We investigate dendrimers of generation 2 to 10 (G2 to G10) for the formation of inorganic-organic hybrid colloids, whereas previous reports employed only low generation dendrimers (G6 and below). Our approach relies on the attraction between charged dendrimers and oppositely charged metal ions. Performing chemical reactions on the inorganic precursor that is physically attached to the dendrimer should produce colloid structures that are controlled by the dendrimer. The concept of using charged, solvent-penetrable nano-polymer-particles as templates in aqueous solution was first applied to polyelectrolyte microgels.¹⁰⁶ This is in contrast to the specific coordination chemistry, i.e. Complexation of metal ions by amine groups, used by other authors and is presumed to be more general. In this study, we use the reduction of gold as a classical model reaction. Transmission electron microscopy (TEM), small angle neutron scattering (SANS) and small angle x-ray scattering (SAXS) are employed to characterize the resulting organic-inorganic nanocomposites. We also investigate how the reaction rate and other parameters influence the colloid formation.

3.1.3 Experimental

3.1.3.1 Synthesis

Poly(amidoamine) (PAMAM) dendrimers of generations 2 to 4 were purchased from Aldrich Chemical Company and generation 5 to 10 were supplied by Dendritech (Michigan Molecular Institute). Aqueous solutions with a dendrimer mass fraction of 0.1 % to 1 % were prepared by diluting concentrated dendrimer/methanol solutions (dendrimer mass fraction of 20 % to 25 %) with deionized water. Dilute aqueous solutions of PAMAM dendrimers were mixed with aqueous solutions of HAuCl_4 at controlled stoichiometries. After stirring these solutions for 1 h, sodium borohydride in basic aqueous solution (0.025 mol/L to 0.5 mol/L sodium hydroxide) was added. The light yellow dendrimer/ HAuCl_4 solutions immediately turned brown or red, indicating the formation of colloidal gold.

UV-VIS spectra of the dendrimer-gold colloid solutions were obtained on a Perkin-Elmer Lambda 9-spectrometer in the wavelength range of 400 nm to 800 nm. TEM was also performed on these solutions as well as on dialyzed samples. The resulting TEM images for both cases are the same. For the SANS experiments, samples were either dialyzed against deuterium oxide or directly synthesized in deuterium oxide.

3.1.3.2 Transmission Electron Microscopy (TEM)

Carbon coated copper grids, 300-mesh, were washed in chloroform reflux in order to remove formvar. Grids were then treated for (2 to 5) s in a glow-discharge tube in partial vacuum to impart hydrophilic character to the carbon substrate. Stained specimens were prepared by depositing the sample solutions on the grid and inverting the grid on a

drop of aqueous phosphotungstic acid solution that had been neutralized with NaOH (mass fraction of phosphotungstic acid = 2 %). The grid was then blotted on filter paper and air-dried. TEM images were obtained at 120 kV with a Phillips 400T at a magnification of 46000 X and 100000 X. The relative error is within 10 % of the magnification.

3.1.3.3 Small Angle Neutron Scattering (SANS)

Samples for SANS measurements were transferred into optical quality quartz banjo cells with 2 mm path length. SANS studies were performed at the Center for Neutron Research at the National Institute of Standards and Technology in the normal manner. Measurements were made using the 30 m SANS instrument with a neutron wavelength $\lambda = 0.6$ nm and wavelength spread of $\Delta\lambda/\lambda = 0.15$

3.1.3.4 Small Angle X-ray Scattering (SAXS)

SAXS data were collected at the Advanced Polymer Beamline at Brookhaven National Laboratory, X27C in the normal manner. The radiation spectrum from the source was monochromated using a double multilayer monochromator and collimated with three 2° tapered tantalum pinholes to give an intense X-ray beam at $\lambda = 1.307$ Å. Two configurations were used with a linear position sensitive detector (European Molecular Biology Laboratory, EMBL) or a 2D image plate detector (BAS2000, Fuji). The sample to detector distance was varied between (1 to 1.5) m. The span of scattering vector magnitudes q was in the range $0.15 \text{ nm}^{-1} < q < 3.2 \text{ nm}^{-1}$ and $0.2 \text{ nm}^{-1} < q < 4.4 \text{ nm}^{-1}$ for the two configurations used.

The scattering curve $I(q)$ was Fourier transformed into the pair distance distribution function $P(r)$ using the program ITP (*Indirect Transformation for the Calculation of $P(r)$*) by O. Glatter.¹¹⁶⁻¹¹⁸ This includes smoothing of the primary data by a weighted least square procedure (estimation of the optimum stabilization parameter based on a stability plot) and transformation into real space by the indirect transformation method with minimized termination effects.

3.1.4 Results and Discussion

3.1.4.1 Nanocomposite Synthesis

The nanotemplating by dendrimers in aqueous solution is depicted schematically in Figure 55. The addition of H₂AuCl₄ to a neutral dendrimer with primary and tertiary amine groups results in a protonated dendrimer with AuCl₄⁻ counterions. The gold ions are then reduced to metallic gold without the formation of a macroscopic metal precipitate. The stable brown to red solutions of colloidal gold formed indicate that the metal colloids were stabilized by the dendrimer. The brown or red color of the solutions and UV-visible spectra (Figure 56) are typical of gold colloids in the size range of (1 to 5) nm. In the following discussion, we will show that the location of the gold colloid

inside the dendrimer as sketched in Figure 55 is an accurate representation of the dendrimer-colloid structure.

3.1.4.2 Optimization of the Reaction Conditions

The stabilization of gold colloids in aqueous solution by the PAMAM dendrimers is possible over a wide range of reaction conditions. In order to control the size of the particles, one needs to optimize the ratio of the added gold ions to dendrimer, the dendrimer concentration in solution, as well as the reduction rate. In the first step, the gold/dendrimer ratio has to be adjusted so that no precipitation occurs. We found that gold could be added to the solution without precipitation of the dendrimer up to the amount corresponding to a gold salt to dendrimer end-group ratio of 1:1. We refer to the number of end groups as a reference value and do not imply any specific binding to the end groups. Furthermore, the dendrimer contains an equivalent number of inner, tertiary amine groups, which can also be protonated.

At higher concentration (dendrimer mass fraction $\geq 2\%$), precipitation occurs upon reduction of the gold salt. When the concentration of the dendrimer is sufficiently low (for example a dendrimer mass fraction of 1%) a stable colloidal solution is formed, but the resulting gold colloids are relatively polydisperse. It is only when the dendrimer mass fraction is 0.12% or lower that the reduction can result in uniform gold colloids, and the dendrimer acts as a true template. Therefore, we employ a dendrimer mass fraction of 0.12% for all subsequent experiments. The third parameter to be optimized is the reaction rate, i.e. Mass transfer and growth in comparison to nucleation. We performed the reduction with sodium borohydride in order to control the reduction rate by the pH of the solution.¹¹⁹ If the reduction is fast (NaBH_4 in (0.025 to 0.1) mol/L NaOH), again polydisperse colloids are observed (Figure 57). For slower reduction rates (NaBH_4 in 0.3 mol/L NaOH), uniform encapsulated particles can be formed (Figure 57). Under much slower reduction conditions (NaBH_4 in 0.4 mol/L NaOH), a red-violet precipitate is observed. Thus the dendrimer is an effective template only when sufficiently slow reduction rates are used. This trend corresponds to results for other systems, but the specific optimal conditions are different. We have chosen the slowest reduction that results in stable colloidal solutions (NaBH_4 in 0.3 mol/L NaOH) for further investigations, hereafter referred to as “slow reduction”. Furthermore, the precipitate obtained at even slower reduction is also a dendrimer-metal composite material since the color indicates nanometer dimensions of the metal. This complex material is an interesting hybrid system, but is not the focus of this study.

3.1.4.3 Characterization of the Hybrid Particles

The particles synthesized are investigated by TEM, SANS and SAXS. The characterization procedure is demonstrated for a representative G9-gold sample (loading ratio 1:1, slow reduction) in this section. TEM on the dendrimer-gold-particles was performed after staining the dendrimer; thus both components are evident in Figure 57b. The image indicates that the colloid particles are formed inside the dendrimer. Under these slow reaction conditions, one gold particle per dendrimer is predominantly formed.

The gold colloids observed are relatively monodisperse. The sizes estimated for the dendrimer and gold are 13 nm and 4 nm, respectively. The measured dendrimer size corresponds to previous reports of the size of the unmodified PAMAM dendrimers.²⁰ The TEM image in Figure 57b suggests that some of the dendrimers aggregate. From the TEM experiments one cannot determine whether the aggregates are present in the parent solution or formed while casting on the grid. Solution characterization methods must be applied to resolve this issue.

SANS measurements were performed on solutions of the dendrimer-gold hybrid-particles in deuterium oxide. Scattering curves for the unmodified dendrimer and the gold containing dendrimers are shown. For the dendrimer-gold hybrid particles, the radius of gyration obtained from Guinier extrapolation is (5.1 ± 0.1) nm. This is within the experimental error the same as for the unmodified dendrimer. The result indicates that the hybrid particles also do not form larger aggregates in solution. Furthermore, the higher order sphere form factor features, which are pronounced in case of the unmodified dendrimer, nearly completely disappear for the hybrid samples. This will be understood in the context of the SAXS results.

SAXS provides more detailed information about the colloid structures. In Figure 59, data for an unmodified G9 dendrimer are shown. Figure 60 shows data for dendrimer-gold hybrid-particles, which correspond to the TEM sample in Figure 57b. The scattering curves $I(q)$ (Figure 59a and Figure 60a) can be Fourier transformed yielding the pair distance distribution functions $P(r)$ (Figure 59b and Figure 60b).

Transformation into real space, which does not include geometric assumptions about the particle, demonstrates the different particle features more obviously than the inverse space scattering curves, in this case. The shape of the $P(r)$ for the unmodified dendrimer in Figure 59b corresponds to a homogenous sphere of 13 nm diameter, which is in agreement with earlier modeling results.²⁰ In contrast, the shape of the $P(r)$ for the hybrid particle in Figure 60b is typical of a layered sphere. An estimate of the dimensions of the inner sphere and outer sphere diameter confirms the diameters of the gold (4 nm) and the dendrimer (13 nm) estimated from TEM. More importantly, this result proves that the gold is formed inside the dendrimer.

A further deconvolution of the pair distance distribution function $P(r)$ under the assumption of a specific geometry (which has been deduced from the $P(r)$ function itself) generally leads to the particle electron-density-profile, $\rho(r)$. In case of the hybrid particles (Figure 60), by assuming spherical symmetry, a satisfactory description of the $P(r)$ function, specifically the relative peak heights, is not possible. Deviation from strict spherical particle symmetry is one possible reason for such a discrepancy.

Additional modeling has been performed in order to understand this issue: We calculated the scattering curves and the pair distance distribution functions for several model layered particles. At this point, one can compare the scattering curves or the real-space pair distance distribution functions in order to understand the basic trends. We will refer to the pair distance distribution functions here, since the effects are more obvious.

Figure 61a displays the calculated pair distance distribution functions for layered spheres with different relative contrast of the inner sphere. The variation does not allow the modeling of the basic shape of the experimental pair distance distribution function (Figure 60b). This points to deviations from a perfect spherical symmetry, as was already indicated by the problem with the deconvolution of the $P(r)$. When considering potential structures with non-spherical symmetry, one has to remember that the maximal diameter of the unmodified dendrimer and the gold containing dendrimer is the same (Figure 59b and Figure 60b). Thus, the best hypothesis for non-spherical symmetry in our system is a non-centered placement of the gold particle within the dendrimer. In Figure 61b we calculated pair distance distribution functions for layered particles with constant relative contrast, but an increasing offset of the inner sphere from the center of the outer sphere. The experimental pair distance distribution function (Figure 60b) is best represented for an offset of 4.7 nm (Figure 61b, bold line). Thereby it is clearly indicated that the gold particle is offset from the center of the dendrimer. We do not perform a quantitative curve fitting within this model, since no new information is expected. The displacement of the gold from the dendrimer-center is also visible in some of the particles in the TEM in Figure 57b. (Because the TEM is a two-dimensional projection, only a fraction of the gold colloids appears off-centered.) In addition, this off-center placement of the gold in relation to the dendrimer can also explain the loss of sharp features in the SANS scattering curve shown above.

Thus we have shown that the gold colloid is inside the dendrimer and it is located with an offset from the center as was depicted schematically in Figure 55. The good agreement between the gold colloid diameter determined from TEM and SAXS allows a quantitative comparison with the model sketched: The G9 dendrimer was loaded with gold salt corresponding to a gold-ion to end-group ratio of 1:1, i.e. 2048 gold ions per dendrimer molecule. Assuming the formation of one gold colloid from the loading of one dendrimer molecule upon reduction, one would expect a gold particle consisting of 2048 gold atoms. This means an expected particle size of 4 nm when assuming bulk density for the gold. This calculated value is in good agreement with the experimental results. Thus, the postulate that the gold ions from the load of one dendrimer form one particle has been demonstrated to be true. The gold-colloid formation is indeed templated by the dendrimer. We will hereafter refer to this template mechanism as “fixed loading law”.

3.1.4.4 Influence of the Gold to Dendrimer Loading Ratio

As stated above, the maximal loading of the dendrimer with gold (1:1 molar ratio of gold ions to dendrimer end groups) is determined by the solubility of the gold salt loaded dendrimer. Although we have extensively studied the structure of the hybrid formed under these maximal loading conditions, we have also investigated the variation of the structures formed with loading ratios below the maximum value. We have studied systems with gold-ion to dendrimer end-group ratios of 1:1, 1:2 and 1:4. UV-VIS spectra for samples formed upon reduction were shown in Figure 56, SAXS results for the G9 sample are given in Figure 62. It can be seen from the SAXS data as well as from TEM (not shown) that a lower loading yields smaller particles. Gold diameters of 4 nm, 3.3 nm

and 2.5 nm (within ranges of ± 0.2 nm) for 1:1, 1:2 and 1:4 loading are observed. Again, this corresponds well with the expected values for 2048, 1024 and 512 atoms.

In other polymer template systems, it has been observed that one part of the polymer particles ends up “fully” filled with gold while another part is completely empty, indicating a more complicated growth mechanism.¹⁰⁶ In contrast, with the dendrimers investigated here, the size of the metal colloids formed is precisely determined by the number of gold atoms that were added per dendrimer, introduced before as the “fixed loading law”.

Although one might be interested in putting as much gold as possible into a single dendrimer, the samples resulting from a lower loading also represent well-defined composite particles which may be of importance for certain applications. For example, dendrimer-stabilized metal colloids represent an interesting system for heterogeneous catalysis in aqueous solution. The hybrid particles containing smaller metal colloids may be more effective because of the larger surface area provided per mass, or changed selectivity due to their different morphology.^{120,121}

3.1.4.5 Effect of Dendrimer Generation on Colloid Size

Table 1 summarizes some TEM and SAXS results for hybrid structures obtained for different generation dendrimers under the same reduction conditions (1:1 loading, slow reduction). The effect of the dendrimer generation on the colloid size is not simple, i.e. For G2, the colloids formed are larger than those obtained with G4. For G6 to G9 the gold diameter increases with increasing generation number. For G10, multiple smaller gold particles per dendrimer are formed. In the following paragraphs we describe the results of the particle characterization and discuss the different structures. In this context, one has to consider how the dendrimer structure itself changes with generation: G2 is a star-like molecule with 16 end groups, G3 to G5 have star-like as well as sphere-like features, and higher generation dendrimers show a spherical structure.³⁷

For G2 and G4 dendrimers, gold colloids of 4 nm and 2 nm diameter, respectively, are detected by TEM as well as by SAXS. In addition, we observe the existence of larger dendrimer aggregates. For the G4 sample these have a well-defined dimension of 7 nm as evident from the pair distance distribution function as well as from our TEM staining experiments. Larger particles obtained with G2 rather than G4 dendrimer are in agreement with recent results from other authors who are studying these lower generation dendrimers as colloid stabilizers.¹²² A schematic of multiple dendrimers attached to one gold colloid was inferred in that work, but not verified experimentally. Small angle scattering and Guinier analysis revealed aggregated structures formed upon colloid preparation using a G4 dendrimer by Beck Tan et al.¹²³ Thus, our results for low generation dendrimers are in agreement with the results of other authors.

The formation of multiple dendrimer aggregates may be understood because for these “small” molecules a single dendrimer cannot provide enough material to stabilize the surface of one gold colloid. In addition, very small metal clusters are less stable, so that colloids from the gold loading of more than one dendrimer are formed. This results in a hybrid structure of a metal colloid surrounded by several dendrimers. The colloid-formation mechanism for these low generation dendrimers is different than for high generation dendrimers. The gold colloids are not formed inside a “pre-existing container”, but the nanostructure organizes only when the colloid is produced chemically. This resembles the concept of double-hydrophilic block copolymers in mineralization.^{124,125} In contrast, the dendrimers are chemically uniform and no complex architectures result. From this point of view, the colloid stabilization can be considered as an analogue to the classical stabilization mechanism with low molar mass molecules like citric acid. The molecules can become attached to the colloid surface and act as stabilizers, but they do not template the colloid.

While the analysis of the G5 hybrid structure proved to be more difficult, for the G6 sample, a gold colloid of about 2 nm diameter is observed, thus the size corresponds to 1:1 loading. However, the dendrimers at least partially aggregate in solution in this case. For G7 to G9, individual dendrimer molecules containing single gold colloid particles are found. The TEM for the G8 sample is shown in Figure 63a. The structure of the hybrid particles corresponds to the G9 sample discussed before. Pair distance distribution functions obtained from SAXS data for G7, G8 and G9 (Fig.10b, solid lines) show the increasing gold colloid size with increasing dendrimer size. The colloid diameters of 2.5 nm, 3.2 nm and 4 nm (within ranges of ± 0.2 nm) agree well with the expected sizes.

The mid-generation dendrimers (G6 to G9) obviously offer the best conditions in terms of a “host-guest nanoscale” synthesis. This may be explained by the fact that their structure provides sufficient polymer to stabilize the surface of the forming colloidal particle, along with enough flexibility for the growth of only one particle from all of the gold ions loaded in the dendrimer. Thereby, the number of gold atoms that build one colloid can be precisely controlled with these dendrimers (“fixed loading law”).

For G10, multiple smaller gold particles inside one dendrimer are observed in the TEM (Figure 63b). In addition, the decreased gold diameter in comparison to the G9 sample is evident in the $P(r)$ function (Figure 64b, dotted line). In general, the growth of a colloid is determined by the free energy of the crystal formation and surface tension. However, when the colloid grows inside a polymeric matrix the elastic forces of the surrounding polymer become important. The growth of a nucleated colloid is limited by the finite extension of neighbouring polymer chains. In this context, one must note that with each generation number G the mass of the dendrimer is roughly doubled, while the size increases only linearly (mass: $M_w \sim 2^G$, radius: $R \sim G$, volume: $V \sim G^3$, compare Table 1). This means, as the generation number increases, the internal dendrimer segment density increases slightly³⁷ and the flexibility of the dendrimer chains decreases. The volume of a single gold nanocluster would double with each generation, yet the space available for its formation would decrease. For the G10 dendrimer, it may be that the

chain flexibility is not sufficiently high to allow for the growth of one colloidal particle. On the other hand, the increased surface to be stabilized for multiple smaller particles is likely to be provided by the G10 dendrimer. From this point of view, the G10 dendrimer still realizes a host-guest nanotemplating, and the different dendrimer structure results in a different colloid morphology. Similarly, in microgels of high cross-linking density only multiple small colloid particles can be formed, while the larger flexibility of lower cross-linking density microgels allows for the formation of continuous structures through the microgel.¹⁰⁶ But for the case of dendrimer nanotemplates, the “fixed-loading law” remains valid. About four 3 nm-gold colloids inside one G10 dendrimer are formed, which is in good agreement with the expected amount of 4096 atoms.

3.1.5 Conclusions

PAMAM dendrimers are shown to be effective as nanotemplates in the formation of inorganic colloids. They not only stabilize the colloidal metal in aqueous solution, but also determine the architecture of the forming nanostructures. G2 to G4 dendrimers behave more like low molecular mass colloid stabilizers, i. E. Several dendrimers become attached to the surface of the metal particle formed. G6 to G10 dendrimers act as effective “polymeric” templates. One colloid particle is completely formed inside one dendrimer, a template mechanism known as “host-guest nanoscale synthesis” or “exotemplating”.¹⁰⁶ For G6 to G9, the size of the inorganic colloid can be precisely controlled by the dendrimer generation without changing the morphology of the hybrid structure. Also, hybrid particles with different morphology can be synthesized in a well-defined manner (G10). To our knowledge, this is the first time such a transition has been shown from colloid “stabilization” by low molecular mass molecules to “polymer nanotemplating” with increase of molecular mass but unchanged chemistry of the stabilizing species.

A detailed study has been presented on the parameters that influence the colloid formation for the reduction of gold salt. With respect to future applications, it is certainly interesting to extend this concept to other chemical reactions leading to different inorganic colloids. For this purpose, we have also synthesized other metal colloids like copper, silver and platinum inside the dendrimers as well as cadmium sulfide nanoclusters, which will be subject of future reports. These examples demonstrate that the dendrimer nanotemplating is not restricted to a specific chemistry, but it represents a fundamental mechanism, which may be widely applied. The inorganic “filled” dendrimers in solution are promising candidates for multiple applications due to the colloidal size of the inorganic crystal, e.g. Specific optical and electrical behaviour caused by quantum size effects, or catalytic activity enhanced by the large surface area. Since the hybrid particles also represent well-defined inorganic colloids in a polymeric matrix, they pave the way to new materials, which combine the mechanical properties of polymers with special colloidal effects. Furthermore, incorporating the gold-dendrimer hybrids further within a polymeric matrix could lead to promising solid composite materials.

3.2 Hydrophobically Modified Dendrimers

3.2.1 Synopsis

Poly(propyleneimine) dendrimers with stearyl end groups are investigated as inverse micelles in toluene. While these dendrimers exhibit a spherical structure with a collapsed core, solubilization of metal salt hydrate leads to the formation of cylindrical multi-dendrimer structures with swollen, metal-salt filled dendrimer cores. The cylindrical structure can be deduced from both small angle neutron (SANS) and x-ray scattering (SAXS) pair distance distribution function. While the neutron scattering leads to a two-step cross section density profile, the x-ray scattering visualizes only the inner, metal-salt-stained part. Chemical reduction was performed on the salt-filled inverse micelles to form colloidal particles. Upon reduction, the cylindrical structure breaks up and spherical colloids are formed. This indicates that the inorganic matter from several dendrimers is combined.

3.2.1.1 Introduction

Higher generation dendrimers appear as homogeneous spheres in solution.²⁰ There is sufficient space available inside the dendrimer molecule that allows them to act as a “host” for smaller guest molecules. Meijer first showed encapsulation of Bengal rose as a guest into the “dendritic box” of poly(propyleneimine) dendrimers modified with amino acids.¹⁰⁷ This observation has motivated a number of further studies and initiated the consideration of a variety of potential applications in areas such as drug delivery, catalysis or gas detection.

The “molecular encapsulation” has been applied to different kinds of dendrimers and modified dendrimers in different solvents: Hydrophobically modified PAMAM dendrimers have been shown to transport copper(II)sulfate from an aqueous solution into an organic phase.¹²⁶ Dendrimers with a fluorinated shell are soluble in supercritical carbon dioxide and can extract an ionic dye from water into supercritical carbon dioxide.³³ Sulfonate-terminated amphiphilic dendrimers with hydrophobic carbosilane cores were demonstrated to enhance the solubility of lipophilic molecules in water.¹²⁷ In all of these experiments, the amphiphilic dendrimer is basically acting as a micelle, or inverse micelle, solubilizing the guest in a solvent of different polarity. Thus a dendrimer may be considered an “unimolecular micelle”.

Several studies on the binding of the guest to the dendrimer-host have been performed by photometric measurements and different kinds of spectroscopy. In this study, we are interested in characterizing the nanoscale structure of dendrimers acting as inverse micelles. We use dendrimers with a hydrophilic poly(propyleneimine) cores which have been modified with hydrophobic chains attached to the dendrimer terminal groups.

We investigate how the structure changes when filling a hydrophobically modified dendrimer with a gold salt hydrate $\text{HAuCl}_4 \cdot 3\text{H}_2\text{O}$ in toluene solution. The use of the gold salt hydrate not only allows for the addition of a very well defined number of water molecules, but also allows study of the structure formed by scattering techniques. The water provides contrast for a small angle neutron scattering (SANS) experiment when using deuterated toluene as solvent, and the gold can provide contrast for a small angle x-ray scattering (SAXS) experiment. Furthermore, the gold salt hydrate can serve as a precursor to investigate if dendrimeric micelles can be used as confined reaction space for the formation of noble metal colloids.

3.2.2 Experimental

Fifth generation (G5) poly(propyleneimine) dendrimers (PPI)⁸ with 64 primary amine groups (DAB-dendr-(NH_2)₆₄) that were modified with octadecanoic acid were provided by DSM.^{58,128} Mass Fraction 1% solutions of G5 fatty acid modified dendrimer were prepared at 55 °C in toluene. The desired amount of $\text{HAuCl}_4 \cdot 3\text{H}_2\text{O}$ is added as a solid salt and the solution is gently stirred at 55 °C resulting in a clear yellow solution. For SANS experiments, deuterated toluene is used as solvent. Reduction of the gold is performed by addition of a solution of sodium borohydrate in diglyme.

Samples for SANS measurements were transferred into optical quality quartz banjo cells with 1 mm path length. SANS studies were performed at the National Center for Neutron Research at the National Institute of Standards and Technology. Measurements were made using the 30 m SANS instrument with a neutron wavelength $\lambda = 0.6$ nm and wavelength spread of $\Delta\lambda/\lambda = 0.15$. All measurements were performed at 55 °C.

SAXS data were collected at the Advanced Polymer Beamline at Brookhaven National Laboratory, X27C in the normal manner. The span of scattering vector magnitudes was in the range $0.15 \text{ nm}^{-1} < q < 3.2 \text{ nm}^{-1}$. All measurements were performed at 55 °C.

The scattering curve $I(q)$ is Fourier transformed into the pair distance distribution function $P(r)$ using the program ITP (*Indirect transformation for the calculation of $P(r)$*) by O. Glatter,¹¹⁶⁻¹¹⁸ which includes smoothing of the primary data by a weighted least square procedure (estimation of the optimum stabilization parameter based on a stability plot), desmearing and transformation into real space by the indirect transformation method with minimized termination effects. For the SANS measurements, we include desmearing by the wavelength distribution of the incident beam as well as the measured beam profile. For the SAXS measurements, the wavelength distribution $\Delta\lambda/\lambda$ is smaller than 1 % and the beam is focused via a pinhole collimation system to (100 to 200) μm diameter. Therefore smearing effects are not accounted for in case of the SAXS data analysis.

Scattering-length-density and electron-density profiles are calculated from the pair distance distribution function $P(r)$ by calculation of the convolution square root

(“deconvolution”) using the program DECON by O. Glatter.¹²⁹⁻¹³¹

Carbon coated copper grids, 300-mesh, were extensively washed in chloroform reflux in order to remove formvar. Specimens were prepared by depositing the sample solutions on the grid and drying in air at 55 °C. TEM images were obtained at 120 kV with a Phillips 400T at a magnification of 46000 X.

3.2.3 Results and Discussion

3.2.3.1 Structure of Inverse Micelles

When stirring solutions of hydrophobically modified poly(propyleneimine) dendrimer over solid $\text{HAuCl}_4 \cdot 3\text{H}_2\text{O}$, the color of the solution turns yellow, indicating the solubilization of the gold salt in the dendrimers. We have prepared samples with an excess of gold salt as well as samples with controlled stoichiometries of gold salt. The maximum amount that is completely dissolved in the toluene solution corresponds to a stoichiometric ratio of gold salt to dendrimer terminal amine groups (64 per dendrimer-molecule) of 1:1. In addition, the UV absorption of the gold salt in different solutions agrees with the saturated and the 1:1 loaded solution. Solutions with loading ratios 1:2, 1:4 and 1:8 show a smaller absorption.

The scattering results from a sample with a maximum load of gold salt, i.e. A molar ratio of 1:1 to dendrimer end groups are shown in Figure 65. It shows the SANS scattering curve for the initial plain dendrimer and the SANS and SAXS scattering curves after solubilization of gold salt. Diagrams are also given which show the areas of high contrast in the dendrimers for the different scattering experiments.

The initial dendrimer exhibits a spherical structure. The radius of gyration for the scattering curve shown is 2.2 nm. This is in agreement with previous reports on the single-chain form factors of the fatty acid and the dendrimer components of these hydrophobically modified dendrimers⁵⁸ and their size in different solvents at different temperatures.³ The size of the dendrimer measured under these conditions is for a collapsed dendrimer core plus a fatty acid shell.

The neutron scattering curve for the sample after addition of gold salt hydrate shows a shift of the first minimum to lower scattering vector, q , i.e. The size of the structure increases, Figure 66. This is due to the swelling of the dendrimer upon solubilization of the gold salt hydrate. In addition, the shape of the scattering curve also changes. In order to analyze the structure of the gold-filled dendrimers in more detail, we Fourier transform the scattering curve $I(q)$ into the pair distance distribution function $P(r)$, which is shown in Figure 67. The $P(r)$ shows a shape typical of a cylindrical structure. The diameter of the cylinder is about 6 nm (inflection point after the maximum), while the length of the cylinder, i.e. The largest correlation found, is about 21 nm. The 21 nm dimension corresponds to the smallest q measured and could possibly represent an experimental limit. However, the fit of the data is stable and the error bars of the calculated $P(r)$ do not dramatically increase for higher r -values, so that we consider

21 nm a good estimate for the length of the cylinder. While the cylinders might in fact be longer, the scattering results clearly show that they are not shorter than 21 nm. In addition, some polydispersity in average length cannot be excluded. Most importantly, the scattering result shows the existence of a cylindrical structure in solution, which has to result from an aggregation of multiple dendrimers, since the length is clearly larger than the diameter of one dendrimer.

Since the data gives conclusive evidence of the cylindrical structure from the $P(r)$, we can now assume cylindrical geometry as input for further calculations. We repeat the Fourier transform of the scattering curve from Figure 67, this time using the zero-order Bessel function $J_0(qr)$ -transformation instead of the $\sin(qr)/(qr)$ -transformation used before, and thereby calculate the cross-section pair distance distribution function $P_c(r)$ of the cylinder. The result is shown in Figure 68. From this, a better estimate of the diameter can be made, giving 6.4 nm. In addition, the shape of this cross-section $P(r)$ roughly indicates a circular cross section. Furthermore, we deconvolute this cross-section pair distance distribution function into a radial scattering length density profile of the cylinder. First, we allow a multiple step density profile. The resulting radial profile is shown in Figure 68 as the dotted line. Secondly, we estimate from this multiple step profile how many actual steps are present in the density profile and the range in which they are located. We then calculate the radial density profile again, under the assumption of a one-step, a two-step and a three-step profile, respectively, looking for the simplest solution that gives the best fit to the cross-sectional $P(r)$. The result is shown in Figure 69 as solid line. We find two pronounced steps in the radial density profile: an inner part with a radius of 1.9 nm, plus an outer shell of 1.3 nm thickness. The total diameter is 6.4 nm. The resolution of the fit values due to the limited q range measured is expected to be within the range of ± 1 nm .

The measured two-step density profile of the cylinder cross-section can be interpreted as a swollen dendrimer core plus a fatty acid shell. The diameter of the “swollen dendrimer” of 3.8 nm is in agreement with previous measurements on G5 polypropyleneimine dendrimer (without fatty acid chains attached) in aqueous solution.²⁰ The thickness of the fatty acid shell is also in agreement with the length of C₁₈-alkyl chains. Since the hydrogen-containing dendrimer is filled with aqueous salt-hydrate, the contrast of the inner core is higher than the contrast of the outer shell.

In order to further confirm the cylindrical structure, we have performed SAXS on the same sample. In the x-ray experiment, only the inner gold-containing core gives contrast, since the electron density difference between the fatty acid chains and the toluene is relatively small. The scattering curve and resulting pair distance distribution function are shown in Figure 70 and Figure 71, respectively. Again, the $P(r)$ reveals a cylindrical structure. The diameter estimated is 4 nm, while the length is 20 nm. The cross-section pair distance distribution function is given in Figure 71 and the cross-section density profile in Figure 72. One obtains a one step-profile, the diameter of the cylinder being confirmed as 4 nm. This corresponds well to the gold-salt filled inner part of the cylindrical structure, i.e. The first step of the neutron density profile from Figure 67.

Figure 73 displays a schematic of the multi-dendrimer cylindrical structure that has been deduced from the SANS and SAXS.

It is interesting to consider the approximate relative volumes in the dendrimer-nanostructures. A G5 poly(propyleneimine) dendrimer, having a molecular mass of 7166 g/mol, having a density of 1.01 g/mL, has a volume of 11.8 nm³, i.e. In a collapsed spherical state a radius of 1.4 nm in agreement with the experimental results. As mentioned before, an amount of gold salt to dendrimer end groups of 1:1 was added, i.e. 64 molecules of HAuCl₄·3H₂O, which means 192 water molecules, were solubilized per dendrimer molecule. These 192 water molecules have an additional volume of 5.74 nm³.

If the analogy of the hydrophobically modified dendrimers to surfactant micelles is valid, then the same factors may determine the phase behaviour. The relative volume of the inner hydrophilic part and the outer hydrophobic part, or more accurately the ratio of the surface area of the dendrimer end group to the volume of the inner part, may determine whether spherical or cylindrical structures are formed. Upon solubilization, the volume of the hydrophilic part increases, i.e the ratio of surface area to volume decreases and cylindrical structures are favored. To confirm of this postulate, however, different samples with a variation of these parameters would be needed.

As mentioned before, we have also prepared samples with different loading ratios. The SANS curves from the saturated and the 1:1 filled sample are the same as would be expected from the UV-vis results which give similar spectra. However, it was not possible to perform the SANS measurements on the samples that had less than stoichiometrically loading, since the ions became reduced when exposed to the neutron beam for a time period needed to perform the scattering measurement. It is known that gold salts can be easily reduced when exposed to x-ray or neutron beams. Why the samples with less gold salt are less stable than the 1:1 loaded, is not apparent. An investigation of the influence of the loading ratio on the structure formed should be possible if metal salts of less noble metals are used, which is an issue that will be addressed in future studies.

3.2.3.2 Use of Dendrimeric Micelles as Confined Reaction Space

Although the poly(propyleneimine) dendrimers are not unimolecular micelles when filled, but rather consist of multiple dendrimers, the expression emphasizes the difference from classical surfactant micelles. Due to the highly branched structure of the inner core, the dynamics are different from those of conventional micelles. Block-copolymer micelles have been claimed to have advantages over low-molecular mass surfactant based micelles for use as a confined nano-scale reaction space, not only because of the larger size range covered, but also due to the different dynamics of the system. Due to the slower exchange of surfactant molecules, the stability of the nanoreactor is enhanced. This feature is obviously further improved in a “unimolecular” or “few-molecular” dendrimeric micelle, which should therefore be an interesting new system for use as a potential nanoreactor. This approach has been recently used with

inner-crosslinking of block-copolymer micelles, after the micelles have formed, but prior to their use as a nanoreactor.

We have therefore tested the use of dendrimeric “few-molecular” micelles as a confined reaction space for the reduction of gold salt. Upon addition of reducing agent, the solution turns purple, indicating the formation of colloidal gold. No macroscopic precipitate is observed. The SANS curve of the reduced sample is shown in Figure 74 and a TEM of the gold colloids is shown in Figure 75. As is evident from the shape of the scattering curve and the TEM, reduction of the gold salt yields spherical dendrimer structures and spherical gold particles. This can be due to the density difference of the reduced gold compared to the gold-salt hydrate. For all of the reducing methods tested, the gold colloids are bigger than expected when formed within one dendrimer. This may be explained by the intermediate connection of dendrimers in the gold salt-filled structure. Thereby, the amount of gold salt from multiple dendrimers is combined, forming one colloidal particle.

All experiments described previously have been performed at 55 °C, since the fatty acid modified dendrimer is not soluble in toluene at lower temperatures. When cooling the gold-colloid containing solution to room temperature, the gold precipitates with the dendrimer, as can be seen from the purple color of the precipitate, while a clear toluene solution remains. This observation proves that the gold colloids are indeed connected to the dendrimers. It also allows for an easy separation of the hybrid material from the solvent. The precipitate can be easily redissolved in toluene when re-heated to 55 °C.

Although the hydrophobically modified dendrimers form cylindrical structures when filled with gold salt, these cylinders cannot be used as template for the formation of cylindrical metal particles. This is in agreement with experiments on the use of cylindrical micelles or hexagonal morphologies as confined reaction spaces. However, we consider the large gold particles produced by the reduction as a further evidence of the intermediate cylindrical connection of multiple dendrimers.

3.2.4 Conclusion

The structure of poly(propyleneimine) dendrimers modified with stearyl end groups in toluene changes from mono-molecular spherical dendrimers to cylindrical multi-dendrimer structures when filled with gold-salt hydrate. Upon reduction of the gold salt to metallic gold, spherical gold colloids are formed and the cylindrical structure splits up. Small angle neutron scattering and small angle x-ray scattering have been used as a powerful tool for the characterization of the solution-structures.

The dendrimer-gold hybrid particles may have certain properties that could allow for them to be incorporated into other polymer systems, or their use as selective catalysts. Although the volume change upon reduction of gold is large, other reactions leading to inorganic materials of lower density could eventually be performed without destruction of the multi-dendrimer cylinders. This issue will be investigated in future studies.

Factor	Question	Application	SANS	SAXS	TEM
Segment Distribution	Uniform or Diffuse?	Solubilization	+	++	+
Type of Branching	Important Differences?	Major Cost Differences	+	+	+
Terminal Group Location	Surface or Interior?	Attachment Networks	++	+	-
Dendrimer-Dendrimer Interactions	Interpenetration or Collapse?	Ordering Nanostructures	+	++	+
Size Variation with Solvent	Large Changes of Stable Size?	Standards Release	+	+	-

Table 1 Major technological issues. Key to symbols, ++, best technique for measurement; +, acceptable technique for measurement; -, unsuitable for measurement.

	Dendrimer	Dendrigrraft	Hyperbranched
Interior Branching	High	High	High
Terminal units	Small	Linear Chains	Small
Molecular Mass Distribution	Narrow	Narrow	Broad
Shape – Low Generation	Dense Star	Star-like	Polydisperse, Diffuse
Shape – High Generation	Dense Sphere	Uniform Center Star-like Exterior	Polydisperse, Diffuse
Synthetic Steps	4-20	2-5	1
Purification Steps	4-20	2-5	0
Cost	Very High	Moderate	Low

Table 2 Comparison of different dendritically branched polymer types, see Figure 7.

Generation	Branches		Graft Polymer		
	M_n (g/mol)	M_w/M_n	M_w (g/mol)	$f_w(\text{tot})$	Branching Density
0	4,300	1.03	5.7×10^4	12	0.25
1	4,600	1.03	5.7×10^5	120	0.20
2	4,200	1.04	3.2×10^6	720	0.11
3	4,400	1.05	2.4×10^7	5200	0.15

Table 3 Characteristics of Arborescent Polymers with 5000 g/mol Branches

	M_w / M_n	M_w	M_n
D-PS	1.03	4300	4170
	1.03	26600	25800
	1.51	102900	68100
	1.04	244000	235000
	1.05	424900	404700
D-PVME	2.05	8280	4040

Table 4. Characteristics of deuterated polystyrene and deuterated poly(vinyl methyl ether).

Measurement Method	G6	G7	G8	G9	G10	G11
The average size in IPN from TEM (Average in Image)			9.6 ± 0.4	11.7 ± 0.8	14.7 ± 1.6	
The average size in IPN from TEM (FFT of Image)			9.5 ± 1.0	12.2 ± 1.2	14.3 ± 1.4	
The average size in IPN from SAXS (low concentration)		8.0 ± 0.8	9.6 ± 1.0		13.7 ± 1.4	
The average size in IPN from SAXS (mass fraction 10 %)	5.9 ± 0.6				11.4 ± 1.1	13.4 ± 1.3
The average size on a surface from TEM	6.9 ± 0.5	8.0 ± 0.7	10.2 ± 0.8	12.4 ± 0.5	14.7 ± 1.1	
The average size in methanol from SAXS	7.3 ± 0.7	8.4 ± 0.8	10.0 ± 1.0	11.8 ± 1.2	14.0 ± 1.4	15.5 ± 1.6

Table 5. Diameter of G6 – G11 PAMAM dendrimers in methanol solution and in IPN's as measured by SAXS and TEM at mass fraction 1 % and 10 %.

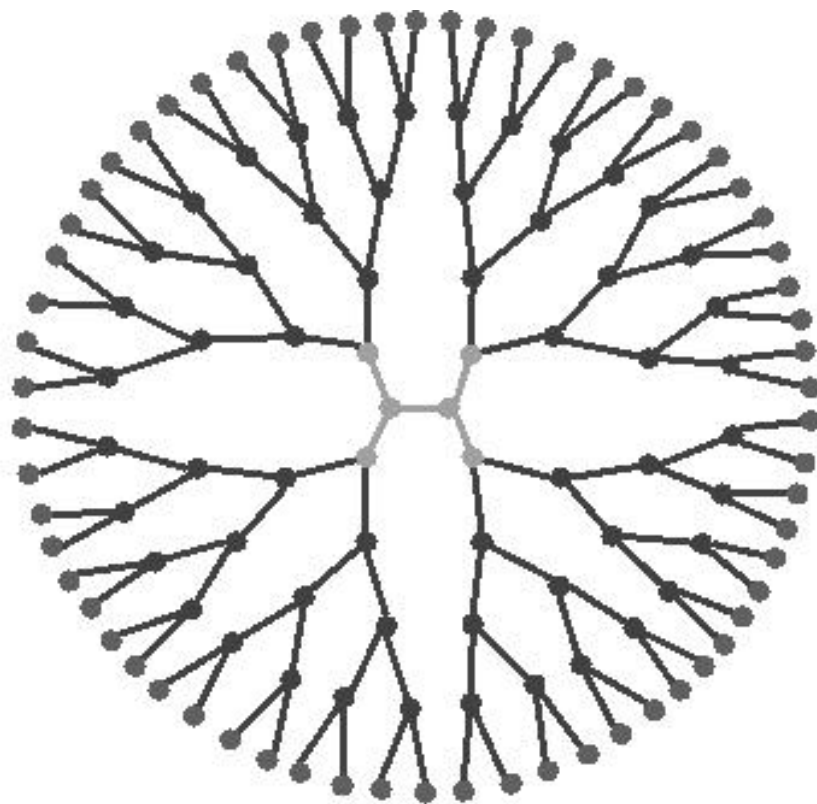


Figure 1 Classical dendrimer cartoon showing core, branch points and terminal groups.

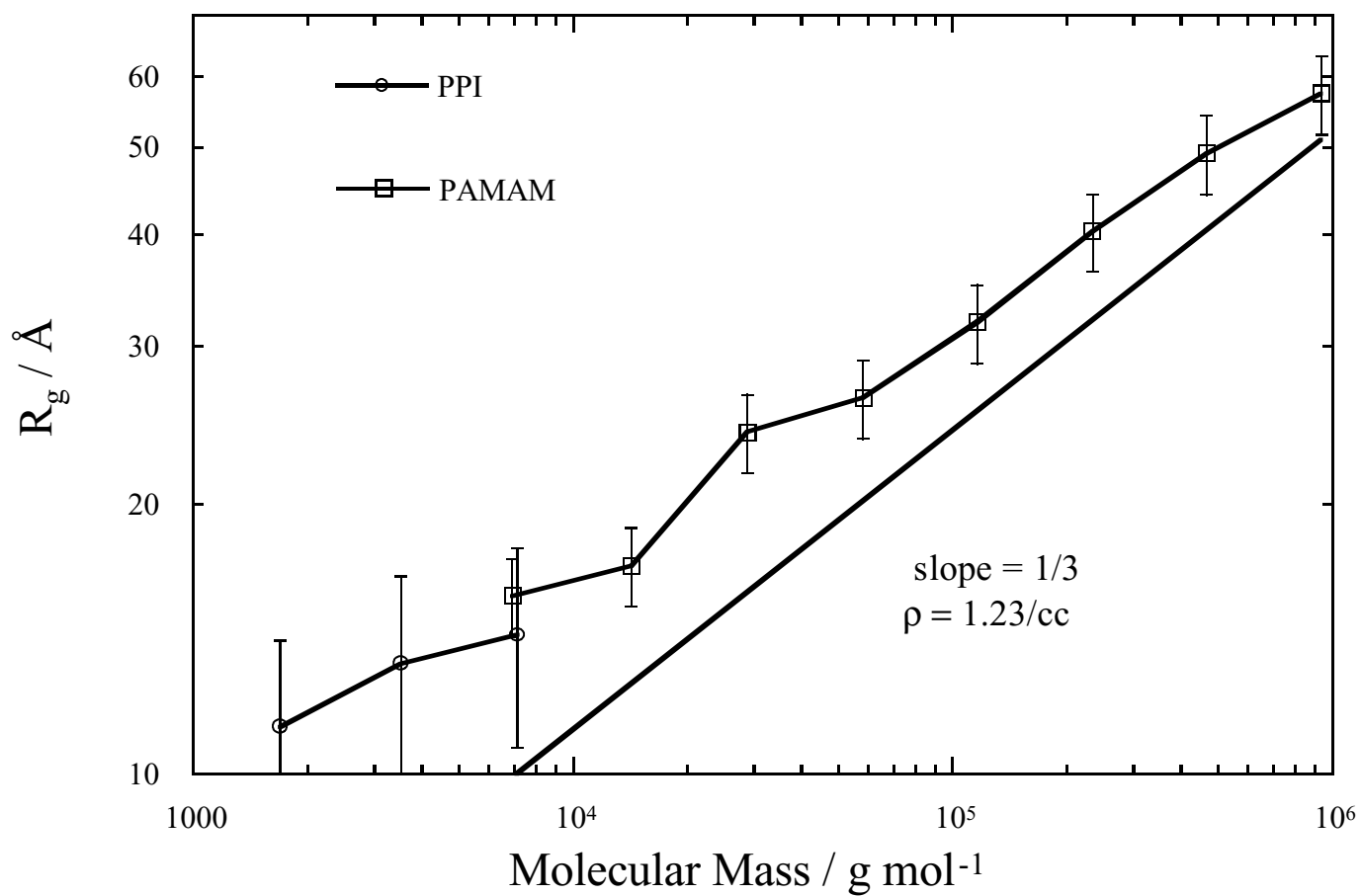


Figure 2 SAXS R_g of PPI and PAMAM dendrimers. Straight line is the limit of PAMAM dendrimers collapsed to bulk density. The 1/3 power law suggests uniform spherical shape.

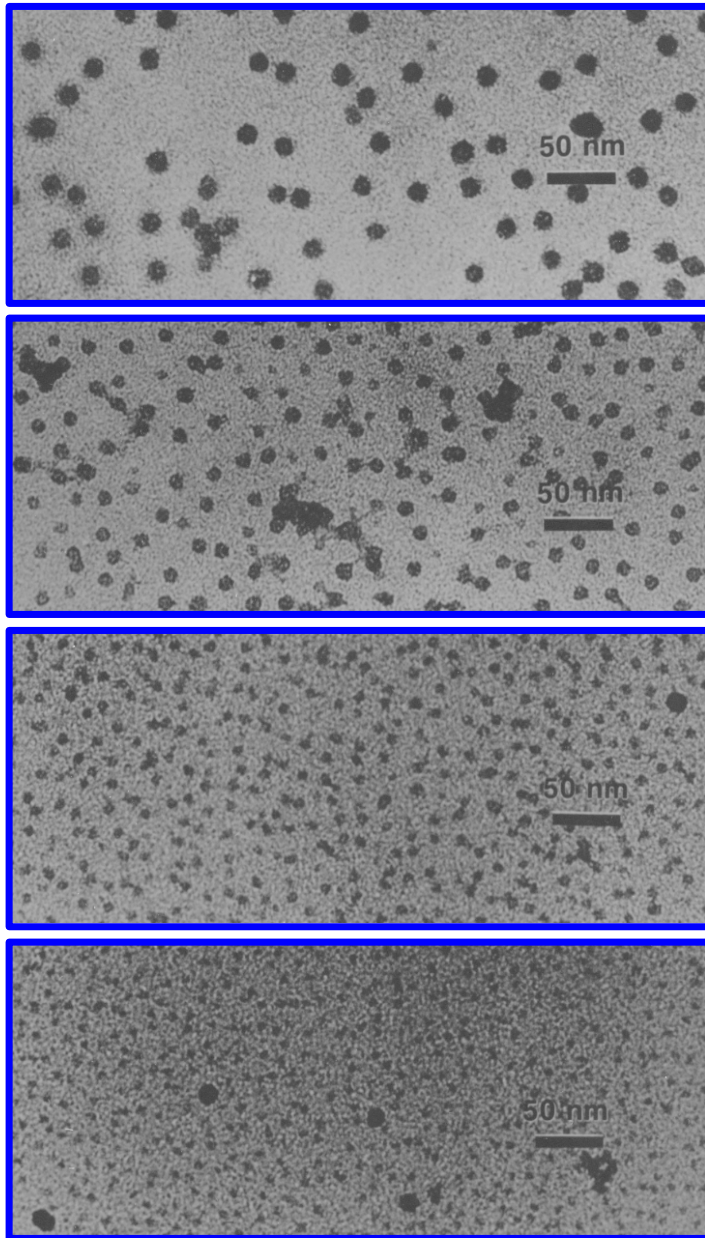


Figure 3 TEM of G5, G6, G8, and G10 PAMAM dendrimers. Individual molecules are seen.

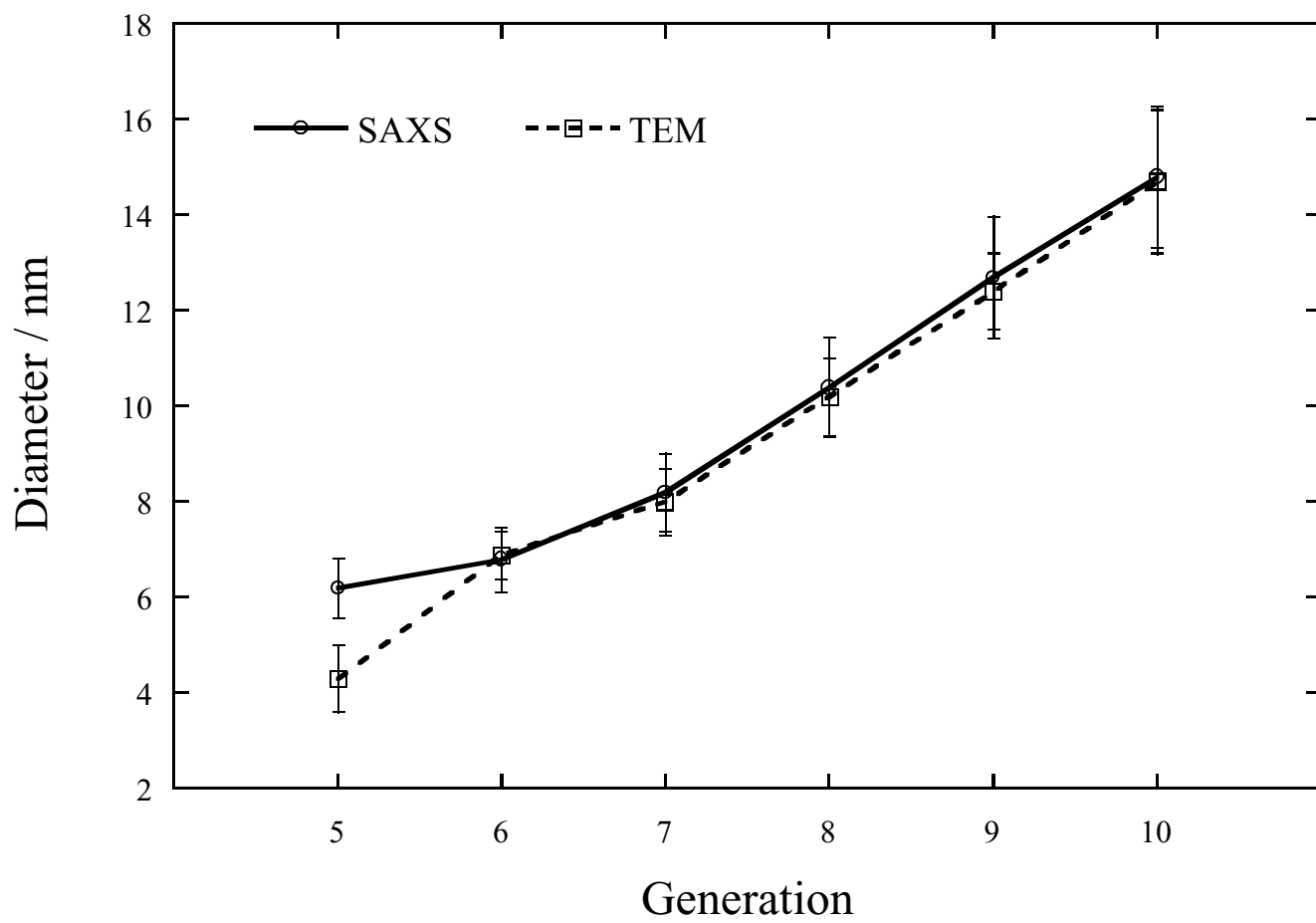


Figure 4 PAMAM dendrimer diameter from SAXS and TEM.

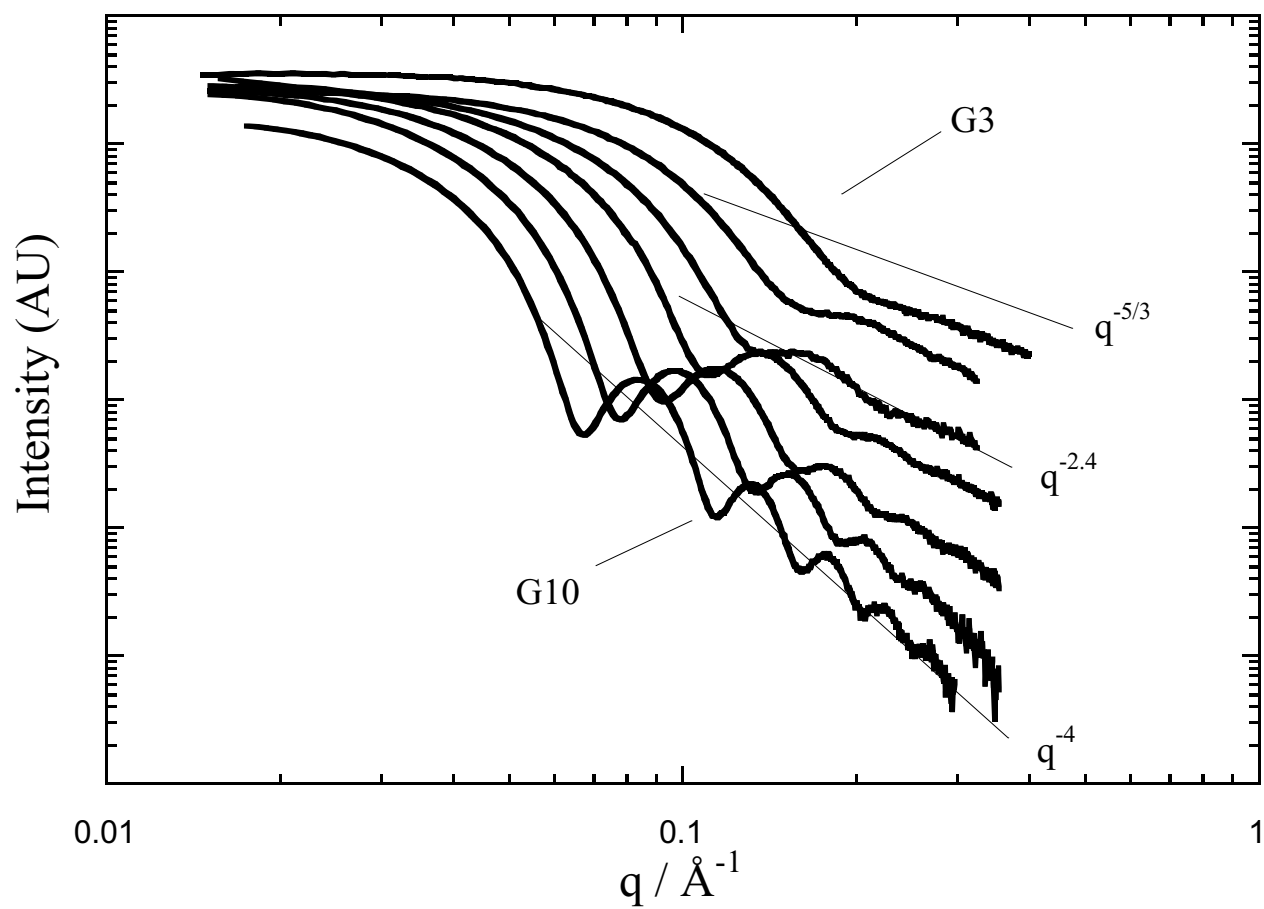


Figure 5 SAXS curves for PAMAM mass fraction 1% dendrimer/methanol solutions of generation G3 (top) through G10 (bottom). Power law behavior continuously varies from $-5/3$ to -4 .

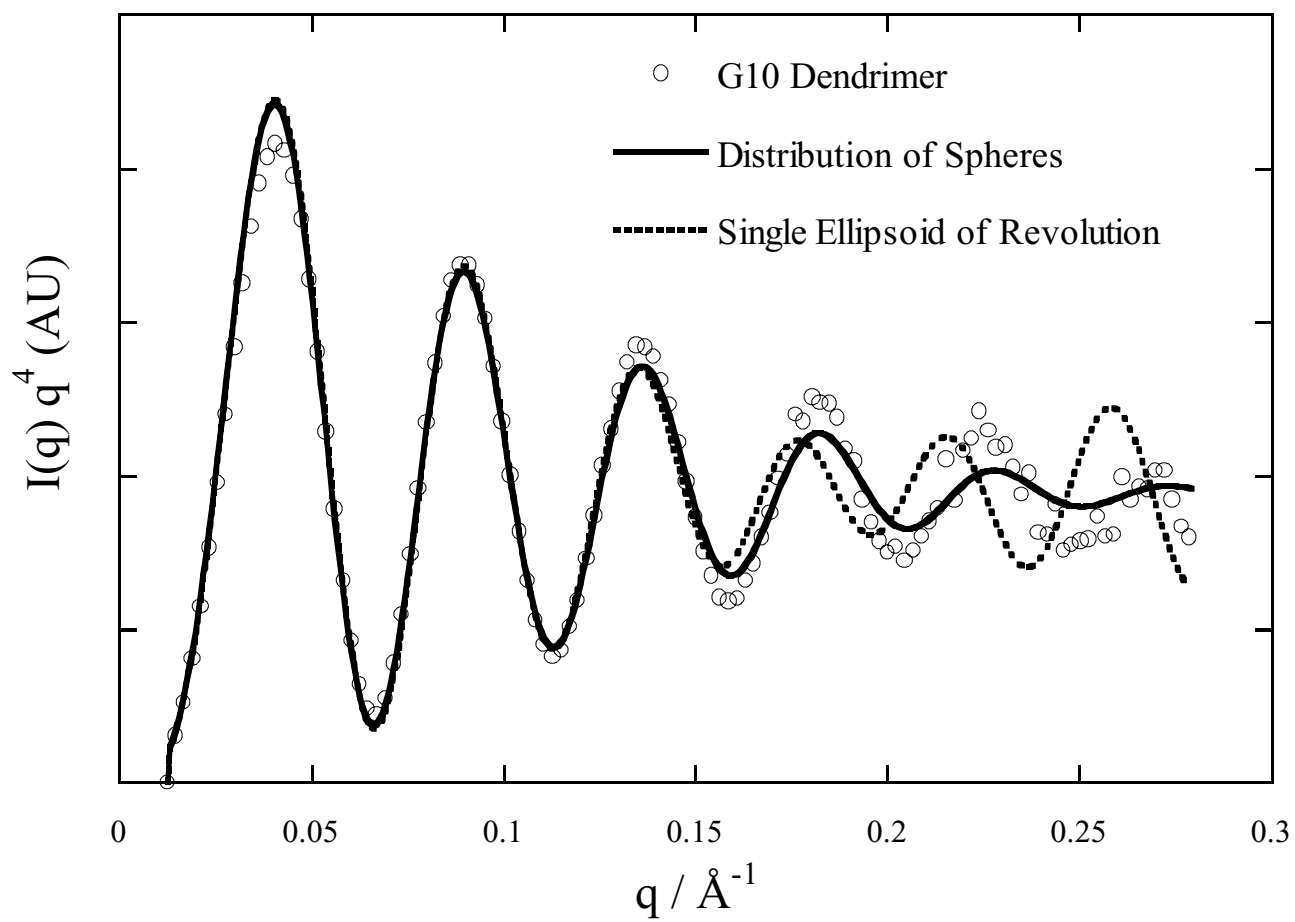
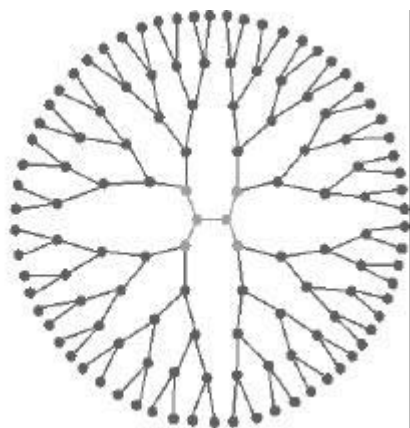
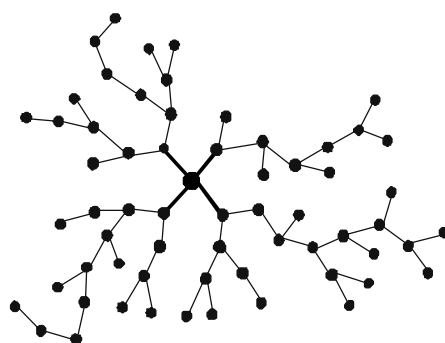


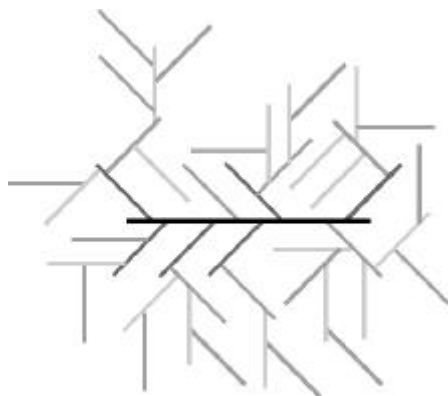
Figure 6 Fits of the G10 PAMAM dendrimer data to a distribution of spheres and a single ellipsoid of revolution



a) Dendrimer



b) Hyperbranched



c) Dendrigraft

Figure 7 Cartoons representing dendritically branched polymers listed in Table 2

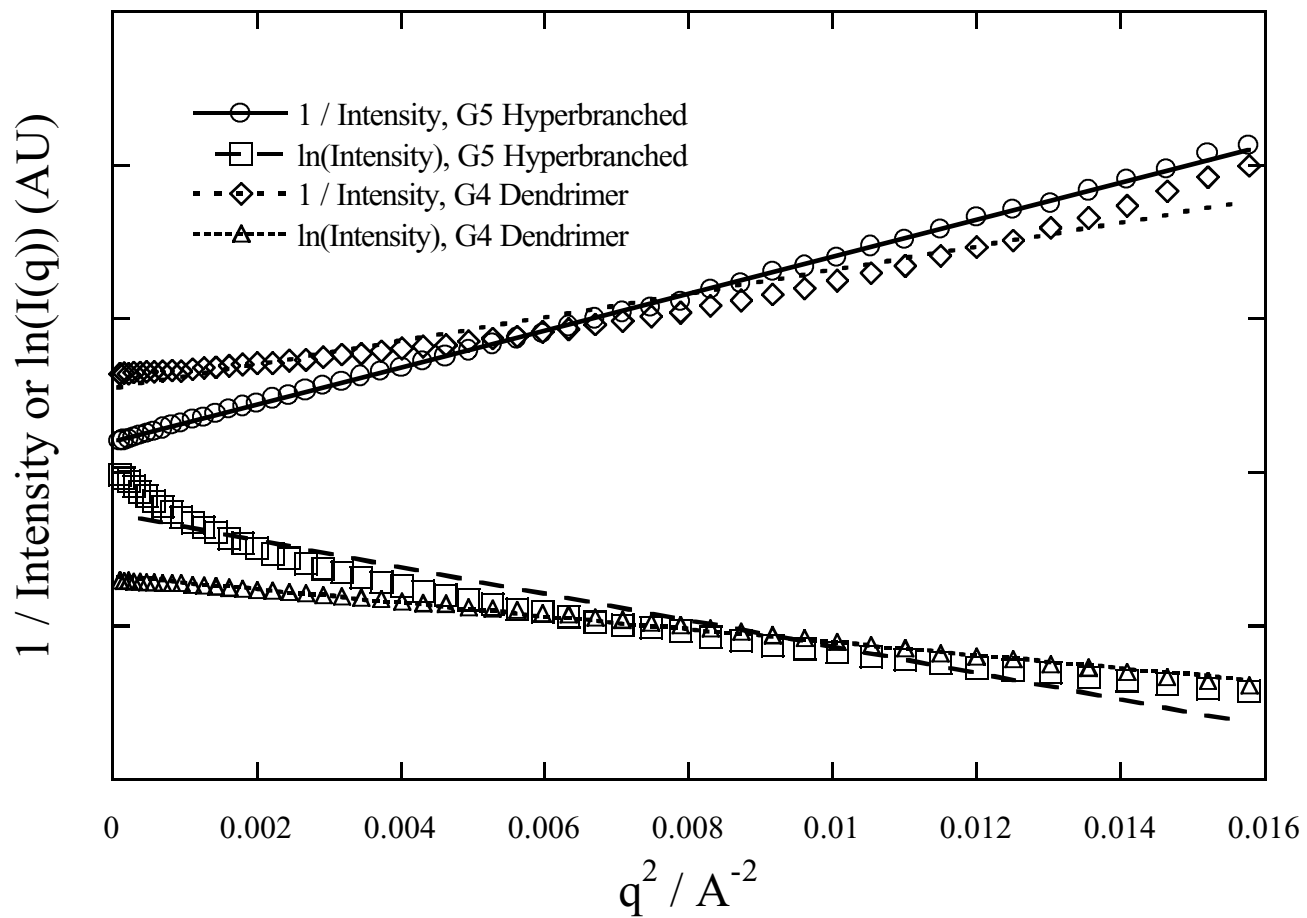


Figure 8 Zimm and Guinier plots of G4 PAMAM dendrimer and G5 hyperbranched polyol. The dendrimer fits Guinier (Spherical) and the hyperbranched fits Zimm (Gaussian).

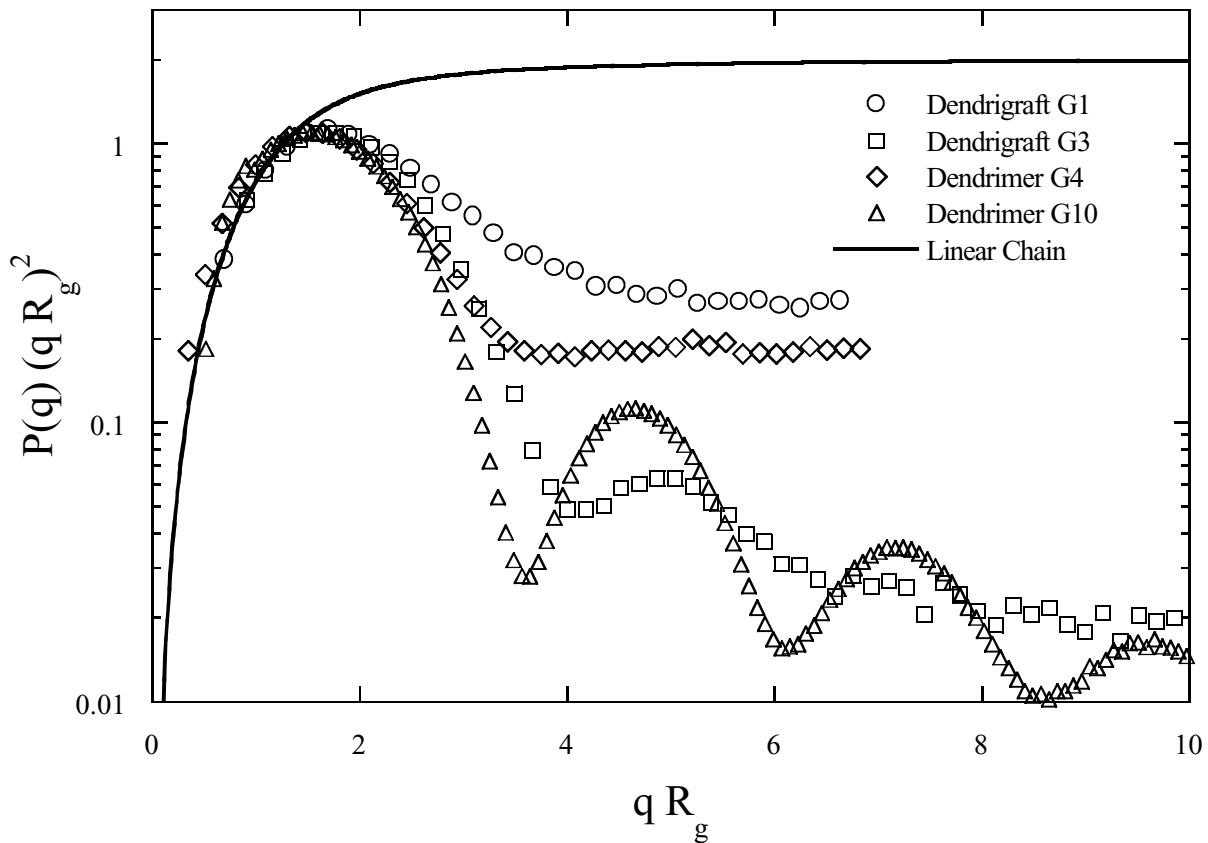


Figure 9 Kratky plots of G1 PS dendrigraft, G3 PS dendrigraft, G4 PAMAM dendrimer, and G10 PAMAM dendrimer. . Flat high q shows star-like structure, higher order features shows sphere-like structure.

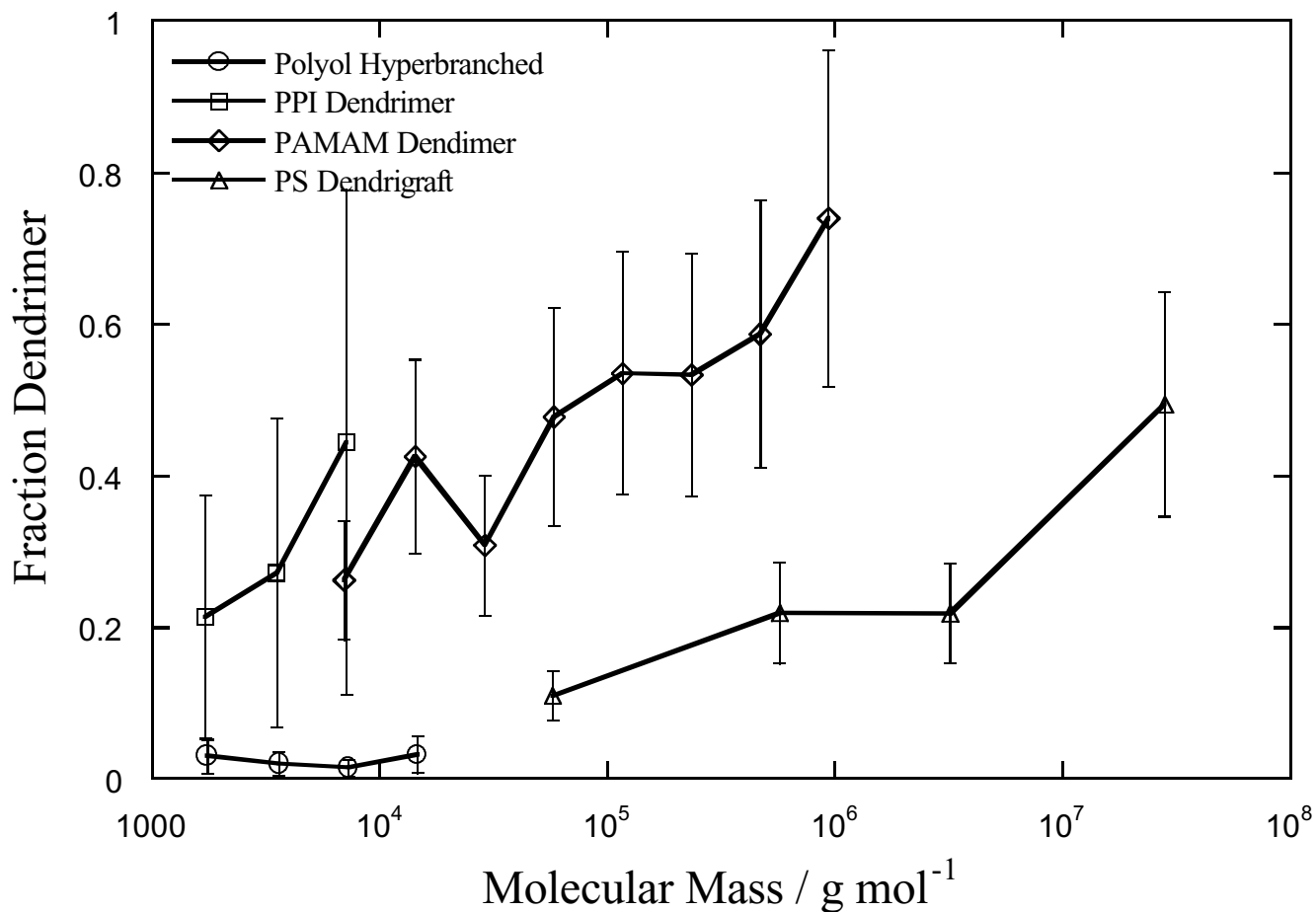
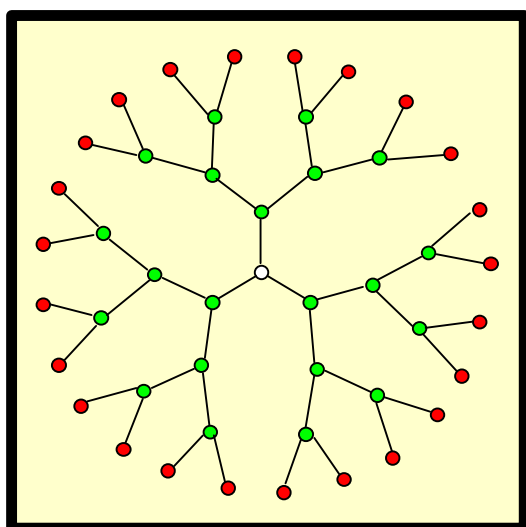
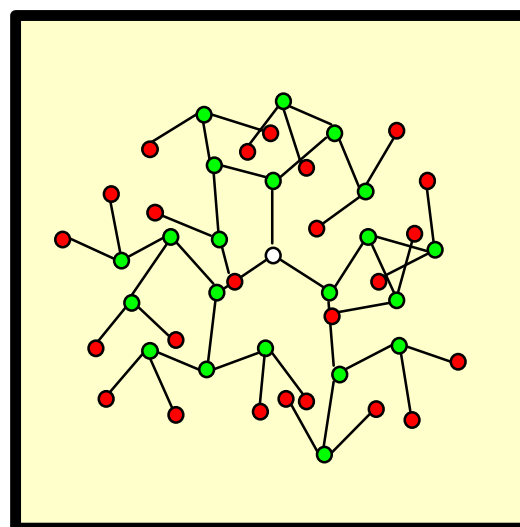


Figure 10 Volume fraction interior polymer segments in dendrimer solution. PPI dendrimer in methanol, PAMAM dendrimer in methanol, hyperbranched polyol in methanol, and PS dendrigrraft in cyclohexane.



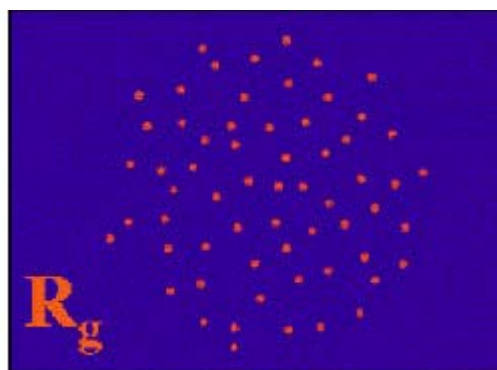
a) End groups – Outside



b) End groups Backfolded



c) Contrast Match – Outside



d) Contrast Match - Backfolded

Figure 11 Cartoon of possible end group locations. A) whole dendrimer end groups outside, b) whole dendrimer end groups backfolded, a) matched dendrimer end groups backfolded, a) matched dendrimer end groups backfolded. Outside end groups have a larger R_g .

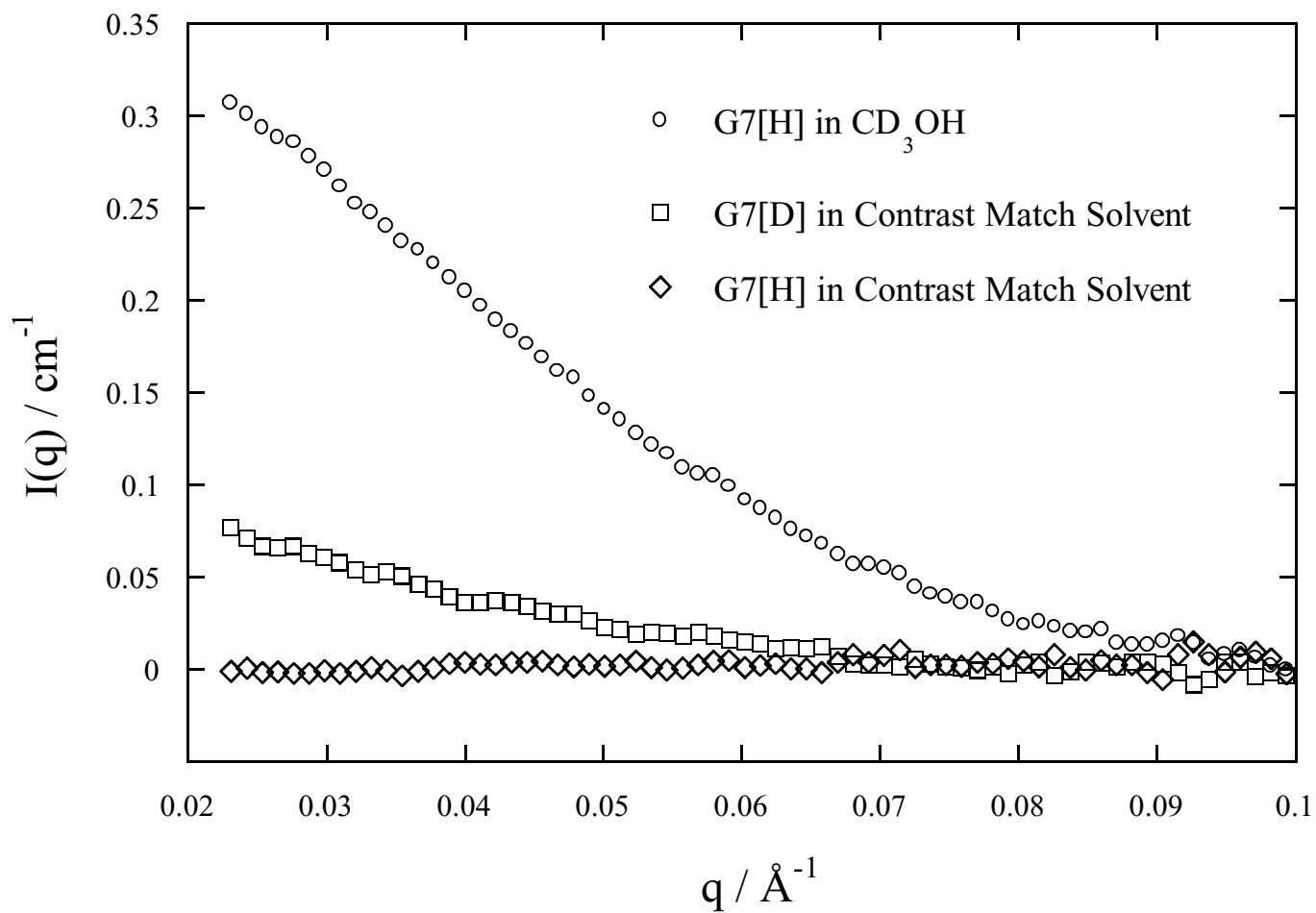


Figure 12 SANS of G7(H) in CD_3OH , G7(D) in contrast match methanol, and G7(H) in contrast match solvent. Labeled dendrimer in core match solvent shows scattering from labeled terminal generation.

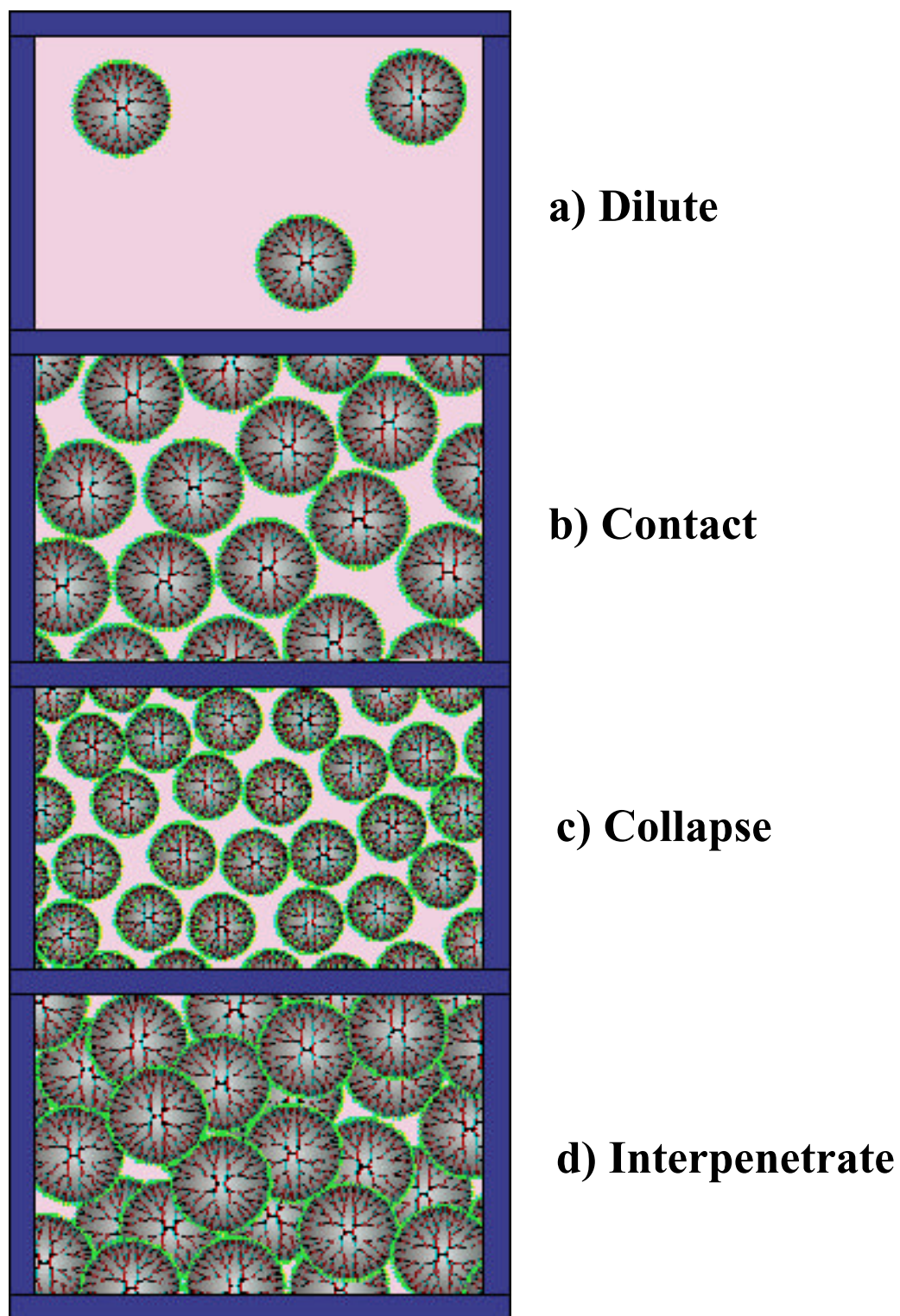


Figure 13 Cartoon showing dendrimers at different concentrations.

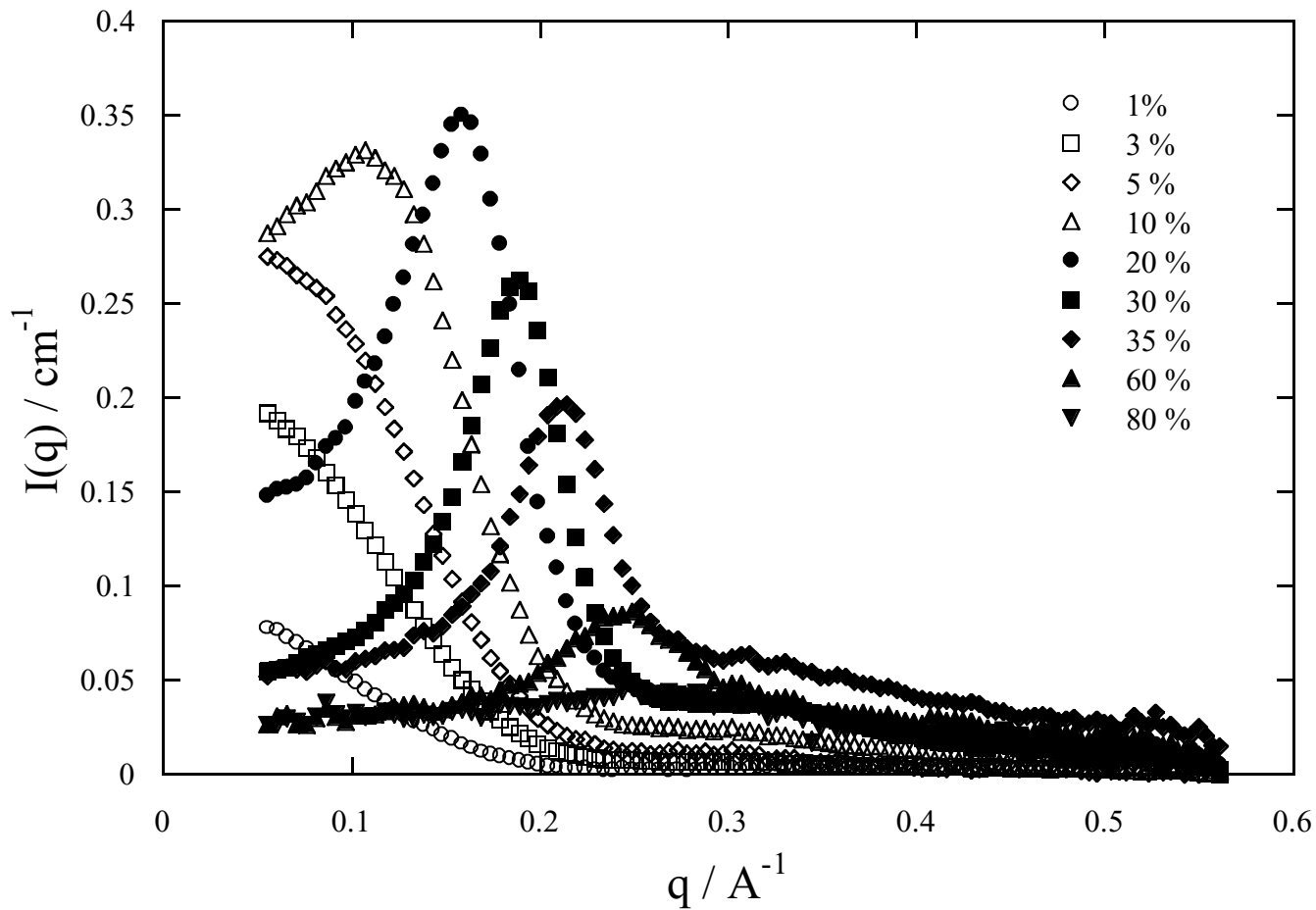


Figure 14 SANS of G5 PPI dendrimer at various mass fractions. Peaks move to higher q (smaller separation distance) with increased concentration.

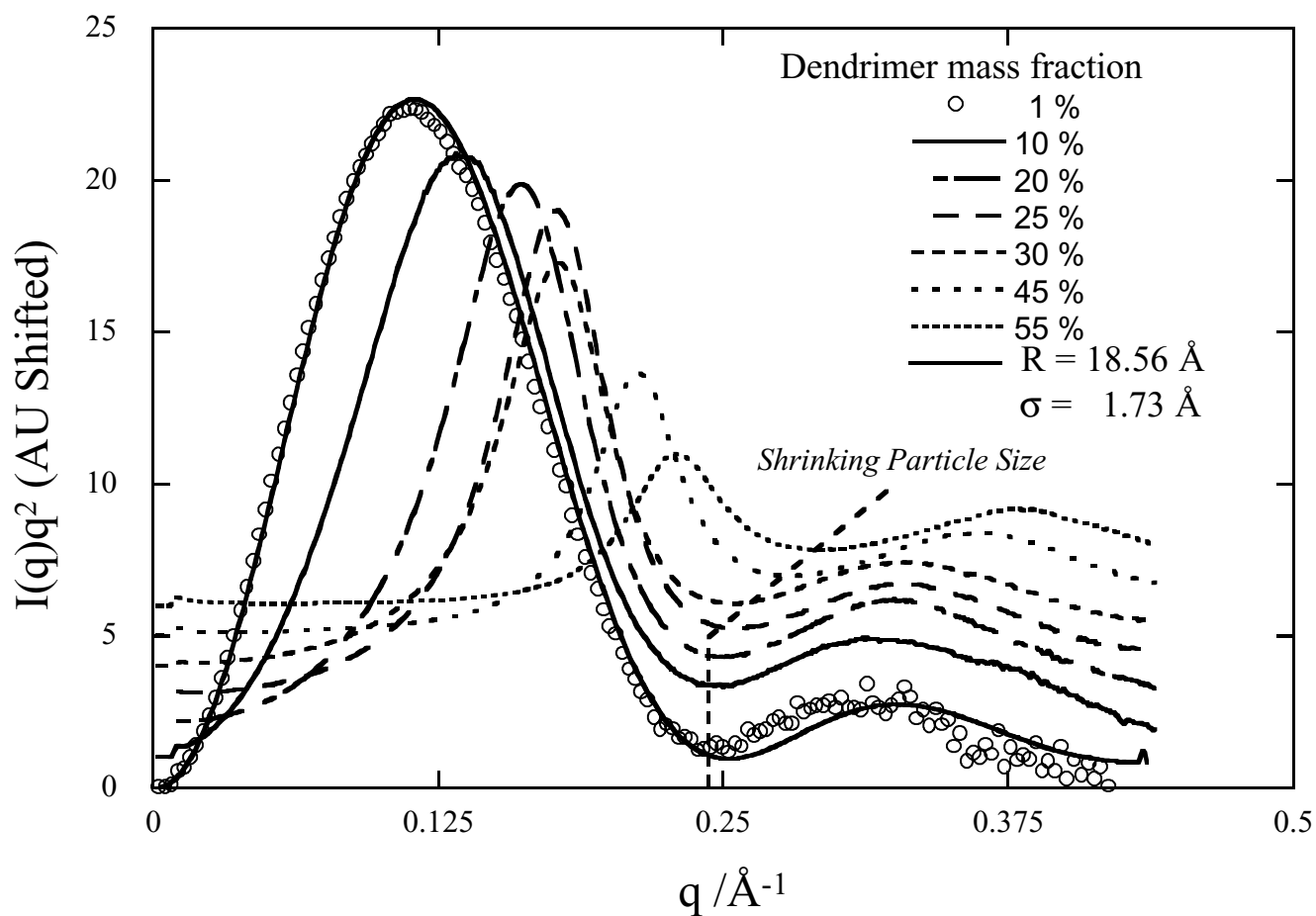


Figure 15 Kratky plot of SAXS of G5 PPI dendrimer at various mass fractions. Higher order feature moves to higher q suggesting shrinkage with increased concentration.

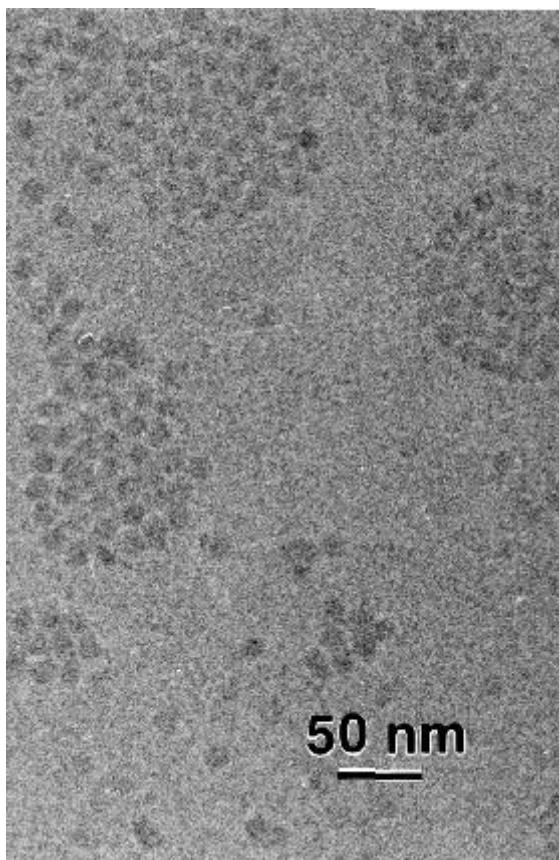


Figure 16 TEM of aqueous PAMAM G10. Note dendrimers are touching but not interpenetrating.

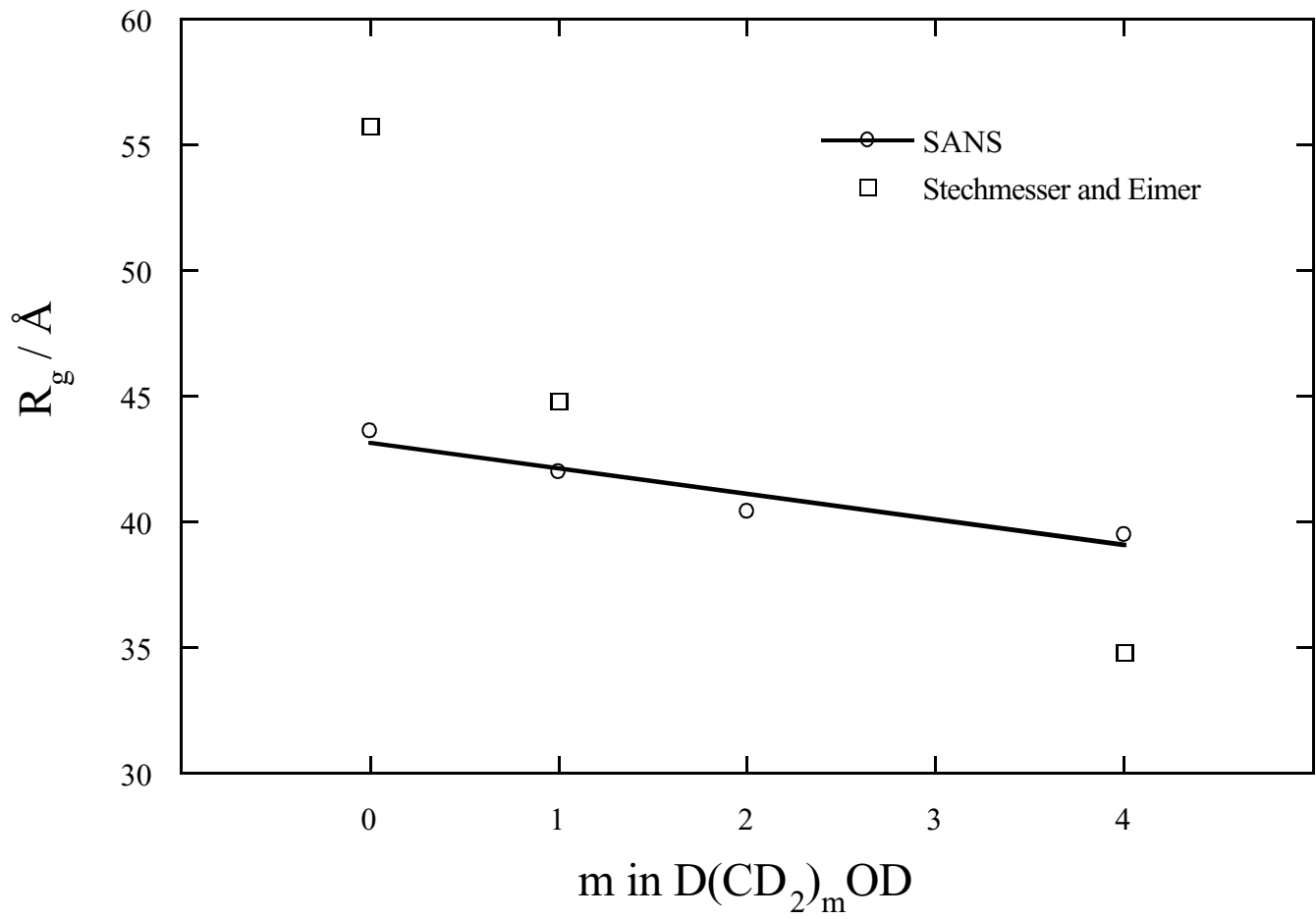


Figure 17 R_g of G8 PAMAM dendrimer in alcohol of various types from SANS. R_g of G8 PAMAM dendrimer calculated from HRS results in reference.⁵²

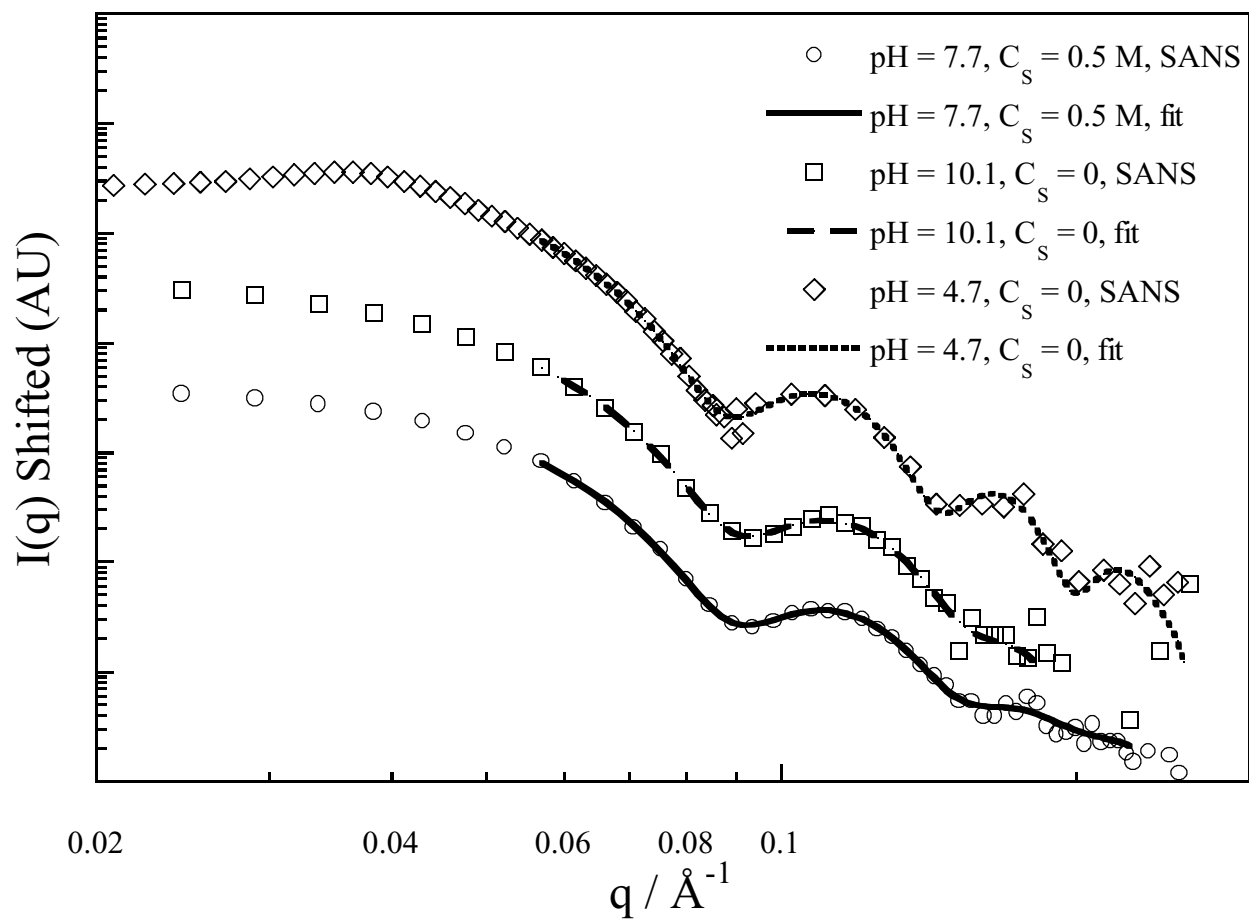


Figure 18 SANS from G8 PAMAM dendrimer with and without acid and salt additions. Note constant position of higher order features showing constant size.

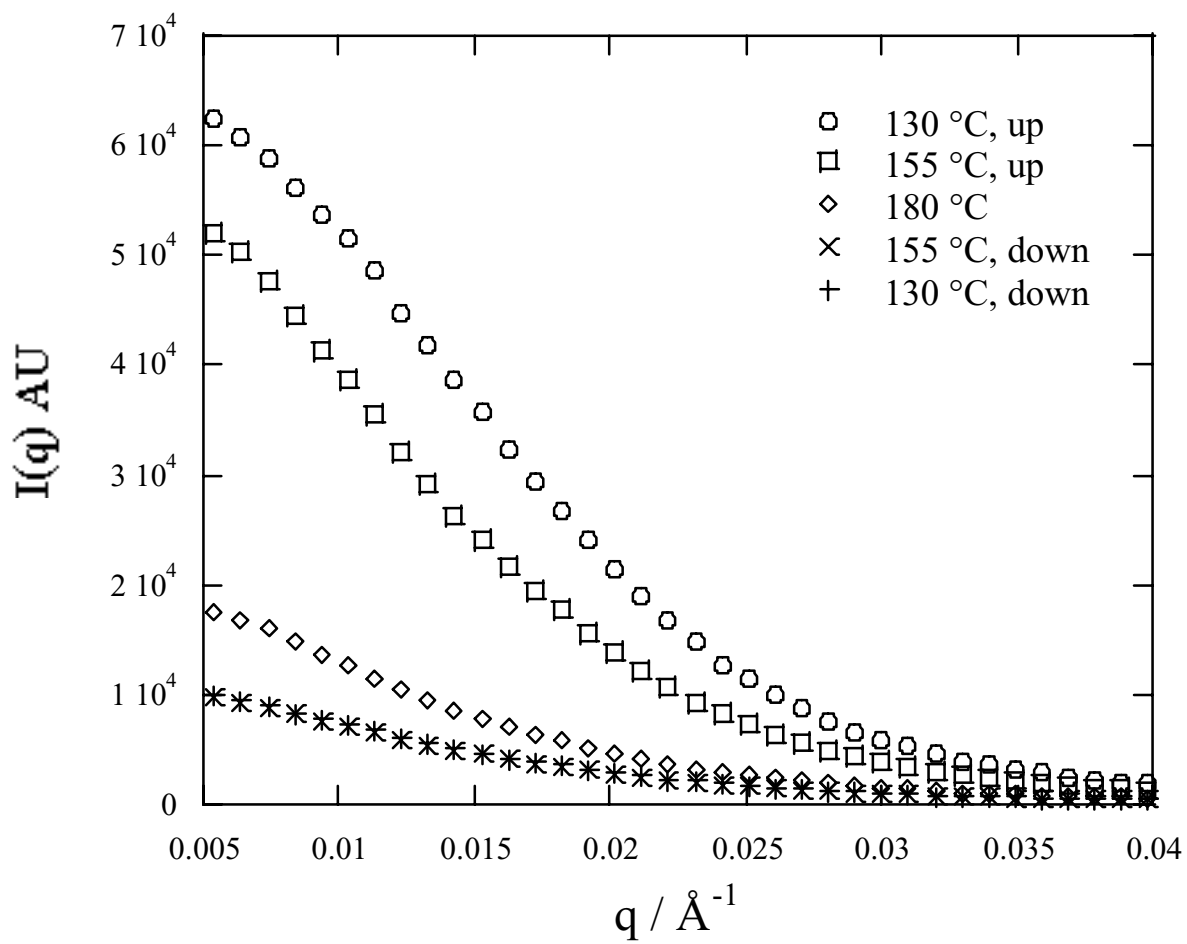


Figure 19 SANS from blends of G4 PAMAM and PMMA-r-PMAA.

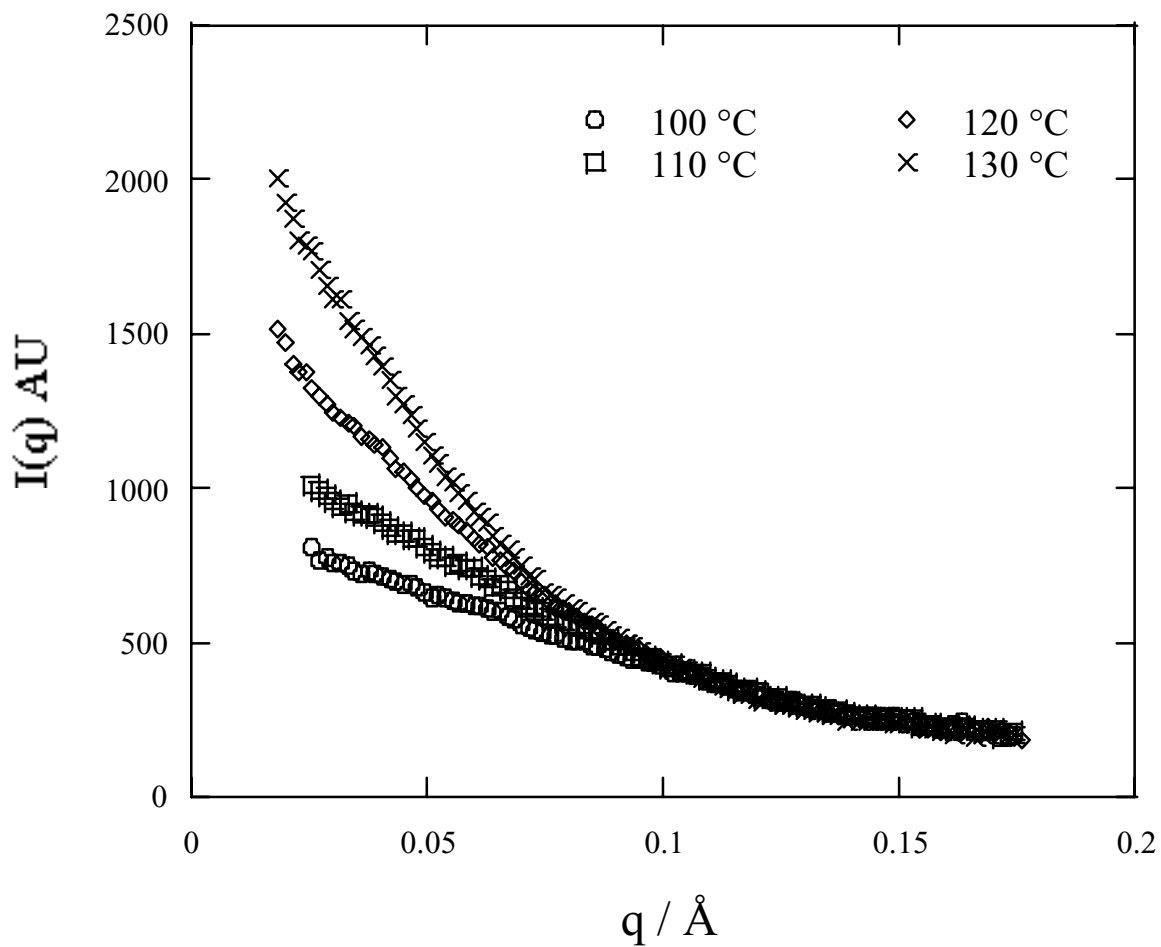


Figure 20 SANS from Blends of G4.5 PPI and PMMA-r-PMAA. Parameter of the plot is the temperature as indicated in the figure.

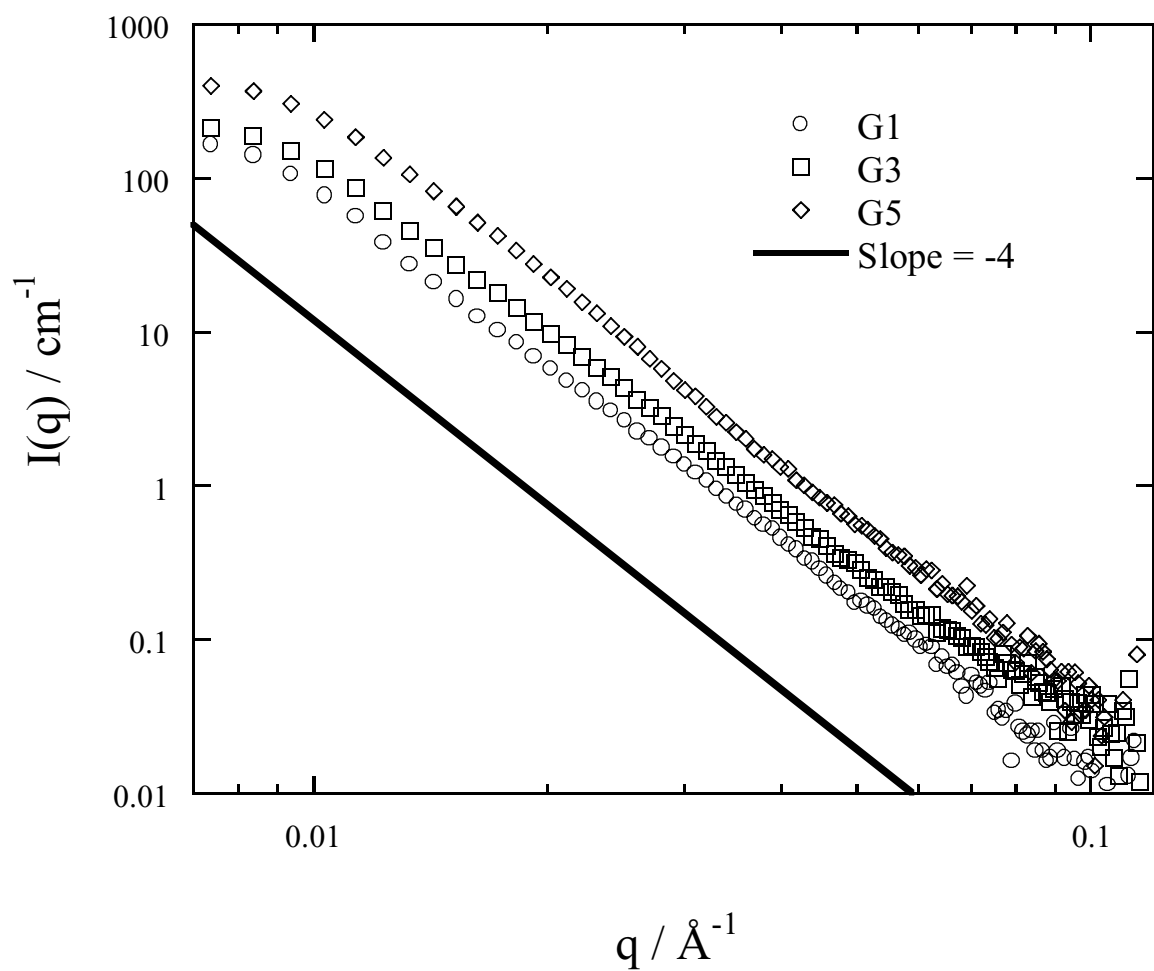


Figure 21 SANS from blends of mass fraction 2% dendrimer-h in 98% mass fraction HDPE-d₄. (○), G1; (□), G3; (◇), G5.

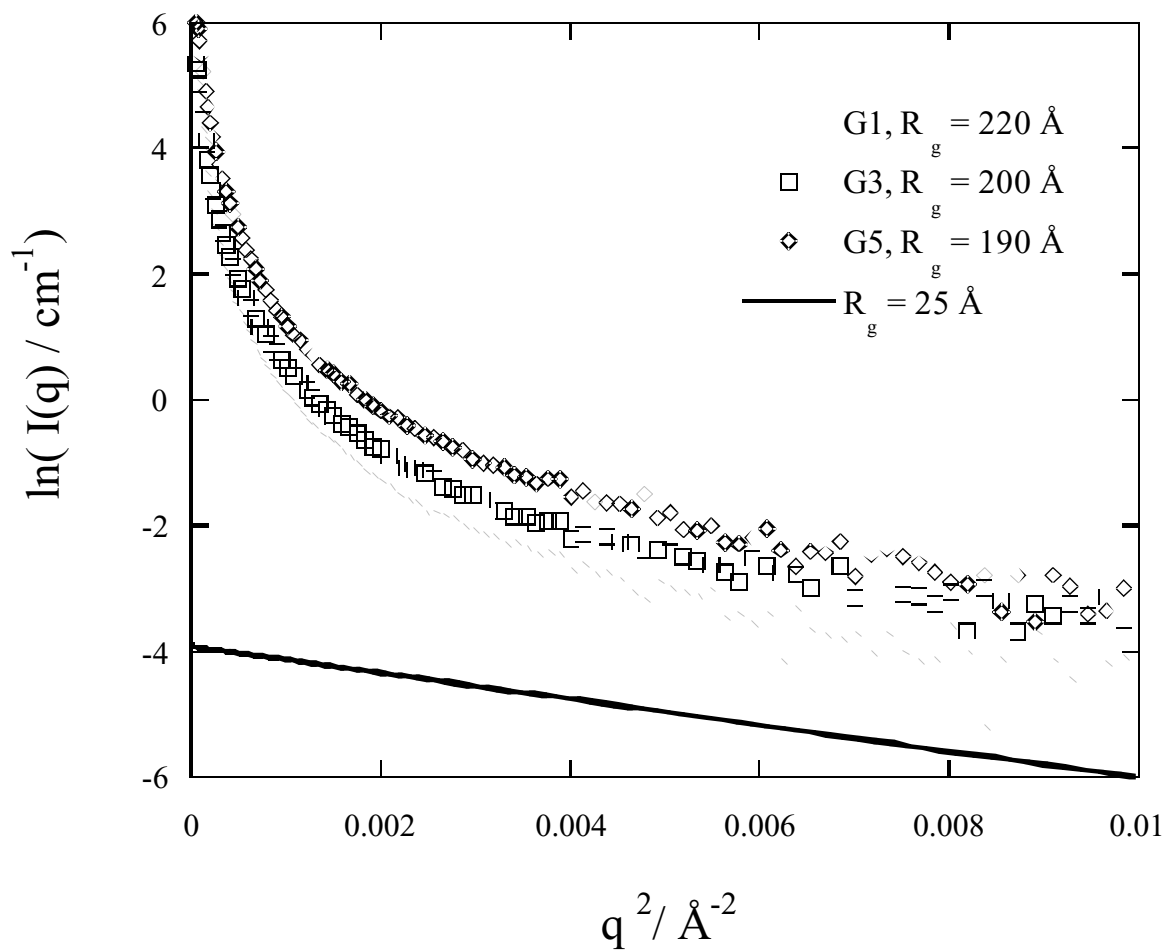


Figure 22 Guinier plot of the scattering from blends of 2% mass fraction dendrimer-h in HDPE-d₄. Symbols are the same as in Figure 21.

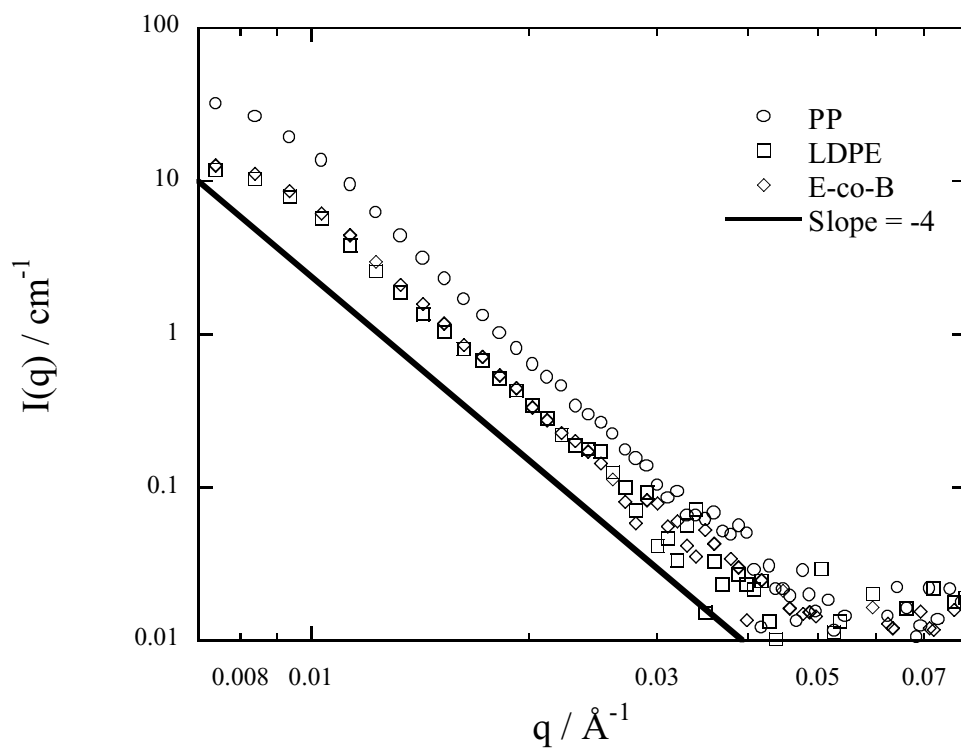


Figure 23 Mass fraction 2% G5 Dendrimer-d in PP, (○); LDPE, (□); and E-co-B, (◇).

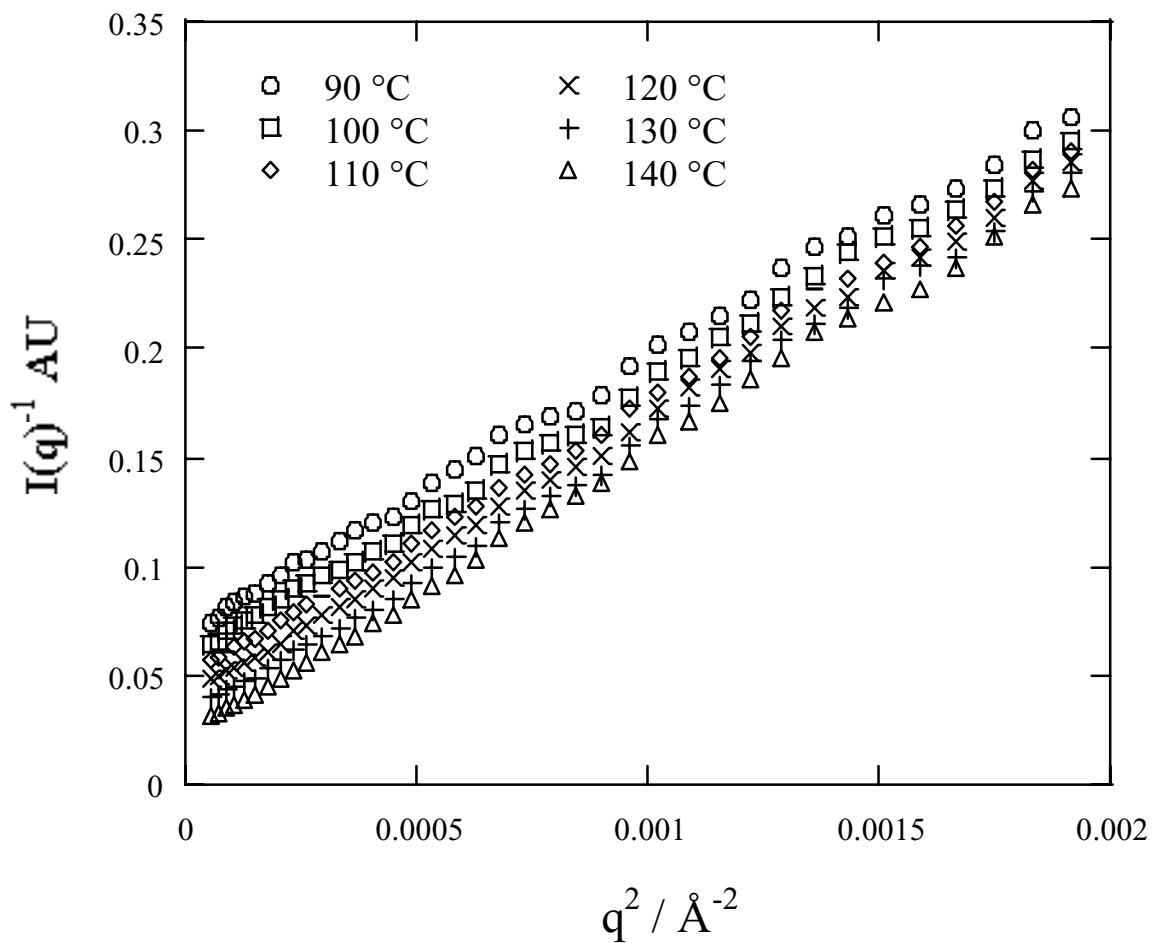


Figure 24 SANS from a 1:9 PSD/PVME blend that contains a mass fraction of 1% PPI- C_8 dendrimer for temperatures in the range $90\text{ °C} \leq T \leq 140\text{ °C}$.

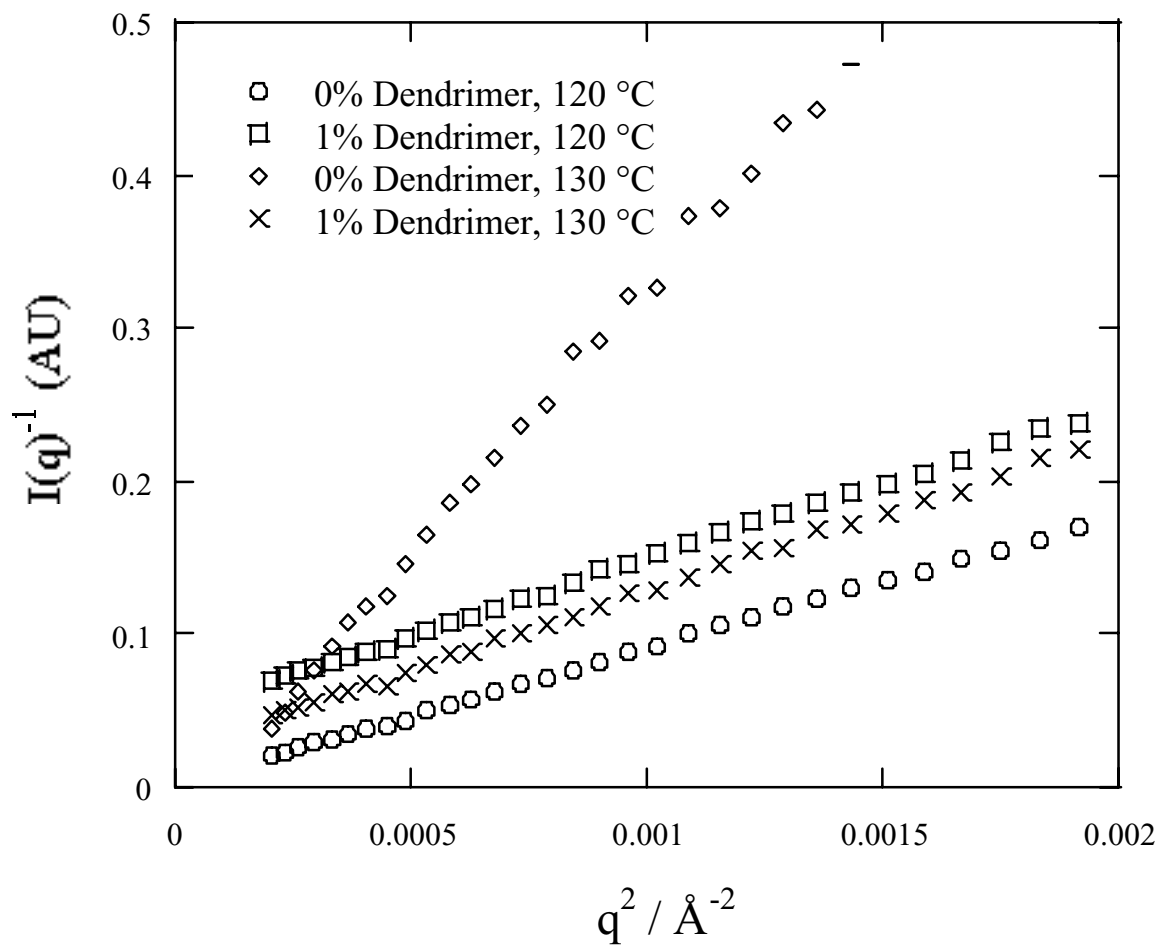


Figure 25 SANS from 3:7 PSD/PVME blends that contain a mass fraction 0% and 1% PPI-C₈ dendrimer.

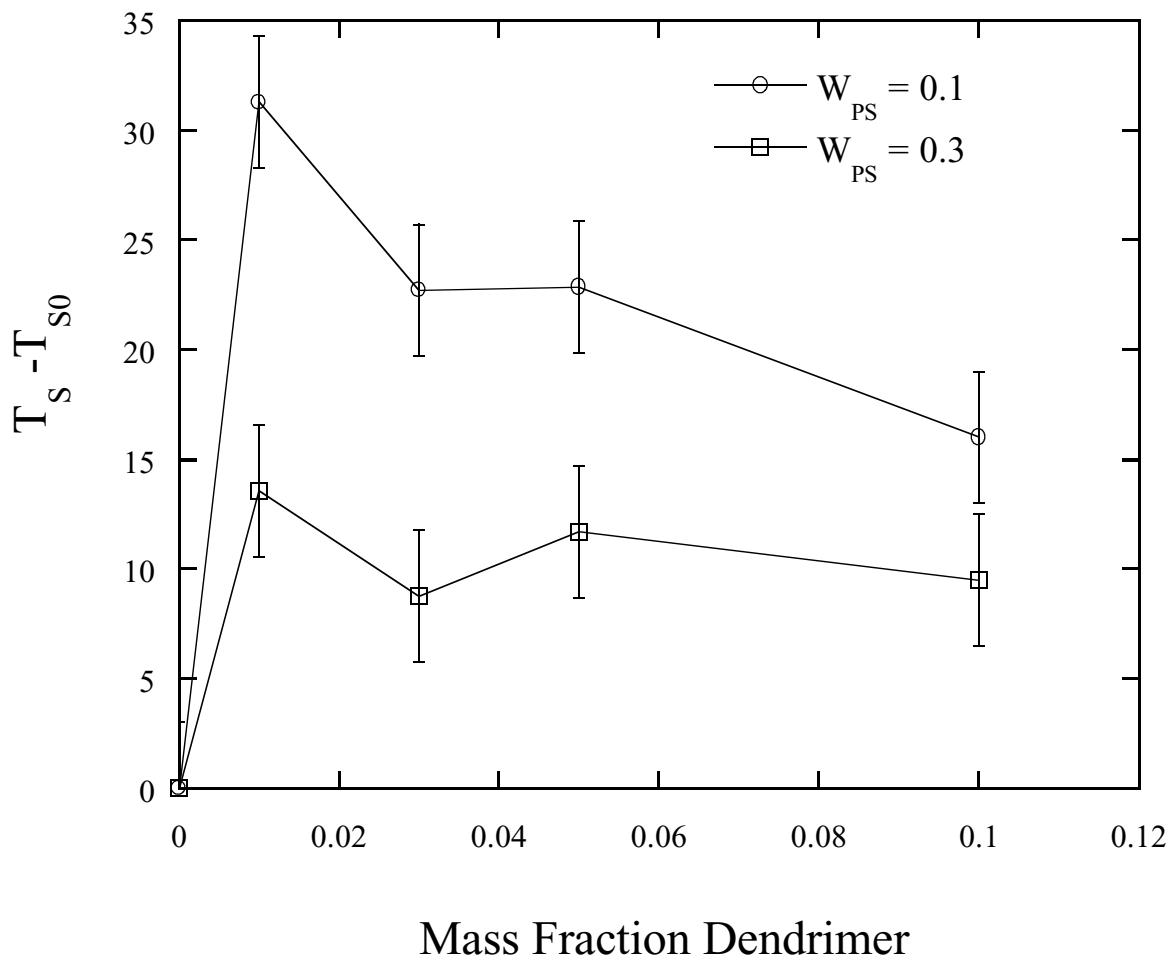


Figure 26 . Effect of the dendrimer PPI-C₈ on the spinodal temperature of PSD/PVME blends

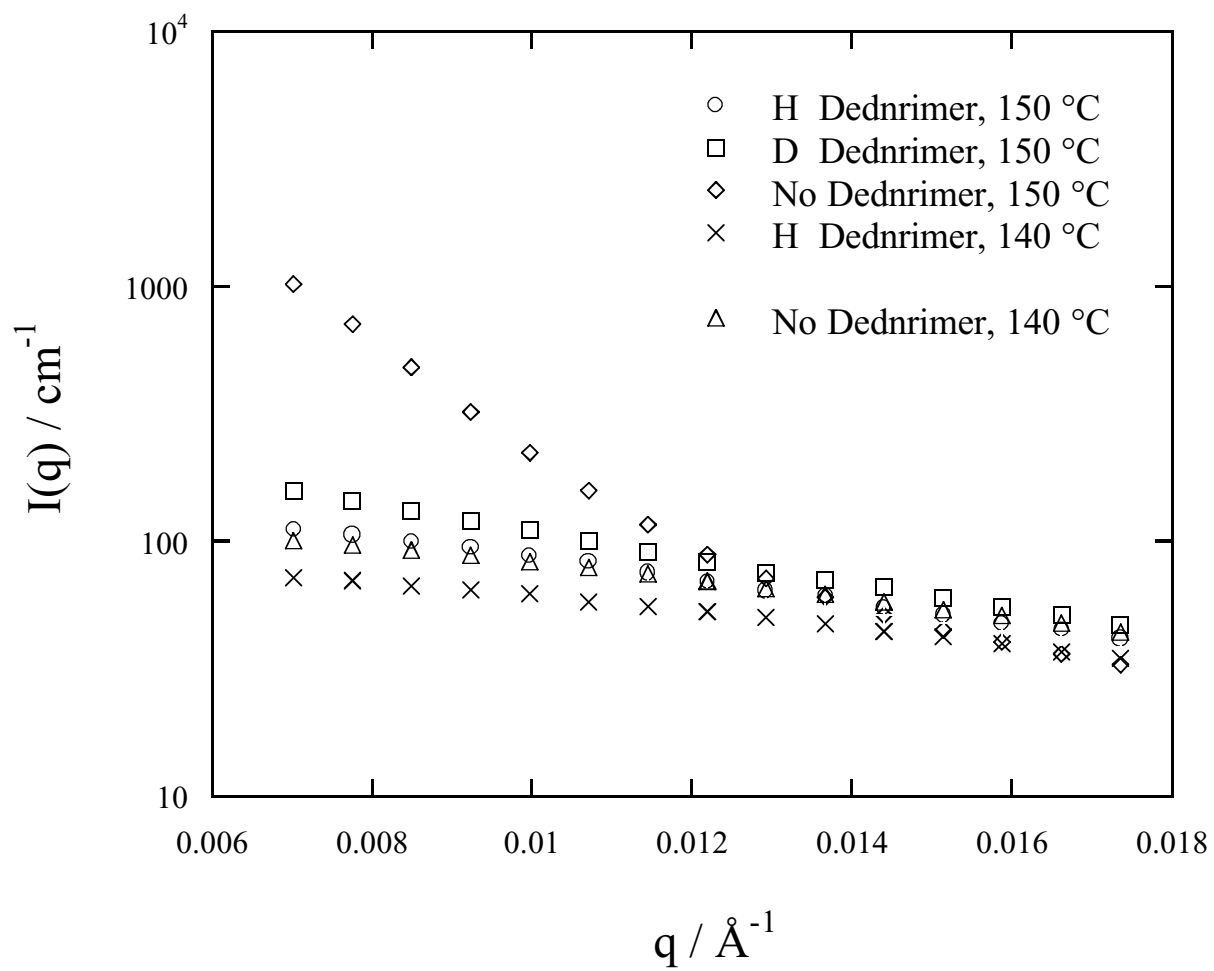


Figure 27 SANS of PSD/PVME = 1/9 with and without mass fraction 1 % dendrimer at 140 °C and 150 °C.

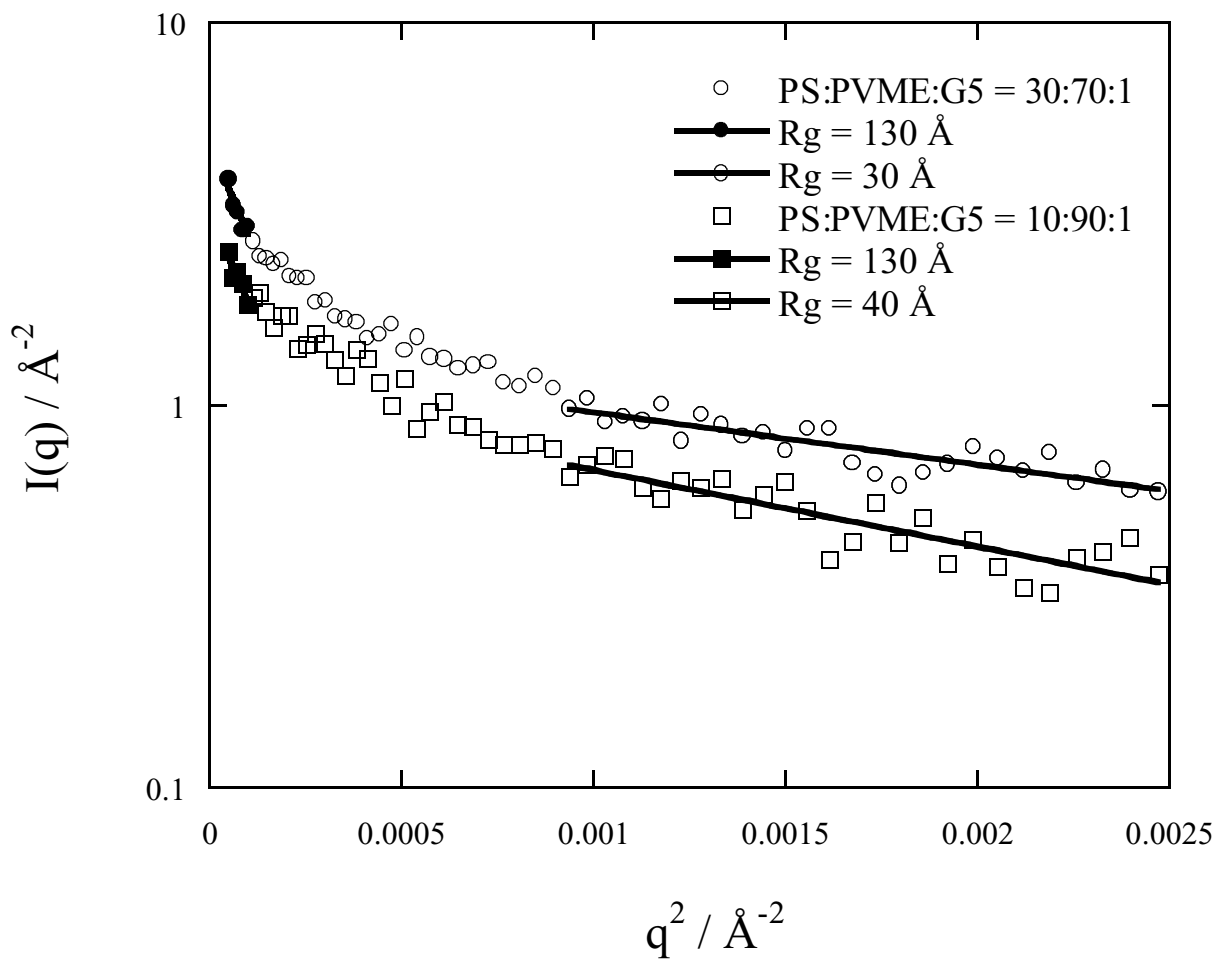


Figure 28 SANS of PSD/PVME = (1/9 and 3/7) with and without mass fraction 1 % dendrimer at 70 °C.

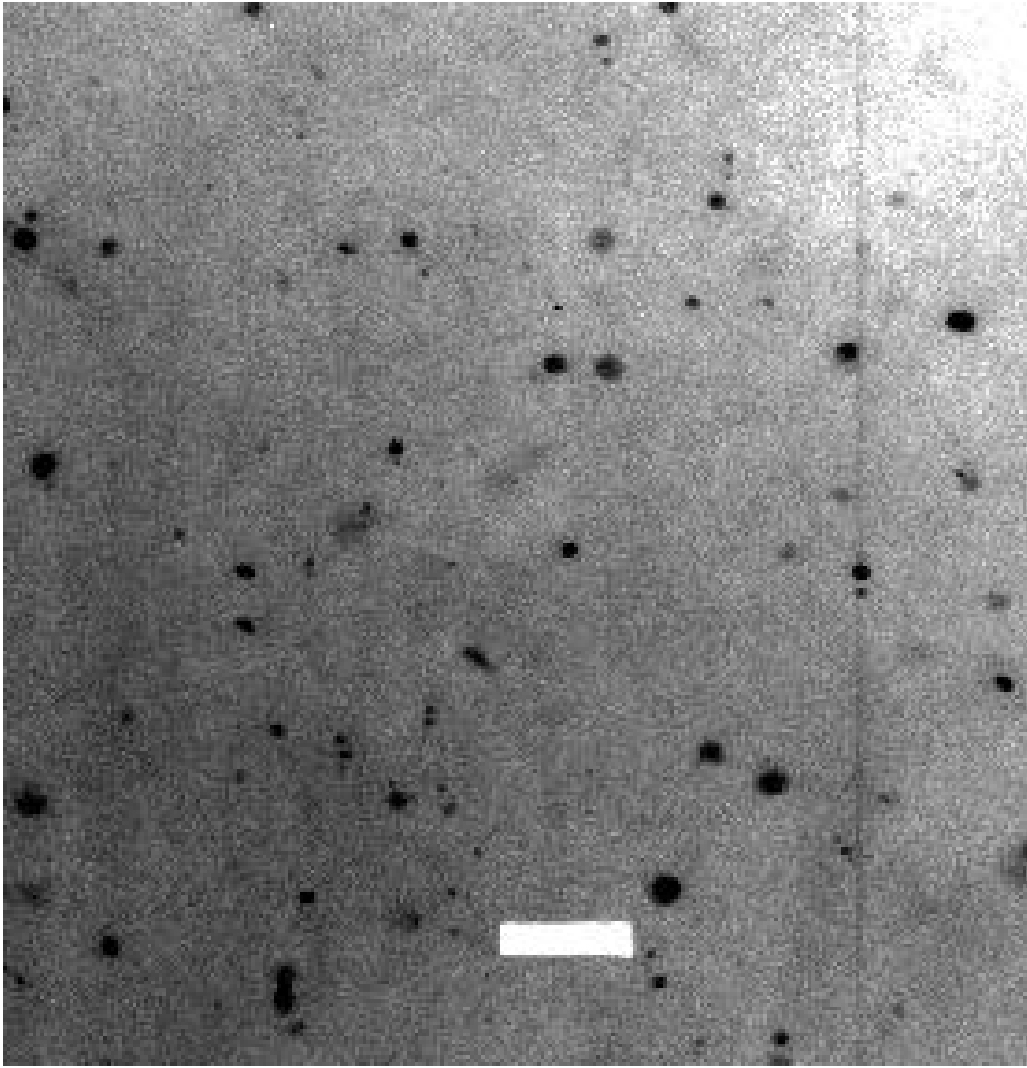


Figure 29 TEM of PSD/PVME blend ED-1. The scale bar is one micron.

Arborscent Polymers

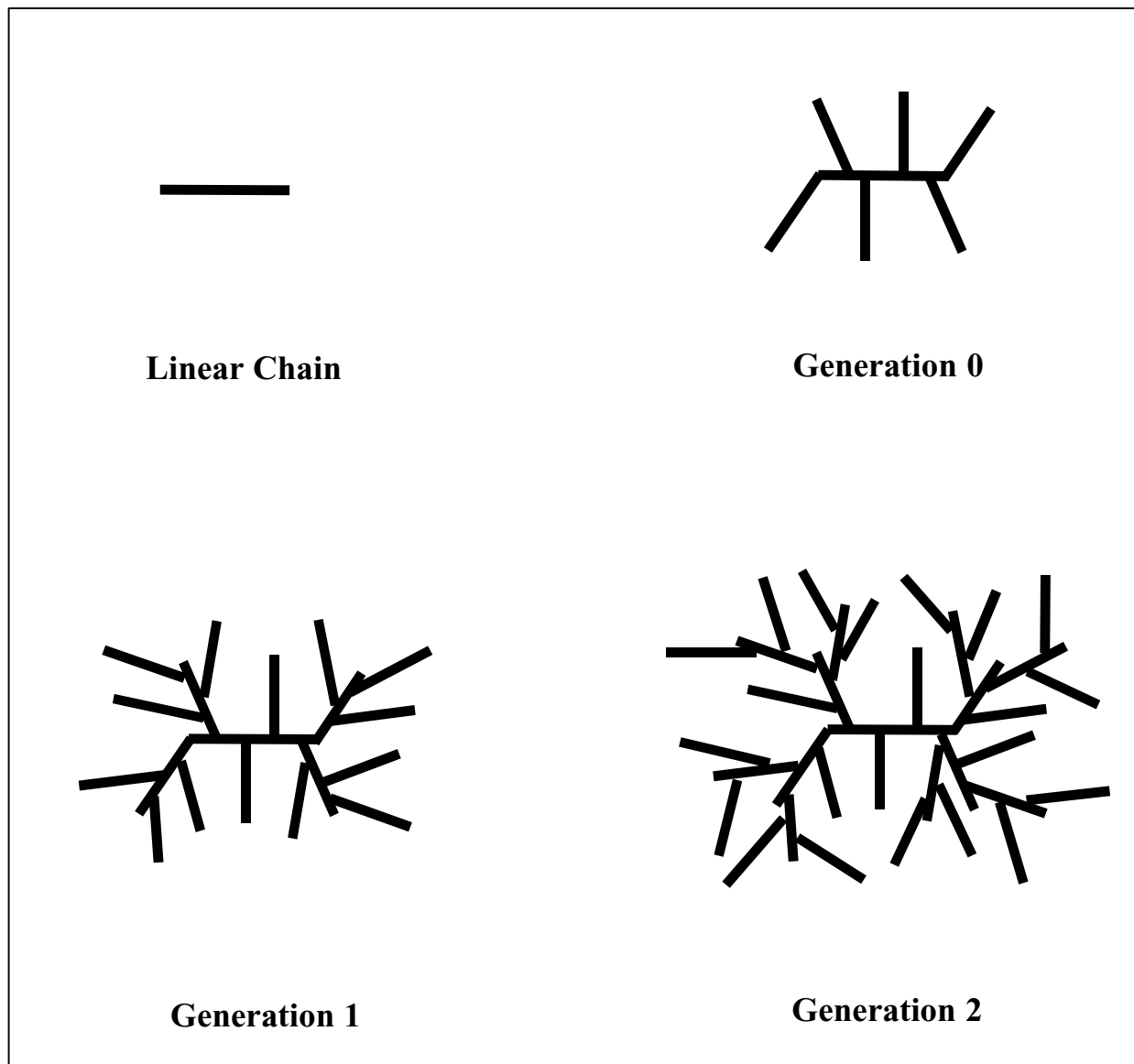


Figure 30 Schematic representation of the growth of arborescent polymers by successive grafting reactions.

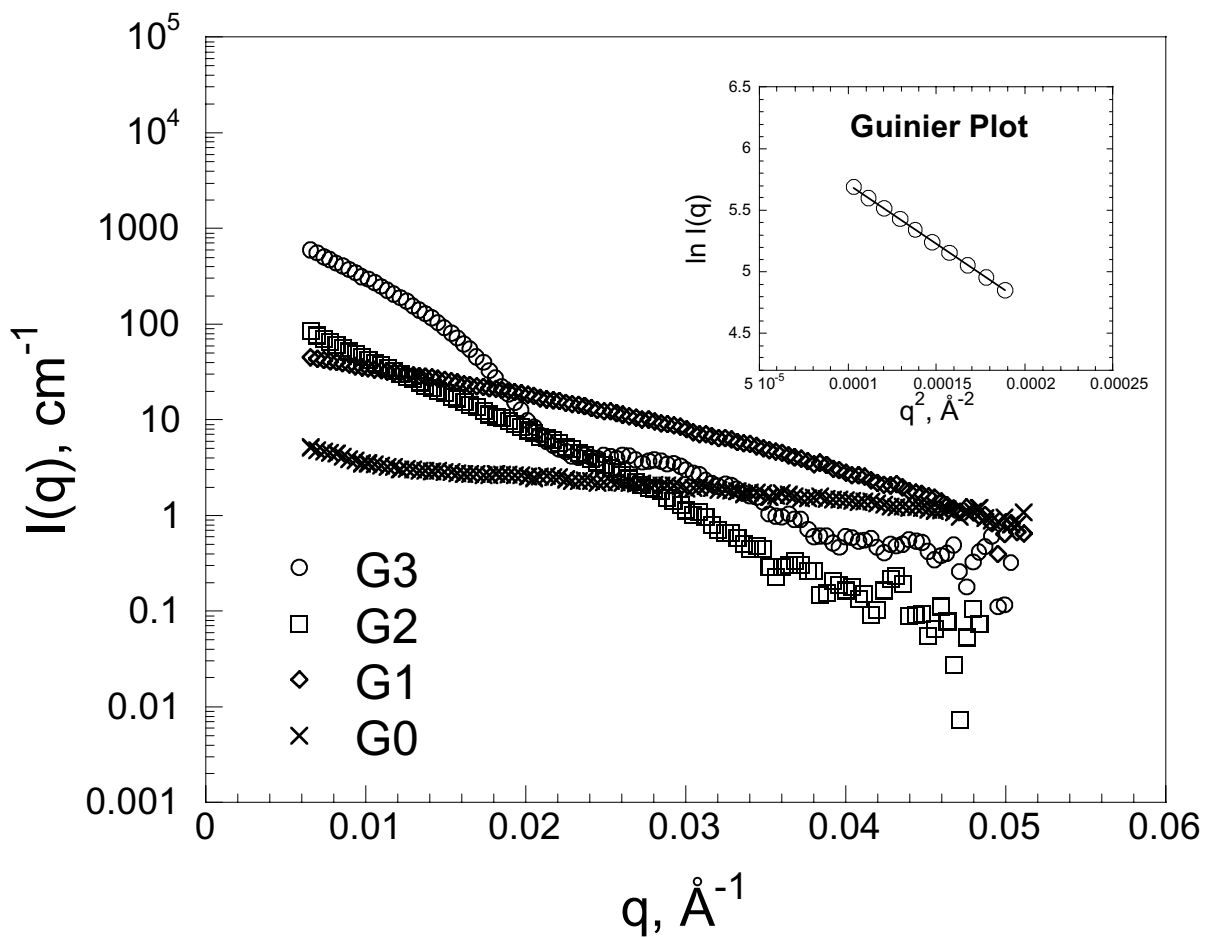


Figure 31 SANS curves for all arborescent polymer generations in d-polystyrene at 120 °C.

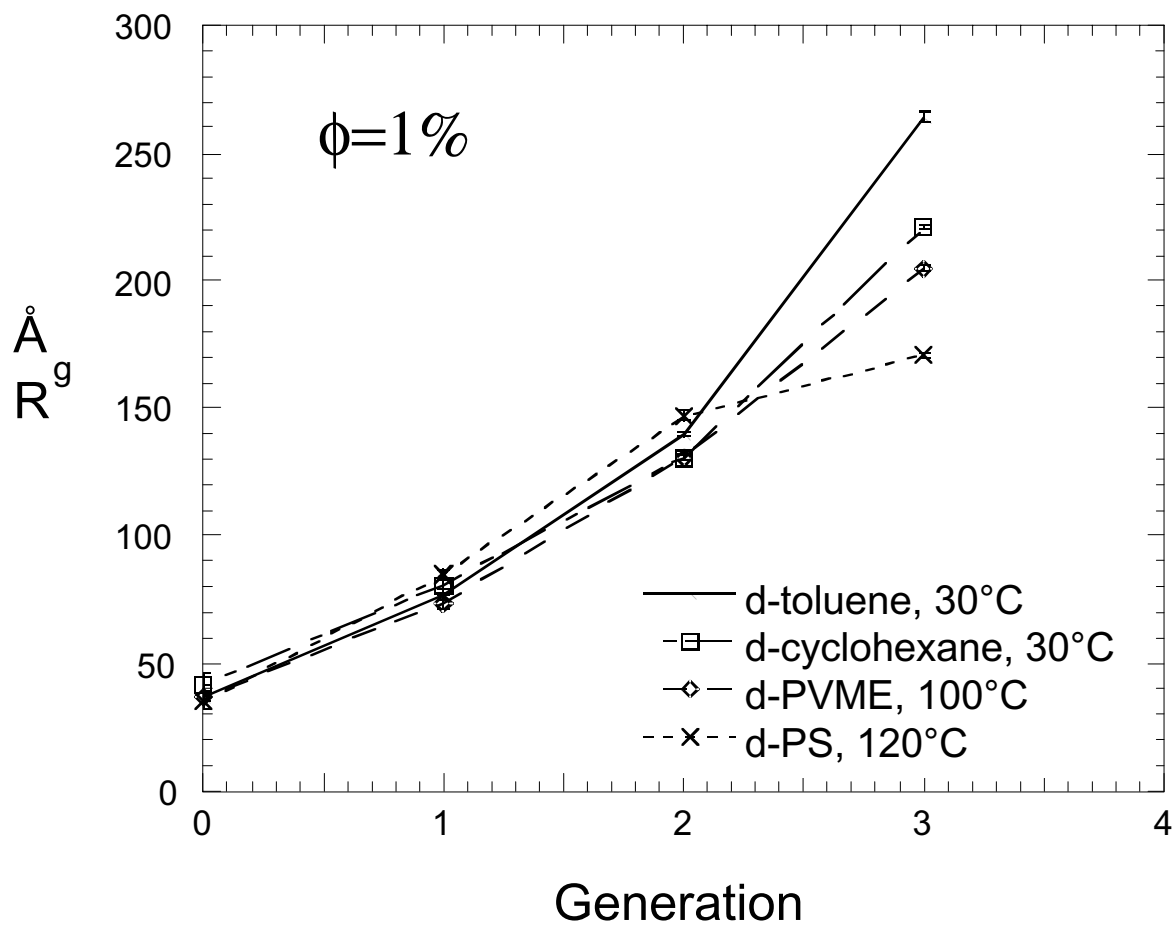


Figure 32 R_g of arborescent polymers in solutions and in blends as a function of generation number.

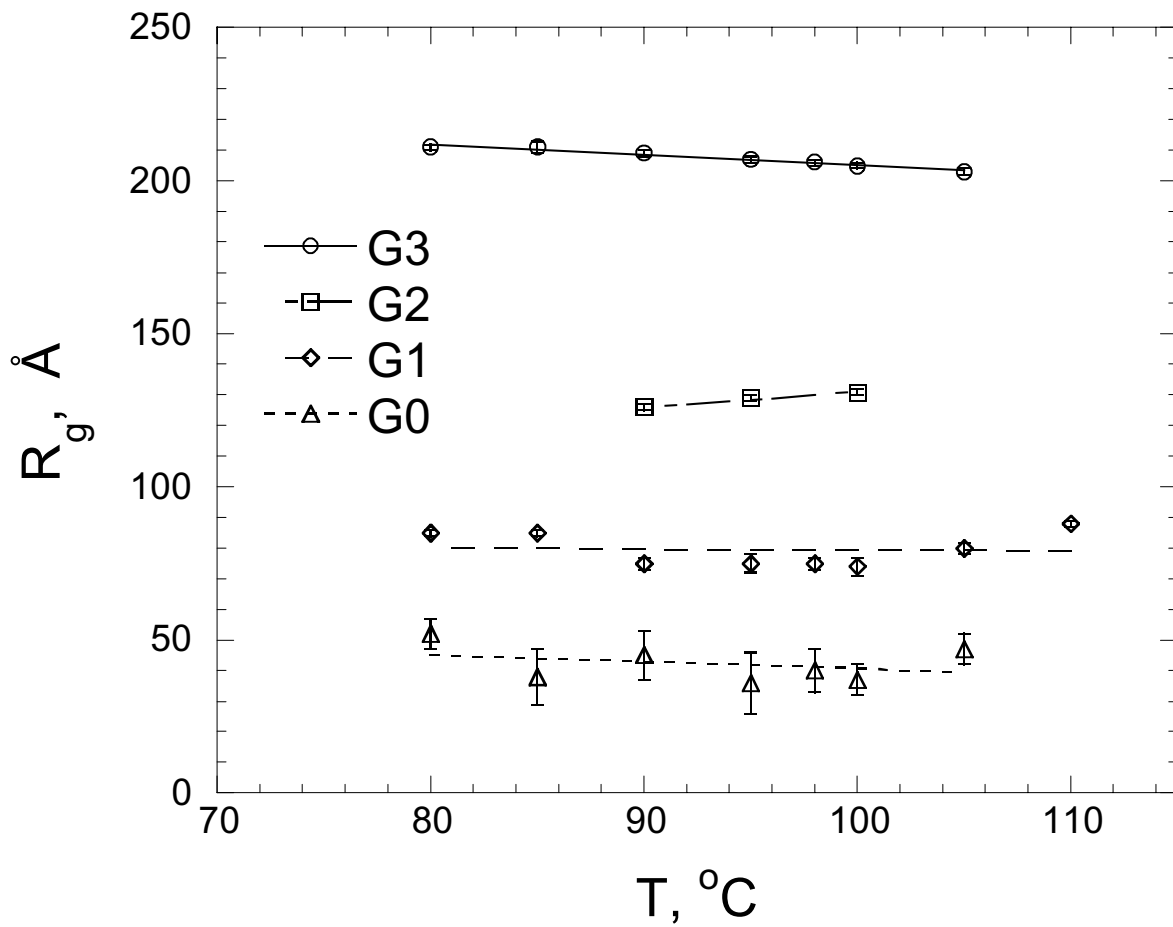


Figure 33 Temperature dependence of R_g for arborescent polymers in d-PVME

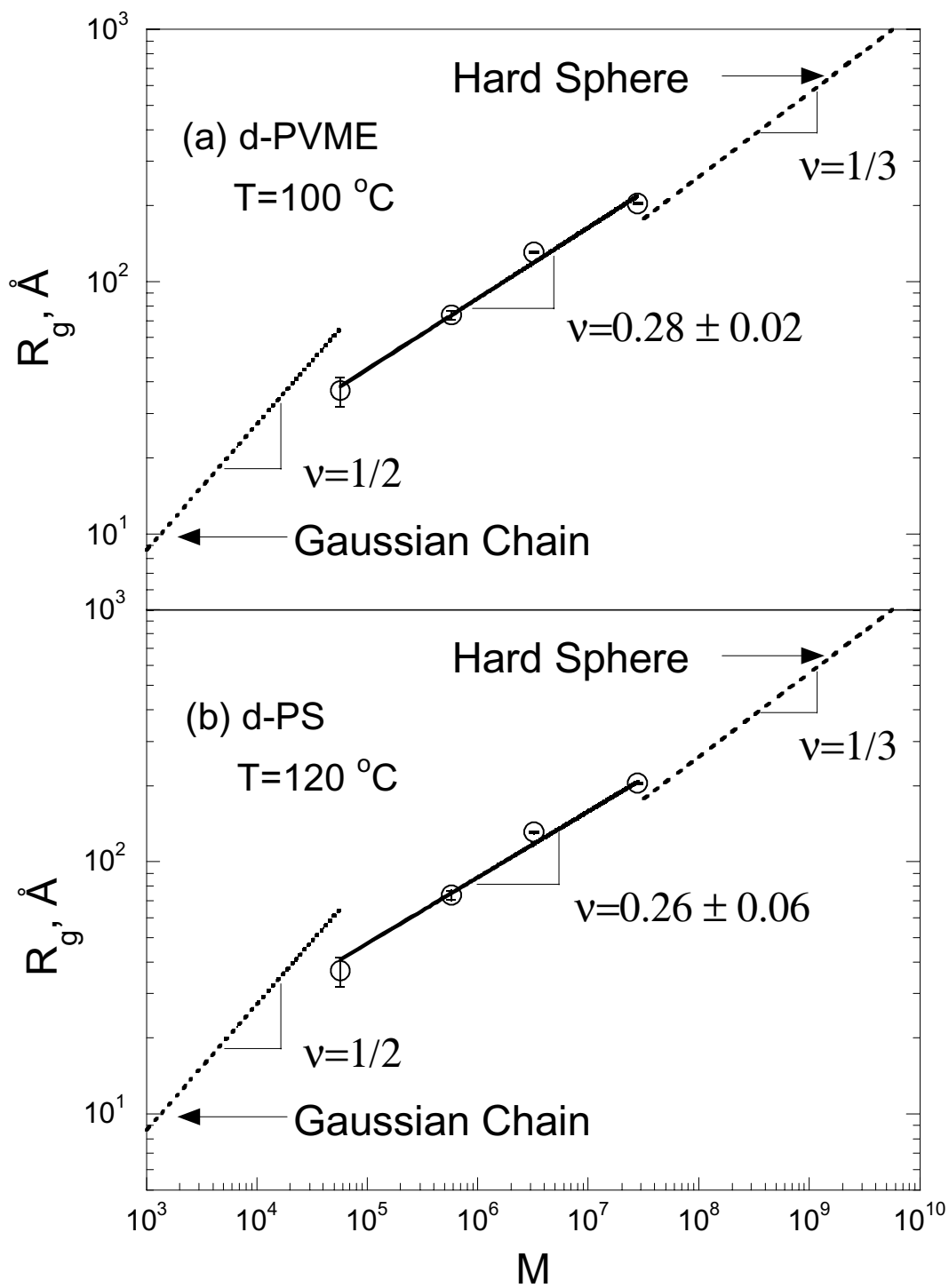


Figure 34 (a) R_g versus molecular mass for arborescent polymers in d-PVME. (b) R_g versus molecular mass for arborescent polymers in d-polystyrene.

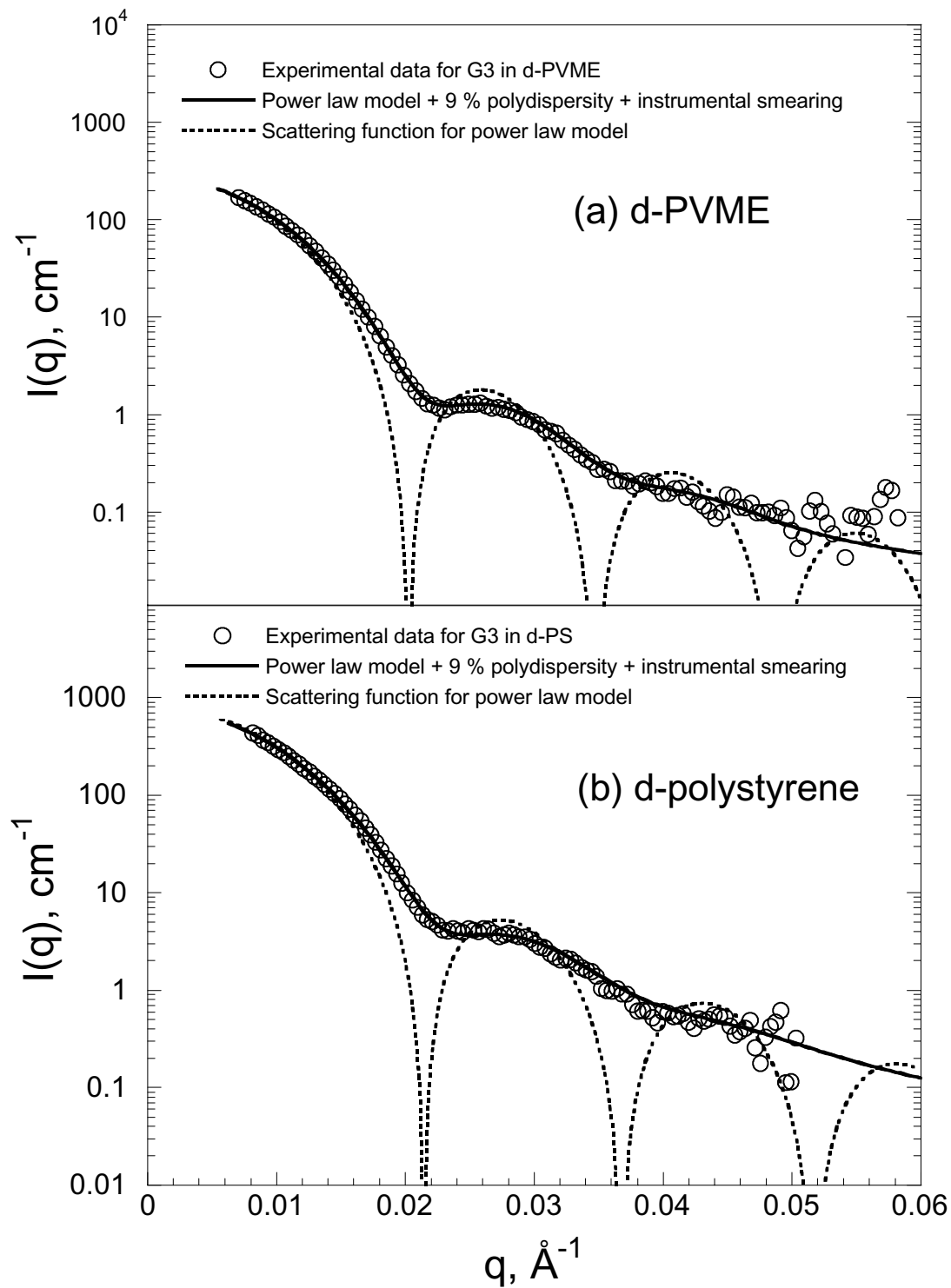


Figure 35 (a) Scattering functions for power law model compared with G3 polymer in d-PVME. (b) Scattering functions for power law model compared with G3 polymer in d-polystyrene.

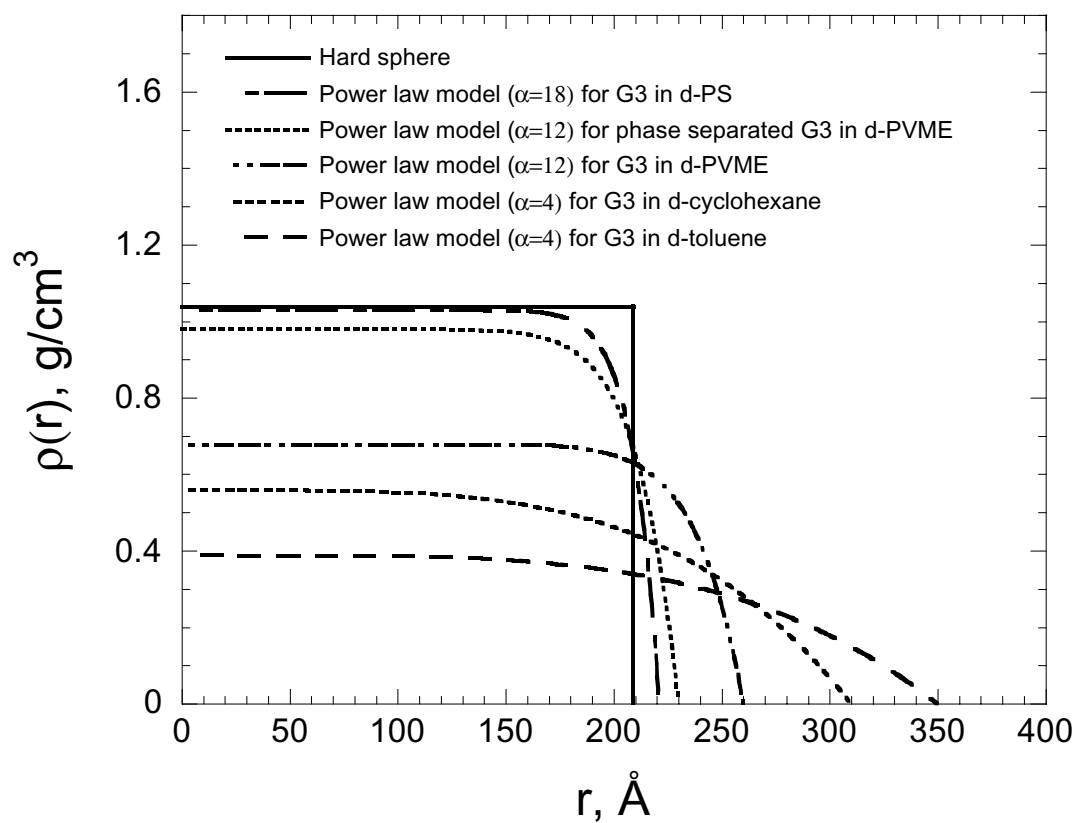


Figure 36 Density profiles for G3 arborescent polymer in solutions and blends.

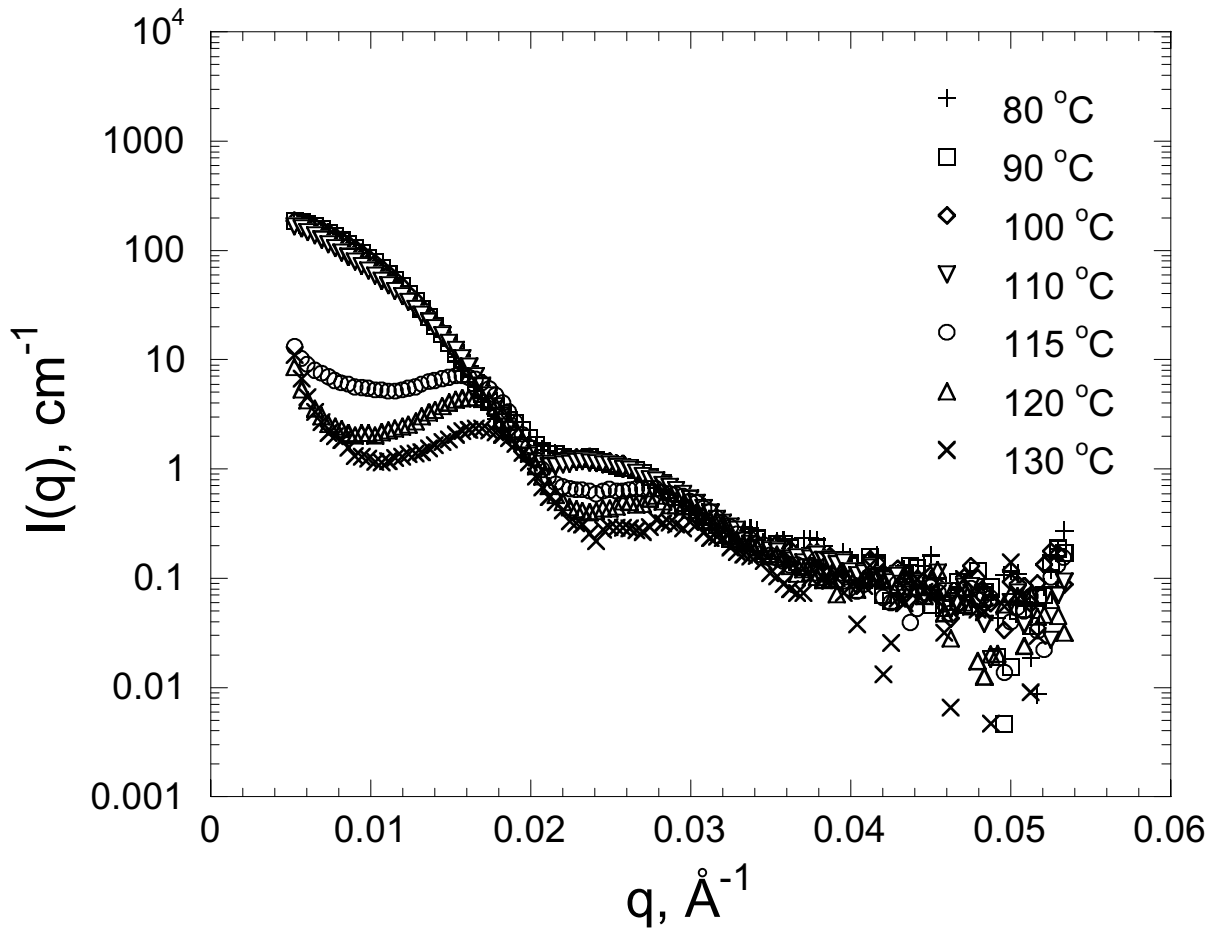


Figure 37 $I(q)$ versus q for G3 polymer in d-PVME from 80°C to the phase separation temperature.

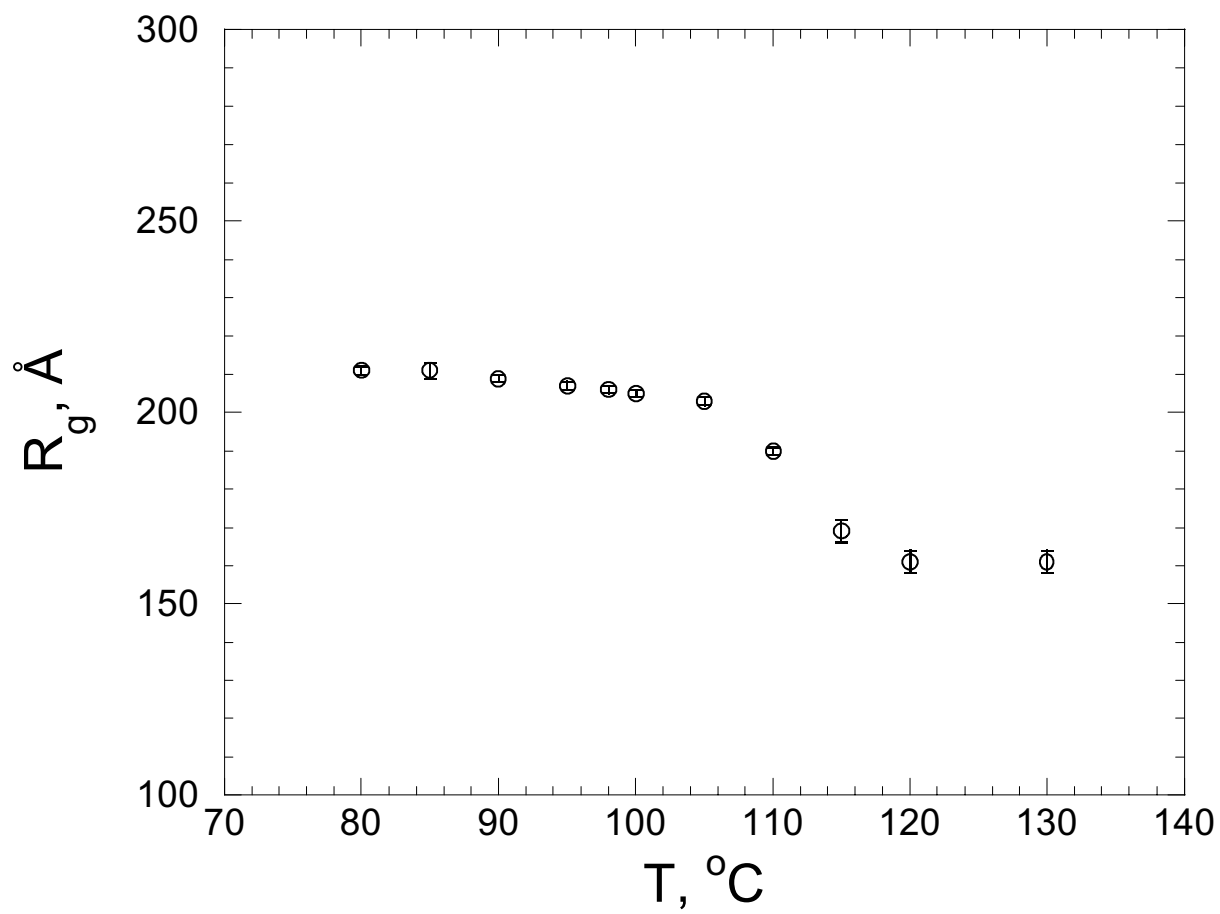


Figure 38 Temperature dependence of R_g for G3 polymer in d-PVME.

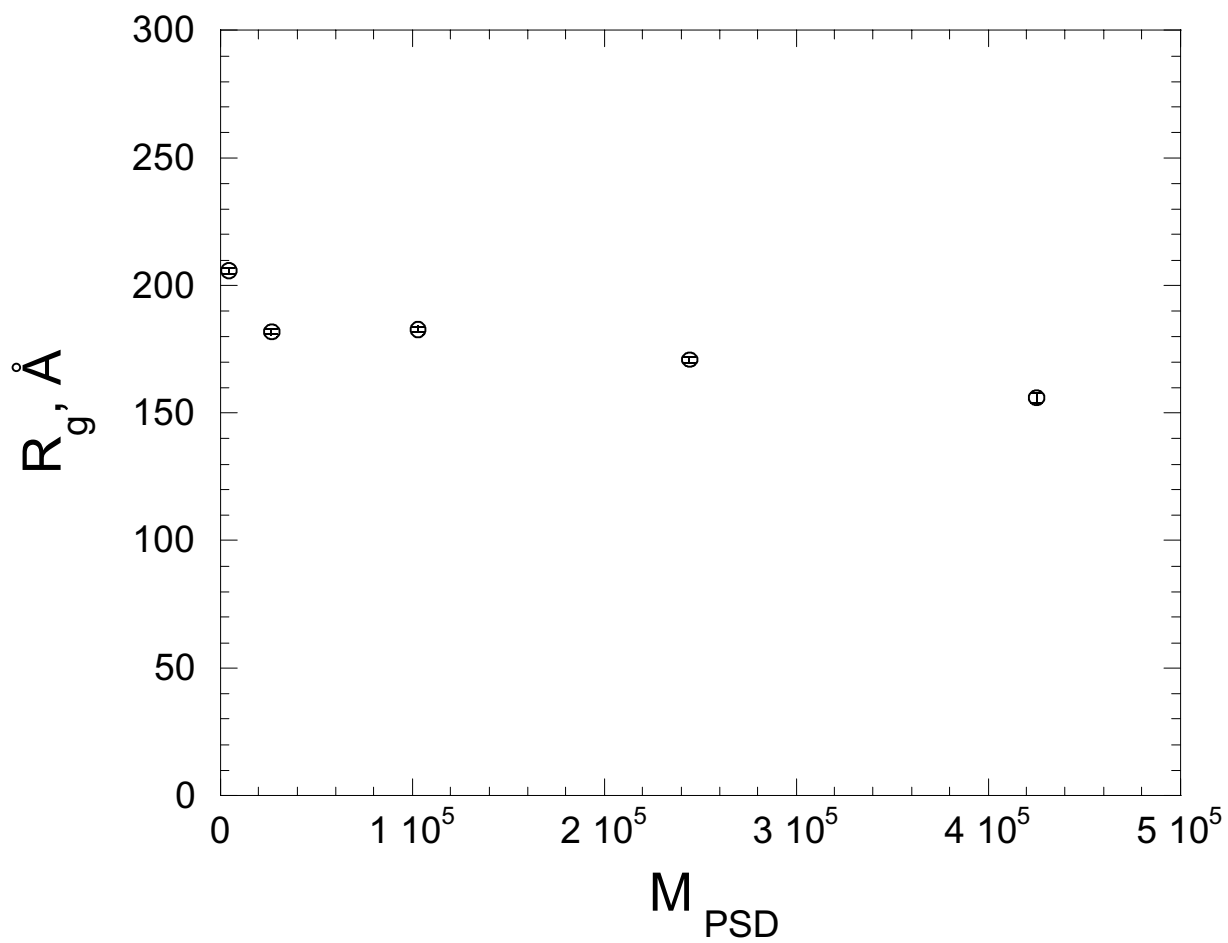


Figure 39 R_g of G3 arborescent polymer as a function of molecular mass of the matrix d-polystyrene.

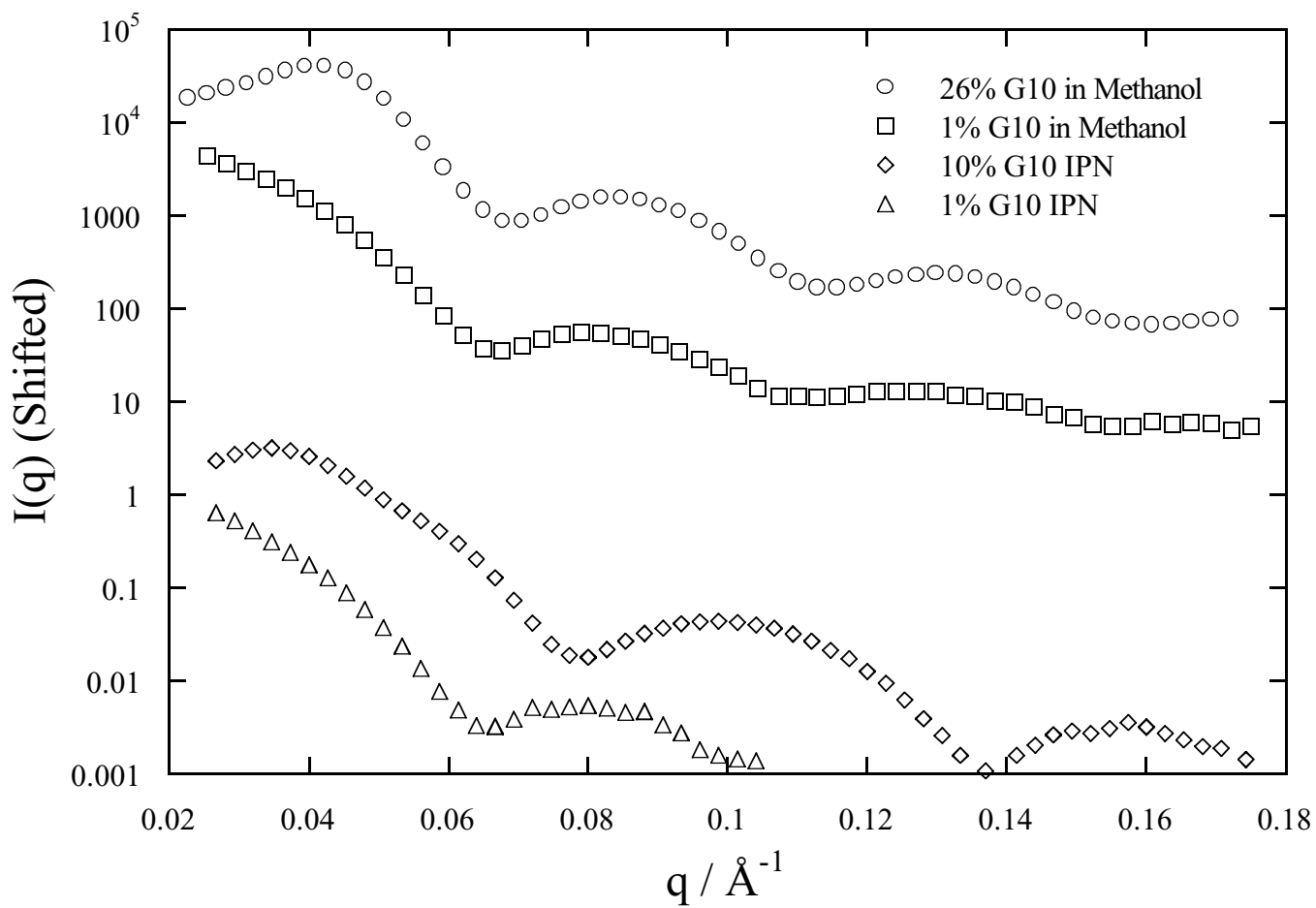


Figure 40 SAXS for G10 dendrimer solution and IPN's. High concentration low q peaks are indicative of dendrimer ordering. The first minimum in the scattering indicates dendrimer size. The shift to higher q of the minimum for the mass fraction 10% dendrimer in the IPN shows shrinking.

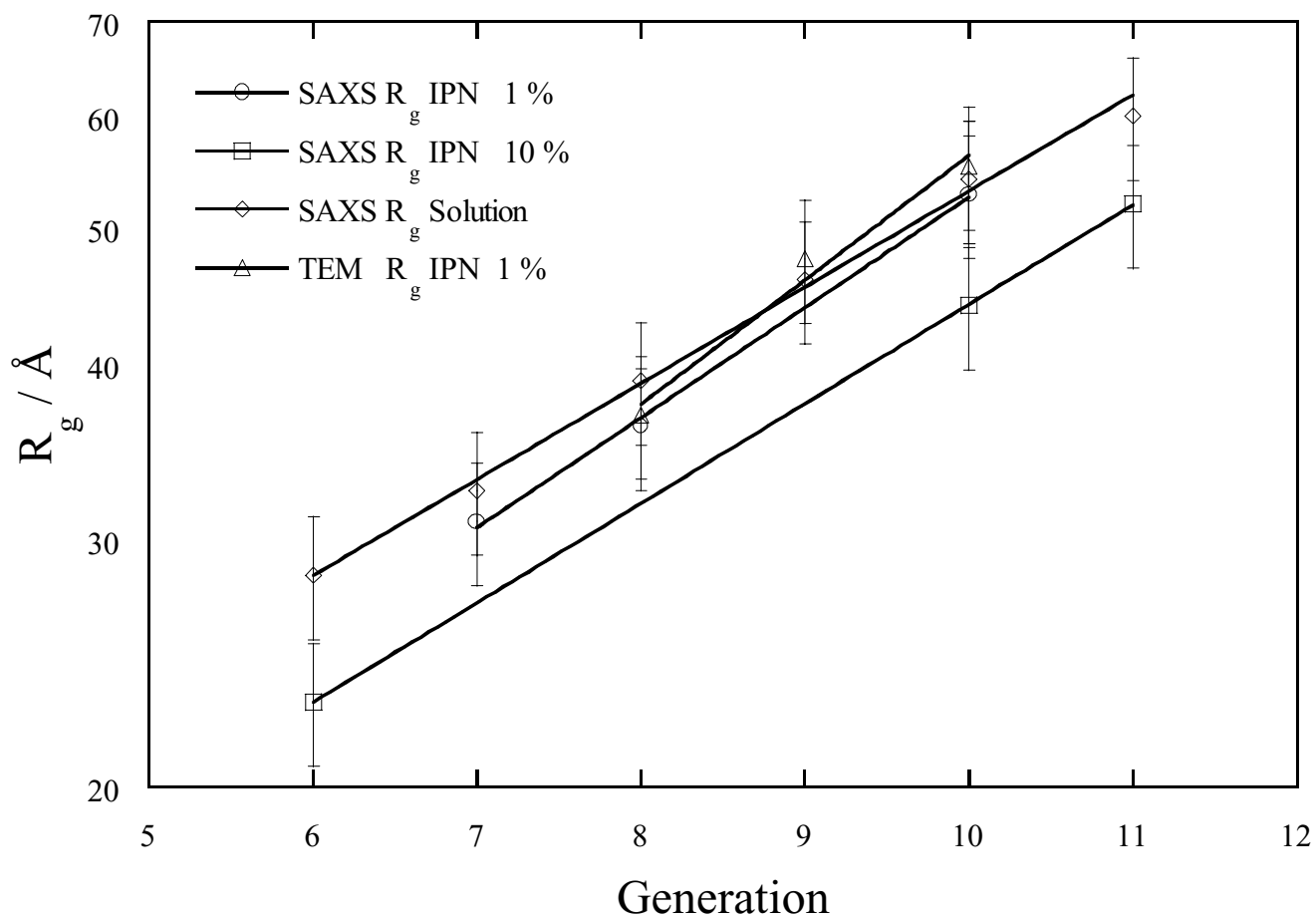


Figure 41 SAXS and TEM-FFT dendrimer R_g in solution and IPN's. The size in mass fraction 10 % dendrimer in the IPN is considerable smaller than in dilute solution or IPN.

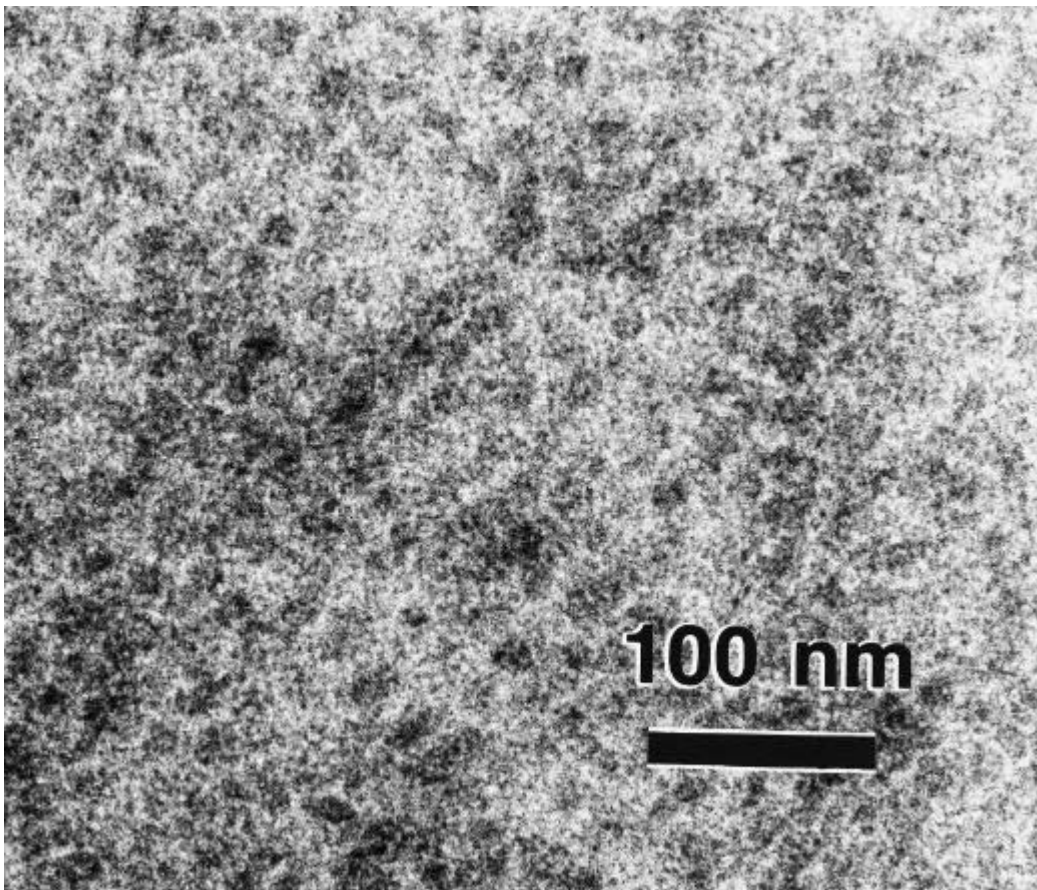


Figure 42 TEM of mass fraction 10 % G11 dendrimer in the IPN with OsO_4 staining. Picture contains images of dendrimers at different levels.

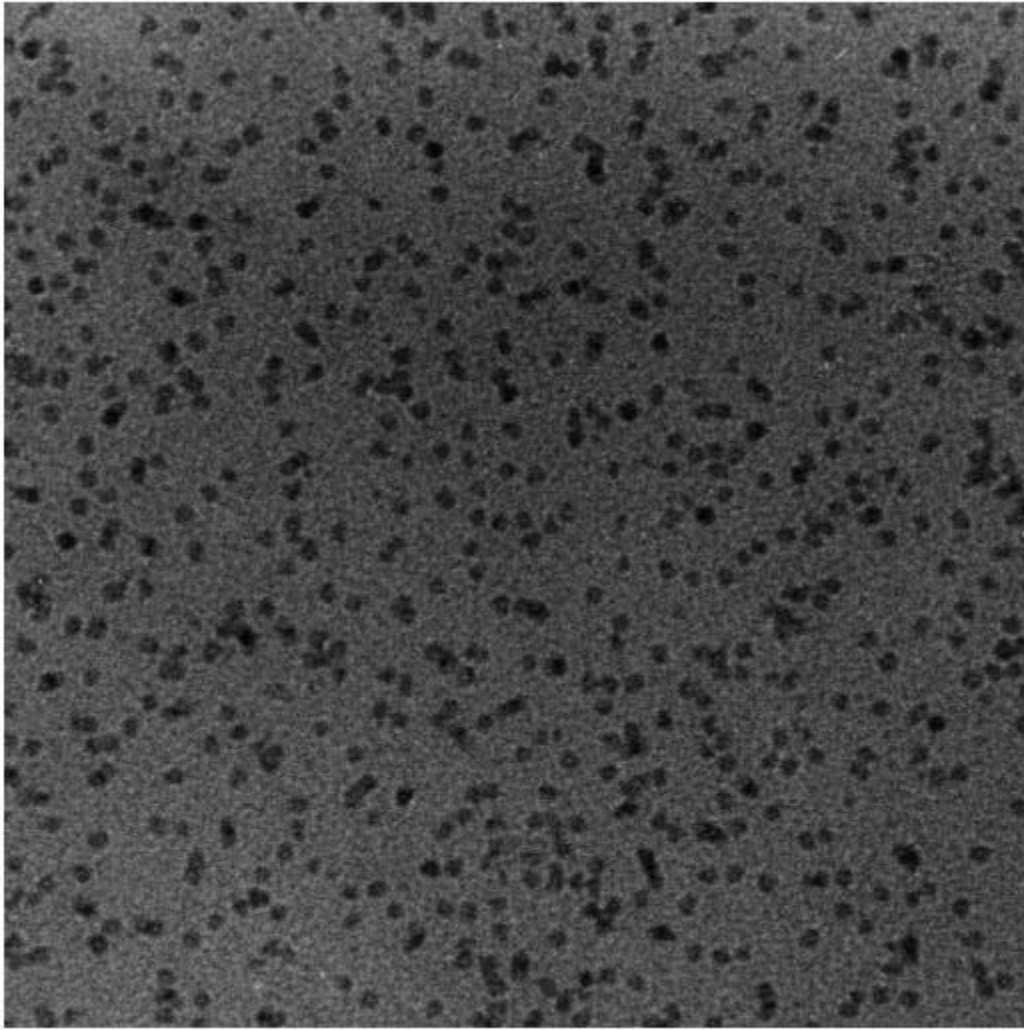


Figure 43 TEM of mass fraction 1 % G10 dendrimer in PHEMA with Phosphotungstic acid staining

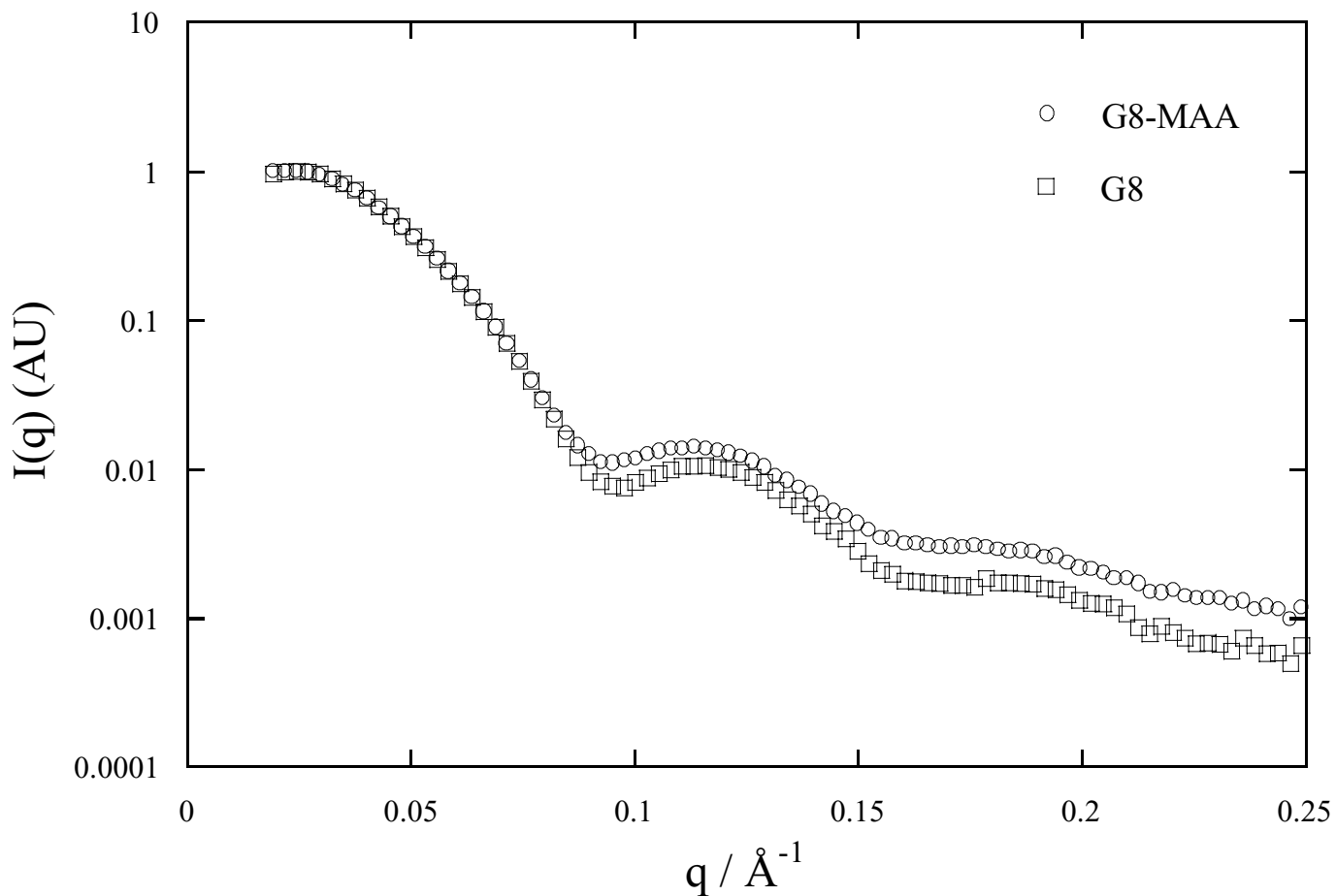


Figure 44 SAXS of mass fraction 2 % G8 PAMAM dendrimer and mass fraction 2 % G8-MAA dendrimer stained with phosphotungstic acid. Leveling off at low q is an incipient peak showing uniform spacing. Peak at higher q shows spherical nature and first minimum gives information on size.

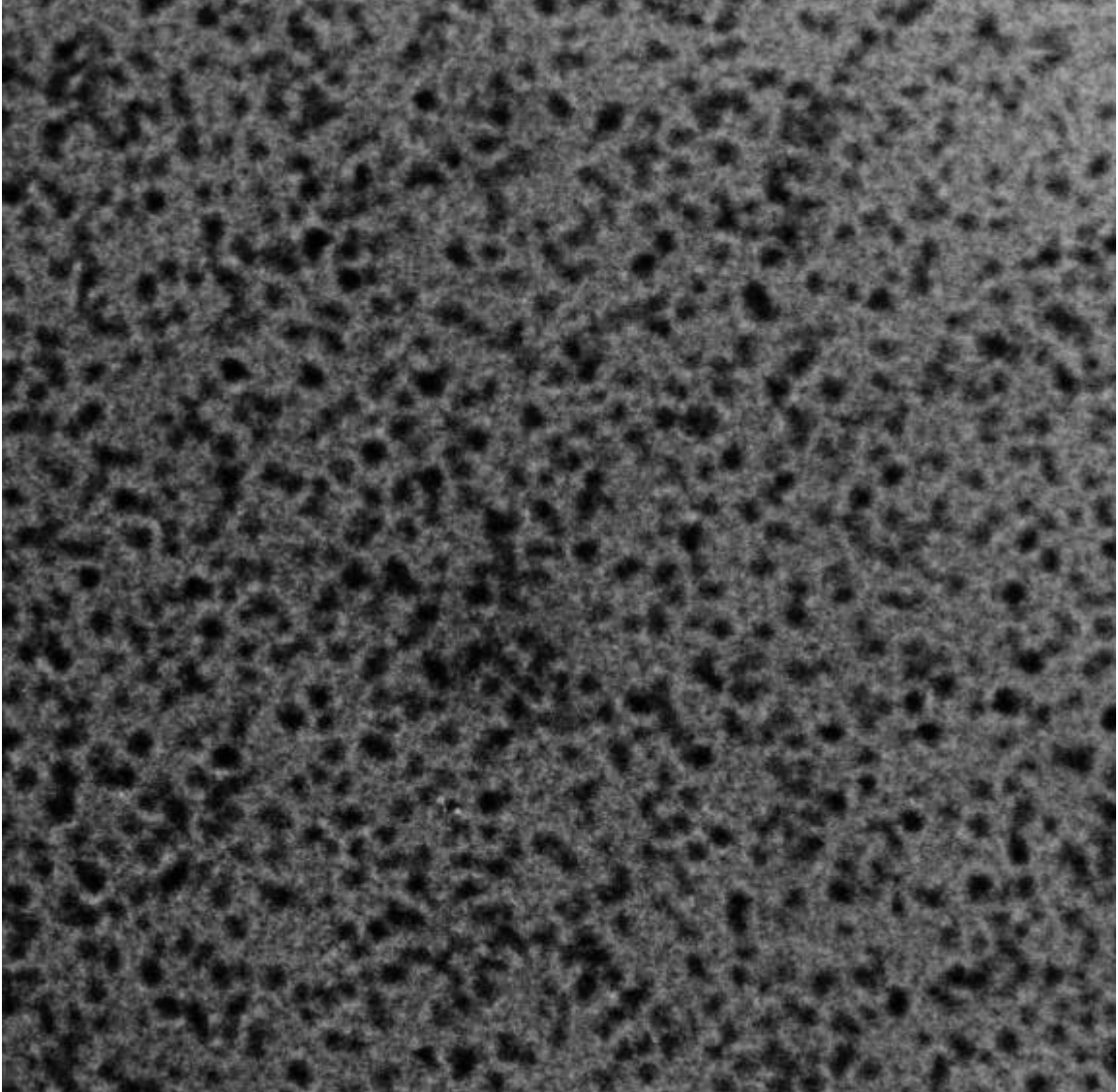


Figure 45 TEM of mass fraction 2% G8 dendrimer in PHEMA with Phosphotungstic acid staining

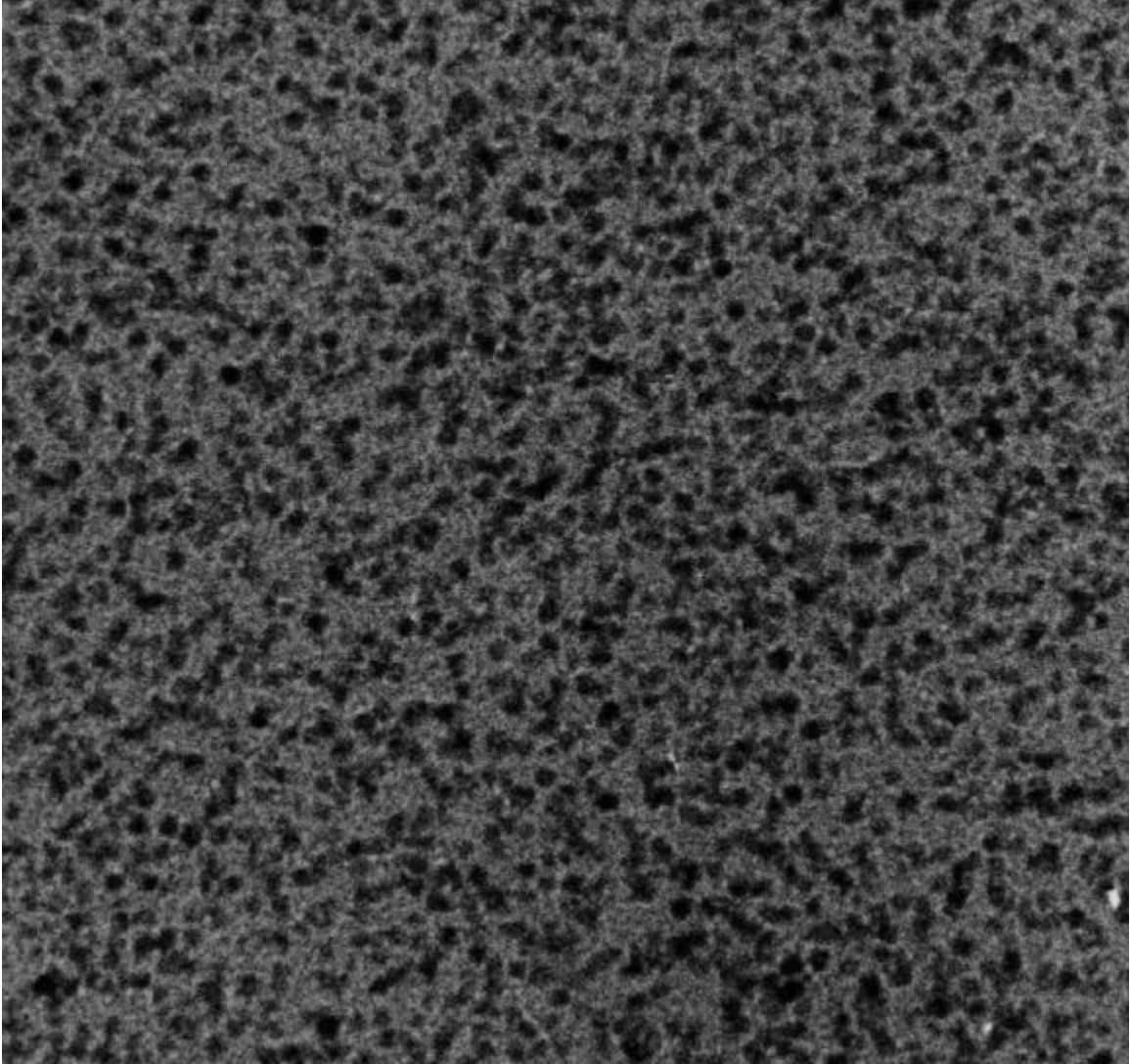


Figure 46 TEM of mass fraction 2 % G8 PAMAM dendrimer in PHEMA-co-PMAA with Phosphotungstic acid staining

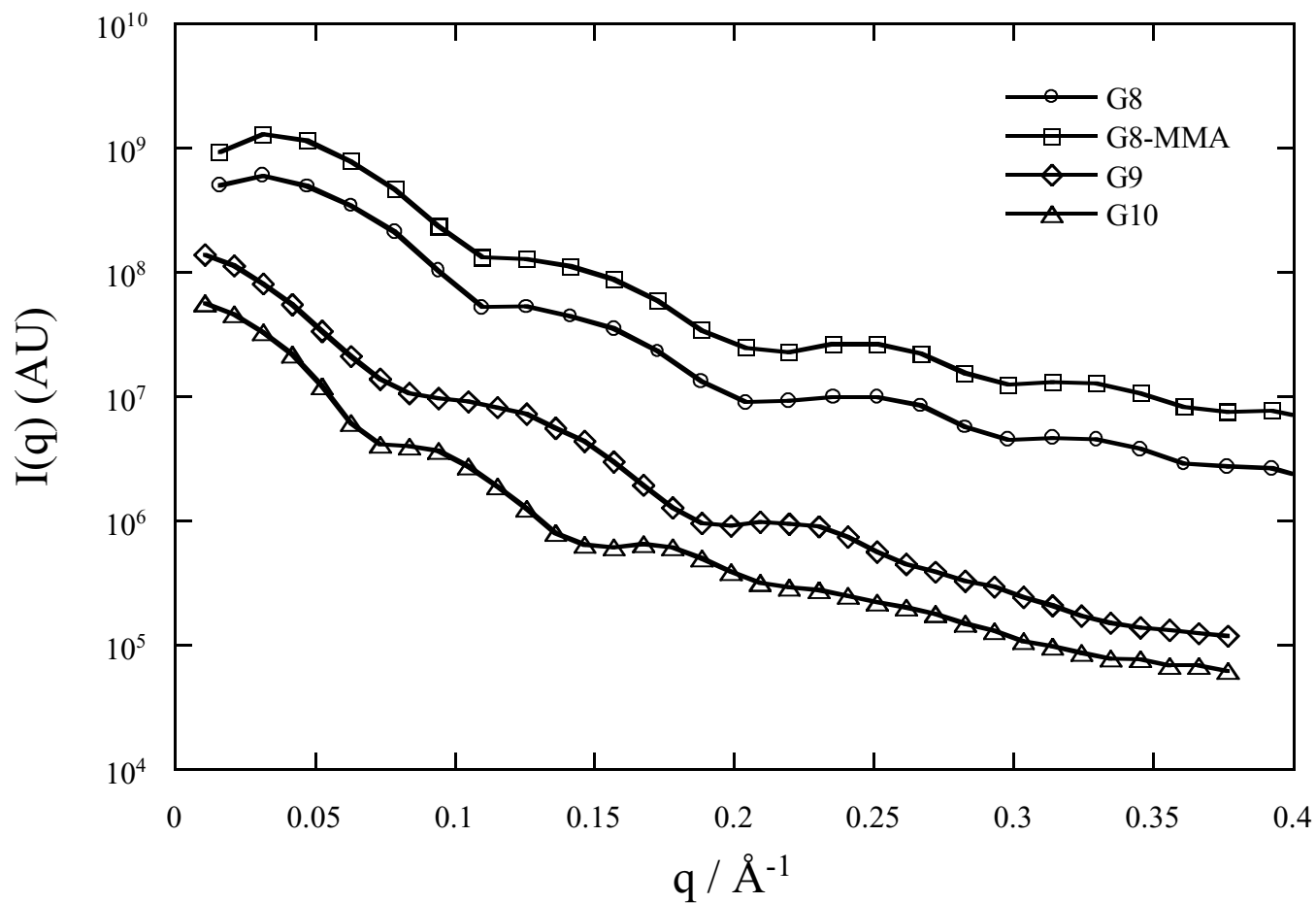


Figure 47 Fast Fourier transform of TEM micrographs. Features at high q are representative of spherical shape, the first minimum indicates an average R . Peak in mass fraction 2 % G8 PAMAM dendrimer samples at low q represents incipient ordering and is not seen for the mass fraction 1 % G9 or G10.

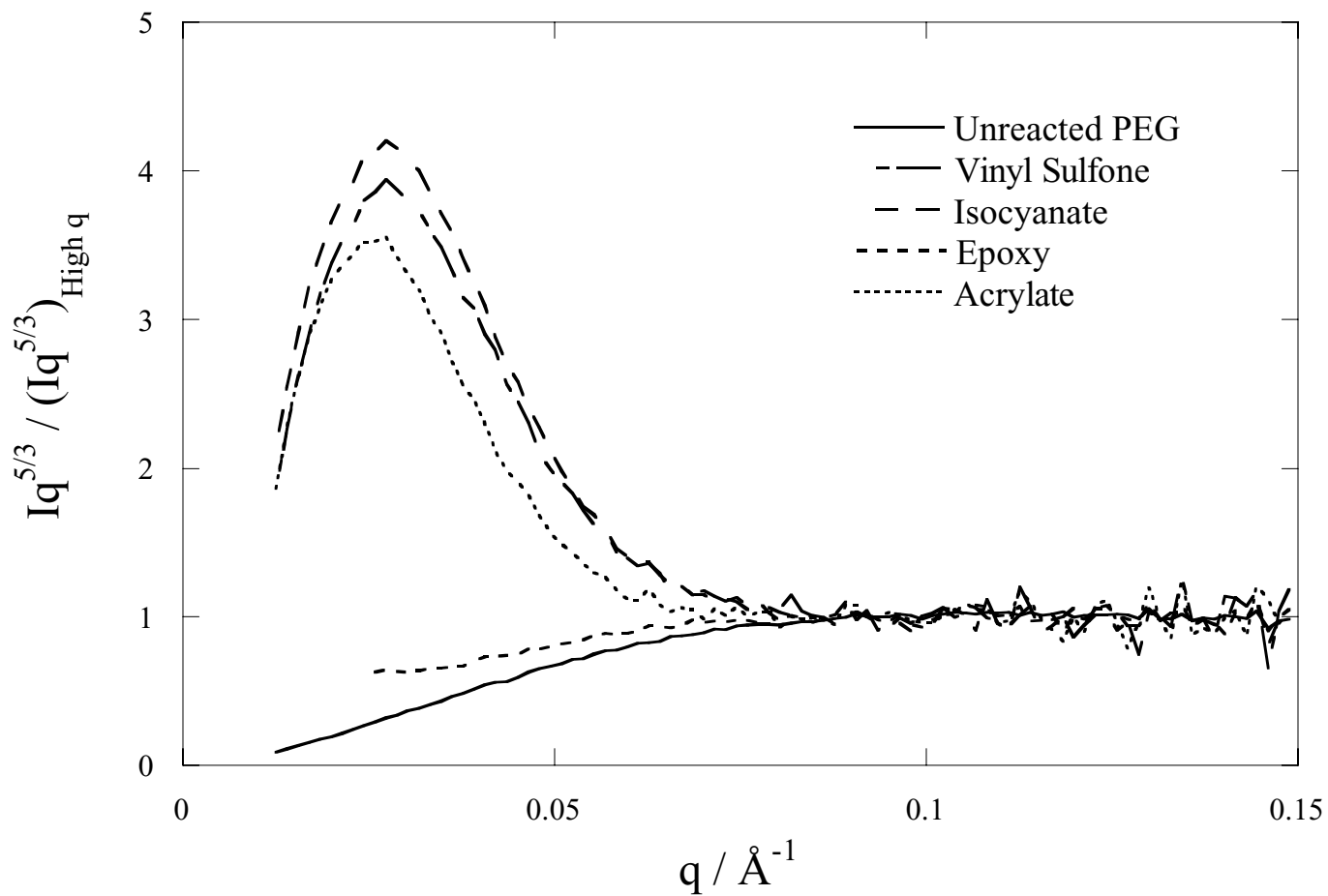


Figure 48 Kratky plots of 32 arm stars with DSM G5 cores. The choice of endlinking chemistry will affect the ultimate number of arms added.

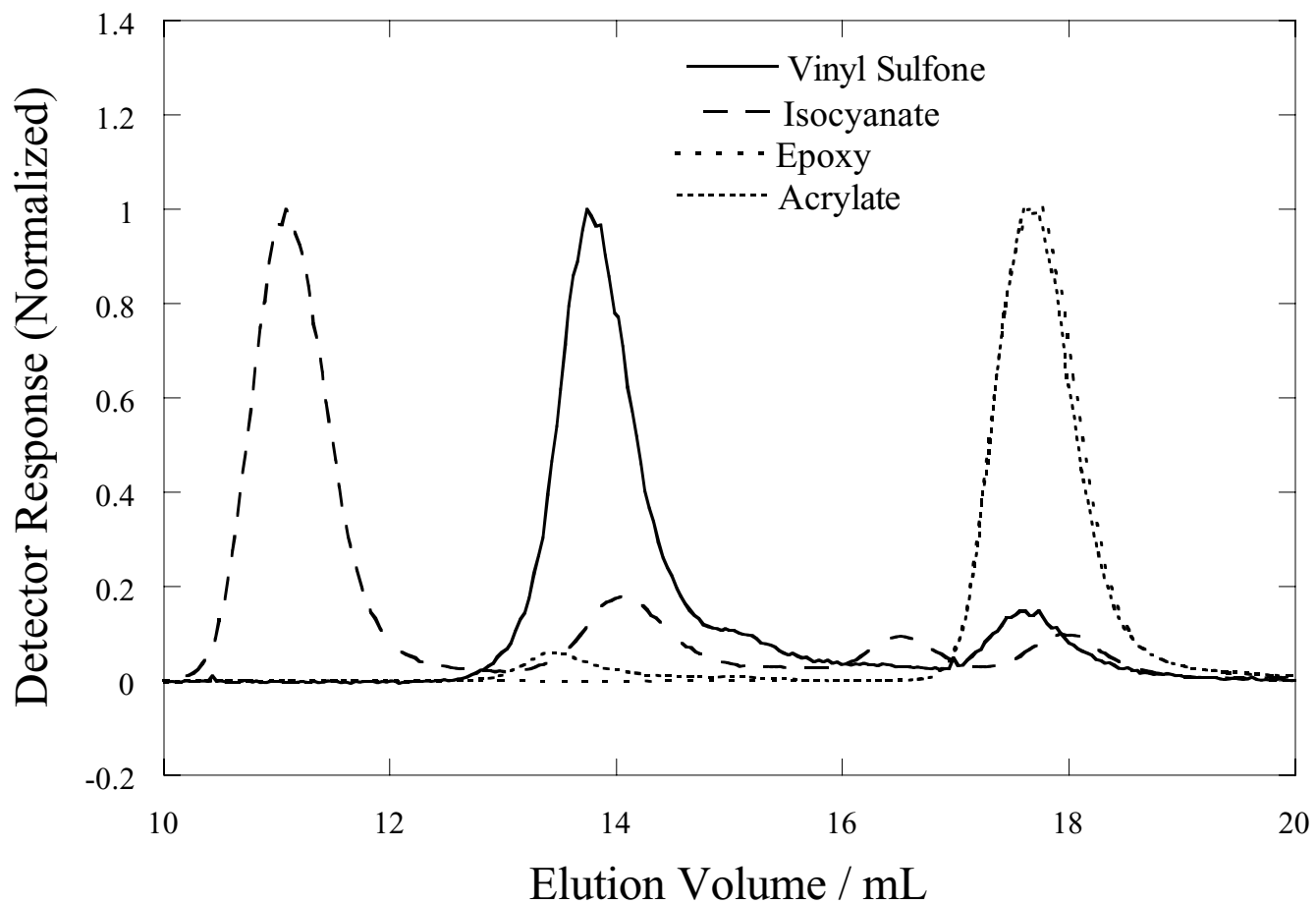


Figure 49 GPC on the 32 arm stars (Figure 48) demonstrating the differences in reactive endlinking chemistries.

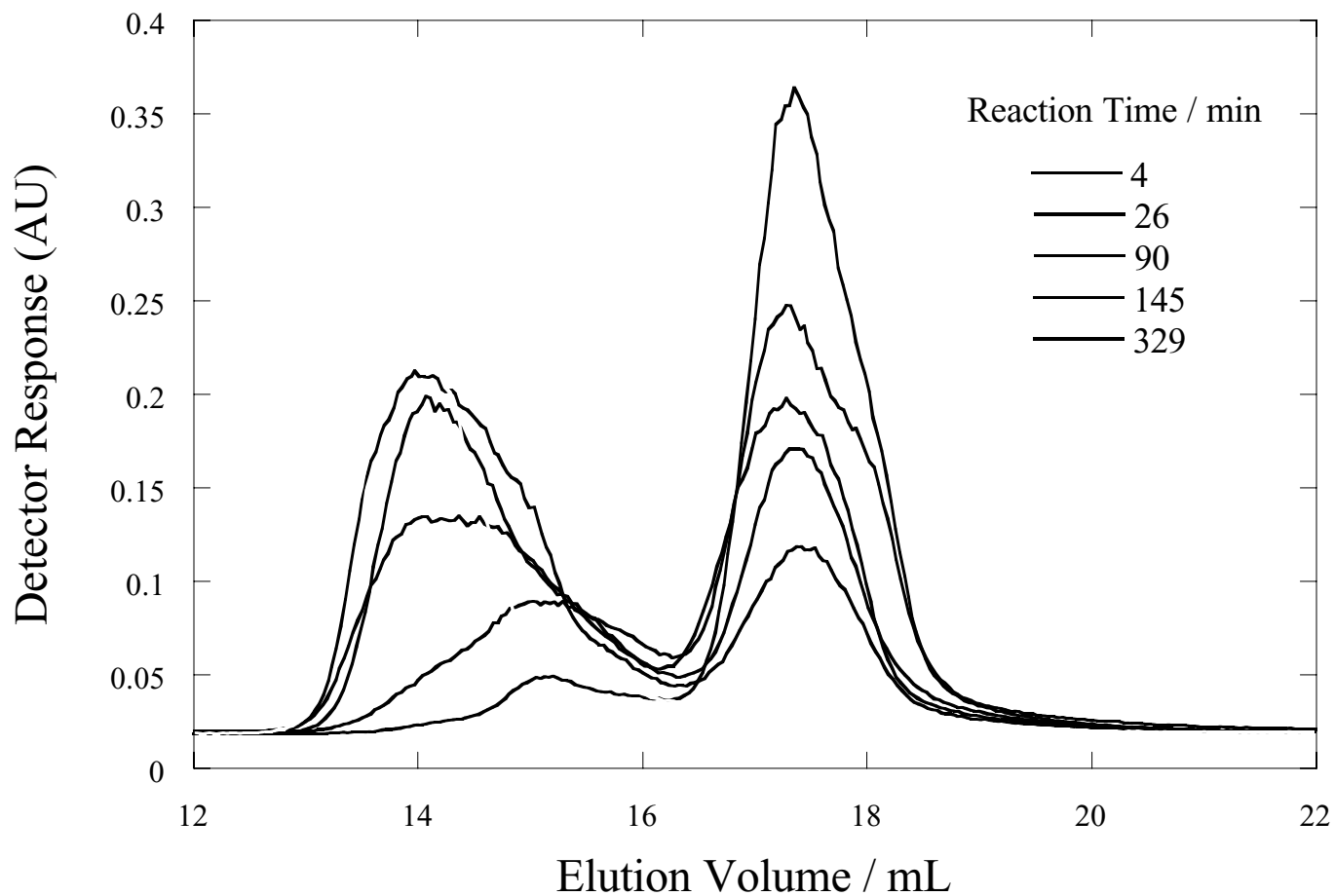


Figure 50. Kinetically Resolved GPC on DSM G4 stars of expected functionality 32. The star (at low elution volumes) is clearly delineated from the free, reacting arms. A ratio of the two peaks provides a measure of the conversion.

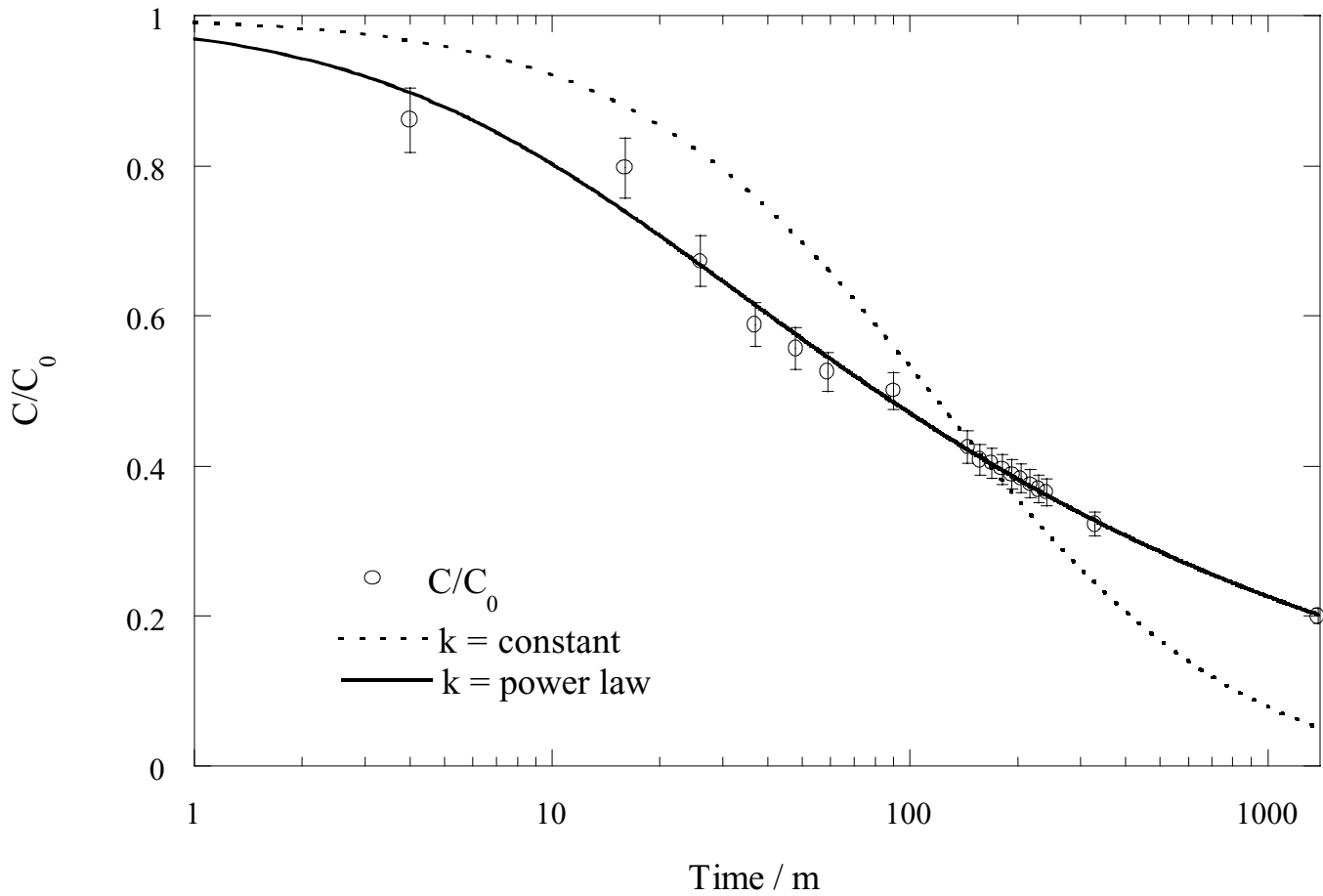


Figure 51 Kinetic Analysis of Figure 50. The dotted line demonstrates the fit expected from Equation (2.12). A better fit is obtained when the reaction order is allowed to float (Equation (2.13)). This demonstrates that arms add very rapidly in early stages, but further addition is very sterically hindered at late stages.

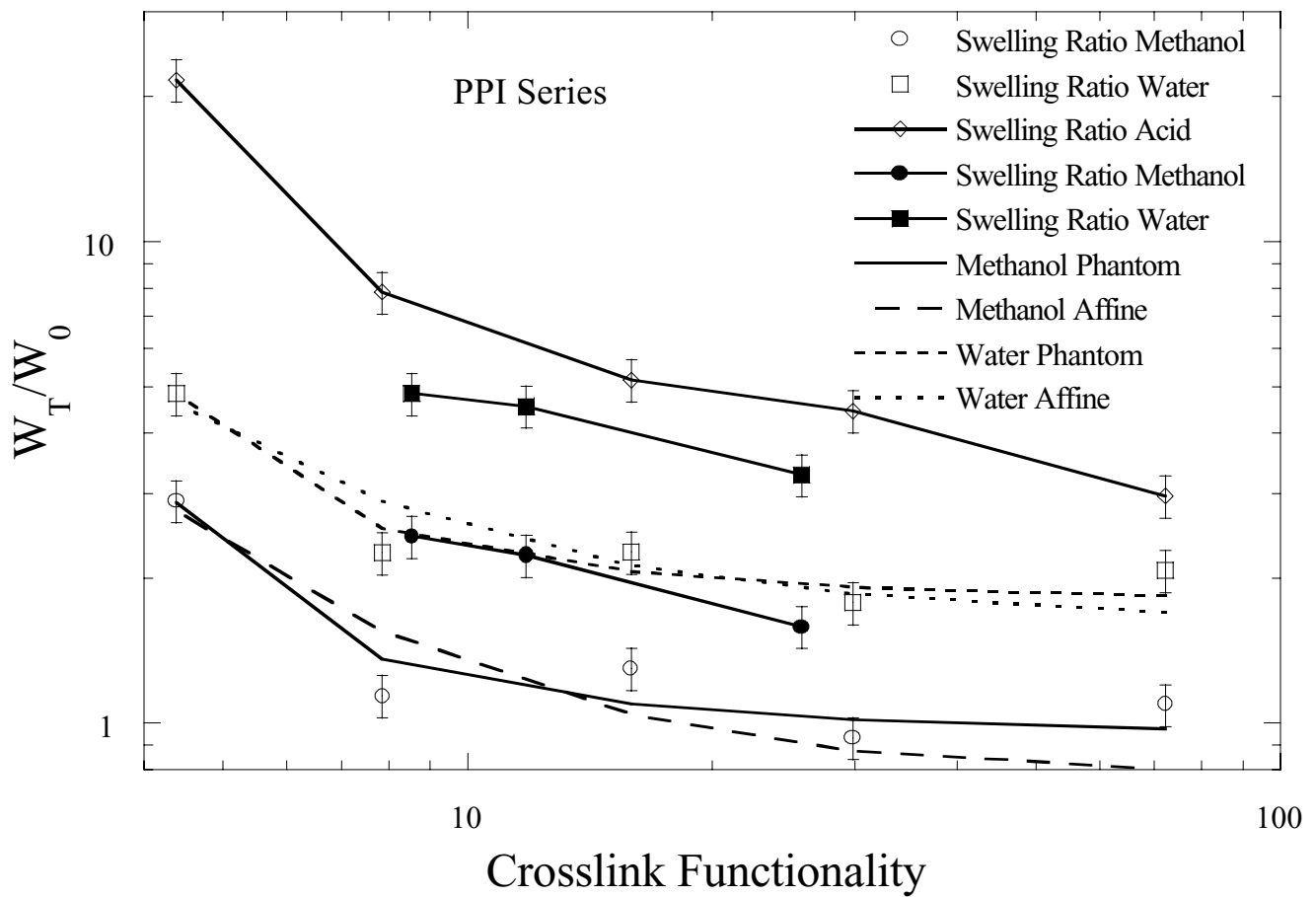


Figure 52. DSM G5 networks with differing PEG/DSM stoichiometry. The most lightly crosslinked gels swell most, and there is little variance in swelling for high crosslink functionality in accord with Equation (2.14) and (2.15)

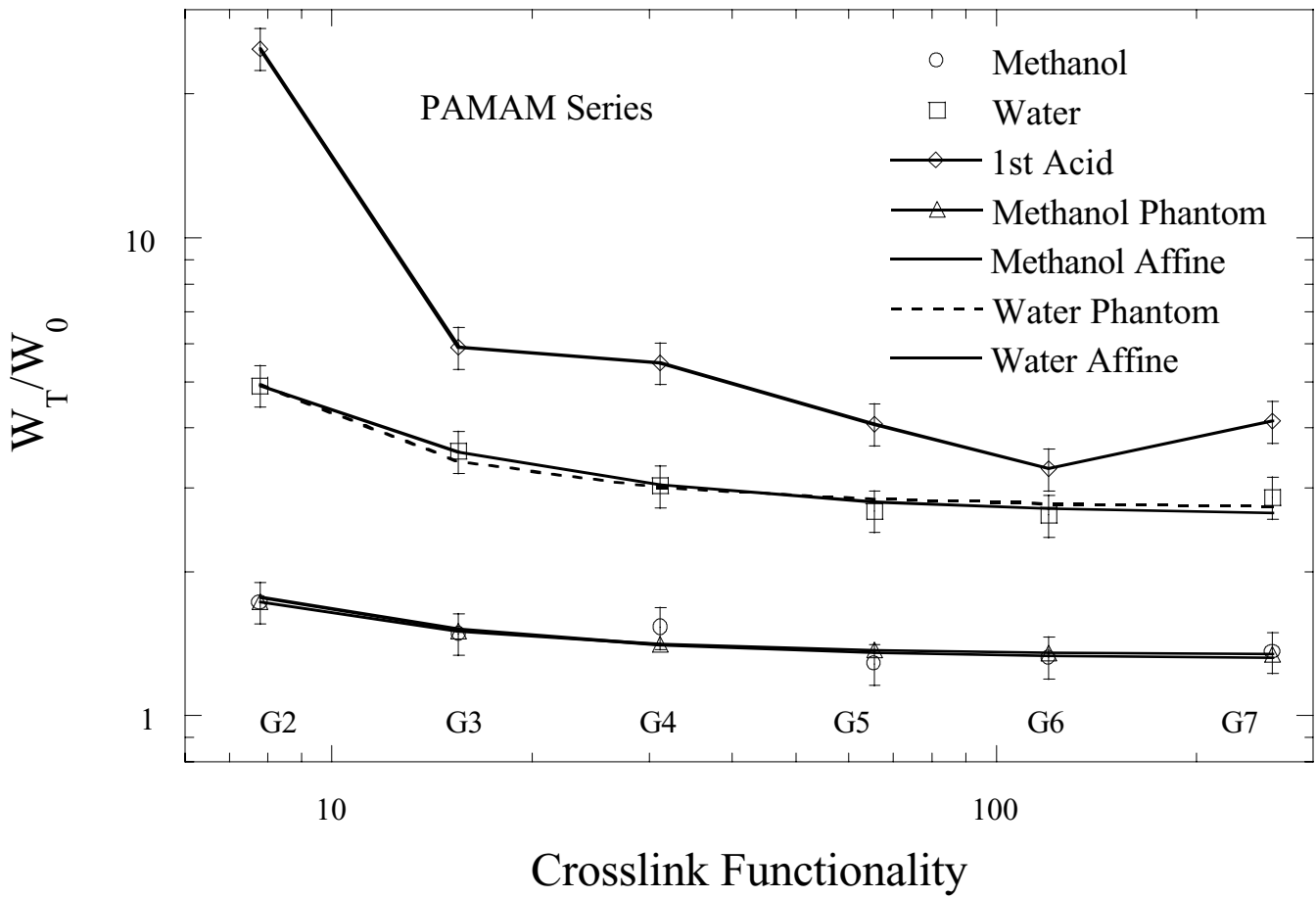


Figure 53. PAMAM G4 networks with differing PEG/PAMAM stoichiometries (see. Figure 52)

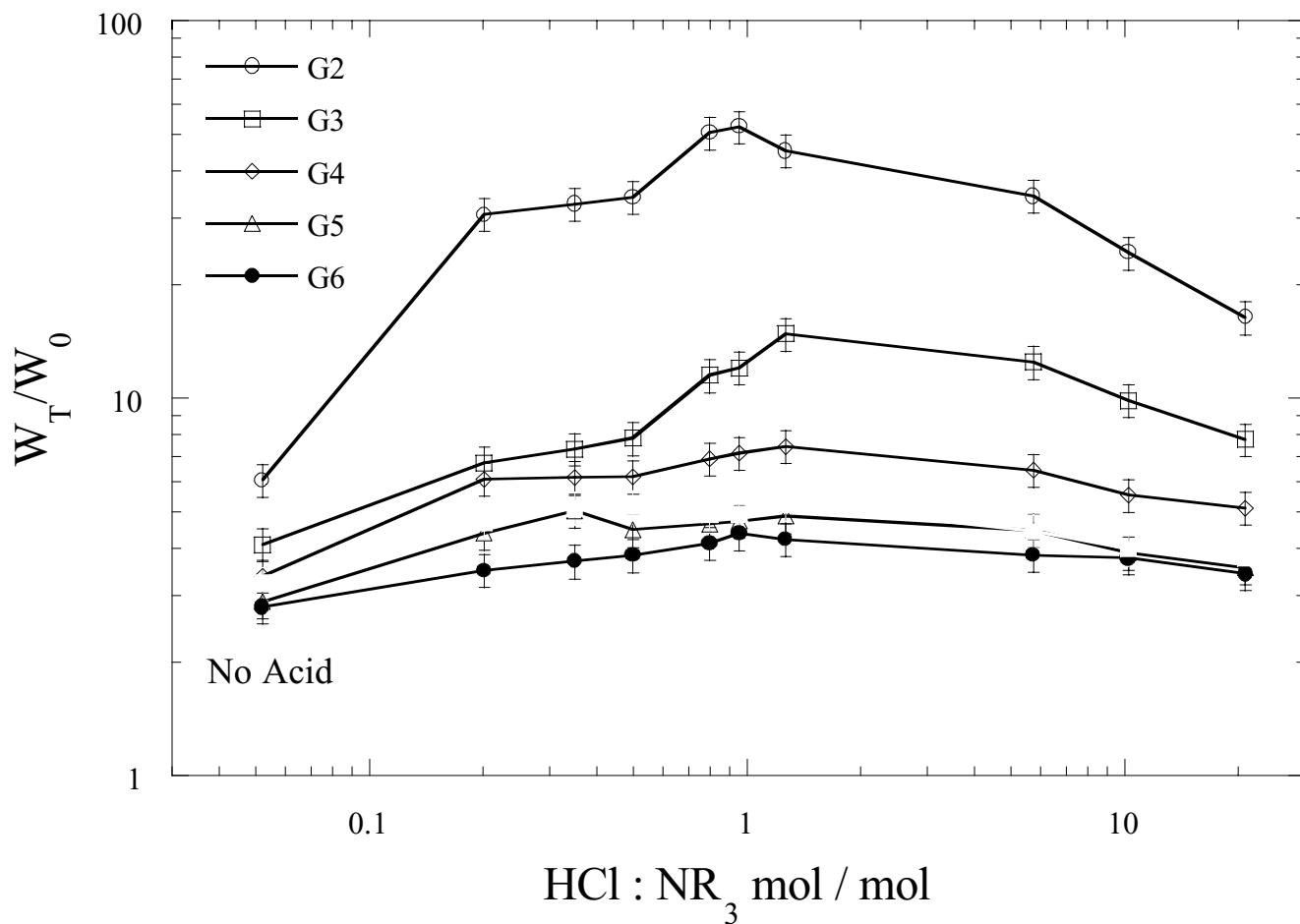


Figure 54. PAMAM networks swollen in solutions of decreasing ph. Gels with the lowest functionality swell the most, and all gels demonstrate a maximum in swelling due to repulsion of the (acid charged) dendrimers. The swelling decreases at lower ph (higher HCl:NR₃) due to screening of the repulsive interactions.

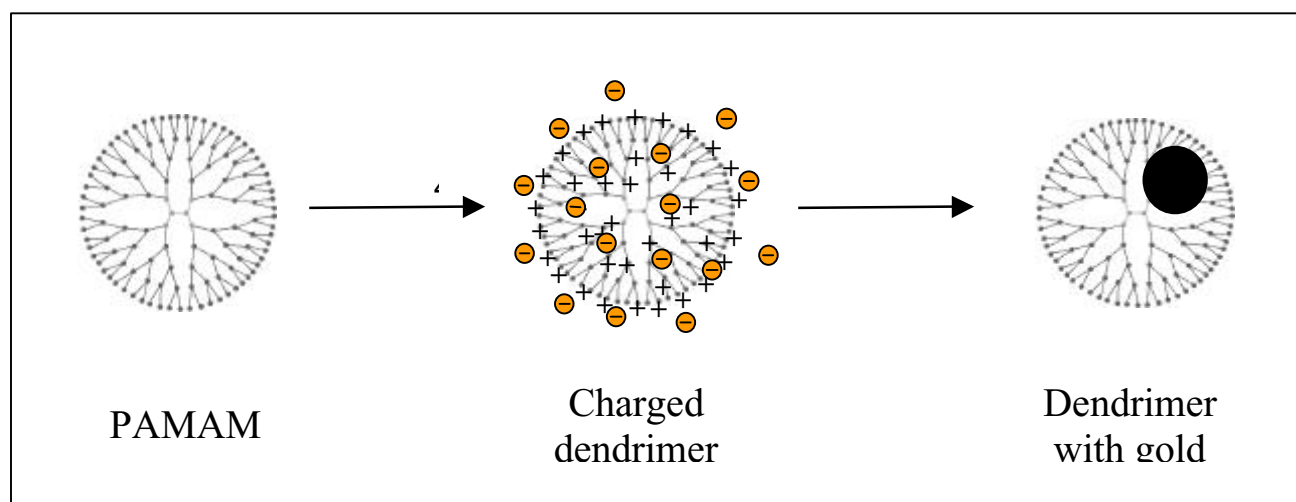


Figure 55. Dendrimer nanotemplating in aqueous solution. In a first step, the dendrimer is loaded with a precursor salt ($H^+ AuCl_4^-$) resulting in a charged dendrimer with the precursor as counterions. In a second step, the chemical reduction is performed which yields a colloid inside the dendrimer.

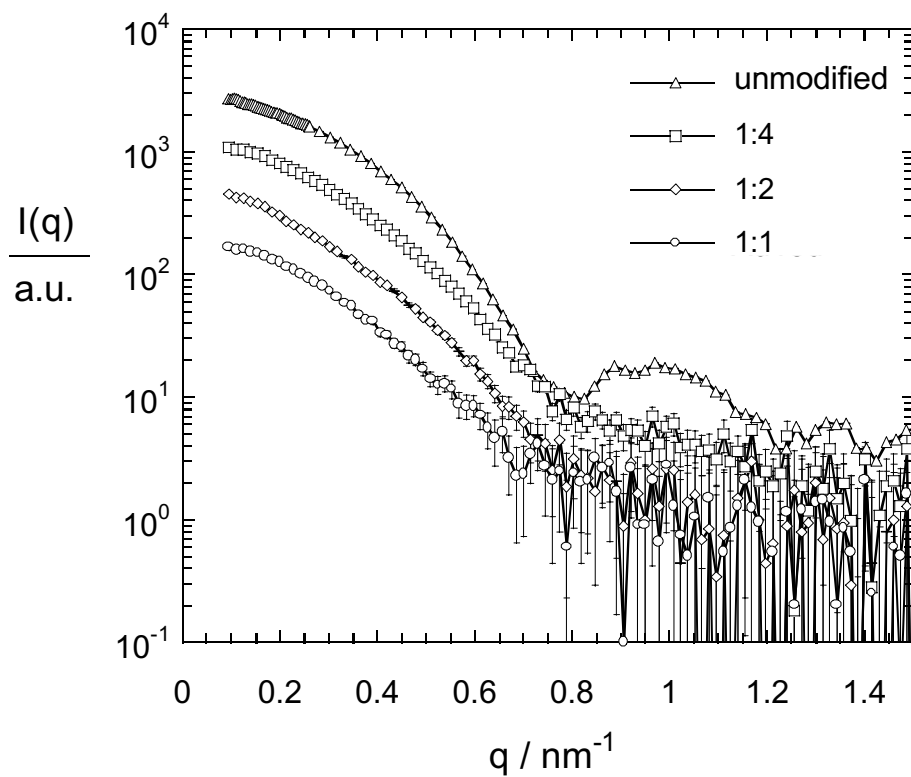


Figure 56 UV-VIS spectra for gold-dendrimer hybrid colloids in aqueous solution. The spectra correspond to G9-PAMAM dendrimer samples loaded with different amounts of gold (the molar ratio of gold ions to dendrimer end groups is indicated in the figure.)

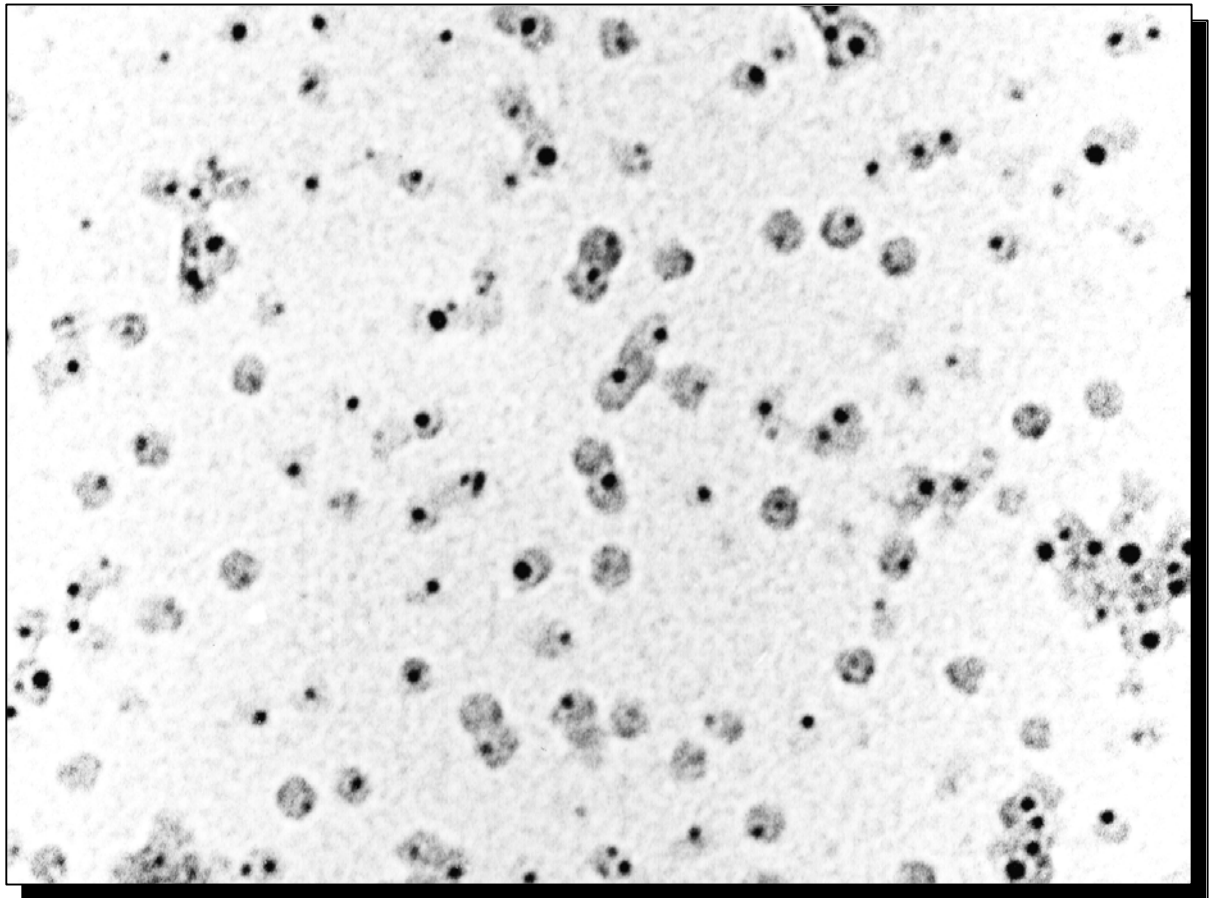


Figure 57. TEM of gold containing G9 PAMAM-dendrimer obtained for 1:1 loading. The dendrimer has been stained with phosphotungstic acid, it appears gray, the gold appears black. A: fast reduction (NaBH_4 in 0.1 mol/L NaOH) b: slow reduction (NaBH_4 in 0.3 mol/L NaOH)

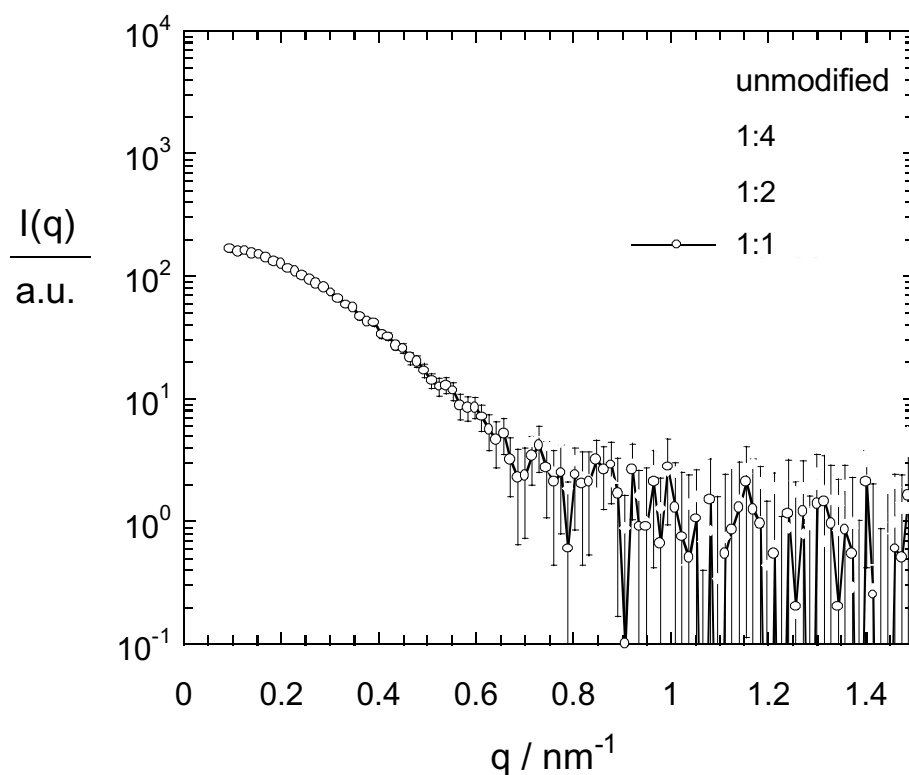


Figure 58. a) Small angle x-ray scattering curve $I(q)$ for the plain G9 PAMAM-dendrimer along with fit to the data. Error bars are the measured standard deviation in $I(q)$. b) Pair distribution function $P(r)$ obtained by indirect Fourier transformation of the scattering data $I(q)$ (program ITP). A homogenous sphere structure with a diameter of 13 nm becomes evident

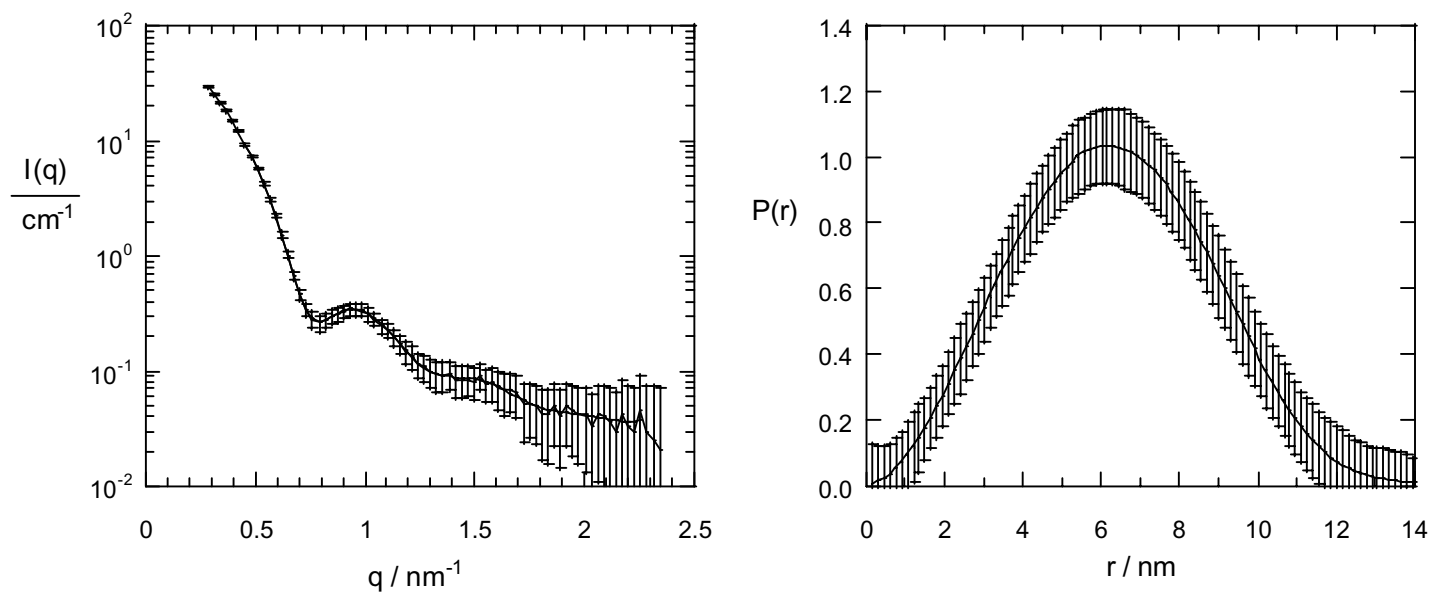


Figure 58 a: Small angle x-ray scattering curve $I(q)$ for the plain G9 PAMAM-dendrimer along with fit to the data. Error bars are the measured standard deviation in $I(q)$.
 B: Pair distribution function $P(r)$ obtained by indirect Fourier transformation of the scattering data $I(q)$ (program ITP). A homogenous sphere structure with a diameter of 13 nm becomes evident.

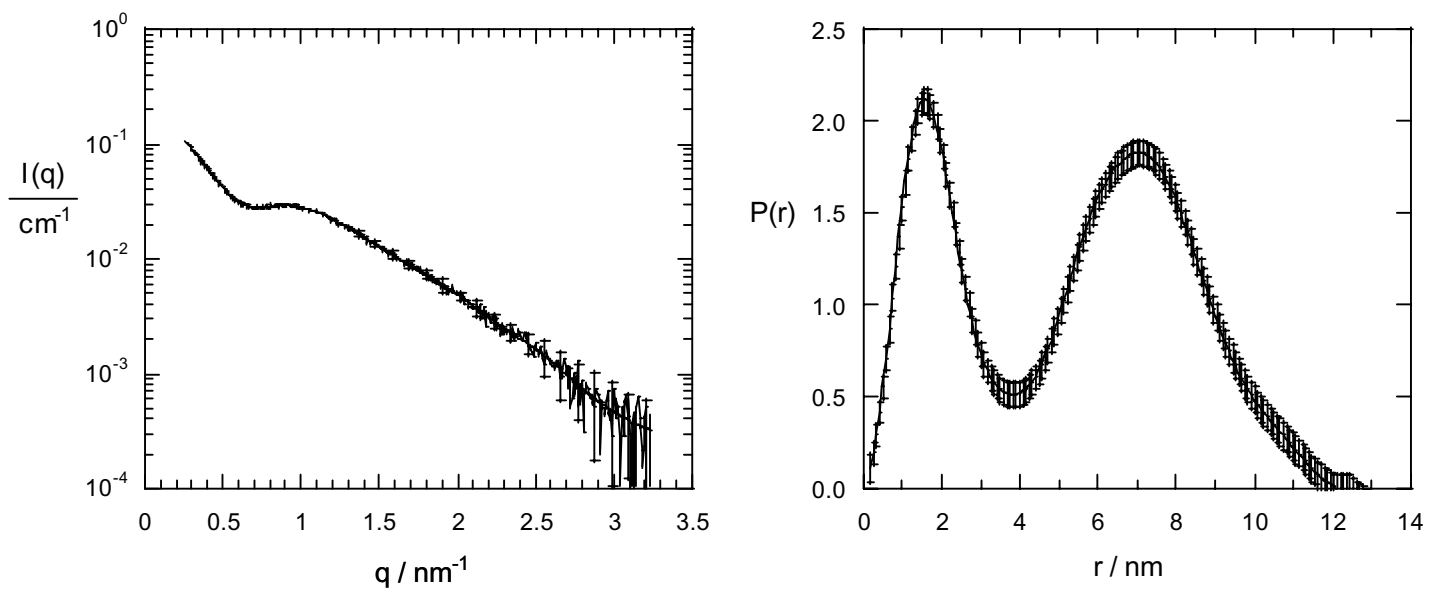


Figure 59 a) Small angle x-ray scattering curve $I(q)$ for the gold containing G9 PAMAM-dendrimer of figure 3 along with fit to the data. B) Pair distribution function $P(r)$ obtained by indirect Fourier transformation of the scattering data $I(q)$ (program ITP). A layered-sphere structure with a total diameter of 13 nm becomes evident.

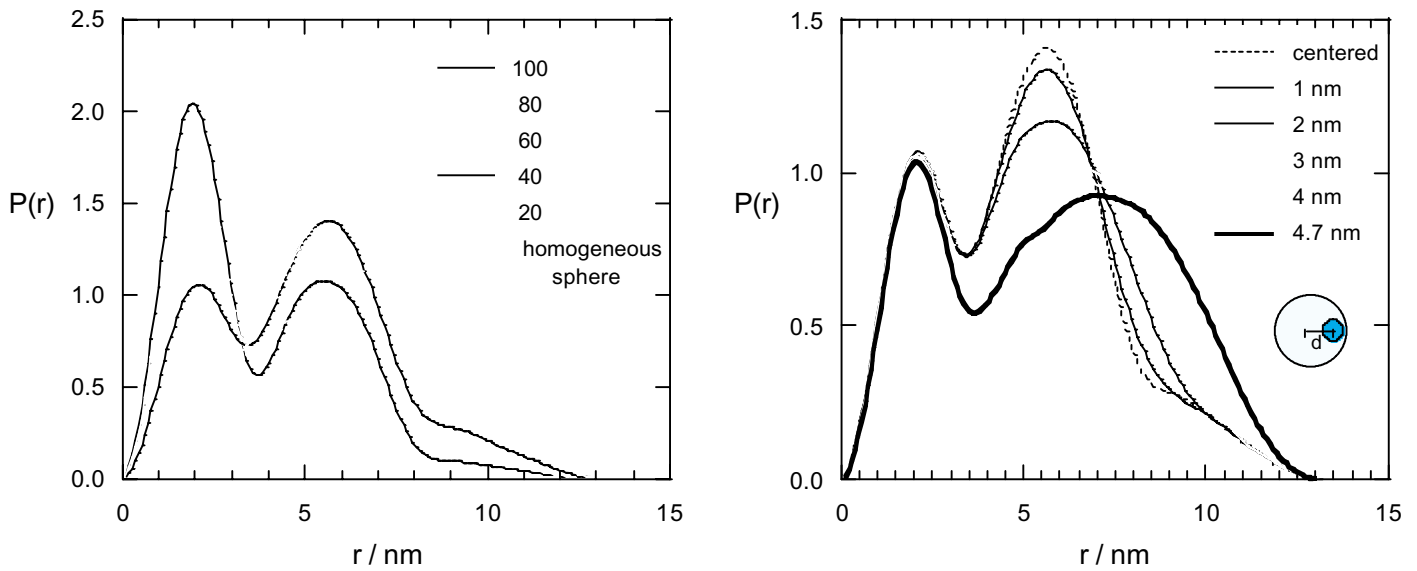


Figure 60 a) Theoretical pair distribution function $P(r)$ calculated for layered spheres with different relative contrast of the inner sphere (solvent contrast = 0, outer sphere contrast = 1, inner sphere contrast as given in the figure). The basic shape of the experimental function in Figure 4b cannot be modeled.

B) Theoretical pair distribution function $P(r)$ calculated for layered spheres with different offset of the inner sphere inside the outer sphere (outer sphere radius = 6.6 nm, inner sphere radius = 1.8 nm, offset d between centers given in the figure). The basic shape of the experimental function is much better represented.

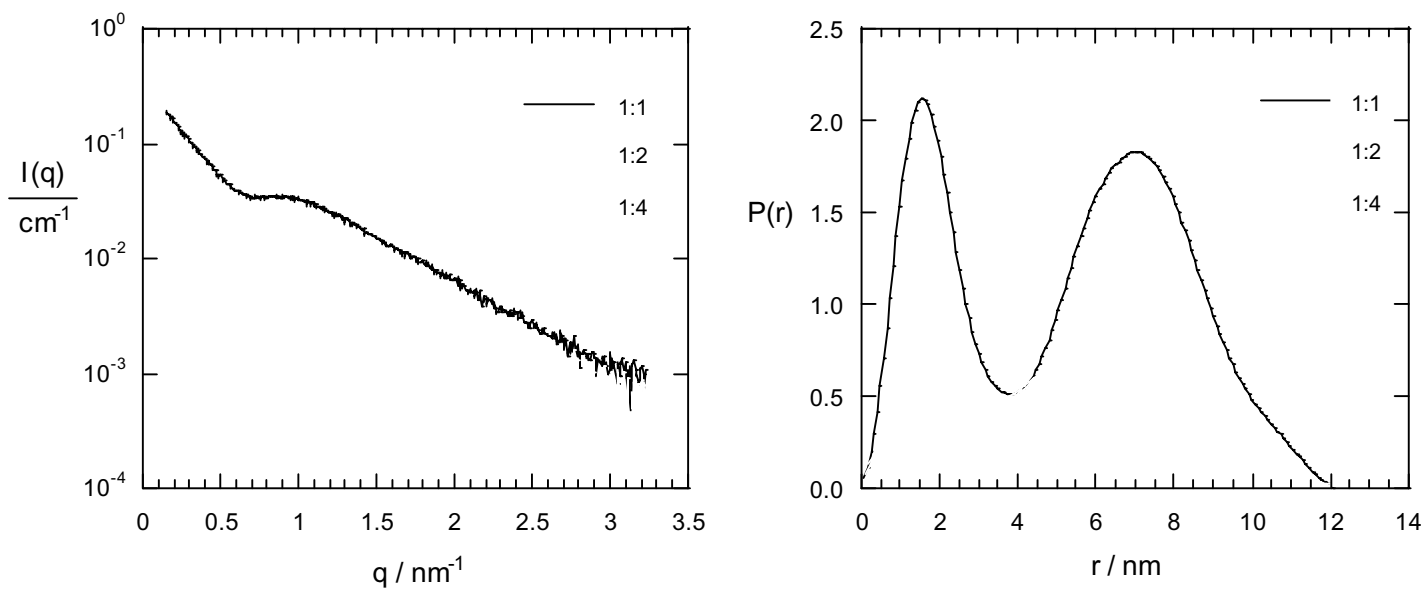


Figure 61 a) Small angle x-ray scattering curves $I(q)$ for gold containing G9 PAMAM-dendrimers obtained for different loading ratios 1:1, 1:2 and 1:4. Pair distribution functions $P(r)$ obtained by indirect Fourier transformation of the scattering data $I(q)$ in b) The decreasing gold diameter but constant dendrimer diameter upon decreasing loading is visible.

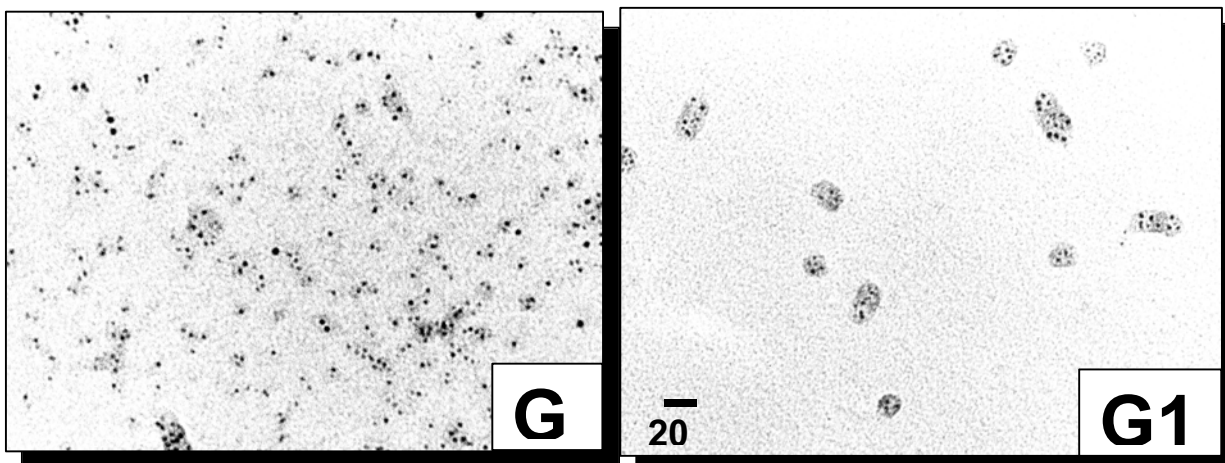


Figure 62 a) TEM of gold containing G8 PAMAM dendrimer obtained for 1:1 loading and slow reduction. (The dendrimer has been stained with phosphotungstic acid.) b) TEM of gold containing G10 PAMAM dendrimer obtained for 1:1 loading and slow reduction. (The dendrimer has been stained with phosphotungstic acid.)

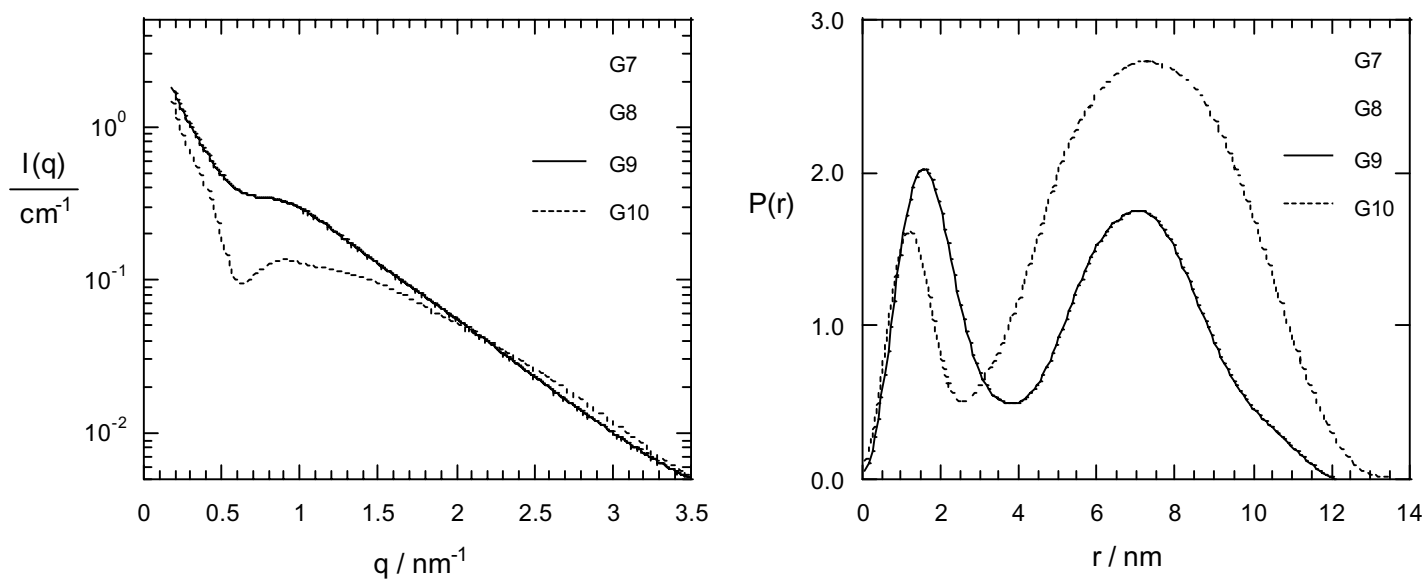


Figure 63 a) Small angle x-ray scattering curves $I(q)$ for gold-dendrimers hybrid structures obtained with PAMAM dendrimers of generation 7 to 10. b) Pair distribution functions $P(r)$ obtained by indirect Fourier transformation of the scattering data $I(q)$ in a). For G7 to G9 (solid lines) an increasing gold diameter with increasing dendrimer diameter is seen. Contrary, for G10 (dotted line) the gold diameter is decreased though the dendrimer diameter is further increased.

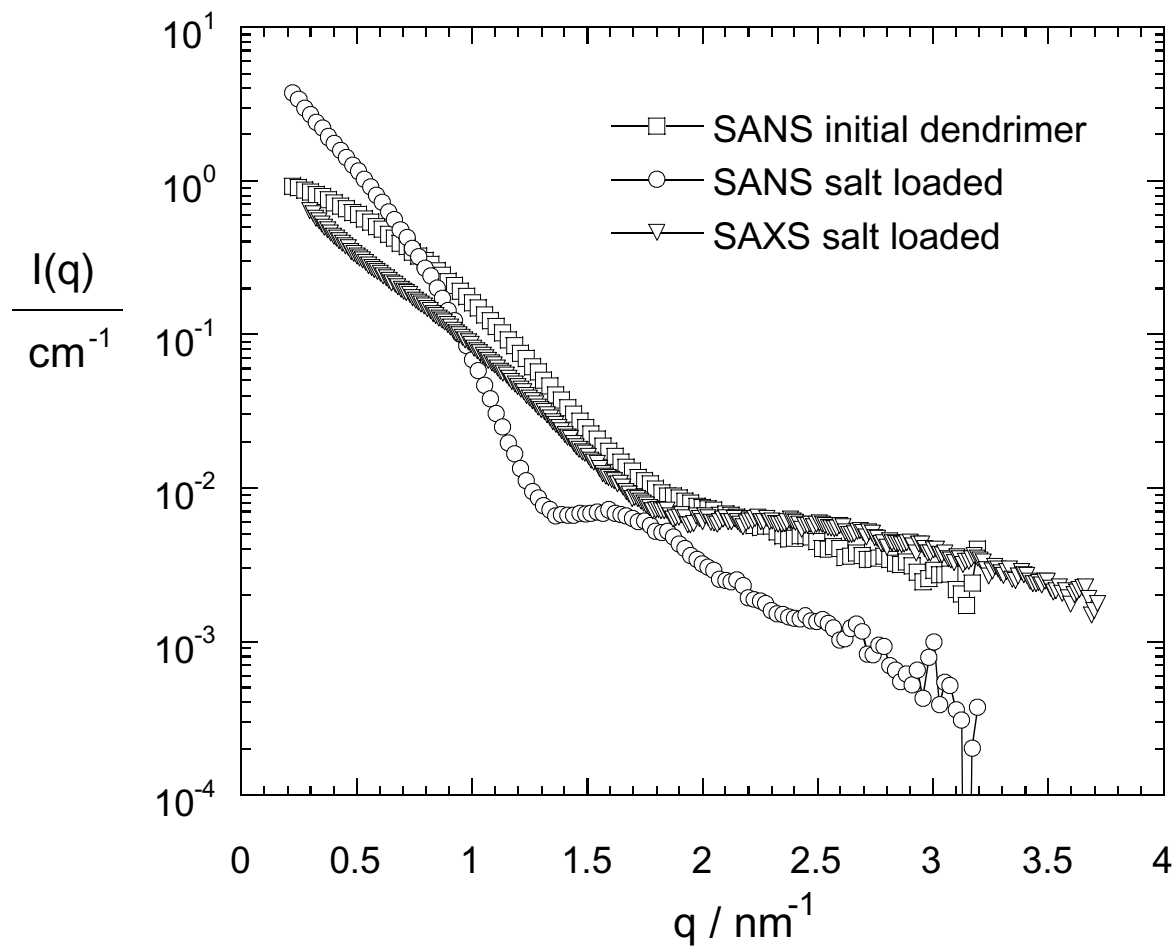


Figure 64 Small angle neutron scattering curve for the initial G5 poly(propyleneimine) dendrimer in toluene at 55°C and small angle neutron scattering curve and small-angle x-ray scattering curve after solubilization of gold salt.

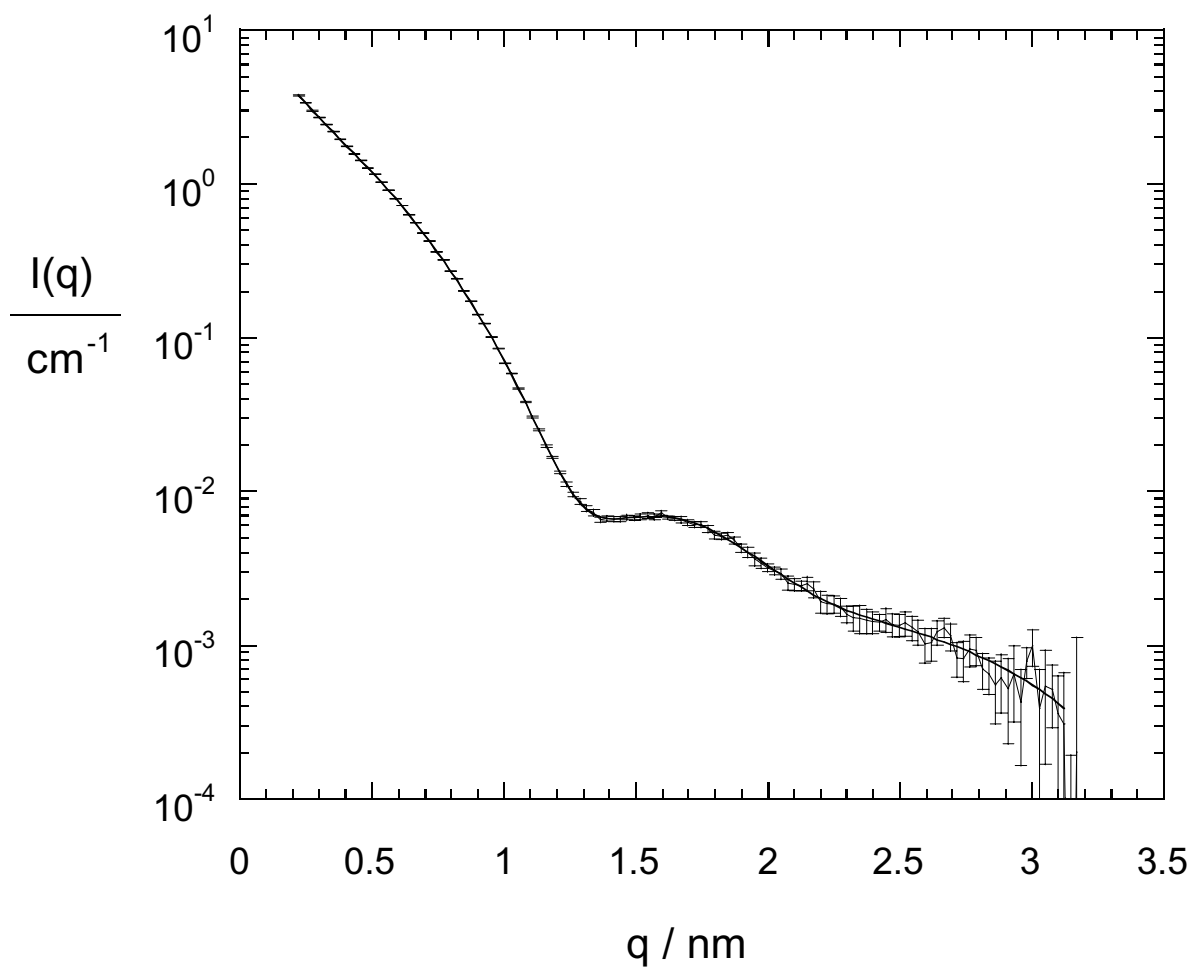


Figure 65 Small angle neutron scattering curve $I(q)$ for the gold-salt loaded G5 poly(propyleneimine) dendrimer along with fit to the data.

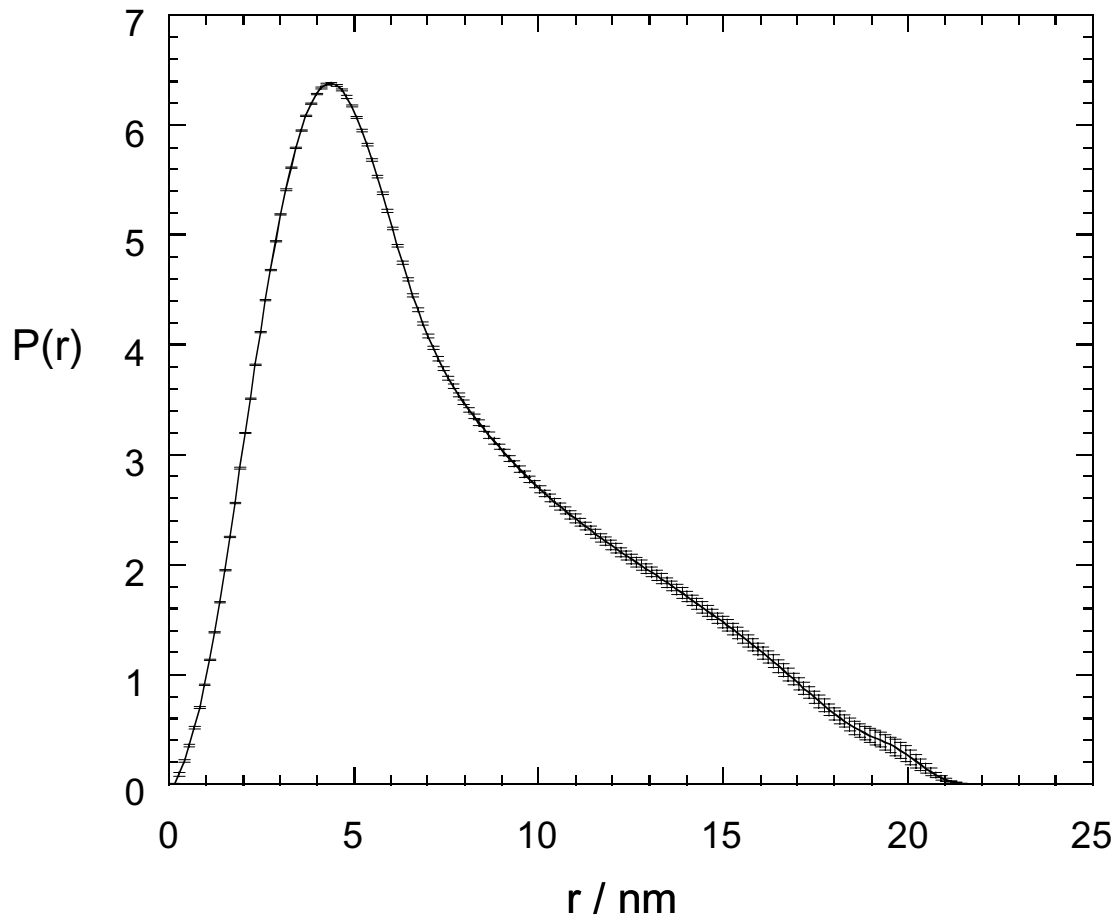


Figure 66 Pair distance distribution function $P(r)$ obtained by indirect Fourier transformation of the scattering data $I(q)$ (program ITP). A cylindrical structure with a diameter of 6 nm and a length of 21 nm becomes evident.

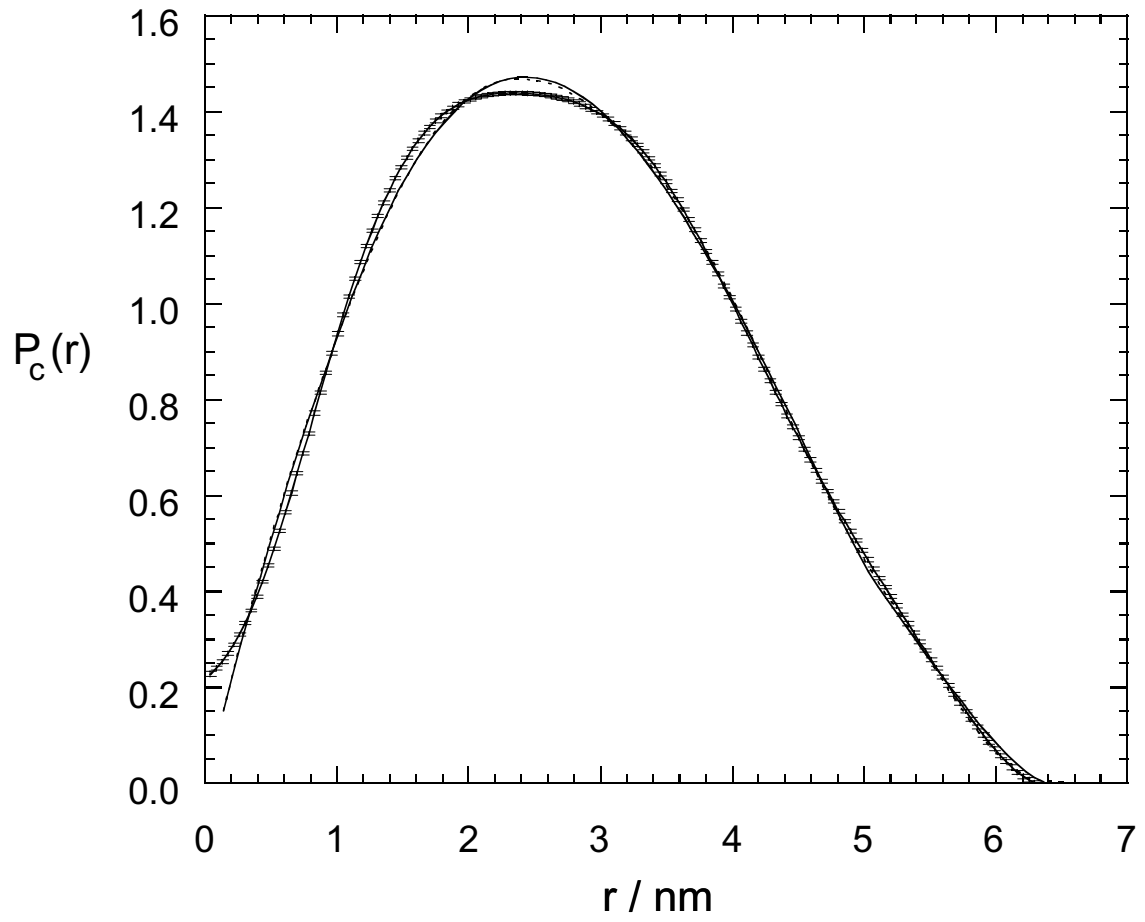


Figure 67 Cross-sectional pair distance distribution function $P_c(r)$ obtained by indirect Fourier transformation of the scattering data $I(q)$ under assumption of a cylindrical particle geometry

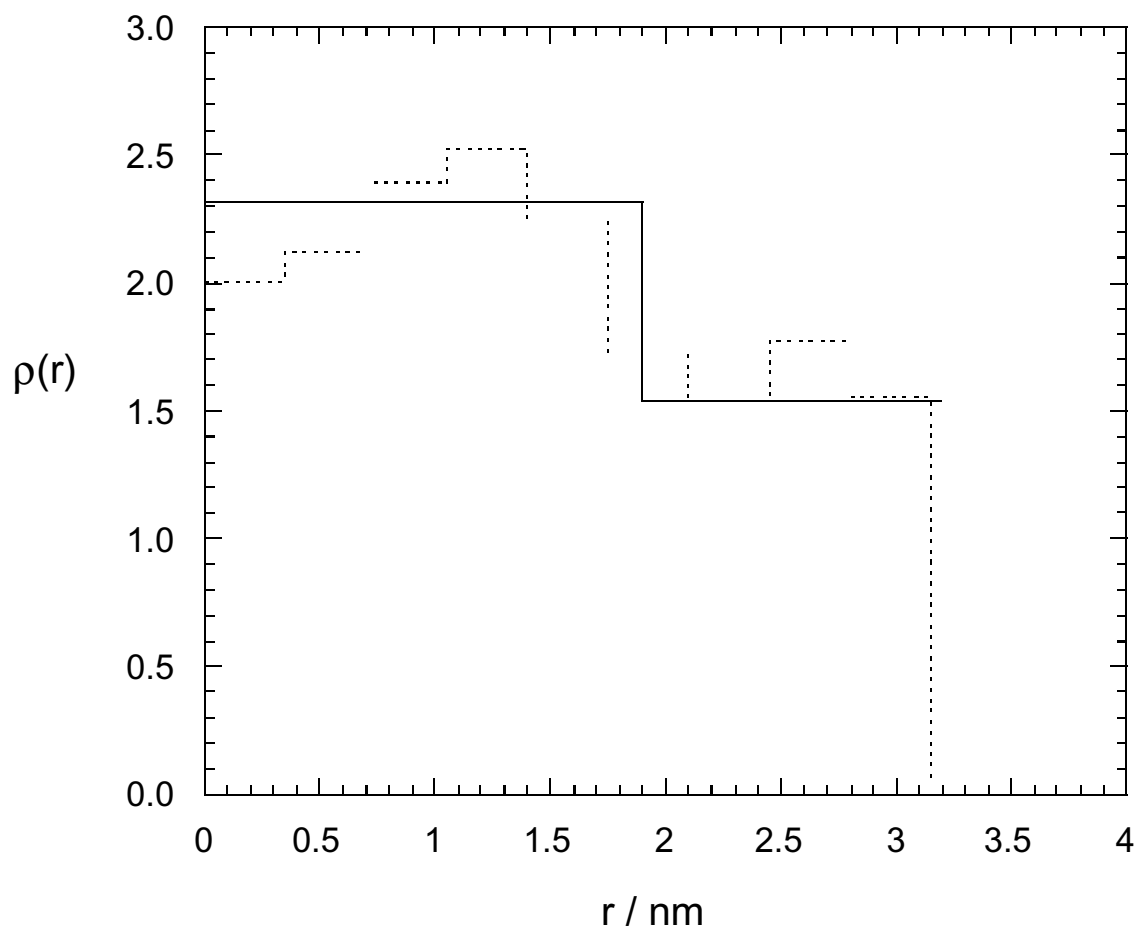


Figure 68. Radial scattering length density profile $\rho(r)$ obtained by square-root deconvolution of the cross sectional pair distance distribution function $P_C(r)$ in figure 68. The dotted line represents the result from the first multi-step approximation. The solid line represents the final solution, i.e. the easiest profile corresponding to the best fit of the data: A two step cross-sectional profile becomes evident.

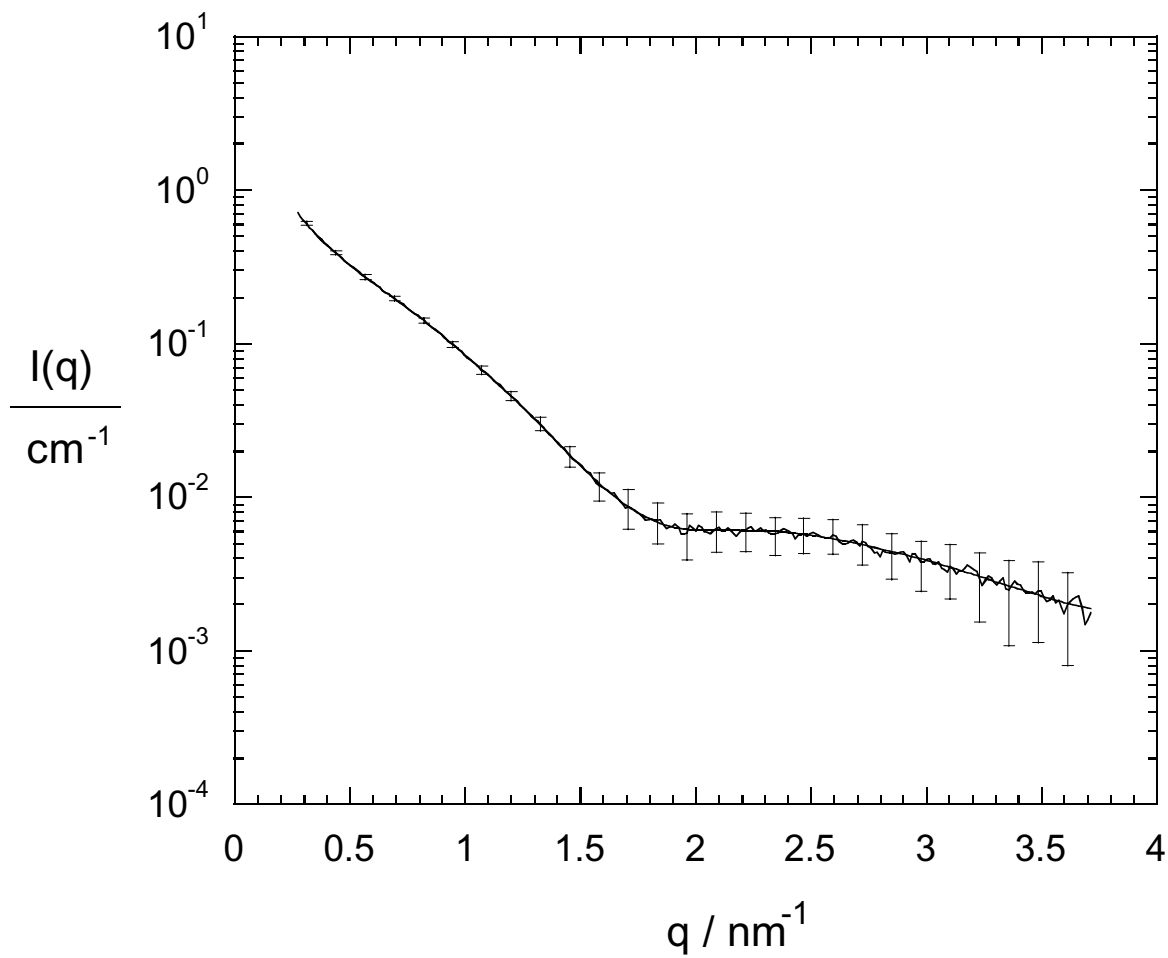


Figure 69 Small angle x-ray scattering curve $I(q)$ for the gold-salt loaded G5 poly(propyleneimine) dendrimer along with fit to the data

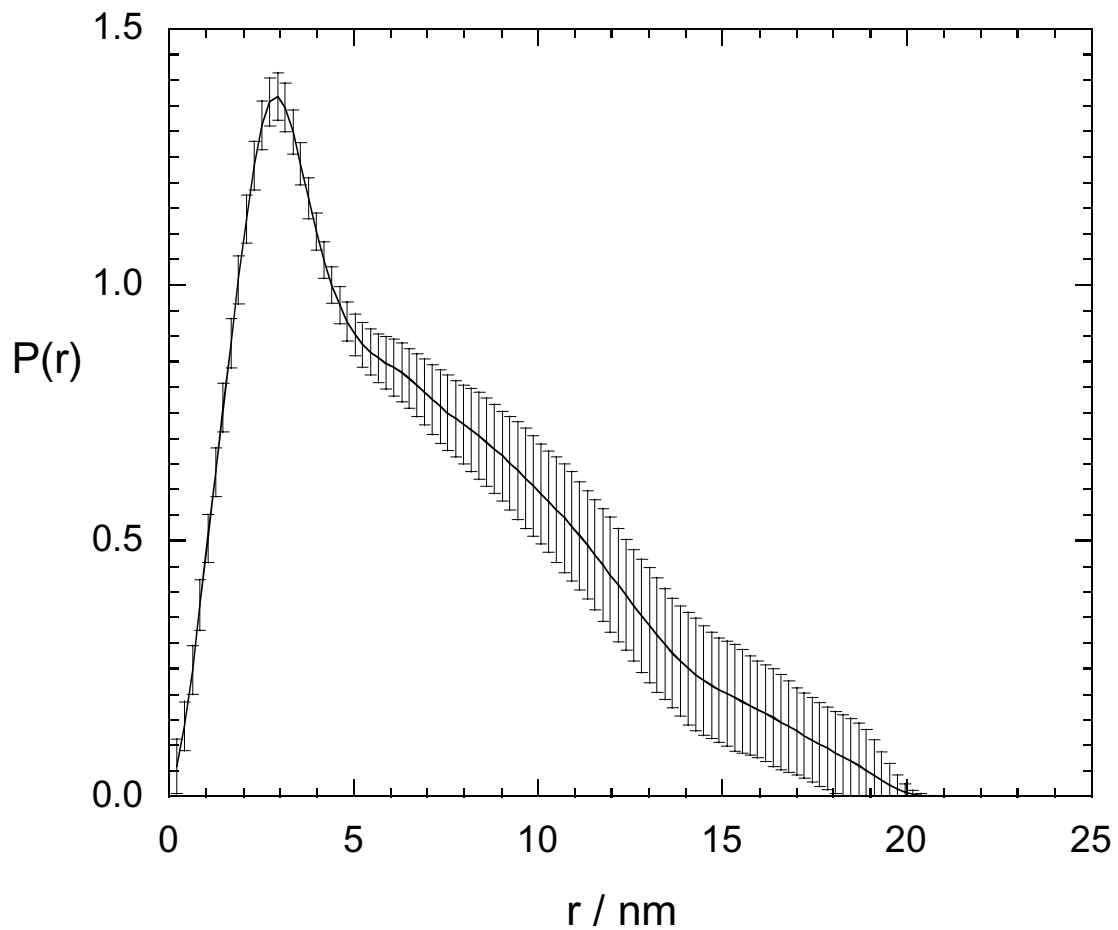


Figure 70 Pair distance distribution function $P(r)$ obtained by indirect Fourier transformation of the scattering data $I(q)$ (program ITP). A cylindrical structure with a diameter of 4 nm becomes evident.

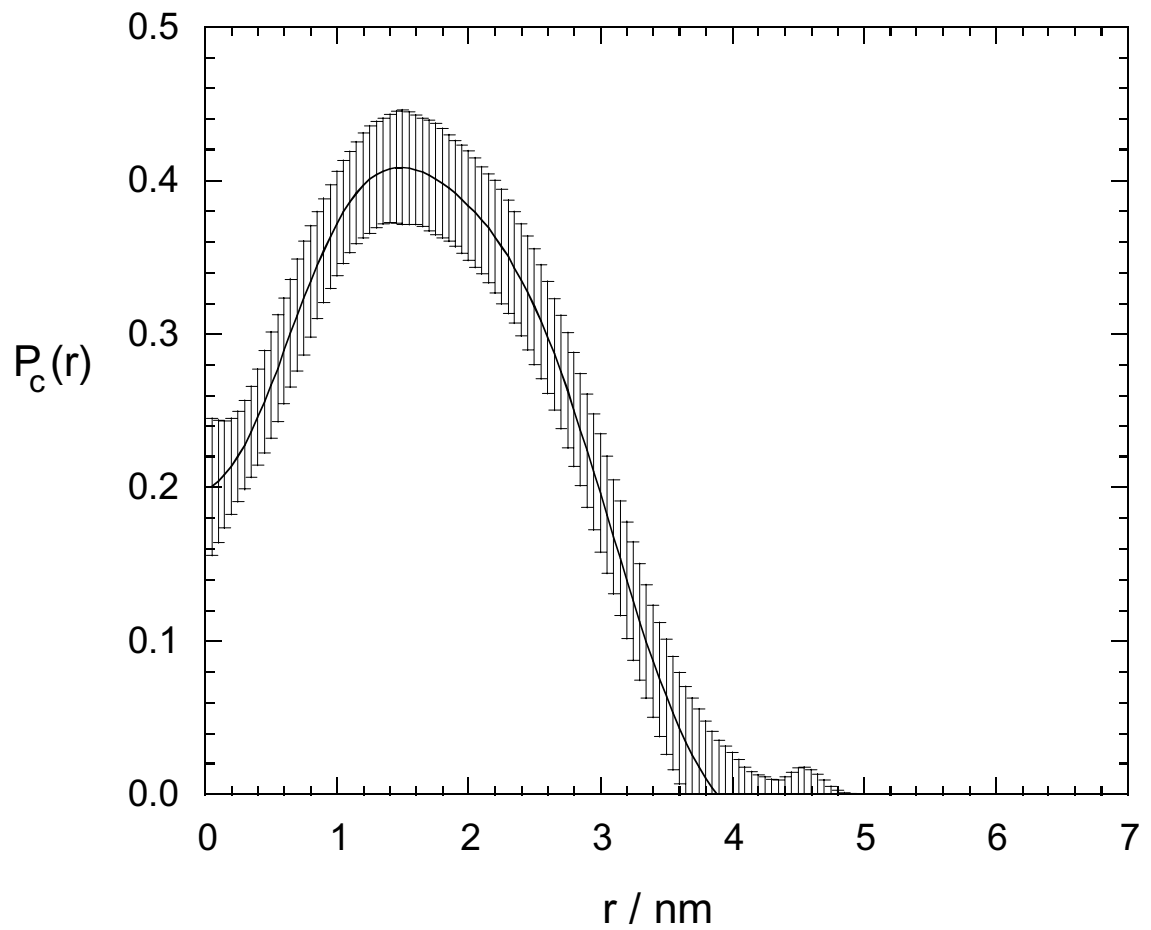


Figure 71 Cross-sectional pair distance distribution function $P_c(r)$ obtained by indirect Fourier transformation of the SAXS data $I(q)$ under assumption of a cylindrical particle geometry (program ITP).

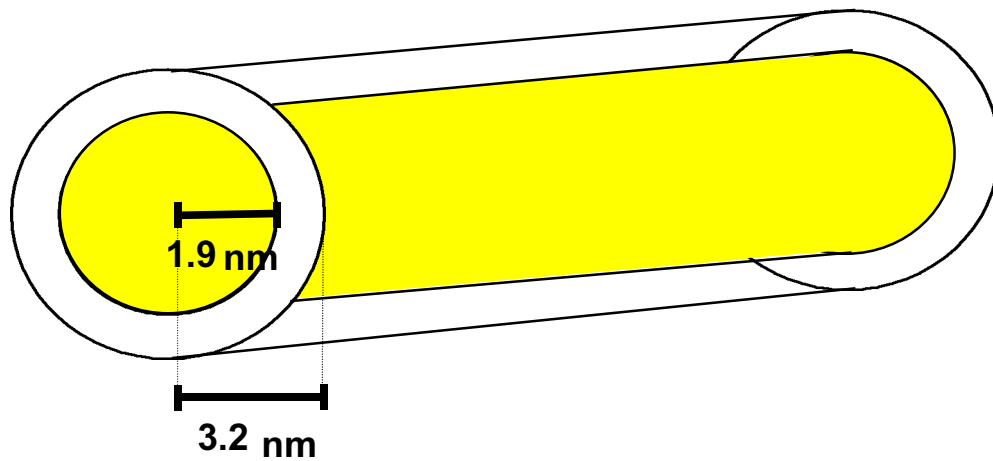


Figure 72 Schematic of the multi-dendrimer cylindrical structure as deduced from the SAXS and SANS results.

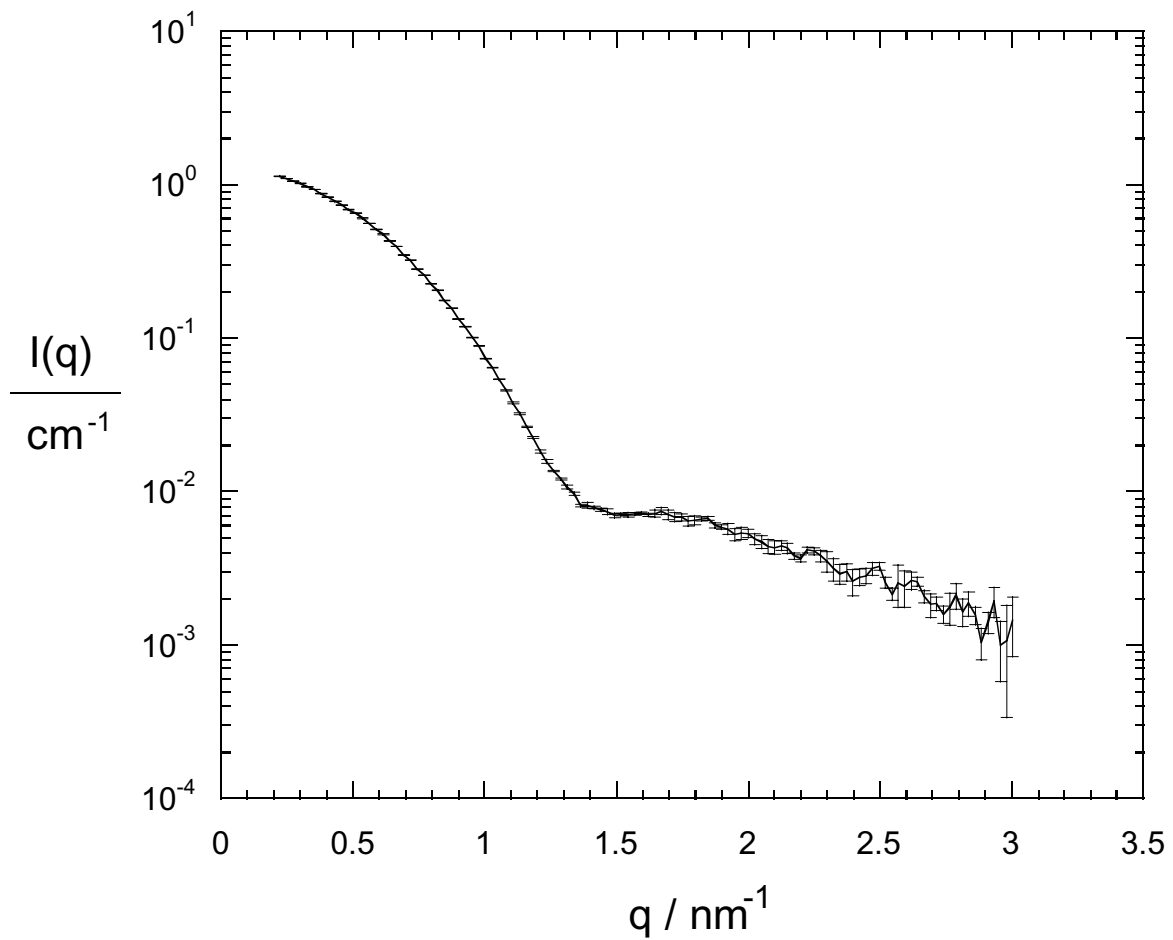


Figure 73 Small angle neutron scattering curve $I(q)$ for gold-dendrimer hybrid structures.

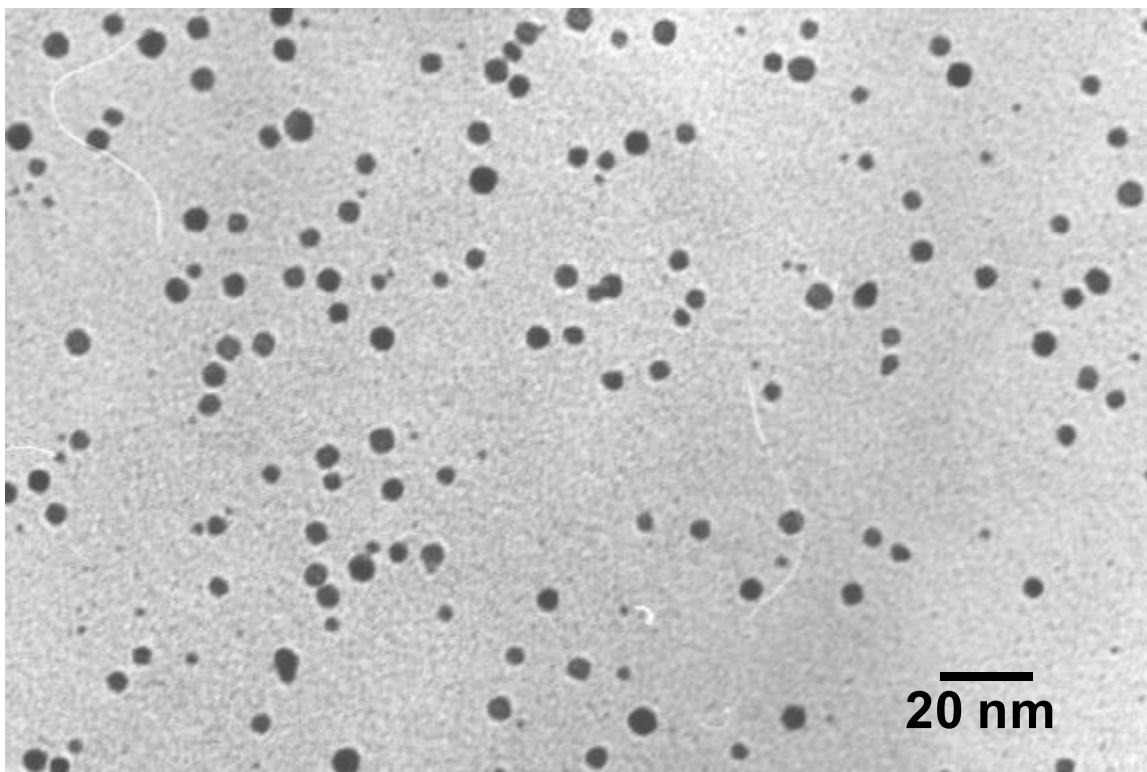


Figure 74 TEM of gold colloids obtained from hydrophobically modified G5 poly(propyleneimine) dendrimers loaded with gold-salt after reduction with sodium borohydrate.

References:

- 1)Amis E. J., B. B. J., Topp A., Prosa, T. J., Liu, D.-W., Jackson, C. L., Karim, Douglas, J. *Nistir 6183* **1997**.
- 2)Amis E. J., B. B. J., Topp A. , Prosa, T. J., Liu, D.-W., Jackson, C. L., Karim, A., Ermi, B., Barnes, K., Nakatani, A., Nisato, G., Ivkov, R. *Nistir 6151* **1998**.
- 3)Amis E. J., B. B. J., Groehn, F., Prosa, T. J., Liu, D.-W., Barnes, K. A., Jackson, C. L., Viers, B. D., Karim, A., Douglas, J. F. **1999**, *Nistir 6353*.
- 4)Tomalia, D. A.; Naylor, A. M.; Goddard, W. A. *Angewandte Chemie-International Edition In English* **1990**, *29*, 138-175.
- 5)Hawker, C. J.; Wooley, K. L.; Frechet, J. M. J. *Journal Of The Chemical Society-Perkin Transactions 1* **1993**, 1287-1297.
- 6)Hawker, C. J.; Fréchet, J. M. J. *Three-Dimensional Dendritic Macromolecules: Design, Synthesis And Properties*; Ebdon, J. R. And Eastmond, G. C., Ed.; Blackie: Glasgow, Uk, 1995, Pp 290-330.
- 7)Newkome, G. R.; Morefield, C. N.; Vögtle, F. *Dendritic Molecules: Concepts, Synthesis, Perspective*; Vch: Weinheim, Germany, 1996.
- 8)Debrabandervandenberg, E. M. M.; Meijer, E. W. *Angewandte Chemie-International Edition In English* **1993**, *32*, 1308-1311.
- 9)Debrabandervandenberg, E. M. M.; Nijenhuis, A.; Mure, M.; Keulen, J.; Reintjens, R.; Vandenbooren, F.; Bosman, B.; Deraat, R.; Frijns, T.; Vanderwal, S.; Castelijns, M.; Put, J.; Meijer, E. W. *Macromolecular Symposia* **1994**, *77*, 51-62.
- 10)Dvornic, P. R.; Tomalia, D. A. *Macromolecular Symposia* **1995**, *98*, 403-428.
- 11)Hummelen, J. C.; Vandongen, J. L. J.; Meijer, E. W. *Chemistry-A European Journal* **1997**, *3*, 1489-1493.
- 12)Uppuluri, S.; Keinath, S. E.; Tomalia, D. A.; Dvornic, P. R. *Macromolecules* **1998**, *31*, 4498-4510.
- 13)Aharoni, S. M.; Murthy, N. S. *Polymer Communications* **1983**, *24*, 132-136.
- 14)Potschke, D.; Ballauff, M.; Lindner, P.; Fischer, M.; Vogtle, F. *Macromolecules* **1999**, *32*, 4079-4087.
- 15)Kleppinger, R.; Reynaers, H.; Desmedt, K.; Forier, B.; Dehaen, W.; Koch, M.; Verhaert, P. *Macromolecular Rapid Communications* **1998**, *19*, 111-114.
- 16)Omotowa, B. A.; Keefer, K. D.; Kirchmeier, R. L.; Shreeve, J. M. *Journal Of The American Chemical Society* **1999**, *121*, 11130-11138.
- 17)Bauer, B. J.; Hammouda, B.; Briber, R. M.; Tomalia, D. A. *Acs Pmse Preprints* **1993**, *69*, 341-342.
- 18)Bauer, B. J.; Hammouda, B.; Barnes, J. D.; Briber, R. M.; Tomalia, D. A. *Acs Pmse Preprints* **1994**, *71*, 140-141.
- 19)Bauer, B. J.; Topp, A.; Prosa, T. J.; Amis, E. J. *Acs Pmse Preprints* **1997**, *77*, 140-141.
- 20)Prosa, T. J.; Bauer, B. J.; Amis, E. J.; Tomalia, D. A.; Scherrenberg, R. *Journal Of Polymer Science Part B-Polymer Physics* **1997**, *35*, 2913-2924.
- 21)Tomalia, D. A.; Baker, H.; Dewald, J.; Hall, M.; Kallos, G.; Martin, S.; Roeck, J.; Ryder, J.; Smith, P. *Macromolecules* **1986**, *19*, 2466-2468.

- 22)Newkome, G. R.; Moorefield, C. N.; Baker, G. R.; Saunders, M. J.; Grossman, S. H. *Angewandte Chemie-International Edition In English* **1991**, *30*, 1178-1180.
- 23)Jackson, C. L.; Chanzy, H. D.; Booy, F. P.; Drake, B. J.; Tomalia, D. A.; Bauer, B. J.; Amis, E. J. *Macromolecules* **1998**, *31*, 6259-6265.
- 24)Sheiko, S. S.; Gauthier, M.; Moller, M. *Macromolecules* **1997**, *30*, 2343-2349.
- 25)Degennes, P. G.; Hervet, H. *Journal De Physique Lettres* **1983**, *44*, L351-L360.
- 26)Lescanec, R. L.; Muthukumar, M. *Macromolecules* **1990**, *23*, 2280-2288.
- 27)Mansfield, M. L.; Klushin, L. I. *Macromolecules* **1993**, *26*, 4262-4268.
- 28)Mansfield, M. L. *Polymer* **1994**, *35*, 1827-1830.
- 29)Murat, M.; Grest, G. S. *Macromolecules* **1996**, *29*, 1278-1285.
- 30)Boris, D.; Rubinstein, M. *Macromolecules* **1996**, *29*, 7251-7260.
- 31)Naylor, A. M.; Goddard, W. A.; Kiefer, G. E.; Tomalia, D. A. *Journal Of The American Chemical Society* **1989**, *111*, 2339-2341.
- 32)Uhrich, K. *Trends In Polymer Science* **1997**, *5*, 388-393.
- 33)Cooper, A. I.; Londono, J. D.; Wignall, G.; McClain, J. B.; Samulski, E. T.; Lin, J. S.; Dobrynin, A.; Rubinstein, M.; Burke, A. L. C.; Frechet, J. M. J.; Desimone, J. M. *Nature* **1997**, *389*, 368-371.
- 34)Kim, Y. H.; Webster, O. W. *Journal Of The American Chemical Society* **1990**, *112*, 4592-4593.
- 35)Higgins, J. S.; Benoît, H. C. *Polymers And Neutron Scattering*; Clarendon Press: Oxford, 1994.
- 36)Bauer, B. J.; Briber, R. M.; Hammouda, B.; A., T. D. *Acs Pmse Preprints* **1992**, *67*, 430-431.
- 37)Prosa, T. J.; Bauer, B. J.; Amis, E. J. *Submitted To Macromolecules* .
- 38)Prosa, T. J.; Bauer, B. J.; Topp, A.; Amis, E. J.; Scherrenberg, R. *Acs Pmse Preprints* **1998**, *79*, 307-308.
- 39)Topp, A.; Bauer, B. J.; Amis, E. J.; Scherrenberg, R. *Acs Pmse Preprints* **1997**, *77*, 137-138.
- 40)Yin, R.; Qin, D.; Tomalia, D. A.; Kukowskalatallo, J.; Baker, J. R. *Acs Pmse Preprions* **1997**, *77*, 206-207.
- 41)Gauthier, M.; Moller, M. *Macromolecules* **1991**, *24*, 4548-4553.
- 42)Bauer, B. J.; Briber, R. M.; Han, C. C. *Macromolecules* **1989**, *22*, 940-948.
- 43)Bauer, B. J.; Hanley, B.; Muroga, Y. *Polymer Communications* **1989**, *30*, 19-21.
- 44)Bauer, B. J.; Briber, R. M. *Acs Polymer Preprints* **1990**, *31*, 578-579.
- 45)Choi, S.; Briber, R. M.; Bauer, B. J.; Topp, A.; Gauthier, M.; Tichagwa, L. *Macromolecules* **1999**, *32*, 7879-7886.
- 46)Topp, A.; Bauer, B. J.; Klimash, J. W.; Spindler, R.; Tomalia, D. A.; Amis, E. J. *Macromolecules* **1999**, *32*, 7226-7231.
- 47)Glinka, C. J.; Barker, J. G.; Hammouda, B.; Krueger, S.; Moyer, J. J.; Orts, W. J. *Journal Of Applied Crystallography* **1998**, *31*, 430-445.
- 48)Prask, H. J.; Rowe, J. M.; Rush, J. J.; Schroder, I. G. *Journal Of Research Of The National Institute Of Standards And Technology* **1993**, *98*, 1-13.
- 49)Wooley, K. L.; Klug, C. A.; Tasaki, K.; Schaefer, J. *Journal Of The American Chemical Society* **1997**, *119*, 53-58.
- 50)Topp, A.; Bauer, B. J.; Prosa, T. J.; Scherrenberg, R.; Amis, E. J. *Macromolecules* **1999**, *32*, 8923-8931.

- 51) Ramzi, A.; Scherrenberg, R.; Brackman, J.; Joosten, J.; Mortensen, K. *Macromolecules* **1998**, *31*, 1621-1626.
- 52) Stechemesser, S.; Eimer, W. *Macromolecules* **1997**, *30*, 2204-2206.
- 53) Welch, P.; Muthukumar, M. *Macromolecules* **1998**, *31*, 5892-5897.
- 54) Nisato, G.; Amis, E. J. *To Be Submitted*.
- 55) Zhou, C. L.; Hobbie, E. K.; Bauer, B. J.; Han, C. C. *Journal Of Polymer Science Part B-Polymer Physics* **1998**, *36*, 2745-2750.
- 56) Zhou, C. L.; Hobbie, E. K.; Bauer, B. J.; Sung, L.; Jiang, M.; Han, C. C. *Macromolecules* **1998**, *31*, 1937-1941.
- 57) Bauer, B. J.; Ramzi, A.; Liu, D. W.; Scherrenberg, R. L.; Froehling, P.; Joosten, J. *Journal Of Polymer Science Part B-Polymer Physics* **2000**, *38*, 95-100.
- 58) Ramzi, A.; Bauer, B. J.; Scherrenberg, R.; Froehling, P.; Joosten, J.; Amis, E. J. *Macromolecules* **1999**, *32*, 4983-4988.
- 59), 1995.
- 60) Stevelmans, S.; Vanhest, J. C. M.; Jansen, J.; Vanboxtel, D.; Vandenberg, E.; Meijer, E. W. *Journal Of The American Chemical Society* **1996**, *118*, 7398-7399.
- 61) Mourey, T. H.; Turner, S. R.; Rubinstein, M.; Frechet, J. M. J.; Hawker, C. J.; Wooley, K. L. *Macromolecules* **1992**, *25*, 2401-2406.
- 62) Gauthier, M.; Tichagwa, L.; Li, W. G. *Abstracts Of Papers Of The American Chemical Society* **1994**, *208*, 186-Poly.
- 63) Gauthier, M.; Tichagwa, L.; Downey, J. S.; Gao, S. *Macromolecules* **1996**, *29*, 519-527.
- 64) Frank, R. S.; Merkle, G.; Gauthier, M. *Macromolecules* **1997**, *30*, 5397-5402.
- 65) Gauthier, M.; Li, W. G.; Tichagwa, L. *Polymer* **1997**, *38*, 6363-6370.
- 66) Gauthier, M.; Chung, J.; Choi, L.; Nguyen, T. T. *Journal Of Physical Chemistry B* **1998**, *102*, 3138-3142.
- 67) Flory, P. J. *Principles Of Polymer Chemistry*; Cornell University Press: New York, 1953.
- 68) Zimm, B. H.; Stockmayer, W. H. *Journal Of Chemical Physics* **1949**, *17*, 1301.
- 69) Hawker, C. J.; Barclay, G. G.; Orellana, A.; Dao, J.; Devonport, W. *Macromolecules* **1996**, *29*, 5245-5254.
- 70) Guinier, A. *X-Ray Diffraction*; W.H. Freeman And Co.: San Francisco, 1963.
- 71) Guinier, A.; Fournet, G. *Small Angle Scattering Of X-Rays*; Wiley: New York, 1955.
- 72) Barker, J. G.; Pedersen, J. S. *Journal Of Applied Crystallography* **1995**, *28*, 105-114.
- 73) Mildner, D. F. R.; Carpenter, J. M. *Journal Of Applied Crystallography* **1984**, *17*, 249-256.
- 74) Briber, R. M.; Bauer, B. J.; Hammouda, B. *Journal Of Chemical Physics* **1994**, *101*, 2592-2599.
- 75) Han, C. C.; Bauer, B. J.; Clark, J. C.; Muroga, Y.; Matsushita, Y.; Okada, M.; Qui, T. C.; Chang, T. H.; Sanchez, I. C. *Polymer* **1988**, *29*, 2002-2014.
- 76) Williams, C.; Brochard, F.; Frisch, H. L. **1981**, 433.
- 77) Chu, B.; Ying, Q. C.; Grosberg, A. Y. *Macromolecules* **1995**, *28*, 180-189.
- 78) Sariban, A.; Binder, K. *Makromolekulare Chemie-Macromolecular Chemistry And Physics* **1988**, *189*, 2357-2365.
- 79) Dimarzio, E. A.; Briber, R. M. *Macromolecules* **1995**, *28*, 4020-4022.
- 80) Swislow, G.; Sun, S.; Nishio, I.; Tanaka, T. *Physical Review Letters* **1980**, *44*, 796.

- 81) Park, I. H.; Wang, Q. W.; Chu, B. *Macromolecules* **1987**, *20*, 1965-1975.
- 82) Bauer, D. R.; Ullman, R. *Macromolecules* **1980**, *13*, 392.
- 83) Chu, B.; Park, I. H.; Wang, Q. W.; Wu, C. *Macromolecules* **1987**, *20*, 2833-2840.
- 84) Chu, B.; Wang, Z. L. *Macromolecules* **1989**, *22*, 380-383.
- 85) Dingenouts, N.; Ballauff, M. *Langmuir* **1999**, *15*, 3283-3288.
- 86) Bates, F. S. *Macromolecules* **1984**, *17*, 2607-2613.
- 87) Bates, F. S.; Dierker, S. B.; Wignall, G. D. *Macromolecules* **1986**, *19*, 1938-1945.
- 88) Hashimoto, T.; Tsukahara, Y.; Kawai, H. *Macromolecules* **1981**, *14*, 708.
- 89) Sasaki, K.; Hashimoto, T. *Macromolecules* **1984**, *17*, 2818-2825.
- 90) Hashimoto, T.; Fujimura, M.; Kawai, H. *Macromolecules* **1980**, *13*, 1660.
- 91) Bates, F. S.; Berney, C. V.; Cohen, R. E. *Macromolecules* **1983**, *16*, 1101-1108.
- 92) Jansen, J.; Meijer, E. W.; Debrabandervandenberg, E. M. M. *Macromolecular Symposia* **1996**, *102*, 27-33.
- 93) Aiken, J. D.; Finke, R. G. *Journal Of Molecular Catalysis A-Chemical* **1999**, *145*, 1-44.
- 94) Mazzoldi, P.; Arnold, G. W.; Battaglin, G.; Gonella, F.; Haglund, R. F. *Journal Of Nonlinear Optical Physics & Materials* **1996**, *5*, 285-330.
- 95) Gröhn, F.; Bauer, B. J.; Amis, E. J. *Acs Polymer Preprints* **2000**, *41*.
- 96) Sperling, L. H. *Interpenetrating Polymer Networks And Related Materials*; Plenum Press: New York, 1981.
- 97) Briber, R. M.; Bauer, B. J. *Macromolecules* **1991**, *24*, 1899-1904.
- 98) Briber, R. M.; Liu, X. D.; Bauer, B. J. *Science* **1995**, *268*, 395-397.
- 99) Bauer, B. J.; Topp, A.; Prosa, T. J.; Liu, D. W.; Jackson, C. L.; Amis, E. J. *Proceedings Of The Spe 56th Annual Technical Conference* **1998**, *22*, 2065.
- 100) Bauer, B. J.; Prosa, T. J.; Liu, D. W.; Jackson, C. L.; Tomalia, D. A.; Amis, E. J. *Acs Polymer Preprints* **1999**, *40*, 406-407.
- 101) Kim, G.; Jackson, C. L.; Prosa, T. J.; Liu, D. W.; Bauer, B. J. *Acs Pmse Preprints* **2000**, *82*.
- 102) [Http://Www.Scioncorp.Com](http://www.scioncorp.com) **1998**.
- 103) Briber, R. M.; Bauer, B. J.; Hammouda, B.; Tomalia, D. *Acs Pmse Preprints* **1992**, *67*, 430-431.
- 104) Liu, X. D.; Bauer, B. J.; Briber, R. M. *Macromolecules* **1997**, *30*, 4704-4712.
- 105) Yen D. R., M. E. W. *Acs Polymer Preprints* **1997**, *38*, 531-532.
- 106) Antonietti, M.; Grohn, F.; Hartmann, J.; Bronstein, L. *Angewandte Chemie-International Edition In English* **1997**, *36*, 2080-2083.
- 107) Jansen, J.; Debrabandervandenberg, E. M. M.; Meijer, E. W. *Science* **1994**, *266*, 1226-1229.
- 108) Jansen, J.; Meijer, E. W.; Debrabandervandenberg, E. M. M. *Journal Of The American Chemical Society* **1995**, *117*, 4417-4418.
- 109) Zhao, M. Q.; Sun, L.; Crooks, R. M. *Journal Of The American Chemical Society* **1998**, *120*, 4877-4878.
- 110) Sooklal, K.; Hanus, L. H.; Ploehn, H. J.; Murphy, C. J. *Advanced Materials* **1998**, *10*, 1083-+.
- 111) Balogh, L.; Tomalia, D. A. *Journal Of The American Chemical Society* **1998**, *120*, 7355-7356.

- 112)Tan, N. C. B.; Balogh, L.; Trevino, S. F.; Tomalia, D. A.; Lin, J. S. *Polymer* **1999**, *40*, 2537-2545.
- 113)Zhao, M. Q.; Crooks, R. M. *Advanced Materials* **1999**, *11*, 217-+.
- 114)Garcia, M. E.; Baker, L. A.; Crooks, R. M. *Analytical Chemistry* **1999**, *71*, 256-258.
- 115)Crooks, R. M. *Science* **1999**, *283*, 165.
- 116)Glatter, O. *Acta. Phys. Austriaca* **1977**, *47*, 83.
- 117)Glatter, O. *Journal Of Applied Crystallography* **1977**, *10*, 415.
- 118)Glatter, O. *Journal Of Applied Crystallography* **1980**, *13*, 7.
- 119)Antonietti, M.; Wenz, E.; Bronstein, L.; Seregina, M. *Advanced Materials* **1995**, *7*, 1000-&.
- 120)Klingelhofer, S.; Heitz, W.; Greiner, A.; Oestreich, S.; Forster, S.; Antonietti, M. *Journal Of The American Chemical Society* **1997**, *119*, 10116-10120.
- 121)Zhao, M. Q.; Crooks, R. M. *Chemistry Of Materials* **1999**, *11*, 3379-3385.
- 122)Esumi, K.; Suzuki, A.; Aihara, N.; Usui, K.; Torigoe, K. *Langmuir* **1998**, *14*, 3157-3159.
- 123)Tan, N. C. B.; Bauer, B. J.; Plestil, J.; Barnes, J. D.; Liu, D.; Matejka, L.; Dusek, K.; Wu, W. L. *Polymer* **1999**, *40*, 4603-4614.
- 124)Colfen, H.; Antonietti, M. *Langmuir* **1998**, *14*, 582-589.
- 125)Antonietti, M.; Breulmann, M.; Goltner, C. G.; Colfen, H.; Wong, K. K. W.; Walsh, D.; Mann, S. *Chemistry-A European Journal* **1998**, *4*, 2493-2500.
- 126)Sayedsweet, Y.; Hedstrand, D. M.; Spinder, R.; Tomalia, D. A. *Journal Of Materials Chemistry* **1997**, *7*, 1199-1205.
- 127)Krska, S. W.; Seyferth, D. *Journal Of The American Chemical Society* **1998**, *120*, 3604-3612.
- 128)Bauer B. J., R. A., Liu D.-L., Scherrenberg, R. L., Froehling P., Joosten J. *Journal Of Polymer Science, Physics* **2000**, *38*, 95-100.
- 129)Glatter, O. *Journal Of Applied Crystallography* **1981**, *14*, 101.
- 130)Glatter, O.; Hainisch, B. *Journal Of Applied Crystallography* **1984**, *17*, 435-441.
- 131)Glatter, O. *Journal Of Applied Crystallography* **1988**, *21*, 886-890.